Stony Brook University

The Identification of Novel Components in the RNAi machinery in Fission Yeast *S. pombe*

A Dissertation Presented

by

An-Yun Chang

to

The Graduate School

in Partial Fulfillment of the

Requirements

for the Degree of

Doctor of Philosophy

in

Molecular and Cellular Biology

Stony Brook University

August 2014

Stony Brook University

The Graduate School

An-Yun Chang

We, the dissertation committee for the above candidate for the

Doctor of Philosophy degree, hereby recommend

acceptance of this dissertation.

Robert Martienssen – Dissertation Advisor
Professor and HHMI Investigator, Cold Spring Harbor Laboratory

Rolf Sternglanz - Chairperson of Defense
Distinguished Professor Emeritus, Stony Brook University

David Spector
Director of Research and Professor, Cold Spring Harbor Laboratory

James Hicks
Research Professor, Cold Spring Harbor Laboratory

William Kelly
Professor, Emory University

Emily Bernstein
Associate Professor, Icahn School of Medicine at Mount Sinai

This dissertation is accepted by the Graduate School

Charles Taber
Dean of the Graduate School

Abstract of the Dissertation

The Identification of Novel Components in the RNAi Machinery in Fission Yeast *S. pombe*

by

An-Yun Chang

Doctor of Philosophy

in

Molecular and Cellular Biology

Stony Brook University

2014

RNA interference (RNAi) is a mechanism for post-transcriptional gene silencing by RNA slicing or translational inhibition. Studies in the fission yeast *S. pombe* have demonstrated that RNAi components are additionally involved in transcriptional silencing by signaling chromatin assembly into the silent heterochromatin state. Originally discovered in worms and in plants, RNAi-mediated silencing is conserved in most eukaryotes with a few exceptions, including the budding yeast *S. cerevisiae*. Taking advantage of this observation, I initiated a candidate gene screen to search for novel components in the RNAi machinery.

I identified a putative splicing factor Rct1 as one of the genes that seems to have co-evolved with RNAi components, and demonstrated that Rct1 is required for proper processing of heterochromatic transcripts into siRNAs. My results showed that Rct1 guides heterochromatic transcripts to the RNAi machinery and prevents transcript targeting by the exosome. Surprisingly, Rct1 is dispensable for H3K9 methylation, suggesting siRNAs do not in themselves mediate heterochromatin assembly. In addition to Rct1, I identified five more genes that are specific to *S. pombe*, with no apparent *S. cerevisiae* homolog and yet are conserved in higher eukaryotes, which are required for robust heterochromatic silencing. Taken together, my study identified several potential novel RNAi factors and demonstrated that siRNA biogenesis and H3K9

methylation could be uncoupled while intact RNAi machinery is present, indicating an additional role of RNAi machinery in heterochromatin assembly.

Dedication Page

I would like to dedicate this thesis to my parents, who are the best parents a daughter could ever wish for.

Table of Contents

List of Figures

List of Tables

List of Abbreviations

5-FOA	5-Fluoroorotic acid
ac	acetylation
act1	actin 1
ade	adenine
Ago	Argonaute
Air1	Arginine methyltransferase-interacting RING finger protein 1
arb	argonaute binding protein
ARC	Argonaute siRNA Chaperone
Ark1	Aurora kinase 1
Atf1	Activating transcription factor 1
ATP	Adenosine Triphosphate
bp	base pair
brdrRNA	siRNAs derived from Dcr1 processing BORDERLINE precursor RNA
C-terminus	carboxyl-terminus, COOH-terminus
Ccq1	Coiled-coil quantitatively-enriched protein 1
Cdc20	Cell division cycle mutant 20, encodes DNA polymerase epsilon catalytic subunit Pol2
cdk9	cyclin-dependent kinase 9
cDNA	complementary DNA
cen	centromere
cenH	centromere homology
CHD	Chromodomain, Helicase, DNA binding
ChIP	Chromatin Immunoprecipitation
chp	HP1 family chromodomain protein
cid	caffeine induced death
clr	cryptic loci regulator
CLRC	Cryptic Loci Regulator Complex

cnt	central core domain
cox1	cytochrome oxidase 1
CT	cycle threshold
CTD	RNA Polymerase II Carboxy-Terminal Domain
cul	cullin family protein
cwf	complexed with Cdc5p
cyn-14	cyclophilin-14
DAPI	4',6-diamidino-2-phenylindole
Dcr	Dicer
dg	dogentai (kinetochore, in Japenese)
DIC	Differential Interference Contrast
dis3	defective in sister chromatid disjoining 3
dos	delocalization of Swi6
dsRNA	double-strand RNA
ely5	embryonic large molecule derived from yolk sac
EMS	ethyl methanesulfonate
eri1	enhanced RNAi 1
FL	full length
G1 phase	Growth 1 or Gap 1 Phase
G2 phase	Growth 2 or Gap 2 Phase
GFP	Green Fluorescent Protein
GST	Glutathione S-Transferase
H3K14	histone H3 lysine 14
H3K27	histone H3 lysine 27
H3K4	histone H3 lysine 4
H3K9	histone H3 lysine 9
H3S10	histone H3 serine 10
H4K16	histone H3 lysine 16
H4K20	histone H4 lysine 20
HA	Hemagglutinin
HAT	histone acetyltransferase

HDAC	histone deacetylase
HEN1	HUA enhancer 1
Hhp2	HRR25 homolog from *S.pombe*
HP1	Heterochromatin Protein 1
Hrr1	Helicase required for RNAi-mediated heterochromatin assembly
imr	innermost region
INO80	Inositol requiring 80
IP	immunoprecipitation
IQR	interquartile range
IRC	Inverted Repeats Centromere
ISWI	Imitation Switch
kDa	kilodaltons
lid2	little imaginal discs 2, homolog of the *D. melanogaster* Trithorax protein
LIM domain	named after the LIN-11, ISL-1 and MEC-3 proteins in *C. elegans*
M	Minus
M phase	Mitotic phase
mcl1	minichromosome loss protein 1
ME	Malt Extract
me	methylation
me2	dimethylation
me3	trimethylation
mit1	Mi2-like interacting with clr3 protein 1
mlo3	missegregation and lethal when overexpressed 3
mRNA	messenger RNA
mst2	MYST (Moz, Ybf2/Sas3, Sas2, Tip60) family histone acetyltransferase 2
mtr4	mRNA transport 4
mug70	meiotically upregulated gene 70
N-terminus	amino-terminus, NH2-terminus
N/S	non-selective
ncRNA	non-coding RNA
NFR	Nucleosome Free Region

nt	nucleotides
nup120	nucleoporin 120
OD600	optical density measured at a wavelength of 600 nm
Orc	Origin recognition complex
ori	orientation
otr	outermost region
otr1R::ura4	*ura4* insertion at the outermost region of centromere 1 right arm
P	Plus
p-S2	phosphorylated serine 2
p-S5	phosphorylated serine 5
PBS	Phosphate Buffered Saline
pcr1	*S. pombe* CREB, transcription factor
PNK	Polynucleotide Kinase
Pol	polymerase
Pol II	RNA polymerase II
poly-A	polyadenylation
PPIase	Prolyl-Peptidyl cis-trans Isomerase
PPIL4	Prolyl-Peptidyl Isomerase -Like 4
priRNA	primal RNA
prp	pre-mRNA processing
raf	Rik1-associated factor
rct1	RRM- containing cyclophilin regulating transcription 1
rdp1	RNA-dependent polymerase 1
RDRC	RNA-directed RNA polymerase complex
RdRP	RNA-dependent RNA Polymerase
rik1	recombination in K
RIP	RNA immunoprecipitation
RITS	RNA-Induced Transcriptional Silencing
RNAi	RNA interference
rpb	DNA-directed RNA polymerase II subunit
RPM	Reads Per Million

RRM	RNA Recognition Motif
rrm	RNA recognition motif mutation
rRNA	ribosomal RNA
rrp6	ribosomal RNA processing 3'-5' exonuclease 6
RSC	Remodel the Structure of Chromatin
S phase	Synthesis phase
SCANR	Spliceosome-Coupled And Nuclear RNAi
SEM	standard error from mean
seq	Next Generation Sequencing
SET	Su(var)3-9 and Enhancer of zeste proteins
SHREC	Snf2/Hdac-containing repressor Complex
sir2	silent information regulator 2
siRNA	small interfering RNA
SNP	Single Nucleotide Polymorphism
sp	*S. pombe*
SR proteins	serine and arginine rich proteins
sre2	sterol regulatory element 2
SREBP	Sterol Regulatory Element Binding Protein
ssr4	SWI/SNF and RSC complexes subunit 4
ssRNA	single-strand RNA
stc1	siRNA to chromatin
SUV39H1	Suppressor of variegation 3–9 homolog 1
swi	switching deficient mutant
SWI/SNF	Switching defective/ Sucrose Nonfermentable
tas3	targeting complex subunit 3
taz1	telomereassociated in *S pombe*
TE	Transposable Element
Tf2	Transposon of fission yeast 2
tlh	telomere-linked helicase
TRAMP	Trf4/Air2/Mtr4p Polyadenylation
trf	topoisomerase related function

tRNA	transfer RNA
U	Uridine
ubc	ubiquitin conjugating enzyme
ura	uracil
ura4-DS/E	ura4 deleting StuI-EcoRV portion
WD repeat	Trp-Asp dipeptide repeat
WGD	Whloe Genome Duplication
YES	Yeast Exact with Supplements
ΔC	carboxyl-terminus deletion
ΔIso	Peptidyl-Prolyl cis-trans Isomerase deletion

Acknowledgments

Completing my PhD has been a quite an interesting journey and I could not have done it without many of you standing by my side throughout the years.

First and foremost, I would like to thank my thesis advisor, Robert Martienssen, for giving me this chance to be part of his lab. Rob has always been extremely patient and supportive of my work, and I appreciate the freedom he gave me to explore in my project. I believe this training helped me become a more mature and independent scientist.

I would also like to express my gratitude to my committee members for all their suggestions, positive criticisms and encouragement: Rolf Sternglanz, Emily Bernstein, Jim Hicks, William Kelly and David Spector. They have always been understanding and helpful. Their positive attitude is what carried me on to remain focused with my project.

I would like to thank Stephane Castel and Evan Ernst who analyzed my sequencing data; a large part of this work would not have been possible without their help. Moreover, a special thank you to our lab manager, Joe Simorowski, who spent so many hours proofreading my thesis. Also, Sadie Arana has been amazing in making sure things runs smoothly and on schedule.

This journey would not have been the same without all the members of the Martienssen lab. I am greatly honored to work with this great selection of people, including former lab members Mikel Zaratiegui, Danielle Irvine, Klavs Hansen, Anna Kloc and Sarajane Locke, who have guided me in the first couple years and taught me all the basics about *S. pombe*. I have learned so much from their expertise. Also the current "team *pombe*" for their great ideas and fun discussions: Benjamin Roche, Hyun Soo Kim, Stephane Castel, Jie Ren, Sonali Bhattacharjee and Atsushi Shimada. In addition, other lab members, Jon-Jin Han, Andrea Schorn, Kate Creasey, Joe Simorowski, Almudena Molla-Morales, Chantal LeBlanc, Yannick Jacob, Evan Ernst, Rowan Herridge, Filipe Borges, Mark Donoghue, Seung Cho Lee, Uma Ramu, Michael Regulski, Charles Underwood, Jean-Sebastien Parent, Joseph Calarco, Fred Van Ex, Rebecca Schwab, Patrick Finigan, Milos Tanurdzic, Keith Slotkin, Eyal Gruntman, Alex Cantó Pastor and Roberto Tirado Magallanes, thank you for sharing my frustration and my joy during this journey. I really appreciate this incredible experience; I learned something valuable from each and every one of you.

Finally, I would like to thank my friends and families for their unconditional love and unlimited support. It was your faith in me that led me towards the finish line. I would not be who I am today without you in my life!

Chapter I: Introduction

1.1 The history and significance of heterochromatin

Heterochromatin was first described by Emil Heitz based on the cytogenetic observation that certain regions of *Pellia epiphylla* chromatin remained condensed throughout the cell cycle, while others underwent cycles of condensation and de-condensation (Heitz, 1928). This observation introduced the idea that the chromosome is not a homogeneous structure from end to end. He called the chromatin that remained condensed "heterochromatin", and the chromatin underwent condensation and de-condensation cycles "euchromatin" or "true chromatin". In the 1930s, the first example of position effect variegation (PEV) was described in *Drosophila melanogaster* (Muller, 1930), where it was shown that the affected gene in the mutants displayed variegated expression and that the expression was heritable to the next generation. Further analysis by genomic mapping showed the affected genes had translocated near to heterochromatin regions. Subsequent studies provided evidence that genes placed proximal to heterochromatin were efficiently silenced when compared to genes placed more distal (Demerec and Slizynska, 1937). This was the first indication that the chromatin structure could affect gene expression and that silent heterochromatin had the ability to spread in a sequence-independent manner.

Major heterochromatin blocks are found at the centromeres and telomeres in eukaryotes. These regions are usually gene poor, contain repetitive DNA sequences, and are mostly transcriptionally silent. For a long time, silent heterochromatin was viewed as "junk DNA" and received very little attention. This view was vigorously challenged in the past decades, as increasing amounts of evidence showed that heterochromatin is essential for many different cellular processes.

Constitutive heterochromatin is stable during the cell cycle and present in all cell types in the organism. Large blocks of constitutive heterochromatin found at the centromeres are essential for equal chromosome segregation during M phase, and prevent aneuploidy that is detrimental in the higher eukaryotes (Allshire et al., 1995; Kellum and Alberts, 1995; Steiner and Clarke, 1994). Constitutive heterochromatin at the telomeres

protects the ends of linear chromosomes and inhibits repetitive DNA recombination, which can lead to telomere fusion and cause large-scale genomic rearrangement (Murnane and Sabatier, 2004). Genome instability caused by the loss of constitutive heterochromatin can result in developmental defects or diseases such as cancer (Blasco, 2007; Verdaasdonk and Bloom, 2011; Zaratiegui et al., 2007).

Facultative heterochromatin assembly triggered by cellular signals is found at developmentally regulated loci, and is important to regulate gene activity to specify different cell identities, thus ensuring normal development (Brown, 1966; Trojer and Reinberg, 2007). One example of facultative heterochromatin is in female mammals, in which non-coding RNAs such as XIST trigger heterochromatin assembly at one of the two X chromosomes to regulate gene dosage. This is commonly referred to as X chromosome inactivation (Lyon, 1961; Ohno et al., 1959; Pollex and Heard, 2012). In addition, transposable elements (TE) are silenced by heterochromatin formation to prevent genome mutagenesis by TE insertion, as observed in several model organisms (Lippman and Martienssen, 2004; McClintock, 1950).

1.2 Heterochromatin in *S. pombe*

Fission yeast *Schizosaccharomyces pombe* is widely used as a model organism to study heterochromatin assembly. Similar to another popular yeast model organism, the budding yeast *Saccharomyces cerevisiae*, the genome of *S. pombe* was fully sequenced in 2002 and is amenable to genetic manipulation (Wood et al., 2002). In addition to centromere and telomere heterochromatin that exist in higher eukaryotes, yeast contains a third constitutive heterochromatin region at the mating-type locus (Cam et al., 2005) (Figure 1.1).

Many studies have demonstrated that *S. pombe* is similar to higher eukaryotes in that they both have regional centromeres. In *S. pombe* centromeres, a central core (cnt), which spans 4-7 kb and incorporates the unique histone H3 variant CENP-A (encoded by Cnp1 in *S. pombe*), is flanked by inverted inner most repeats (*imr*) followed by outer repeats (*otr*). The *otr* regions contain multiple *dh* and *dg* subrepeats arranged in tandem, and depending on the number of *dh/dg* repeats, the three centromeres in *S. pombe* range from 40-100 kb in size (Chikashige et al., 1989; Clarke et al., 1986; Fishel et al., 1988;

Murakami et al., 1991; Nakaseko et al., 1986; 1987; Wood et al., 2002). In higher eukaryotes, such as plants and mammals, centromeres are much larger and more complex, but they still resemble the same basic organization as observed in *S. pombe* (Allshire and Karpen, 2008; Zaratiegui et al., 2007). By contrast, *S. cerevisiae* has point centromeres, only about 125 bp in length and with no DNA repeats (Clarke, 1990; Clarke and Carbon, 1985; Cottarel et al., 1989). This is perhaps not surprising, considering *S. pombe* diverged from *S. cerevisiae* more than 300 million years ago (Heckman et al., 2001; Hedges, 2002; Sipiczki, 2000).

Telomeres appear well conserved through evolution in both structure and function, and they consist of extended arrays of tandem repeats and G-overhangs (Blasco, 2007). All higher eukaryotes have an identical 5'-GGGTTA-3' telomeric repeat sequence (de Lange et al., 1990; Zakian, 1995), while *S. pombe* and *S. cerevisiae* contain the more degenerate sequences GGTTACA(G)1–4 and G2-3 (TG)1–4, respectively (Hiraoka et al., 1998; Wang and Zakian, 1990). Nonetheless, together with telomere DNA specific binding proteins, the nucleoprotein structure of telomeres protects the ends of chromosomes from recombination and unwanted initiation of DNA repair and degradation pathways.

Yeast contains additional heterochromatin at the mating-type locus, which includes three DNA cassettes, two of which are transcriptionally silent and one active. In *S. pombe*, mating-type heterochromatin covers a 20 kb domain containing the two silent DNA cassettes, *mat2-P* and *mat3-M*, and the *K*-region between them (Cam et al., 2005). Depending on which one of the silent cassettes gets expressed through translocation to the third active cassette, *mat1*, *S. pombe* cells can display either plus (P) or minus (M) mating type. The choice of which silent cassette gets expressed is not random; in fact, "donor selection" occurs in a cell type specific manner. In *mat1-M* cells, *mat2* is the preferred donor, and *mat1-P* cells, *mat3* is the preferred donor (Abraham et al., 1984; Beach and Klar, 1984; Beach et al., 1982; Egel et al., 1990; Hicks and Herskowitz, 1977; Klar et al., 1982; Oshima and Takano, 1971; Strathern and Herskowitz, 1979). Interestingly, by swapping the two silent cassettes at the mating-type locus, studies showed that the location of the donor loci, rather than their DNA sequences, directs this cell type specific donor choice (Thon and Klar, 1993). This non-random donor choice is

disrupted in mutants that affect heterochromatin silencing, suggesting heterochromatin assembly at this locus is important for mating-type switching in *S. pombe* (Ekwall and Ruusala, 1994; Grewal et al., 1998; Thon and Klar, 1993; Thon et al., 1994; Tuzon et al., 2004).

Interestingly, the heterochromatin regions discussed above share sequence homology in *S. pombe* (Grewal and Klar, 1997; Hansen et al., 2006) (Figure 1.1), and this sequence is sufficient to trigger *de novo* heterochromatin assembly at a euchromatic site (Ayoub et al., 2000; Partridge et al., 2002). Similar to higher eukaryotes, heterochromatin regions in *S. pombe* are highly repetitive and extremely gene poor (Wood et al., 2002). At the molecular level, heterochromatin is characterized by hypo-acetylated histones H3 and H4 (Ekwall et al., 1997; Jeppesen and Turner, 1993; Jeppesen et al., 1992; Turner, 1991), and methylated lysine 9 on histone H3 (H3K9) in most eukaryotes, including *S. pombe* (Cam et al., 2005; Rice and Allis, 2001). Methylated H3K9 serves as a binding site for heterochromatin protein 1 (HP1, encoded by Swi6 and Chp2 in *S. pombe*), leading to epigenetic repression (Bannister et al., 2001; Lachner et al., 2001; Nakayama et al., 2000). This tightly packed and modified chromatin structure probably inhibits RNA Polymerase II (Pol II) accessibility, resulting in transcriptional silencing of those associated sequences. In higher eukaryotes, heterochromatin and gene silencing are also associated with histone H3 lysine 27 (H3K27), histone H4 lysine 20 (H4K20) and DNA methylation. Although H4K20 methylation is present in *S. pombe*, it does not associate with heterochromatin or gene silencing, but rather with DNA damage (Sanders et al., 2004). Furthermore, H3K27 and DNA methylation appear to be missing in *S. pombe*, but are conserved in the filamentous fungus *Neurospora crassa* (Antequera et al., 1984; Aramayo and Selker, 2013; Lachner et al., 2004).

1.3 Epigenetic inheritance

Originally coined by Waddington in 1942, the term “epigenetic” was used to bridge the differences between genotype and phenotype (Waddington, 1942). In my thesis, I will define epigenetics as heritable changes in genome function that occur without DNA sequence alteration, including processes involving histone variants, post-translational histone modifications and DNA methylation. Therefore, heterochromatin

assembly that involves the propagation of essential architectural features of chromosome is subject to epigenetic regulation.

Much like genetic material, epigenetic information must be faithfully inherited from the parental generation by the next, but a certain level of plasticity is carefully regulated to allow cell differentiation during development. Epigenetic inheritance is relatively common in plants, but how epigenetic inheritance is achieved remains poorly understood. In organisms with DNA methylation, epigenetic inheritance can be regulated by the semi-conservative nature of DNA replication. The parental methylated strands received by newly replicated chromatids could be sufficient in guiding replicated DNA methylation and thereby restoring the parental epigenetic state (Bostick et al., 2007; Sharif et al., 2007). However, *S. pombe* lacks DNA methylation (Antequera et al., 1984), and it can be challenging to re-establish the proper heterochromatin state after passage of the replication fork during S phase, during which modified parental histones are stripped off from the nucleosomes. A current model suggests that modified parental histones and newly synthesized histones are deposited onto the DNA strand behind the replication fork in a random fashion, and in order to retain the parental epigenetic state after DNA replication, parental histones can be used as templates to modify naïve neighboring histones (Cam, 2010; Gonzalez and Li, 2012; Heard and Martienssen, 2014).

In *S. pombe*, histone H3K9 methylation is catalyzed by the mammalian histone methyltransferase SUV39H1 homolog, Clr4, which localizes throughout heterochromatin (Rea et al., 2000; Zhang et al., 2008). The SET domain at the C-terminus of Clr4 mediates the catalytic activity, and the chromodomain located in the N-terminus allows Clr4 binding to methylated H3K9 (Ivanova et al., 1998; Nakayama et al., 2001; Zhang et al., 2008). Therefore, Clr4 is both the "writer" and the "reader" of H3K9 methylation (Zhang et al., 2008). This dual property makes Clr4 an excellent candidate to achieve histone modification inheritance in *S. pombe*. Clr4 exists in the CLRC (Cryptic Loci Regulator Complex), and artificially tethering the CLRC to euchromatin is sufficient to trigger *de novo* H3K9 methylation (Kagansky et al., 2009). Additional factors in CRLC include Cul4, Rik1, Dos1 (also known Raf1/Cmc1/Clr8), Dos2 (Raf2/Cmc2/Clr7) and Lid2, and disruption of any of these factors results in compromised heterochromatin assembly and silencing (Hong et al., 2005; Horn et al., 2005; Jia et al., 2005; Li et al.,

2008; Thon et al., 2005). Interestingly, Cdc20, the catalytic subunit of DNA Polymerase ε (DNA Pol ε), interacts with the CLRC components Rik1 and Dos2, and this interaction is required for heterochromatin assembly during S phase. In *cdc20* mutant cells, Rik1 and Dos2 dissociate from pericentromeric heterochromatin and H3K9 methylation is compromised (Li et al., 2011). Additionally, the Origin Recognition Complex (Orc) and DNA Polymerase α subunits Swi7 and Mcl1 interact with Swi6, and are involved in heterochromatin formation in the pericentromeric region (Natsume et al., 2008).

These studies demonstrate that the DNA replication machinery is closely associated with CLRC, which is essential for establishing the silent epigenetic state in *S. pombe*. Furthermore, the coordination of the H3K9 methylation by CLRC during S phase is required to re-assemble heterochromatin.

1.4 Cell cycle dependent heterochromatin assembly via RNAi

After S phase, *S. pombe* spends almost 3/4 of its cell cycle in G2, followed by a short M/G1 phase. Heterochromatin is usually transcriptionally inert and devoid of Pol II binding. However, Pol II binds to pericentromeric heterochromatin specifically during the S phase, and *dh/dg* repeats are transcribed (Chen et al., 2008; Kloc et al., 2008). In agreement with this observation, H3K9 methylation levels are at their lowest in early S phase, indicating that modified histones are being temporarily diluted due to DNA replication. In late S phase, H3K9 methylation levels increase and finally peak in G2 (Kloc et al., 2008). A cell cycle dependent phospho-methyl switch regulates this silent heterochromatin alleviation (Fischle et al., 2003; 2005). During S-phase, histone H3 serine 10 (H3S10) is phosphorylated by aurora kinase Ark1, and this phosphorylation disturbs the association between Swi6 and H3K9 methylation, thereby allowing heterochromatin transcription (Fischle et al., 2003; 2005; Hirota et al., 2005; Kloc et al., 2008). In the early G2, H3S10 phosphorylation is lost, which enables Swi6 binding to methylated H3K9, preparing the cell for mitosis. Swi6 interacts with cohesin at the pericentromeric repeats, which is critical for sister chromatid alignment with the mitotic spindle to ensure proper chromosome segregation (Kloc et al., 2008; Nonaka et al., 2002) .

Heterochromatin formation appears to be a dynamic process that involves transient alleviation of the silent state during S-phase and re-establishment of silent epigenetic marks (Cheutin et al., 2003; 2004 ; Festenstein et al., 2003; Kloc et al., 2008). Transcripts originating from the heterochromatin regions are transcribed by Pol II (Choi et al., 2011; Djupedal et al., 2005; Kato et al., 2005). In *S. pombe*, Pol II consists of 12 different subunits, and the C-terminal domain (CTD) of the largest subunit, Rpb1, contains 28 heptad repeats with a very conserved YSPTSPS sequence. Many types of post-translational modifications target the Pol II CTD, which serves as a platform for recruiting specific RNA processing factors, including capping, polyadenylation and splicing, at different stages of transcription. Similar to euchromatic protein-coding transcripts, pericentromeric transcripts are polyadenylated and spliced (Chinen et al., 2010; Win et al., 2006b). Cells carrying a point mutation (N44T) in the second largest Pol II subunit, Rpb2, have defects in chromosome segregation along with loss of heterochromatic silencing and H3K9 methylation (Kato *et al*. 2005). A mis-sense mutation (G150D) in a small subunit of Pol II, Rpb7, impairs pericentromeric transcription and results in reduced H3K9 methylation (Djupedal *et al*. 2005).

The transcription of pericentromeric repeats by Pol II appears to be required for heterochromatin assembly, and studies showed that these transcripts are rapidly processed by the RNA interference (RNAi) machinery to generate small interfering RNAs (siRNAs) during S-phase (Kloc et al., 2008). Disruption of the RNAi components results in accumulation of the pericentromeric transcripts and defects in siRNA biogenesis. Furthermore, in addition to post-transcriptional silencing of pericentromeric transcripts, RNAi machinery is also required for H3K9 methylation and heterochromatin assembly in *S. pombe.* In cells lacking RNAi factors, H3K9 methylation is decreased and Swi6 delocalizes from pericentromeric repeats, leading to higher rate of lagging chromosome and mini chromosome loss (Hall et al., 2003; Volpe et al., 2002; 2003). Intriguingly, the CLRC and Cdc20 are essential for robust siRNA biogenesis, suggesting that efficient heterochromatin transcript processing by RNAi is dependent on DNA replication and H3K9 methylation (Hong et al., 2005; Li et al., 2005; 2008; 2011).

1.5 The evolution of RNAi in fungi

Originally discovered in *Caenorhabditis elegans* (*C. elegans*) and in plants, RNAi is a mechanism of post-transcriptional gene silencing by RNA slicing or translational inhibition (Fire et al., 1998; Hamilton and Baulcombe, 1999; Vaucheret et al., 1998). The key components in the RNAi machinery are RNA-dependent RNA Polymerase (RdRP), Argonaute (Ago) and Dicer (Dcr). RNAi-mediated silencing is conserved in most eukaryotes from yeast to human, with a few exceptions including the budding yeast *S. cerevisiae* (Aravind et al., 2000; Nakayashiki et al., 2006). I surveyed the phylogenic distribution of RNAi machinery in diverse fungi, and the RNAi machinery appears to be lost in *S. cerevisiae* and its close relatives (Figure 1.2).

S. cerevisiae belongs to the Saccharomycotina subphylum, which can be divided into the CTG clade and the whole genome duplication (WGD) clade. The CTG clade translates CTG into serine instead of leucine. The sequenced species from the CTG clade contain a non-canonical Dicer, and have no RdRP homolog (Nakayashiki et al., 2006). The *Candida* genus of the CTG clade, which includes another popular yeast model organism, *Candida albicans*, contains an Argonaute homolog, thus appearing to have a functional RNAi pathway. Other species from the CTG clade do not contain an Argonaute homolog and are considered RNAi deficient (Drinnenberg et al., 2011; Nakayashiki et al., 2006). The WGD clade underwent whole genome duplication roughly 100 million years ago (Wolfe and Shields, 1997), but about 90% of the duplicated gene pairs were lost over time. As of now, about 500 gene pairs remain in the genome of *S. cerevisiae* (Cliften et al., 2006). The RNAi machinery appears to be lost in the majority of the sequenced species in the WGD clade, with the exceptions *Kluyveromyces polysporus* and *Saccharomyces castellii* (*S. castellii*), both of which contain an Argonaute and a non-canonical Dicer homolog, but no detectable RdRP. Interestingly, the expression of Argonaute and Dicer from *S. castellii* is sufficient to reconstitute the RNAi pathway in *S. cerevisiae* (Drinnenberg et al., 2009).

The yeast centromere is a rapidly evolving region (Bensasson et al., 2008). The loss of RNAi during evolution in certain lineages correlates with point centromere structures, as observed in the yeast species in which the genome assembly is complete. *S. cerevisiae* contains point centromeres, conserved DNA motifs serving as binding sites for

specific kinetochore proteins, thus defining a point centromere by the presence of centromere-specific DNA sequences (Clarke, 1990; Clarke and Carbon, 1985; Cottarel et al., 1989). Most other organisms possess regional centromeres, which are highly repetitive and lack centromere-specific DNA motifs. The formation of regional centromeres relies on a sequence-independent epigenetic mechanisms (Verdaasdonk and Bloom, 2011). Most species from the Saccharomycotina subphylum contain point centromeres, with the exception of the *Candida* genus in the CTG clade, and *S. castellii* in the WGD clade (Cliften et al., 2006; Roy and Sanyal, 2011), both of which coincidentally retain the RNAi machinery (Figure 1.2). *S. castellii* is closely related to *S. cerevisiae*, and these two species diverged well after the whole genome duplication event. Interestingly however, the *S. cerevisiae* centromere is much more similar to some distal species in which their RNAi machinery are also lost (Drinnenberg et al., 2011; Roy and Sanyal, 2011).

The evolutionary success of those RNAi-deficient yeast species can be explained by the ability to acquire and retain "killer" (Drinnenberg et al., 2011), a stable cytoplasmically inherited dsRNA virus system which encodes a secreted protein toxin that can kill nearby cells while providing host cells with immunity (Wickner, 1996). However, the observation that some budding yeast species closely related to *S. cerevisiae* contain a functional RNAi pathway suggests that RNAi might have been lost only very recently, and in the long term, the disadvantage of losing RNAi machinery in these yeast species might become apparent.

1.6 The role of RNAi in heterochromatin assembly

Following the discovery more than a decade ago that RNAi components are involved in co-transcriptional silencing of heterochromatin in *S. pombe* (Hall et al., 2002; Provost et al., 2002b; Volpe et al., 2002), the detailed mechanism has been elaborated. This fission yeast species contains a fully functional RNAi machinery, and each factor in the RNAi pathway is encoded by a single gene (Volpe et al., 2002; Wood et al., 2002).

The co-transcriptional model (Figure 1.3) suggests that heterochromatic transcripts are converted to double-stranded RNAs (dsRNAs) by the action of the RDRC (RNA-

directed RNA polymerase complex) (Motamedi et al., 2004; Sugiyama et al., 2005), which contains RNA-dependent RNA Polymerase (encoded by *rdp1*). Although to a certain extent, dsRNAs can also be generated by bi-directional transcription and/or folding of single-stranded RNAs (Djupedal et al., 2009; Volpe et al., 2002). The RNase III family endonuclease Dicer (encoded by *dcr1*), which is associated with the RDRC complex, processes dsRNA precursors into 22-24 nucleotide long siRNAs (Reinhart and Bartel, 2002; Volpe et al., 2002; Colmenares et al., 2007). These double-stranded siRNAs are first loaded onto the ARC (Argonaute siRNA chaperone) complex, which contains Argonaute (encoded by *ago1*) and two other chaperon proteins, Arb1 and Arb2 (Argonaute binding). Arb1 inhibits the slicer activity of Ago1 in this complex, and the associated siRNAs remain double-stranded (Buker et al., 2007). These double-stranded siRNAs are passed onto another complex termed RITS (RNA-Induced Transcriptional Silencing), which, in addition to Ago1, contains Chp1 and Tas3 (Verdel et al., 2004). The slicer activity of Ago1 in the RITS complex promotes passenger strand release from duplex siRNA, enabling this effector complex to target homologous RNA or DNA through base pairing (Buker et al., 2007; Irvine et al., 2006). LIM domain protein Stc1 (siRNA to chromatin) bridges the interaction between the RITS complex and CLRC (Bayne et al., 2010), helping to recruit CLRC to the pericentromeric heterochromatin for H3K9 methylation (Nakayama et al., 2001; Hong et al., 2005; Horn et al., 2005; Jia et al., 2005; Li et al., 2005; Thon et al., 2005). Methylated H3K9 histones serve as binding sites for chromodomain proteins, including Swi6, Chp1, Chp2 and Clr4 (Doe et al., 1998; Thon and Verhein-Hansen, 2000; Halverson et al., 2000; Partridge et al., 2000; Bannister et al., 2001; Lachner et al., 2001; Sadaie et al., 2004; Zhang et al., 2008). Chp1 binding to methylated H3K9 can further strengthen the association between RITS and heterochromatin, creating a positive feed back loop (Petrie et al., 2005). A second positive feedback loop is created by the binding of Clr4 to methylated H3K9, which in turn promotes H3K9 methylation of the neighboring histones, thus allowing heterochromatin spreading in a sequence independent manner (Al-Sady et al., 2013; Zhang et al., 2008). All components in the RDRC, RITS and CLRC complexes are essential for robust siRNA biogenesis and efficient H3K9 methylation at pericentromeric heterochromatin in S. pombe.

While both pericentromeric heterochromatin assembly and maintenance require RNAi at the pericentromeric repeats (Volpe et at., 2002; Sadaie et al., 2004), RNAi components are only required for rapid restoration of artificially depleted heterochromatin at the mating-type locus and at telomeres, and are dispensable for maintenance in these regions (Volpe et al., 2002; Hall et al., 2002; 2003; Jia et al., 2004; Sadaie et al., 2004; Yamada et al., 2005). For this reason the pericentromeric repeats, and reporter genes integrated within them, have become the most important model for RNAi mediated heterochromatin assembly in *S. pombe*.

1.7 Small RNAs

In agreement with the specific role of the RNAi machinery in pericentromeric heterochromatin assembly and maintenance, an early study has shown that Dcr1 dependent small RNAs in *S. pombe* mapped to *dh* pericentromeric repeats (Reinhart and Bartel, 2002). Subsequent work done by high-throughput small RNA sequencing demonstrated that in addition to centromeres, RITS-bound small RNAs are generated from rRNAs, tRNAs and mRNAs, although the majority (about 55%) map to repeat regions (Bühler et al., 2008). Small RNAs derived from the *dh/dg* repeats constitute most of the small RNAs in *S. pombe*, and these small RNAs map to both forward and reverse strands, and are 21-24 nt in length (Bühler et al., 2008; Cam et al., 2005; Halic and Moazed, 2010). Interestingly, Ago1-associated small RNAs show a strong 5' uridine (U) bias. This bias has been proposed to be largely due to the preferential loading of small RNAs that begins with U onto the RITS complex, and, to a lesser extent, favored cleavage before a uracil in the dsRNA precursor by Dcr1 (Bühler et al., 2008).

Closer examination of these repeat-associated small RNAs show that 85% of them mapped to pericentromeric regions, while the remaining 15% mapped to the subtelomeres and the mating-type locus, all of which are heterochromatic. A smaller portion of the small RNAs mapped to the pericentromeric heterochromatin are derived from IRC (Inverted Repeats, Centromere) regions, which are located just beyond the heterochromatin and euchromatin boundary (Bühler et al., 2008; Cam et al., 2005) (Figure 1.1). Several tRNA clusters flank the pericentromeric heterochromatin and serve as barrier elements in *S. pombe* to prevent heterochromatin spreading into euchromatin

and the central core (Scott et al., 2006; 2007). However, tRNA genes are absent from the right side of centromere 1 (IRC1-R), and research focused on how heterochromatin is restricted at this location lead to the discovery of a special class of small RNAs, termed border RNAs (brdrRNAs). BrdrRNAs depend on Dcr1 for their biogenesis, but unlike canonical pericentromeric siRNAs, brdrRNAs rarely load onto Ago1 and are incapable of triggering H3K9 methylation (Keller et al., 2013). Instead, the brdrRNA precursor, BORDERLINE, has been proposed to prevent heterochromatin spreading into neighboring euchromatin by binding to Swi6 and evicting RNA-bound Swi6 from chromatin (Keller et al., 2012). However, the role of the brdrRNA themselves is unclear, as Dcr1 does not impact spreading in this region.

Deep sequencing of Ago1-associated small RNAs in RNAi mutants revealed a class of small RNAs that does not require Dcr1 or Rdp1 for their biogenesis. They appear to be degradation products of abundant transcripts (Halic and Moazed, 2010; Marasovic et al., 2013). Consistent with this idea, in cells lacking both Dcr1 and exosome subunit Rrp6, Dcr1-independent Ago1-associated small RNAs were increased by 10 fold. These small RNAs, termed primal RNAs (priRNAs), have been proposed to trigger the initial step of heterochromatin assembly, and are required for subsequent amplification of Dcr1-dependent small RNA biogenesis. RNA of size range from 23-27 nt associate with Ago1, and are further trimmed by 3'- 5' exonuclease Triman into 22-23 nt long priRNAs. priRNAs have a comparable size distribution and 5' nucleotide preference to Dcr1-dependent small RNAs and therefore might function in a similar way to establish H3K9 methylation (Halic and Moazed, 2010; Marasovic et al., 2013).

At the molecular level, small RNAs in *S. pombe* are 5' monophosphorylated and 3' hydroxylated (OH), consistent with Dcr1 product in other organisms. In *C. elegans*, however, the majority of the small RNAs are mostly 5' triphosphorylated secondary small RNAs generated by RdRP (Pak and Fire, 2007; Sijen et al., 2007). Duplex small RNAs produced by Dcr1 show a signature 2 nt 3'-OH overhang, which is generated by the staggered positions of RNase III domains around the dsRNA groove (Bernstein et al., 2001; Elbashir et al., 2001; Lee et al., 2003; Ma et al., 2004; Provost et al., 2002a; Zhang et al., 2002; 2004). The signature 2 nt overhang is required for additional small RNA modification by HEN1 in plants. *HEN1* encodes a 2'-O-methyltransferase that

specifically deposits a methyl group onto the 2'OH of the 3' terminal ribonucleotide of 21-24 nt small RNAs (Yang et al., 2006). This small RNA modification prevents 3' end uridylation and truncation that lead to small RNA degradation (Ji and Chen, 2012). *HEN1* is conserved across many species, including *S. pombe* (systemic ID SPBC336.05c), but whether or not small RNAs are indeed methylated in *S. pombe* remains to be determined.

A conserved 3'-5' exoribonuclease, Eri1, which was originally identified in *C. elegans* by its function in negatively regulating RNAi machinery, has also been shown to mediate small RNA stability in *S. pombe* (Iida et al., 2006; Kennedy et al., 2004). Eri1 specifically degrades dsRNA or RNA-DNA hybrids. High levels of pericentromeric small RNAs have been shown to accumulate in *eri1Δ* mutant cells, concomitant with increased transgene silencing and decreased *dh* transcripts. In agreement with Eri1 degrading small RNAs produced by RNAi, this enhanced silencing is RNAi dependent. Interestingly, although *eri1Δ* mutant cells grew normally in non-selective medium, the overexpression of Eri1 caused severe growth defects, possibly due to non-specific degradation of RNA substrates (Bühler et al., 2007; Iida et al., 2006).

1.8 The RNA processing machinery in heterochromatin assembly

In addition to components in the RNAi machinery, other RNA processing factors have been shown to affect heterochromatic silencing, including splicing factors, polyadenylation components and exosome subunits.

In *S. pombe*, mRNA-type introns have been identified in both *dh* and *dg* pericentromeric repeats by their conserved splice site sequences. At least in *dg* repeats, this mRNA-type intron is indeed spliced albeit at low levels (Chinen et al., 2010). Interestingly, several splicing factors are required for efficient pericentromeric silencing, including *prp5*, *prp8*, *prp10*, *prp12*, *prp13*, *prp39* and *cwf10*. Splicing factor mutants show defects in siRNA biogenesis and fail to establish silencing in both endogenous pericentromeric repeats and integrated reporter genes (Bayne et al., 2008; Chinen et al., 2010). However, heterochromatin structure, marked by H3K9 dimethylation (H3K9me2) and Swi6 binding, is only modestly disrupted in splicing mutants. Similar to RNAi mutants, Prp10 and Cwf10 do not affect silencing at the mating-type locus. Prp10 and Cwf10, along with Prp5 and Prp12, directly interact with RDRC complex component

Cid12, thus providing a direct link with the RNAi machinery. Furthermore, silencing is alleviated when the RITS component Tas3 is artificially tethered to *ura4* transcripts in *cwf10-1* mutant cells, suggesting that Cwf10 functions downstream of RITS recruitment and might be involved in amplification of the siRNA signal (Bayne et al., 2008). Interestingly, silencing and splicing defects observed in these mutants can be uncoupled, as silencing defects can be observed under permissive temperature where splicing was not affected. In addition, *dg* transcripts are still spliced in *prp13-1* mutant cells in which silencing is compromised. This has lead to the idea that specific splicing factors nucleate at pericentromeric non-coding RNAs to facilitate RDRC complex recruitment for robust siRNA amplification and efficient silencing (Bayne et al., 2008; Chinen et al., 2010).

In addition to splicing, proper gene expression requires mRNA 3' end polyadenylation (poly-A) in eukaryotes by canonical poly-A polymerase. The pericentromeric transcripts are polyadenylated, and the 3' end of siRNAs derived from this region contains mismatches enriched with A, U and C at the last 2 nucleotides, suggesting they are targeted by nucleotidyltransferases (Halic and Moazed, 2010; Win et al., 2006b). The genome of the fission yeast *S. pombe* encodes six non-canonical poly-A polymerases, and two members of this family, Cid12 and Cid14, are nuclear proteins which have been shown to be involved in heterochromatic silencing, and that their polyadenylation activities are required. The other four members in this family, Cid1, Cid11, Cid13 and Cid16, are all cytoplasmic proteins and are not needed for heterochromatin silencing (Saitoh et al., 2002; Wang et al., 2008).

Cid12, along with Rdp1 and Hrr1, constitute the RDRC complex (Colmenares et al., 2007; Motamedi et al., 2004; Sugiyama et al., 2005). Consistent with its role in the RNAi machinery, *cid12* has no apparent *S. cerevisiae* ortholog (Goffeau et al., 1996; Wood et al., 2002). In *S. pombe* cells lacking Cid12, siRNA biogenesis is severely impaired, although to a lesser extend than *rdp1Δ* mutant cells (Halic and Moazed, 2010; Motamedi et al., 2004). Furthermore, overexpression of Rdp1 in *cid12Δ* mutant cells can restore functional *dh/dg* siRNAs to a wild type level; however, siRNAs corresponding to the IRC elements are not restored. It has been demonstrated that Cid12 assembly into the RDRC complex stimulated its adenylation activity, but Cid12 appeared to target the single stranded RNA template rather than the synthesized second strand since the

catalytic activity of Rdp1 was not required for Cid12 mediated adenylation. Instead of polyadenylating the substrate, Cid12 only adds a single A nucleotide, probably remains bound to the RNA and marks the RNA for Rdp1 targeting (Halic and Moazed, 2010).

In the *cid12Δ* mutant cells, pericentromeric transcripts are still polyadenylated, suggesting that at least one other poly-A polymerase is involved for pericentromeric RNA polyadenylation (Win et al., 2006b). Another non-canonical poly-A polymerase, Cid14, mediates silencing at all major heterochromatin blocks, and is essential for robust siRNA levels in the cell (Bühler et al., 2007; Wang et al., 2008). Unlike Cid12, Cid14 is capable of adding up to 25 adenines to its RNA substrate in vitro, and does not need to be associated in a complex for its activity (Bühler et al., 2007). Cid14 has two *S. cerevisiae* orthologs, Trf4 and Trf5, both of which form a complex with Air1 and Mtr4, termed TRAMP4 (Trf4-Air1-Mtr4 polyadenylation) and TRAMP5 (Trf5-Air1-Mtr4 polyadenylation), respectively (Houseley et al., 2006; LaCava et al., 2005; Vanácová et al., 2005; Wyers et al., 2005). In *S. cerevisiae*, these complexes polyadenylate RNA substrates and stimulate exosome activity (Mitchell et al., 1997). Exosome is a highly conserved protein complex that serves as a major part of the RNA surveillance pathway to process and/or degrade RNA produced by the three major RNA polymerases. In *S. pombe*, Cid14 associates with Air1 and Mtr4, thus forming a TRAMP-like complex, termed spTRAMP, which possesses a similar function to degrade heterochromatic transcripts (Bühler et al., 2007; Keller et al., 2010; Wang et al., 2008; Win et al., 2006a). Paradoxically, the additional deletion of *cid14* in *ago1Δ* mutant cells restores pericentromeric heterochromatin (Reyes-Turcu et al., 2011).

In agreement with the idea that the spTRAMP complex mediates heterochromatic transcript degradation by the exosome, pericentromeric transcripts accumulate in exosome mutant cells. The eukaryotic exosome contains a catalytically inactive core that creates a channel-like structure, and it's binding with ribonuclease Dis3 gives rise to a fully functional exosome. In the nucleus, this exosome complex can further associate with Rrp6, the nonessential 3′-5′ exoribonuclease that is strictly nuclear (Houseley et al., 2006).

A point mutation in the catalytic module of *dis3* (Dis3-P509L) reduces its ribonuclease activity and alleviates heterochromatic silencing at pericentromeric repeats,

mating-type region and subtelomeres. Swi6 binding to the pericentromere in this mutant is reduced, but siRNA biogenesis and loading onto RITS are not affected (Murakami et al., 2007; Wang et al., 2008). Similarly, H3K9me2 levels are decreased in cells lacking Rrp6, but siRNA biogenesis remains unaffected. More pericentromeric transcripts accumulate and H3K9me2 levels are further reduced in *rrp6Δago1Δ* double mutant cells, suggesting that the exosome pathway functions in parallel with RNAi machinery to silence heterochromatin (Bühler et al., 2007; Reyes-Turcu et al., 2011). These results suggest that exosome machinery is not required for siRNA biogenesis and can trigger H3K9 methylation independently of RNAi. In cells lacking Rrp6, the RNAi machinery promotes siRNA production and H3K9 methylation at Tf2 retrotransposable elements that are normally silenced by Rrp6, suggesting that RNAi and Rrp6 compete for the same RNA substrates (Yamanaka et al., 2013). The precise mechanism of exosome-mediated heterochromatic silencing is still not well understood.

Intriguingly, the spTRAMP complex interacts with RNA exporting factor Mlo3, which also associates with Clr4, Rik1, Chp1 and pericentromeric transcripts, and is a substrate of Clr4 methyltransferase activity. Mlo3 and its ability to be methylated by Clr4 are necessary for the robust siRNA production (Zhang et al., 2011). However, despite endogenous pericentromeric transcript accumulation and the severe siRNA reduction, *mlo3* mutant cells have no defect in H3K9me2 and transgene silencing at the pericentromeric heterochromatin. Furthermore, the additional deletion of *mlo3* in RNAi mutant cells restores the functional pericentromeric heterochromatin without rescuing the siRNA biogenesis defect, but this rescue is still depended on Clr4 (Reyes-Turcu et al., 2011).

1.9 The role of histone deacetylase in heterochromatin silencing

Histones and their post-translational modifications mediate heterochromatin assembly in eukaryotes. Heterochromatin is characterized by both H3K9 methylation (Cam et al., 2005; Rice and Allis, 2001) and histone H3 and H4 hypoacetylation (Ekwall et al., 1997; Jeppesen and Turner, 1993; Jeppesen et al., 1992; Turner, 1991). While Clr4 is likely to be the sole H3K9 methyltransferase in *S. pombe*, several histone deacetylases (HDAC) facilitate heterochromatin assembly by histone deacetylation and nucleosome

repositioning, both of which limit Pol II access to chromatin. Unlike RNAi machinery, which has a dominant role at centromeric heterochromatin, HDACs are required for heterochromatin assembly at all three major heterochromatin regions, and HDAC mediated heterochromatin silencing is conserved in the budding yeast *S. cerevisiae*.

Clr3 is homologous to the mammalian class II HDACs and specifically deacetylates acetylated histone H3 lysine 14 (H3K14ac) (Bjerling et al., 2002). Clr3 associates with Clr1, Clr2 and Mit1 to form SHREC (Snf2/Hdac-containing REpressor Complex) that is present at all three heterochromatin regions. Different, yet in some cases overlapping, DNA-binding factors mediate SHREC recruitment to different regions. Swi6 and Chp2 bridge SHREC recruitment at the pericentromeric repeats. Swi6 and Chp2, together with Atf1/Pcr1, are responsible for SHREC associating with the mating-type locus. At the telomeric heterochromatin, Taz1/Ccq1 mediates SHREC localization (Motamedi et al., 2008; Sugiyama et al., 2007; Yamada et al., 2005). Although not required for SHREC recruitment to the nucleation site at the mating-type locus, HDAC activity is essential for SHREC spreading across the mating-type region and subsequent silencing of the region (Yamada et al., 2005). Clr3 functions in parallel with RNAi machinery to establish silencing and H3K9 methylation at the mating-type locus and pericentromeric region (Jia et al., 2004; Yamada et al., 2005). Consistent with its RNAi independent function, in the absence of an intact SHREC complex, heterochromatin silencing is compromised without impairing siRNA biogenesis. In fact, the combination of intact RNAi machinery and impaired heterochromatin silencing in SHREC mutant cells causes elevated levels of pericentromeric siRNAs (Motamedi et al., 2008; Sugiyama et al., 2007). Additionally, Clr3 also contributes to silent heterochromatin assembly partly by the elimination of the nucleosome free region (NFR) found within the repeats, therefore inhibiting Pol II engagement (Garcia et al., 2010; Yamane et al., 2011).

Clr6 is a class I HDAC and was originally identified by its ability to silence mating-type locus transcripts. In *clr6* mutant cells, pericentromeric transgene silencing was partially alleviated, and this silencing was further impaired in combination with *clr3* deletion (Grewal et al., 1998; Nicolas et al., 2007). In contrast to Clr3, Clr6 is essential for cell viability and is capable of deacetylating a broad set of substrates, including histones H3 and H4, which are acetylated at different lysines (Bjerling et al., 2002). Clr6

exists in two functionally distinct complexes that show different preferences in target sites (Nicolas et al., 2007). Interestingly, although both the *clr3* and *clr6* single mutants do not impair siRNA biogenesis alone, the combinatorial effect of the *clr3Δclr6-1* mutant cells abolished siRNAs derived from *dh/dg* repeats (Zaratiegui, unpublished), in agreement with their synergistic effect in pericentromeric transcript accumulation (Hansen et al., 2005).

Sir2 is a conserved class III HDAC that shows strong deacetylation activity towards acetylated H3K4, H3K9, H3K14 and H4K16 histone tails. Sir2 mediates heterochromatin silencing at all three major heterochromatin blocks (Alper et al., 2013; Freeman-Cook et al., 2005; Shankaranarayana et al., 2003). The catalytic activity of Sir2 is essential for silencing at the telomeres, as *tlh* transcripts accumulate and H3K9ac levels increase in Sir2 catalytic mutant (N247A) cells. Furthermore, H3K9me2 is lost in the Sir2 catalytic mutant cells, suggesting that Sir2 functions upstream of Clr4 and is needed for H3K9 methylation at telomeric heterochromatin. However, at pericentromeric regions, Sir2 functions redundantly with Clr3 to fully assemble silent heterochromatin, but is required for *de novo* H3K9me2, possibly by facilitating Clr4 recruitment. Like other HDACs, loss of Sir2 does not effect siRNA biogenesis, suggesting an RNAi independent role in heterochromatin assembly (Alper et al., 2013).

Interestingly, loss of H3K14 histone acetyltransferase (HAT) Mst2 bypasses the requirement of RNAi in pericentromeric heterochromatin maintenance but not establishment. Mst2 is the catalytic subunit of H3K14 HAT complex, and removing its activity, or certain other components from this complex, also bypasses the requirement for RNAi machinery. However, only RNAi machinery is dispensable in the *mst2* mutant background, as HP1, HDACs and the components in CLRC and SHREC are still required for pericentromeric silencing (Reddy et al., 2011).

1.10 Summary of dissertation

In *S. pombe*, it is well established that the RNAi machinery processes precursor transcripts into siRNAs to trigger pericentromeric heterochromatin assembly. Pericentromeric siRNA biogenesis correlates with efficient silencing and H3K9 methylation at the endogenous *dh/dg* repeats flanking *S. pombe* centromeres in most

mutants described so far. In addition, enzymatic activities of RNAi components are required for pericentromeric H3K9 methylation, further supporting the direct role of siRNAs in heterochromatin assembly (Sugiyama et al., 2005; Irvine et al., 2006; Colmenares et al., 2007).

However, artificial siRNAs introduced by a hairpin RNA fail to assemble H3K9 methylation in *trans* despite efficient siRNA production (Bühler et al., 2006; Iida et al., 2008). The ability of siRNAs to trigger H3K9 methylation in *trans* depends on the genomic location of their target sequences. Convergent transcription and proximity to the pre-existing H3K9 methylation site both facilitate *de novo* heterochromatin formation by artificial siRNAs (Iida et al., 2008). An inefficient poly-adenylation signal at the 3' end of the target sequence also promotes artificial siRNA triggered H3K9 methylation in *trans* (Yu et al., 2014). Furthermore, reporter transgenes integrated into pericentromeric repeats generate much less siRNAs than the repeats themselves, and yet are far more dependent on Ago1 and Dcr1 for H3K9 methylation (Irvine et al., 2006; Volpe et al., 2002). The over-expression of a catalytically dead Dcr1 in *rdp1Δ* mutant cells results in a partial rescue of the H3K9 methylation defect (Yu et al., 2014), and catalytically inactive Ago1 is still recruited to heterochromatin despite the loss of siRNAs and the loss of reporter gene silencing (Irvine et al., 2006).

These results suggest that, in addition to siRNA biogenesis, the RNAi machinery contributes to heterochromatin assembly in a way that is not yet understood. During my studies, I was interested in identifying novel components involved in the RNAi machinery. Taking advantage of the observation that *S. cerevisiae* has lost all the RNAi components (Aravind et al., 2000; Nakayashiki et al., 2006), we hypothesized that any gene that is specific to *S. pombe*, with no apparent *S. cerevisiae* homologue and yet is conserved in other eukaryotes, could potentially be involved in the RNAi pathway, or have co-evolved with RNAi machinery to support its function.

Chapter II presents a detailed study of an RNA-binding protein Rct1 (RRM-containing Cyclophilin regulating Transcription), which is of one of the conserved genes that are specific to *S. pombe*. I show that Rct1 is essential for proper processing of pericentromeric transcripts into siRNAs, and that the RNA recognition motif is required for this process. In agreement with the defect in siRNA biogenesis, pericentromeric

silencing is impaired in *rct1Δ* mutant cells. I also demonstrate that *rct1* shares similar genetic interactions with RNAi factors, strongly supporting the idea that Rct1 functions in the RNAi machinery. Surprisingly, severely compromised siRNA biogenesis in *rct1* mutant cells had no effect on H3K9 methylation, suggesting siRNAs do not in themselves mediate heterochromatin assembly. Furthermore, the additional deletion of exosome catalytic subunit *rrp6* recues the silencing defect in *rct1Δ* mutant cells and also increases pericentromeric siRNA production. Together, my results suggest that Rct1 is not directly involved in the siRNA biogenesis, but rather acts upstream to direct transcripts to the RNAi pathway and away from the exosome. Finally, we provide evidence that Rct1 is a putative splicing factor, and propose that the fate of Pol II transcripts towards the RNAi machinery could be regulated though splicing efficiency.

In Chapter III, I present the candidate gene screen for novel components involved in the RNAi machinery based on the observation that *S. cerevisiae* has lost all the key RNAi components as compared to *S. pombe*. We composed a list of 538 *S. pombe* specific genes that are also conserved in other eukaryotes, including *rdp1*, *dcr1* and *ago1*. I screened 268 genes by RT-PCR to test pericentromeric transcript expression levels. In additional to several known RNAi or CLRC components, I identified a putative chromatin remodeler *ssr4* that is required for pericentromeric silencing. Further characterization demonstrated that siRNA biogenesis is partially impaired in *ssr4Δ* mutant cells, and this mutant is sensitive to UV. However, the detailed mechanism(s) related to Ssr4 function requires further study.

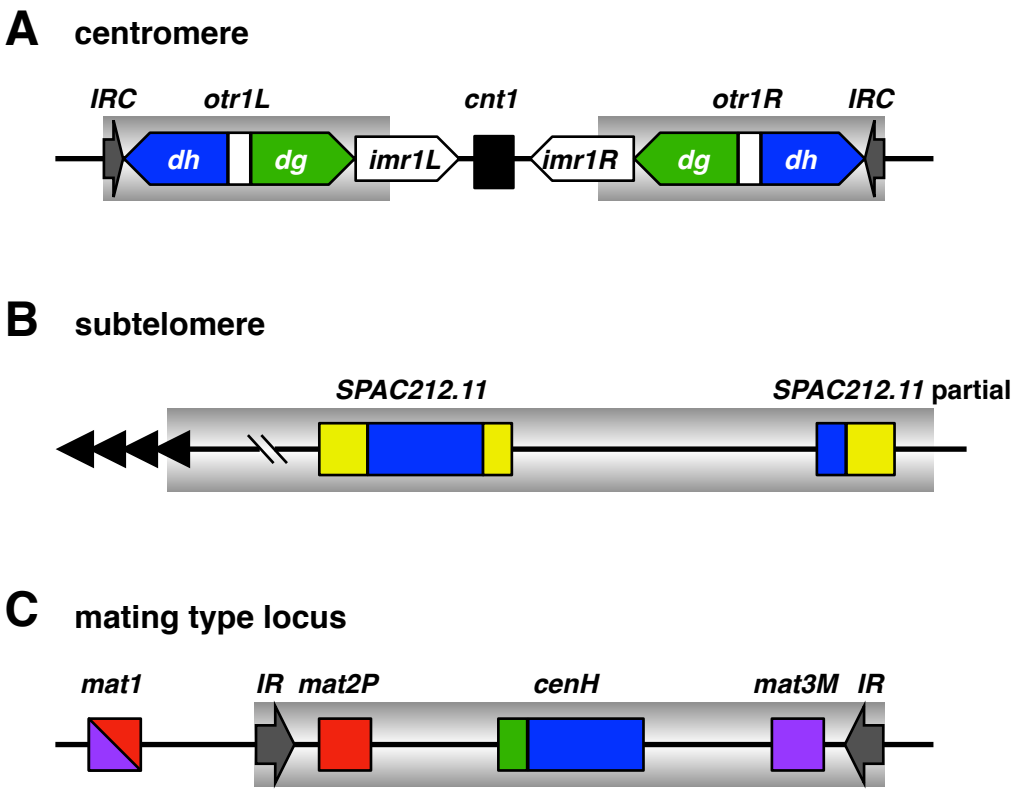

Figure 1.1 Heterochromatin in *S. pombe*

Schematic representation of constitutive heterochromatin regions in *S. pombe*. Silent heterochromatin regions are covered by grey box.
Sequences similar to pericentromeric repeats (*dh*, blue; *dg*, green) can be found at mating type locus and subtelomere regions.
(A) Centromere 1. Centromere core (*cnt*), the site of kinetochore formation, is flanked by inverted repeats *imr* (white) and *otr*. Otr consists of *dh* (blue) and *dg* (green) repeats, which the number and organiztion varies in different centromeres. Inverted repeats (*IR*, grey arrow) are located at euchromatin and heterochromatin boundary, and along with tRNA clusters, define the border between euchromatin and heterochromatin.
(B) Subtelomere of chromosome 1 left arm. Full length and a partial sequence of SPAC212.11 (yellow), a RecQ helicase gene, is located at the subtelomere heterochromatin. A centromere repeat-like sequence is embeded in SPAC212.11 coding sequnce. Telomere repeats are shown as black triangles.
(C) Mating type locus located at chromosome 2. *mat1* (red/purple) is transcriptionally active while *mat2P* (red) and *mat3M* (purple) resides in the 20 kb silent mating type region. *cenH* located in between *mat2P* and *mat3M* share sequence homology with centromere *dh/dg* repeats, and serves as heterochromatin nucleations site at the mating type locus.

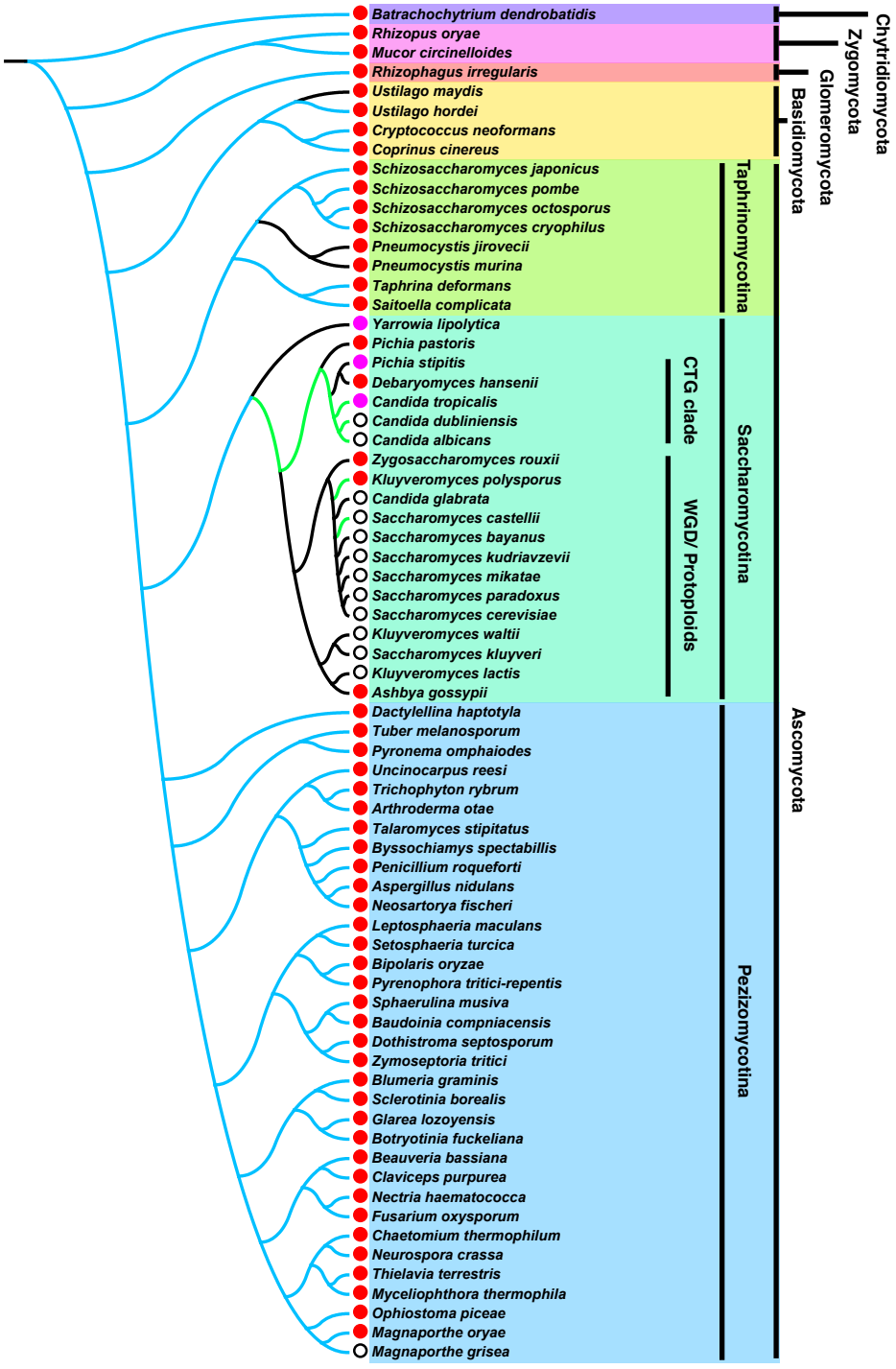

Figure 1.2 The distribution of RNAi machinery in the diverse fungi

rdp1, *dcr1*, *ago1* and *rct1* amino acid sequences from *S. pombe* were compared to assembled sequences from indicated species. Fungal species containing *rdp1*, *dcr1* and

ago1 are labeled in blue line. Species containing only *ago1* and non-canonical *dcr1* are labeled in green line. Species containing no RNAi genes or containing only non-canonical *dcr1* is labeled in black line. Red circles indicate species containing Rct1 protein. Purple circles indicate species containing Rct1-like protein. White circles indicate species with no obvious Rct1 protein based on protein sequences. This figure is generated with MEGA 6.0 (Tamura et al., 2013).

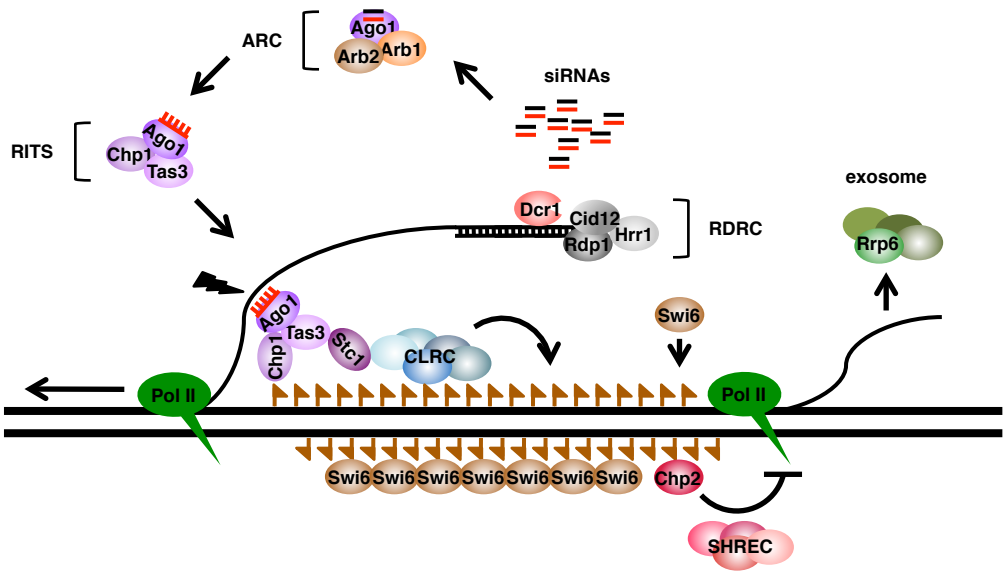

Figure 1.3 The pericentromeric heterochromatin assembly pathways in *S. pombe*

A summary of pericentromeric heterochromatin assembly pathways in *S. pombe*. In brief, Pol II transcribes pericentromeric repeats during S phase and generates the nascent transcript. RDRC complex recongnizes the nascent transcript and converts it into double stranded RNA (dsRNA) by the action of *rdp1*. Dcr1 further processes dsRNA into small interfering RNAs (siRNAs). siRNAs are first loaded into the ARC complex then passed on to the RITS complex, where the passenger strand is released. RITS complex is directed to the heterochromatin region by both siRNA base pairing and chromodomain protein Chp1 binding to methylated H3K9 (brown flag). The activity of Ago1 slices the nascent transcript leading to post-transcriptional silencing. Co-transcriptional silencing is achieved by Stc1 linking RITS and CLRC, which contains H3K9 methyltransferase Clr4. H3K9 are methylated by Clr4, and serves as binding site for heterochromatin protein Swi6 and Chp2. Chp2 recruits SHREC, which contains histone deacetylase Clr3, to inhibit Pol II transcription. In addition, the exosome machinery is targeted to the pericentromeric transcripts to ensure heterochromatin silencing.

Chapter II: The Conserved RNA Binding Protein, Rct1, Regulates Small RNA Biogenesis and Splicing Independent of Heterochromatin Assembly

2.1 Introduction

Budding yeast *S. cerevisiae* and fission yeast *S. pombe* are two well established model organisms, both of which have completely sequenced and assembled genomes (Goffeau et al., 1996; Wood et al., 2002). Interestingly, *S. cerevisiae* has lost all the key RNAi components as compared to *S. pombe* (Aravind et al., 2000; Nakayashiki et al., 2006). We hypothesized that any gene that is specific to *S. pombe*, with no apparent *S. cerevisiae* homologue and yet is conserved in other eukaryotes, could potentially be involved in the RNAi pathway, or have co-evolved with RNAi machinery to support its function. Therefore, we composed a list of *S. pombe* specific genes that are also conserved in other eukaryotes. This list contains 538 genes including *rdp1, hrr1, cid12*, *dcr1, chp1* and *ago1*.

We noticed one of the genes on this list is *rct1,* and previous studies in *C. elegans* had shown that the Rct1 homolog CYN-14 regulates transgene silencing (WG. Kelly, personal communication). Our collaborator in William Kelly's group used transgenic GFP reporter *C. elegans* strains, in combination with extrachromosomal arrays, to screen for new genes that are required for transgene silencing in *C. elegans*. They found that the cc629 mutant line lost the ability to silence repetitive GFP transgene. Characterization of the cc629 mutant line revealed that this mutant contains a single recessive allele of *cyn-14*. The *cyn-14* mutation introduced an early stop codon in this gene, which resulted in severely truncated *cyn-14* in cc629 mutant line. The same silencing defect was also observed in *cyn-14* RNAi knockdown animals. Additionally, *cyn-14* is required for embryo development and normal growth of *C. elegans* (Jeong Hyun Ahn, unpublished). CYN-14 belongs to a conserved protein family called cyclophilins, and proteins in this

family contain a PPIase (Prolyl-Peptidyl Isomerase) domain, the activity of which catalyzes proline peptide bond isomerization from *trans* to *cis* (Fischer et al., 1984).

In *S. pombe*, there are nine members of the cyclophilin family present in the genome, and all nine have homologs in *Homo sapiens* (*H. sapiens*), *Drosophila melanogaster* (*D. melanogaster*) and *Arabidopsis thaliana* (*A. thaliana*) (Aravind et al., 2000; Pemberton and Kay, 2005). The *cyn-14* homolog in *S. pombe* is *rct1*, and like its homolog in higher eukaryotes, Rct1 contains a Prolyl-Peptidyl Isomerase (PPIase) domain at the N-terminus, followed by a conserved RNA recognition motif (RRM) (Gullerova et al., 2007; Gullerova et al., 2006). The Rct1 homolog in *A. thaliana,* AtCyp59, binds to RNA *in vivo* and *in vitro*, with higher affinity towards GC rich sequences (Gullerova et al., 2006). In a human embryonic kidney cell lines, the Rct1 homolog PPIL4 interacts with polyadenylated transcripts (Baltz et al., 2012). Interestingly, AtCyp59 binding to RNA molecules negatively regulates its PPIase activity (Bannikova et al., 2013). In *S. pombe*, Rct1 has five of its six conserved isomerase catalytic sites substituted by other amino acids, and PPIase activity has never been demonstrated (Pemberton and Kay, 2005). Rct1 associates with Pol II in both *S. pombe* and *A. thaliana*, and negatively regulates Pol II C-terminal domain (CTD) phosphorylation . In addition, Rct1 inhibits meiotic gene splicing during vegetative cell growth, possibly through interaction with SR proteins or the transcript itself (Gullerova et al., 2007; Gullerova et al., 2007). It has been shown that recombinant GST-Cyp59 interacts with several SR proteins *in vitro* and this interaction is not mediated by RNA molecules (Gullerova et al., 2006).

Rct1 appears to be closely linked to the Pol II transcription machinery, which transcribes both protein-coding genes and non-coding RNAs. By blasting Rct1 amino acid sequences to a wide range of fungal species, the existence of Rct1 strongly correlates with the presence of RNAi in other fungi (See Chapter I Figure 1.2). Here I present evidence that in *S. pombe*, Rct1 is involved in RNAi and is essential for robust siRNA biogenesis. In cells lacking Rct1, pericentromeric heterochromatin silencing was derepressed, but H3K9 methylation was preserved. I show that the RRM of Rct1 is required for pericentromeric siRNA biogenesis, while the PPIase domain and the C-terminal region are dispensible for this process. Although siRNA biogenesis was severely

compromised in *rct1Δ* mutant cells, the additional deletion of *rrp6* could rescue this defect and produce functional siRNAs. These results suggest that Rct1 is not directly involved in siRNA biogenesis, but rather acts upstream to direct transcripts to the RNAi pathway and away from the exosome. Finally, I show that Rct1 is needed for efficient RNA splicing, and propose a model linking splicing to transcript processing by the RNAi machinery.

2.2 Results

2.2.1 Rct1 is not an essential gene

Pol II transcribes both protein-coding genes and non-coding RNAs, but these two types of transcripts are recognized differently and directed to different downstream RNA processing pathways in the cell. The mechanism to distinguish these transcripts is not well understood. Pol II is hyper-phosphorylated in *rct1*$^{+/-}$ mutant cells (Gullerova et al., 2007), and to test if transcribing by different Pol II isoforms contributes to this distinction, I generated *rct1*$^{+/-}$ heterozygous diploid mutant cells. These *rct1*$^{+/-}$ mutant cells grew normally with no obvious morphological phenotypes, and consistent with the previous study, Pol II is hyper-phosphorylated in these cells (Figure 2.1A). If transcription by different Pol II phosphorylation isoforms is needed to distinguish between coding and non-coding transcripts, in *rct1*$^{+/-}$ mutant cells, where Pol II phosphorylation is mis-regulated, pericentromeric transcripts will no longer be targeted to the RNAi pathway, resulting in pericentromeric transcript accumulation. To test this, I performed semi-quantitative RT-PCR to analyze *dh/dg* transcript levels in *rct1*$^{+/-}$ mutant cells, but no accumulation was detected (Figure 2.1B).

Rct1 was designated as an essential gene in *S. pombe* database (http://www.pombase.org/) based on a previous study (Gullerova et al., 2007). Surprisingly, I was able to obtain complete *rct1* deletion haploid mutants by tetrad dissecting the *rct1*$^{+/-}$ diploid mutant cells (Figure 2.2A). Although not essential, *rct1Δ* mutant cells showed severe growth retardation and morphological defects (Figures 2.2B and C). To confirm if Pol II was hyper-phosphorylated in *rct1Δ* mutant cells, I performed western blot with antibodies specific to different Pol II isoforms, including phosphorylated serine 2 (p-S2) and serine 5 (p-S5) among the heptad repeats (YSPTSPS). Intriguingly, I consistently observed a decrease in the total Pol II protein level in *rct1Δ* mutant cells, although the percentage of the phosphorylated Pol II increased slightly (Figures 2.3A and B). To rule out the possibly that this is due to the Pol II antibody (8WG16) recognition bias towards non-phosphorylated Pol II, I generated *rct1Δ* mutant cells in the background where the large subunit of Pol II, Rpb1, is tagged by

HA or GFP at its endogenous locus. Total cell lysate from *rct1Δrpb1-HA* mutant cells was subjected to western blot analysis, and Pol II protein levels were analyzed by antibody against HA. My result showed that Pol II protein levels were indeed reduced in *rct1Δ* mutant cells (Figure 2.4A). Furthermore, to test Pol II localization in the *rct1Δ* mutant cells, live *rct1Δrpb1-GFP* mutant cells stained by DAPI were observed under the microscope. In cells lacking Rct1, Pol II localized normally in the nucleus (Figure 2.4B).

2.2.2 Rct1 is essential for *dh* and *dg* derived siRNA biogenesis

Since *rct1Δ* mutant cells were viable, I tested to see if Rct1 is involved in RNAi directly by analyzing siRNA biogenesis in *rct1Δ* mutant cells. I performed small RNA northern blot to detect the siRNAs derived from *dh* and *dg* pericentromeric repeats. In wild type cells, both *dh* and *dg* derived siRNAs were easily detected, but in *rct1Δ* mutant cells siRNAs were barely detectable, similar to what has been observed in RNAi mutants, such as *rdp1Δ* mutant cells (Figure 2.5A). To quantify the extent of siRNA loss in *rct1Δ* mutant cells, I sequenced small RNAs from *rct1Δ, ago1Δ and dcr1Δ* mutant cells. In *rct1Δ* mutant cells, normalized siRNA reads mapped to *dh* and *dg* repeats were only about 1.3 % of the reads in wild type cells, similar to the RNAi mutants *ago1Δ* and *dcr1Δ,* which have less than 0.4%, when compared to wild type (Figure 2.5B). My results indicate that Rct1 is required for robust siRNA biogenesis.

2.2.3 Rct1 is required to establish heterochromatic silencing at the pericentromeric heterochromatin

Pericentromeric precursor transcripts are transcribed by Pol II, and Pol II protein level was reduced in *rct1Δ* mutant cells. To investigate if the loss of siRNAs was due to a defect in either precursor RNA transcription or their processing into siRNAs, I performed RNA sequencing (RNAseq) and semi-quantitative RT-PCR to analyze precursor transcript levels and their origins in *rct1Δ* mutant cells. Transcripts from endogenous *dh* and *dg* pericentromeric repeats are transcribed and accumulated in *rct1Δ* mutant cells, similar to cells lacking the RNAi and CLRC component (Figures 2.6, 2.7A, B and C). Furthermore, by RNAseq, I showed that pericentromeric transcripts accumulated at the same regions where wild type siRNAs were mapped (Figures 2.7A, B and C). These

results suggest a defect in the processing of repeat transcripts into siRNAs instead of impaired transcription in *rct1Δ* mutant cells. In addition, the *ura4* transgene inserted into the *dg* repeat was de-repressed in *rct1Δ* mutant cells (Figure 2.6) to a level comparable to that observed in the *rik1Δ* mutant cells.

Cells lacking RNAi components show no defect in silencing at the mating-type locus, unlike CLRC component mutants which affect all major heterochromatic regions (Kato et al., 2005; Volpe et al., 2002). To test if Rct1 had a specific role in pericentromeric silencing like the RNAi mutants, I generated *rct1Δ* mutant strains in the homothallic (*h90*) background. In wild type *h90* cells, mating-type switching yields an equal amount of P and M cells. Additionally, under nitrogen starvation condition, these P and M cells can mate efficiently and produced spores. However in CLRC mutants, *h90* cells fail to produce an equal number of P and M cells, as one of the mating types is always over represented, which results in reduced spore formation (Aguilar-Arnal et al., 2008; Ekwall and Ruusala, 1994). To test if Rct1 is needed for efficient mating-type switching, I tested the spore formation in *rct1Δ h90* mutant cells by staining with iodine vapors. Under nitrogen starvation, *rct1Δ h90* mutant cells can produce spores but very inefficiently (Figure 2.8A). I also amplified the *mat1P* and *mat1M* cassette by PCR with genomic DNA from *rct1Δ h90* mutant cells. This result showed that in *rct1Δ h90* mutant cells, equal numbers of cells carried *mat1P* and *mat1M* (Figure 2.8B). To further test the effect of the *rct1* deletion in mating type silencing, I performed semi-quantitative RT-PCR to analyze *cenH* transcripts, which are derived from the silent mating-type locus. My result showed that in *rct1Δ* mutant cells, silencing was maintained at the mating-type locus while *cenH* was clearly de-repressed in *clr4Δ* mutant cells (Figure 2.8C). Therefore, despite the high sequence homology between pericentromeric repeats and *cenH*, Rct1 was not required for silencing at the mating-type locus. The observed reduction in spore formation (sterility) was likely related to the slow growth phenotype from the *rct1* deletion.

2.2.4 Rct1 functions in parallel with Clr3 to silence pericentromeric heterochromatin

HDAC Clr3 is part of the SHREC complex that acts in parallel with the RNAi machinery to establish heterochromatic silencing (Sugiyama et al., 2007; Yamada et al., 2005). I generated *rct1Δclr3Δ* double mutant cells to test if, like RNAi, Rct1 also acts in parallel with Clr3. I performed RT-qPCR to quantify *dh* and *dg* repeat transcript expression levels, and the results showed that the pericentromeric silencing was further impaired in *rct1Δclr3Δ* double mutant cells as compared to each individual single mutant strain (Figure 2.9A). To test if Rct1 is indeed functioning in the RNAi pathway, I generated *rct1Δrdp1Δ, rct1Δdcr1Δ* and *rct1Δago1Δ* double mutant strains, and pericentromeric repeat expression levels were analyzed by RT-qPCR in these mutants. The additional deletion of RNAi genes in *rct1Δ* mutant cells did not further impair pericentromeric silencing, supporting the idea that Rct1 functions in the RNAi machinery to achieve silencing (Figure 2.9B).

In cells lacking Clr3, H3K14 acetylation is not efficiently removed, thus engaging active transcription in the presence of RNAi. As a result, pericentromeric siRNAs accumulate in *clr3Δ* mutant cells at a much higher level compared to wild type (Sugiyama et al., 2007). To test the combinational effect of siRNA biogenesis in cells lacking both Clr3 and Rct1, I performed small RNA northern blot to detect the siRNAs derived from *dh* and *dg* pericentromeric repeats in the *rct1Δclr3Δ* mutant cells. Consistent with previous studies, high levels of siRNAs accumulated in *clr3Δ* mutant cells and were barely detectable in cells lacking Rct1, Rdp1 and Rik1. In the *rct1Δclr3Δ* mutant cells, low levels of siRNA were detected from both *dh* and *dg* repeats (Figure 2.10). To quantify the level of siRNAs produced from *rct1Δclr3Δ* mutant cells, I performed small RNAseq in the double mutant along with each individual single mutant. My result showed that *cen* siRNA levels were increased more than 10-fold in *rct1Δclr3Δ* double mutant cells when compared to *rct1Δ* single mutant cells (Figure 2.11A). Consistent with previous studies, my small RNAseq data showed 1.6-fold increase in *cen* siRNAs in cells lacking Clr3 over wild type (Figure 2.11A). These pericentromeric siRNAs in *rct1Δclr3Δ* double mutant cells were further confirmed to be produced by the

RNAi machinery, based on the 5' U bias analysis and size distribution (Figures 2.11B and 2.11C).

However, these siRNA reads mapped to a more confined region of the repeats as compared to wild type cells (Figure 2.12A, B and C). Additionally, in *rct1Δclr3Δ* double mutant cells, the elevated *cen* siRNA reads mapped exactly to the same regions as siRNAs in *clr3Δ* single mutant cells, suggesting an additive effect in siRNA production in the double mutant (Figure 2.12). Surprisingly, siRNAs originating from the IRC boundary elements, just outside of the pericentromeric repeats, were completely absent in *clr3Δ* mutant cells (Figure 2.12). This reveals a previously unidentified role of Clr3 in siRNA biogenesis.

2.2.5 *mlo3* suppresses pericentromeric silencing defect in *rct1Δ* mutant cells independent of siRNA biogenesis

Deletion of RNA exporting factor *mlo3* can restore silencing at pericentromeric heterochromatin in cells lacking RNAi factors, but this process still depends on CLRC components (Reyes-Turcu et al., 2011). To further confirm if Rct1 is involved in RNAi machinery and not CLRC, I generated *rct1Δmlo3Δ* double mutant cells to test if *mlo3* deletion could rescue the pericentromeric silencing defect in *rct1Δ* mutant cells. RT-qPCR showed that the pericentromeric transcripts were efficiently silenced in the *rct1Δmlo3Δ* double mutants cells (Figure 2.13A), indicating that silencing was restored. These results suggest that Rct1 is involved in the RNAi pathway instead of the CLRC or HDAC pathway.

Mlo3 is needed for siRNA biogenesis but is dispensable to maintain H3K9 methylation. It is not yet clear how the deletion of *mlo3* restores silencing without rescuing the siRNA biogenesis defect in RNAi mutants (Reyes-Turcu et al., 2011). To test the siRNA levels in *rct1Δmlo3Δ* double mutants cells, I performed small RNAseq. My result showed that the additional deletion of *mlo3* in *rct1Δ* mutant cells had limited effect on siRNA levels (Figure 2.13B). This is in agreement with the previous study that while deleting *mlo3* restores H3K9 methylation and silencing in RNAi mutants, siRNA levels were not restored (Reyes-Turcu et al., 2011).

2.2.6 Differential *dh* and *dg* repeat region regulation by Rct1

Pericentromeric *dh* and *dg* repeat transcripts accumulated at a similar level in RNAi mutants, whilst *dh* repeat transcript levels were two times higher than *dg* in *rct1Δ* mutant cells (Figure 2.14A). This result indicates that Rct1 regulates endogenous *dh* and *dg* repeats differently. To further test this observation, I generated *rct1Δ* mutant cells in which the *ura4* transgene is inserted at either *dh* or *dg* repeats of the *otr1*, and is transcribed from different orientations (Figure 2.14B). Spot assays on –Ura plates and 5-FOA (5-Fluoroorotic acid) plates were performed to quantify the repression level of the *ura4* transgene at different insertion sites. My results demonstrated that the *ura4* transgene is more efficiently silenced when placed in the *dg* repeats in *rct1Δ* mutant cells, and transgene orientation had limited effect on the silencing intensity (Figure 2.14C). This is in agreement with the observation that in cells lacking Rct1, *dh* pericentromeric transcripts were de-repressed at a higher level when compared to *dg* (Figure 2.14A). However, I observed the same bias in wild type cells in which *ura4* transgene is more robustly silenced when placed in *dg* repeats (Figure 2.14C and Allshire et al., 1995).

2.2.7 The RNA recognition motif of Rct1 is essential for siRNA biogenesis and pericentromeric heterochromatin silencing

To understand how Rct1 is involved in processing heterochromatic transcripts into siRNAs, I mutated specific domains of Rct1 at its endogenous locus. Rct1 is a 51 kDa protein which contains 432 amino acids. It has a PPIase domain at the N-terminus followed by a conserved RRM, with a less conserved C-terminus region enriched in charged amino acids (Gullerova et al., 2007). *rct1ΔIso* mutant cells lacked the first 175 amino acid, which completely deleted the PPIase domain. *rct1-rrm* mutant cells carried two amino acid mutations (Y287D and F289D) at the endogenous *rct1* locus, both of which combined were predicted to abolish the RNA-binding ability of Rct1 (Merrill et al., 1988). In *rct1ΔC* mutant cells, amino acids 333-428 were removed (Figure 2.15A).

I analyzed pericentromeric siRNA levels in these mutants by small RNA northern blot. The result showed that while deleting the *rct1* PPIase domain or the C-terminal tail had no significant effect on *dh* and *dg* derived siRNAs, siRNAs were completely lost in *rct1-rrm* mutant cells (Figure 2.15B). By semi-quantitative RT-PCR, I showed that

pericentromeric *dh* and *dg* transcripts accumulated only in *rct1-rrm* but not in *rct1ΔIso* or *rct1ΔC* mutant cells, as expected from the loss of siRNAs (Figure 2.15C). This result was further confirmed by RT-qPCR (Figure 2.15D). My data suggest that the RRM of *rct1* is required for siRNA biogenesis and heterochromatin silencing.

Additionally, while deleting the *rct1* PPIase domain or the C-terminal tail had no significant effect on cell growth or morphology (Figures 2.16A, 2.16B and 2.17), mutations in *rct1* RRM resulted in severe growth defect and abnormal cell morphology, similar to *rct1Δ* mutant cells (Figures 2.16A, 2.16B and 2.18). Previously, I observed the moderate reduction of Pol II protein levels in *rct1Δ* mutant cells, and this phenotype was also present in *rct1-rrm* mutant cells as shown by western blots (Figure 2.19). These results indicate that the function of Rct1 in RNAi-mediated silencing is largely dependent on its RNA-binding ability.

To confirm these domain specific mutations did not change the Rct1 expression level, I performed RT-qPCR to analyze *rct1* transcript levels in domain-specific *rct1* mutant cells. The *rct1* RNA levels were comparable between mutants and wild type (Figure 2.20). Due to the lack of antibody against Rct1, I generated C-terminal HA-tagged domain-specific *rct1* mutant cells to analyze the mutant protein levels. Adding the HA-tag did not affect the function of Rct1, since the HA-tagged version displayed the same morphological and growth phenotype when compared to the non-tagged version (Figure 2.21A and data not shown). Western blot using an antibody against HA was performed to detect the Rct1 protein levels in these HA-tagged *rct1* mutant cells. While deleting the *rct1* C-terminal tail did not alter Rct1 protein level, it was reduced in *rct1ΔIso* and barely detectable in *rct1-rrm* mutant cells (Figure 2.21B). The observation that *rct1ΔIso* mutant cells grew normally and had no obvious phenotype suggests that low level of Rct1 protein is enough to support its function. Surprisingly, two amino acid mutations at the RRM of Rct1 resulted in dramatic decrease in mutant protein level. These mutations could cause incorrect protein folding thereby leading to protein degradation, or that Rct1 is an unstable protein by itself, and is only stabilized by binding to RNAs.

2.2.8 H3K9 methylation is retained in *rct1* mutants

Based on the current RNAi-mediated heterochromatin assembly model, RITS complex loaded with siRNAs is required to guide the CLRC silencing complex to specific genomic locations in order to establish histone H3K9 methylation. Dimethylated H3K9 (H3K9me2) is the most prevalent H3K9 methylation state in *S. pombe* (Al-Sady et al., 2013). I performed H3K9me2 chromatin immunoprecipitation sequencing (ChIPseq) to test if severely compromised siRNA biogenesis in *rct1Δ* mutant cells could impair H3K9me2 as in cells lacking RNAi components. H3K9me2 was enriched at the pericentromeric region at all three centromeres in wild type cells as expected (Figure 2.22A, B and C). Surprisingly, *rct1Δ* mutant cells retained normal levels of H3K9me2 across the pericentromeric regions for all three centromeres (Figure 2.22A, B and C). Quantitative analysis of enrichment at endogenous *dh* and *dg* repeats demonstrated that deleting Rct1 had no effect on H3K9me2 (Figure 2.23A), while siRNAs generated from these repeats could not be detected (Figure 2.5A). Compared to endogenous repeats, the H3K9me2 at the *otr1R*::*ura4* transgene insertion site is more sensitive to the loss of RNAi components (Irvine et al., 2006; Sadaie et al., 2004). However, I detected no difference in H3K9me2 levels between wild type and *rct1Δ* mutant cells at the *ura4* transgene insertion region (Figure 2.23B), despite the transgene silencing being partially derepressed in the mutant (Figure 2.6).

The chromodomain of Clr4 preferentially binds to trimethylated H3K9 (H3K9me3), the terminal methylation state (Al-Sady et al., 2013). I performed H3K9me3 ChIPseq experiment to test if H3K9 methylation was blocked at a later stage in the *rct1Δ* mutant cells. In wild type cells, H3K9me3 was enriched at the pericentromeric regions, although to a lesser extent than H3K9me2 (compare Figure 2.22 and 2.24), in agreement with H3K9me2 being the main H3K9 methylation state (Al-Sady et al., 2013). In the *rct1Δ* mutant cells, pericentromeric H3K9me3 levels were similar to wild type cells, and no differences were observed at either endogenous *dh* and *dg* repeats (Figure 2.25A) or *otr1R*::*ura4* transgene insertion (Figure 2.25B) by quantitative analysis. H3K9 methylation serves as binding site for heterochromatin protein Swi6 in *S. pombe*. To test if Swi6 can be efficiently recruited to pericentromeric regions in the *rct1Δ* mutant cells, I

performed Swi6 ChIP PCR. My result showed that Swi6 associated with the *dh/dg* repeats and *otr1R*::*ura4* transgene in the *rct1Δ* mutant cells at a level comparable to wild type, consistent with the normal H3K9 methylation levels (Figure 2.26).

I demonstrated previously that Rct1 RRM was essential for the function of Rct1 in processing precursor transcripts into siRNAs, although it remains possible that this is due to a reduced Rct1 protein level in the *rct1-rrm* mutant cells. To test if H3K9 methylation was also retained in *rct1-rrm* mutant cells as observed in the *rct1Δ* strain, I performed H3K9me2 and H3K9me3 ChIPseq experiments in *rct1-rrm* mutant cells (Figures 2.22 and 2.24). As expected from the previous results, the two point mutations in Rct1 RRM did not affect H3K9 di- or trimethylation at endogenous *dh* and *dg* repeats (Figures 2.23A and 2.25A) or *otr1R*::*ura4* transgene (Figures 2.23B and 2.25B). These observations distinguish Rct1 from other RNAi components and suggest that siRNAs do not in themselves mediate heterochromatin assembly.

2.2.9 Pol II accumulates at pericentromeric heterochromatin in *rct1Δ* mutant cells but not in *rct1-rrm* mutant cells

Spreading of H3K9 methylation from heterochromatic repeats into embedded reporter transgenes requires the coupling of Clr4 with the leading strand DNA Pol ε (Li et al., 2011; Zaratiegui et al., 2011). During S phase, when the replication machinery encounters Pol II, the failure to remove Pol II at pericentromeric repeats in *dcr1Δ* mutant cells interferes with fork progression. This results in the loss of H3K9 methylation due to fork restart by homologous recombination (Zaratiegui et al., 2011).

To test if Pol II was efficiently removed from pericentromeric repeats in *rct1* mutant cells in order to allow replication-coupled H3K9 methylation by Clr4, I performed Pol II ChIPseq. Our results showed that Pol II accumulated in *rct1Δ* mutant cells at similar regions observed in other RNAi mutants, but this accumulation extended into the neighboring repeats (Figure 2.27A, B and C). However, *rct1-rrm* mutant cells had only a very limited effect on Pol II accumulation at the pericentromere repeats (Figure 2.27A, B and C). Similar results were observed with p-S2 and p-S5 phospho-isoform Pol II accumulation (Figures 2.28 and 2.29). In RNAi mutants, Pol II accumulates within siRNA clusters (Zaratiegui et al., 2011). Quantification of Pol II

enrichment within these clusters revealed accumulation in *rct1Δ* mutant cells but not in *rct1-rrm* mutant cells (Figure 2.30). In *rct1-rrm* mutant cells, H3K9 methylation was preserved with no Pol II accumulation at pericentromeric regions, indicating Pol II could be released to allow replication-coupled H3K9 methylation spreading in the absence of siRNAs. The Pol II accumulation in *rct1Δ* mutant cells suggests that Rct1 was required for Pol II release at the pericentromeric repeats. However, another domain of Rct1, other than RRM, may be responsible to promote the Pol II release.

2.2.10 Rct1 does not bind to siRNA nor mediate siRNA stability

Pericentromeric siRNAs were lost without affecting heterochromatin assembly in *rct1Δ* mutant cells, suggesting Rct1 could be involved in post-transcriptional gene silencing instead of co-transcriptional gene silencing. One idea was that Rct1 directly binds to siRNAs and mediates siRNA stability. Therefore, in cells lacking either Rct1 or its RNA binding ability, siRNA level is reduced. I tested this idea by two different approaches, one to see if Rct1 binds to siRNAs, the other to test if deleting Eri, an exonuclease that degrades siRNA (Iida et al., 2006), can bypass the requirement of Rct1 in pericentromeric silencing.

To test if Rct1 binds to siRNAs, I generated an Rct1-HA strain and performed RNA-immunoprecipitation (RIP) with HA antibody. I did not detect significant enrichment of siRNAs after immunoprecipitation by HA antibody in Rct1-HA cells, while the control HA-Ago1 strain showed clear enrichment of RNA size 20-24 nt long (Figure 2.31A).

If Rct1 prevents Eri1 mediated siRNA degradation, one would expect *eri1Δ* mutant cells could bypass the requirement of Rct1 in robust siRNA accumulation and silencing. To test this idea, I generated *rct1Δeri1Δ* mutant cells and checked if heterochromatin silencing was restored in this double mutant by RT-qPCR. Pericentromeric transcripts accumulated in *rct1Δeri1Δ* mutant cells at a similar level as *rct1Δ* single mutant cells, suggesting silencing was not restored by the additional deletion of *eri*1 (Figure 2.31B). Taken together, my results suggest that Rct1 neither binds to siRNAs nor does it mediate siRNA stability. This is in agreement with the observation that RRM's primary target is single stranded RNA (ssRNA).

2.2.11 Loss of *rrp6* restores pericentromeric silencing in *rct1* mutant cells

I showed previously that in *rct1Δclr3Δ* mutant cells, siRNA biogenesis was partially restored. This indicates that Rct1 is not directly involved in siRNA biogenesis like RdRP or Dicer. Furthermore, all the RNAi factors have been tagged and immunoprecipitated to identify other components in the RNAi machinery, and the association with Rct1 was never discovered. This observation, along with my results demonstrating the conserved RRM was essential for siRNA levels in the cell, lead me to investigate the possibility that Rct1 binds to ssRNAs and guides the precursor transcripts to the RNAi pathway. To address this idea, I took advantage of the finding that the Rrp6 exosome pathway exists in parallel with the RNAi pathway to process heterochromatic transcripts, but exosome does not process transcripts into siRNAs (Reyes-Turcu et al., 2011; Yamanaka et al., 2013). In addition, these two pathways compete for the same RNA substrates, and so in cells lacking Rrp6, RNA substrates that are normally targeted by Rrp6 can now be targeted by the RNAi machinery.

To test if pericentromeric transcripts in *rct1* mutant cells were mis-targeted by Rrp6, resulting in a loss of siRNAs, I generated *rct1Δrrp6Δ* and *rct1-rrm rrp6Δ* mutant cells. I reasoned that by impairing the competing exosome pathway, pericentromeric transcripts could be channeled into the RNAi machinery more efficiently and could produce siRNAs even in *rct1* mutant cells. I sequenced siRNAs and found that pericentromeric siRNAs were partially restored in *rct1Δrrp6Δ* and *rct1-rrm rrp6Δ* double mutant cells as compared to *rct1Δ* and *rct1-rrm* single mutant cells, including the boundary small RNAs (Figures 2.32A, B and C). Quantitative analysis showed a 20- to 40-fold increase in centromeric siRNA levels in the double mutant cells when compared to *rct1* single mutant cells (Figure 2.33A). Consistent with previous reports, deleting *rrp6* alone had limited effect on *dh/dg* repeat siRNA biogenesis (Figures 2.32 and 2.33A, and (Bühler et al., 2007)). siRNAs derived from *otr1R*::*ura4* transgene were similarly restored in *rct1Δrrp6Δ* and *rct1-rrm rrp6Δ* mutant cells, even though *ura4* siRNAs were produced much less robustly than repeat-derived siRNAs (Figure 2.33B). I noticed an increase in the *ura4* siRNAs levels in *rrp6Δ* mutant cells when compared to wild type cells (Figure 2.33B), indicating that the precursor transcript generated from *otr1R*::*ura4*

transgene is preferentially directed to exosome pathway instead of RNAi machinery under normal conditions, thus explaining the low level of siRNAs derived from *ura4::otr1R* transgene (Bühler et al., 2007).

To confirm if the siRNAs in the *rct1Δrrp6Δ* and *rct1-rrm rrp6Δ* mutant cells are produced by RNAi machinery, we analyzed the 5' nucleotide bias and size distribution of these siRNAs. Our analysis revealed that the siRNAs detected in *rct1Δrrp6Δ* and *rct1-rrm rrp6Δ* mutant cells showed a strong 5' U bias (Figure 2.34A) and were mostly 22-24 nucleotides in length (Figure 2.34B). This result suggests that without the competing exosome pathway, RNAi machinery is able to target pericentromeric transcripts and produce siRNAs in the absence of Rct1 or its RNA-binding ability.

To test if these siRNAs were capable of inducing silencing, I performed RT-qPCR to quantify pericentromeric RNA levels in the *rct1Δrrp6Δ* and *rct1-rrm rrp6Δ* double mutant cells. My result showed that, when compared to the *rct1Δ* and *rct1-rrm* single mutant cells, both *dh* and *dg* repeats were efficiently silenced in *rct1Δrrp6Δ* and *rct1-rrm rrp6Δ* double mutant cells (Figure 2.35). Other than siRNA induced silencing, precursor RNAs processed into siRNAs could also cause the decreased level of *dh* and *dg* transcripts. However, the *cen* siRNAs in the *rct1Δrrp6Δ* and *rct1-rrm rrp6Δ* double mutant cells were only about 15-25% of *cen* siRNAs in the wild type cells (Figure 2.33A), while pericentromeric transcript expression levels were significantly reduced to nearly wild type levels (Figure 2.35). Therefore, the rescue of pericentromeric silencing in *rct1Δrrp6Δ* and *rct1-rrm rrp6Δ* mutant cells could not be explained simply by post-transcriptional processing of the precursors. My results indicate that by impairing the exosome pathway, pericentromeric transcripts can be guided towards RNAi machinery, thereby generating functional siRNAs in the absence of Rct1 or its RNA-binding ability.

2.2.12 Rct1 is required for efficient splicing of Pol II transcripts

My results indicated that in the absence of Rct1 or its RNA-binding ability, Rrp6 targets pericentromeric transcripts, thereby preventing transcript processing by RNAi machinery. In other words, Rct1 prevents pericentromeric transcript targeting by Rrp6 in wild type cells. Rrp6 is directed to unspliced transcripts and mediates their retention at the transcription site (de Almeida et al., 2010; Eberle et al., 2010). Therefore, by

promoting splicing, Rct1 could avoid transcripts targeted to Rrp6. To test if Rct1 is needed for RNA splicing, we analyzed splicing efficiency in *rct1* mutant cells by RNAseq. Our analysis showed a striking upregulation in intron retention in *rct1Δ* and *rct1-rrm* mutant cells while exon expression was largely unaffected (Figure 2.36). In cells lacking Clr3, there are global gene expression changes (Hansen et al., 2005); however, we did not detect any splicing defects in the *clr3Δ* mutant cells, suggesting the splicing defects are specific to *rct1Δ* and *rct1-rrm* mutant cells. A role for Rct1 in splicing is supported by its previously reported direct interaction with SR splicing proteins, Pol II, and RNA (Baltz et al., 2012; Bannikova et al., 2013; Gullerova et al., 2007; Gullerova et al., 2006).

In *S. pombe*, mRNA-type introns have been identified in both *dh* and *dg* pericentromeric repeats by their conserved splice site sequences (Chinen et al., 2010). Our attempt to analyze splicing efficiency in *dh* and *dg* pericentromeric transcript was not conclusive due to the poor splicing efficiency and low expression levels in the wild type cells.

2.2.13 Pol II phosphorylation and heterochromatic silencing

Rct1 negatively regulates Pol II phosphorylation and is associated with Pol II in fungi, plants and worms (Gullerova et al., 2007; Gullerova et al., 2006; Jeong Hyun Ahn, unpublished). To test if the silencing defect in *rct1Δ* mutant cells is caused by Pol II hyper-phosphorylation, I attempted to test if deleting Pol II kinases in an *rct1* deletion background could rescue the silencing defect observed in *rct1Δ* mutant cells. There are three Pol II kinases in *S. pombe*, encoded by *lsk1*, *cdk9* and *mcs6*. While *cdk9* and *mcs6* are both essential for cell viability, *lsk1* is not required. I generated *cdk9* and *mcs6* deletion constructs and transformed them into diploid *S. pombe* cells. Diploid $cdk9^{+/-}$ and $mcs6^{+/-}$ cells were viable. I then transformed an *rct1* deletion construct into the heterozygous cells and followed with tetrad dissection. Diploid $lsk1^{+/-}$ mutant cells were created by crossing *lsk1Δ* haploid mutant cells with wild type haploid cells. I again transformed the *rct1* deletion construct into $lsk1^{+/-}$ cells and followed with tetrad dissection. Although I was able to obtain $rct1^{+/-}$ $cdk9^{+/-}$, $rct1^{+/-}$ $mcs6^{+/-}$ and $rct1^{+/-}$ $lsk1^{+/-}$

diploid cells, I did not recover any haploid double mutants or *mcs6Δ* single mutant cells. This result indicates that *rct1* is synthetic lethal with Pol II kinases.

Despite the severe growth (Figures 2.37A and 2.37B) and morphological defects (Figure 2.37C), I was able to recover *cdk9Δ* single mutant cells. To test if Pol II kinases are required for heterochromatin silencing, I performed semi-quantitative RT-PCR in *cdk9Δ* and *lsk1Δ* mutant cells. My result showed that Cdk9, but not Lsk1, is needed for endogenous *dh/dg* repeat and *ura4* transgene silencing (Figure 2.38A). Additionally, in agreement with impaired silencing, *dh/dg* derived siRNAs were abolished in *cdk9Δ* mutant cells, whereas siRNAs were produced at a wild type level in *lsk1Δ* mutant cells (Figure 2.38B). Lsk1 specifically phosphorylates serine 2 at Pol II CTD heptad repeats, while Cdk9 phosphorylates both serine 2 and serine 5 (Viladevall et al., 2009). These results suggest a potential link between Pol II CTD serine 5 phosphorylation and siRNA mediated heterochromatin silencing (Zaratiegui et al., 2011).

2.2.14 Pol II degradation and heterochromatic silencing

Pol II protein levels were reduced in *rct1Δ* and *rct1-rrm* mutant cells, but at the transcript level, no reduction was observed (Figure 2.39A). This result suggests that Pol II protein might be prone to degradation in *rct1* mutant cells. It has been shown that in *S. cerevisiae*, UBC4 and UBC5 trigger Pol II degradation in response to DNA damage (Somesh et al., 2005). The *UBC4*/*UBC5* ortholog in *S. pombe* is *ubc4*, an essential ubiquitin-conjugating enzyme. I hypothesized that, if the silencing defects in *rct1* mutant cells were caused by Pol II degradation, I should be able to rescue silencing defects by inactivating Ubc4, the enzyme responsible for Pol II degradation. Taking advantage of previously identified *ubc4* mutant allele, *ubc4-G48D* (Irvine et al., 2009), I generated *rct1Δubc4-G48D* double mutant cells.

To analyze the pericentromeric silencing defect, I performed semi-quantitative RT-PCR in the *rct1Δubc4-G48D* double mutant cells. My result showed that the silencing at the pericentromeric *dg* repeat was further impaired in the double mutant cells when compared to each individual single mutant (Figure 2.39B). This result was also confirmed by RT-qPCR (Figure 2.39C). In *S. pombe*, it is not yet clear if *ubc4* mediates Pol II degradation like UBC4/5 in budding yeast, but *ubc4* is needed for efficient mating-type

switching and pericentromeric silencing (Irvine et al., 2009). My results suggest that, although Pol II could be the common target, Rct1 and Ubc4 regulate pericentromeric silencing via different mechanisms.

2.2.15 Suppressor Screen

In addition to the candidate suppressor search, I also employed unbiased suppressor screens to identify genes, other than *rrp6* and *mlo3*, that can suppress Rct1 function in silencing to provide a mechanistic insight for Rct1 mediated heterochromatin silencing.

I started with a classic EMS mutagenesis in *rct1-rrm* mutant cells, selecting for suppressors that rescued the slow growing phenotype. I also did EMS mutagenesis in *ubc4-G48D* mutant cells to identify suppressors that rescued the defect in mating-type switching. Surprisingly, despite the slow growing phenotype of *rct1-rrm* mutant cells, they were not sensitive to EMS treatment. I tested different EMS treatment durations in the mutagenesis process, and while no *ubc4-G48D* mutant cells survived under 3% (v/v) EMS for 90 minutes, the same treatment did not kill *rct1-rrm* mutant cells. In addition, the survival rate of *rct1-rrm* mutant cells after EMS treatment showed no correlation with treatment time length, and I did not recover any colony that grew much faster. On the other hand, EMS mutagenesis of *ubc4-G48D* mutant cells was successful, about half of the cells survived under 3% (v/v) EMS treatment for 45 minutes. Potential *ubc4* suppressors were isolated based on their ability to generate spores, as tested by iodine staining. I isolated 4 strains that stained strongly with iodine, and 11 strains that stained weakly (Figure 2.40).

rct1-rrm mutant cells grew more slowly, partly due to high percentage of cell death under the normal culture condition. I estimated that more than half of the cells die during culture based by survival assay (Figure 2.41). In slow growing cells, prolonged culture conditions naturally select for the cells carrying suppressors that suppress the slow growing phenotype. Therefore, I took a different approach in my *rct1* suppressor screen. Briefly, *rct1-rrm* mutant cells were cultured in complete liquid media until saturation, and cells were then plated on complete solid media and grew until colonies appeared. The large colonies were then picked and cultured in complete liquid media

until saturation. This process was repeated five times, after which I tested the survival rate in the isolated large colonies (Figure 2.41). I was able to isolate 8 suppressors based on improved survival rate. However the actually mutation(s) obtained is likely to be much less, as certain "lineages" consistently showed a higher survival rate among their descendents, suggesting the survival rate improvement is likely due to the same genetic mutation that occurred early in my screening process. Subjecting genomic DNA libraries from these strains to Next Generation Sequencing will identify these potential suppressors. Variant calling programs will be used to identify SNPs in the suppressors and by comparing these with SNPs in the parental *rct1-rrm* mutant cells, the precise mutation(s) responsible for improved survival can be mapped. The mutation(s) will be re-created in *rct1-rrm* mutant cells in order to confirm the suppression phenotype.

2.3 Discussion

2.3.1 Rct1 in siRNA production and gene silencing

Rct1 was identified in our *S. pombe* specific gene list in order to find novel components in the RNAi pathway. Compromised siRNA biogenesis (Figure 2.5) and genetic interactions (Figures 2.9 and 2.13) indicate a strong connection between Rct1 and the RNAi machinery. Protein-protein interaction studies have been done extensively with RNAi factors to identify novel components in the RNAi pathway. Interaction between RNAi factors and Rct1 has never been shown, which indicates that Rct1 does not directly interact with the RNAi machinery. Consistent with this idea, we were not able to detect interactions between Rct1 and siRNAs (Figure 2.31). Additionally, siRNA biogenesis was partially restored in *rct1Δclr3Δ* and *rct1Δrrp6Δ* mutant cells (Figures 2.11 and 2.33), further indicating that Rct1 does not participate in siRNA biogenesis directly as do other RNAi components.

Rct1 is engaged with transcription by interacting with the C-terminal domain of Pol II (Gullerova et al., 2007). Based on our results, we propose that, as transcription proceeds, Rct1 binds to the nascent RNA through its RRM. The splicing machinery is further recruited to this Rct1-bound transcript, and properly spliced transcripts are exported to the cytosol for translation. Non-coding transcripts from centromeric repeats stay in the nucleus to be processed into siRNAs, stimulated by the presence of spliceosomes stalled at weak splice site signals (Bayne et al., 2008). Such signals are found in non-coding transcripts from *dg* repeats, and the introns are partially spliced (Chinen et al., 2010), which is known to stimulate siRNA production in *Cryptococcus neoformans* (Dumesic et al., 2013). In cells lacking Rct1 or its RNA-binding ability, nascent transcripts are not processed (Figures 2.6 and 2.15); therefore unspliced RNAs accumulate in these cells. Rrp6 mediates unspliced transcript retention at the transcription site, preventing RNAi from targeting these transcripts, resulting in impaired siRNA biogenesis (Figure 2.42).

2.3.2 Rct1 in H3K9 methylation and Pol II accumulation

Unlike other RNAi mutants, but strongly resembling other splicing mutants (Bayne et al., 2008), cells lacking Rct1 uncouple siRNA biogenesis and H3K9 methylation. Recently, we proposed a model that bypasses the requirement for siRNAs in RNAi mediated H3K9 methylation (Zaratiegui et al., 2011). In brief, RNAi factors are required for Pol II release during S phase to resolve the collision between the replication and transcription machinery, thus allowing replication to proceed. Continuously engaging the replication machinery during early S phase is necessary to spread H3K9 methylation through the pericentromeric repeats. Rather than requiring high levels of siRNAs, Pol II is removed by RNAi activity itself.

Supporting this model, in *rct1-rrm* mutant cells, Pol II is released from the pericentromeric repeats and H3K9 methylation is assembled. However, Pol II accumulated at pericentromeric repeats in *rct1Δ* mutant cells while H3K9 methylation was retained. There were no differences in Pol II protein levels between *rct1Δ and rct1-rrm* mutant cells (Figure 2.43); therefore the discrepancy of Pol II accumulation between the complete knockout and RRM mutant cells is not due to changes in Pol II protein levels. One possibility is that Rct1 bridges protein interactions with Pol II, thereby promoting Pol II release. Since this interaction is not mediated by RRM, Pol II can be efficiently released in *rct1-rrm* mutant cells. A potential candidate is ubiquitin ligase Cul3, which triggers Pol II degradation in response to DNA damage in *S. cerevisiae* (Ribar et al., 2007). The Rct1 homolog in *Drosophila melanogaster* (*D. melanogaster*), CG5808, exists in a protein complex with Cul3 (Fujiyama-Nakamura et al., 2009), and several protein interactions in this complex are conserved in *S. pombe* (Geyer et al., 2003; Pintard et al., 2004). The link between Rct1 and Cul3 could be a potential mechanism for Pol II removal through degradation during transcription and replication collision. An unbiased approach to identify Rct1 interacting proteins might be required to answer how Rct1 aids in releasing Pol II.

How is H3K9 methylation assembled without Pol II removal in *rct1Δ* mutant cells? The *rct1Δ* mutant cells grew four times slower at 30°C as compared to wild type cells, and it is possible that by slowing down replication, *rct1Δ* mutant cells minimize the collision problem and bypass the requirement of Pol II removal for H3K9 methylation. In

support of this idea, in hydroxyurea arrested *dcr1Δ* mutant cells, which also replicate much slower than untreated cells, Pol II accumulated in wider regions than in cycling *dcr1Δ* mutant cells (Zaratiegui et al., 2011), similar to the Pol II accumulation pattern observed *rct1Δ* mutant cells. Alternatively, the accumulation of Pol II could reflect paused, rather than actively transcribing, Pol II. Impaired transcription is known to bypass RNAi for H3K9 methylation (Reddy et al., 2011), so perhaps a similar mechanism may be at work in *rct1Δ* mutant cells.

2.3.3 Genome-wide role of Rct1 in Pol II transcript regulation

Putative Rct1 binding motifs have been mapped to mRNA transcripts in *A. thaliana*. This RNA motif appears to be widely present in the genome, in both coding and non-coding regions (Bannikova et al., 2013). From our RNAseq analysis, we found that 30% of the transcripts, both coding and non-coding, are differentially expressed in *rct1* mutants, including a few RNAi components and other factors known to be involved in heterochromatic silencing (Table 2.1). However, none of these uncouple siRNA biogenesis and H3K9 methylation, therefore ruling out the indirect effect caused by deleting Rct1. It remains possible that Rct1 might act at the translational level or affect transcription of other unidentified gene(s).

2.3.4 Clr3 dependent small RNAs

Pericentromeric siRNAs were detected in *rct1Δclr3Δ* double mutant cells. Based on the 5' nucleotide bias analysis and size distribution, we concluded that these siRNAs were Dcr1 products, as observed in *rct1Δrrp6Δ* mutant cells (Figure 2.34). However, the siRNAs from *rct1Δclr3Δ* double mutant cells were not able to induce silencing at the pericentromeric repeats (Figure 2.9A). In addition, *rct1Δclr3Δ* double mutant cells showed a synergistic effect on transcript accumulation (Figure 2.9A), indicating that Rct1 functions in a pathway independent of Clr3. The increase of siRNAs in *rct1Δclr3Δ* double mutant cells could be due to the active transcription at repeat region in *clr3Δ* background, and the siRNA level merely reflects more siRNA precursors in the cells.

Interestingly, even though *clr3Δ* cells have been shown to accumulate more siRNAs from centromeric repeats, we noticed a different pattern in the siRNA distribution as compare to wild type cells from our small RNAseq data. The siRNA reads in *clr3Δ* cells mapped to a more confined *dh* and *dg* region than siRNA reads from wild type cells. Strikingly, siRNA reads mapping to the pericentromere boundary were completely lost in *clr3Δ* mutant cells (Figure 2.12). The pericentromeric siRNAs restored in the *rct1Δclr3Δ* mutant cells only mapped to the confined regions, and were still absent from the boundaries. These boundary siRNAs are Dcr1 dependent 22 nucleotide long siRNAs but unlike canonical pericentromeric siRNAs, boundary siRNAs do not load onto Ago1 and are incapable of triggering H3K9 methylation (Keller et al., 2013). Instead, the boundary siRNA precursors have been proposed to prevent heterochromatin spreading into neighboring euchromatin by binding to Swi6 and evicting RNA-bound Swi6 from chromatin (Keller et al., 2012). However, we did not observe H3K9 methylation spreading at the pericentromere boundaries, suggesting boundary siRNA precursors are properly transcribed in *clr3Δ* cells (Figure 2.22). Clr3 contributes to silent heterochromatin assembly partly by the elimination of the nucleosome free region (NFR) found within the repeats, therefore inhibiting Pol II engagement (Garcia et al., 2010). Unlike the *dh/dg* repeats associated NFRs, the NFRs at the pericentromeric boundaries are resistant to Clr3 mediated elimination, suggesting a unique mechanism in boundary element regulation. We revealed an unexpected role of Clr3 in boundary siRNA biogenesis; the significance of this requires further analysis.

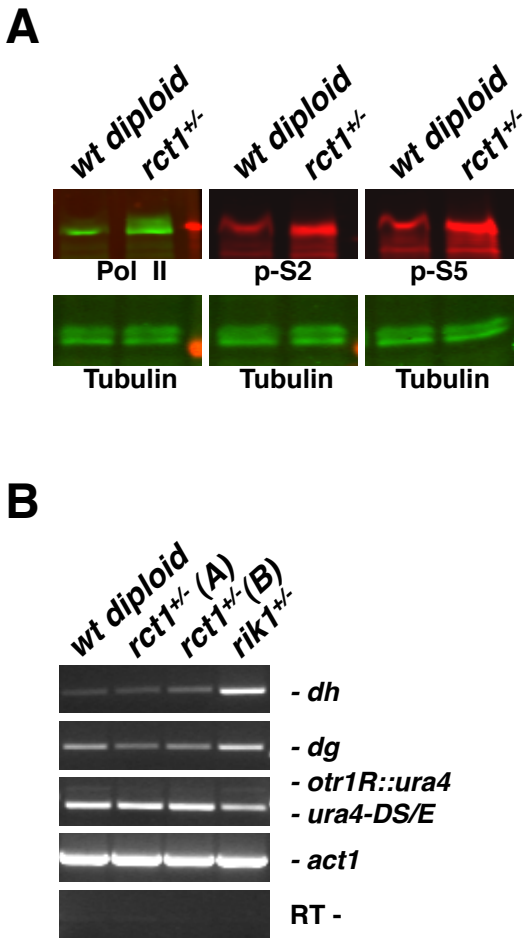

Figure 2.1 Rct1 negatively regulates Pol II phosphorylation and has no effect on pericentromeric silencing in rct1$^{+/-}$ heterozygous cells

(A) Pol II protein levels were analyzed by western blot in indicated strains. Different phosphorylated forms of Pol II were analyzed. Tubulin serves as loading control.
(B) Semi-quantitative RT-PCR of *dh*/*dg* and *otr1R*::*ura4* transcript levels in indicated strains. Two biological replicates were labeled as A and B. Truncated *ura4-DS/E* at endogenous site and *act1* serve as loading controls, RT- omits the reverse transcription step.

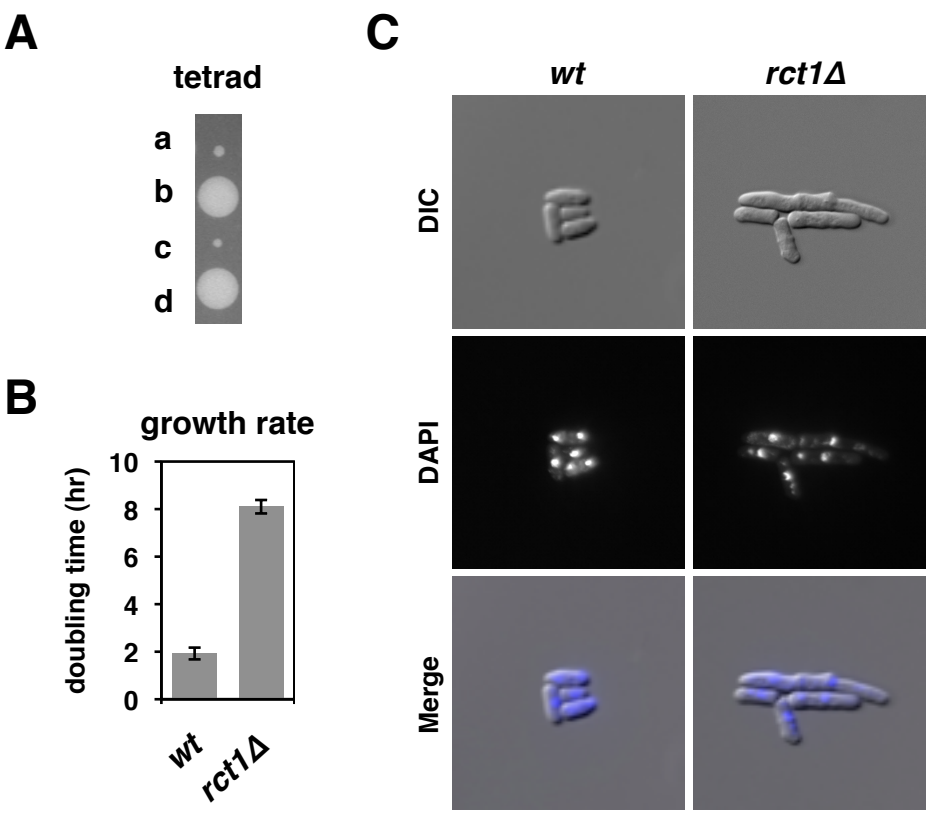

Figure 2.2 *rct1* is a non-essential gene required for normal cell growth and morphology

(A) A full tetrad. a, b, c and d indicate siblings from the same ascus. Haploid cells carrying *rct1* null allele are the small colonies as confirmed by drug resistance and PCR.
(B) Cell growth rate measured by OD_{600} in indicated strains.
(C) Cell morphology in indicated strains. DIC (differential interference contrast) shows the cell shape, DAPI stains nuclei.

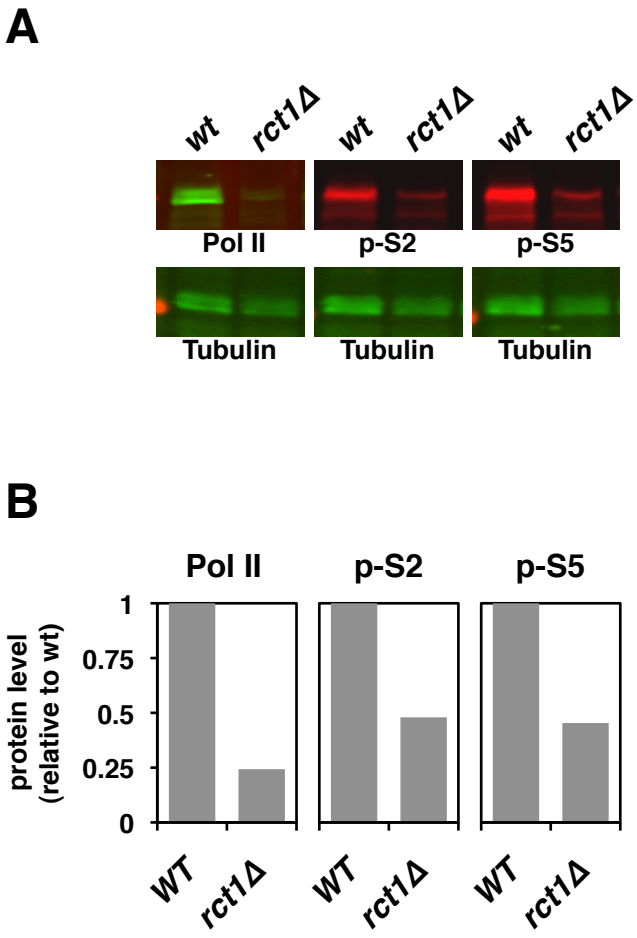

Figure 2.3 Reduced Pol II protein levels in haploid *rct1Δ* cells

(A) Pol II protein levels were analyzed by western blot in indicated strains. Different phosphorylated forms of Pol II were analyzed. Tubulin serves as loading control.
(B) Quantitative analysis of Pol II protein levels in indicated strains by normalizing to corresponding Tubulin signals and wild type.

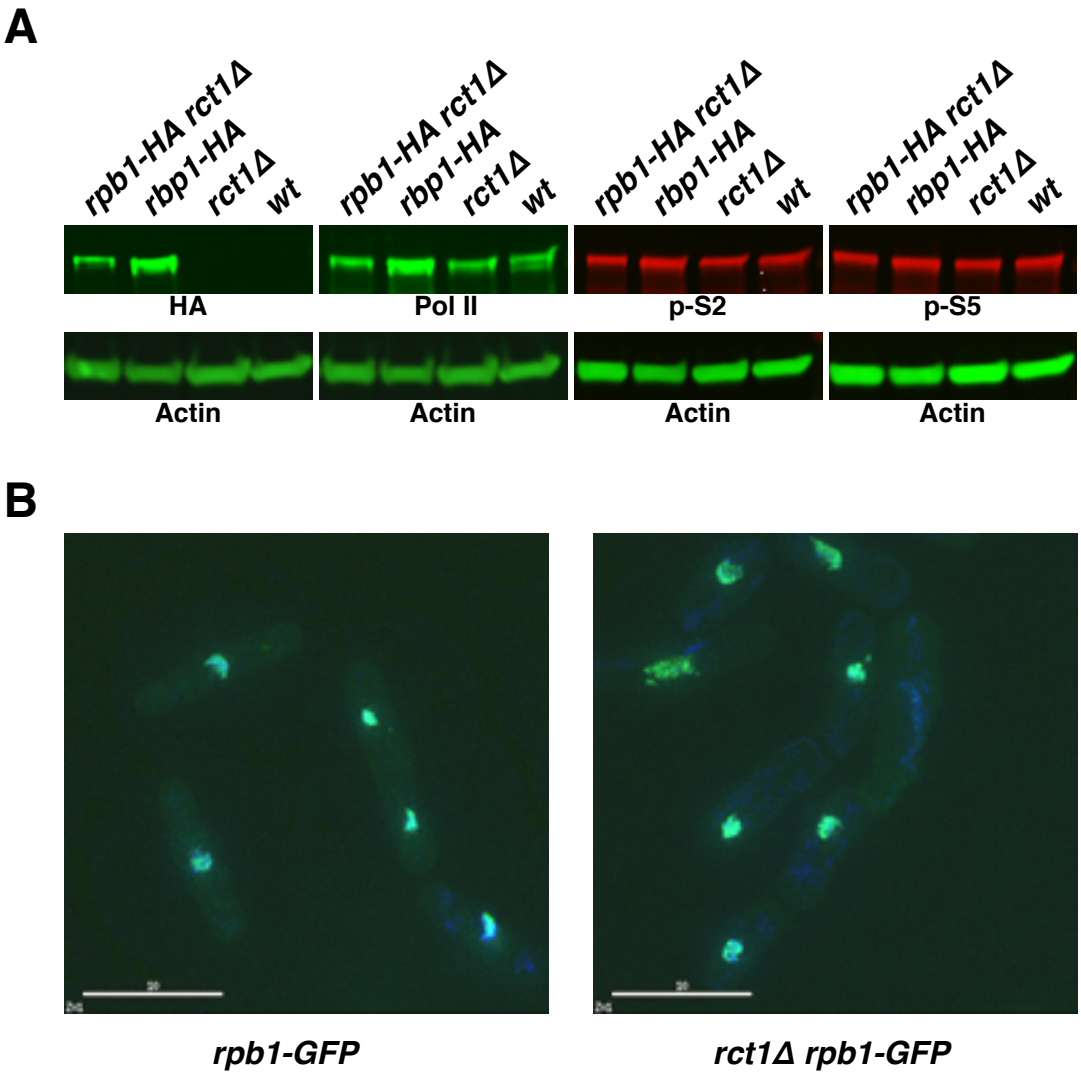

Figure 2.4 Pol II protein levels and localization in *rct1Δ* cells

(A) Pol II protein levels were analyzed by western blot in indicated strains. HA antibody was used to detect total Pol II protein. In addition, different phosphorylated forms of Pol II were analyzed. Actin serves as loading control.
(B) GFP-tagged Pol II localization in wild type and *rct1Δ* cells. DAPI stains nuclei.

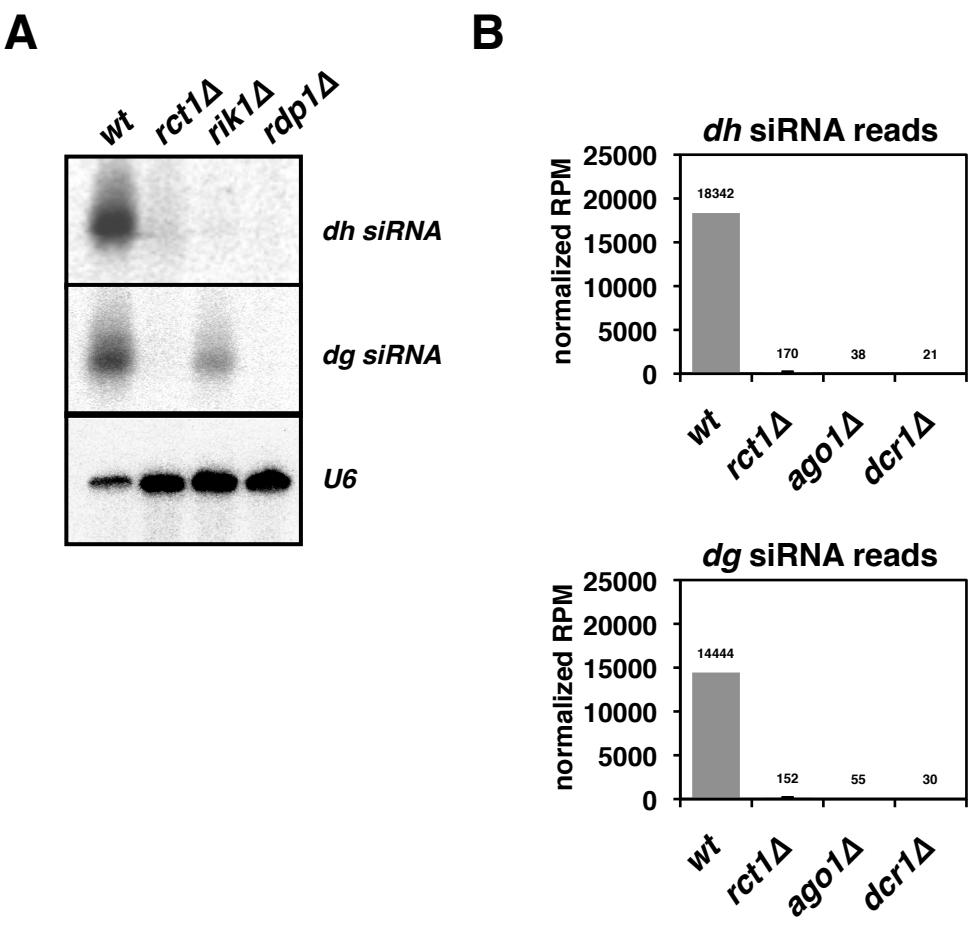

Figure 2.5 Rct1 is essential for pericentromeric siRNA biogenesis

(A) Small RNA northern blots of pericentromeric *dh*/*dg* derived siRNAs. *U6* serves as loading control.
(B) Quantification of *cen* siRNAs in indicated strains. Y-axis represents normalized reads in each library (read per million). Normalized reads mapped to *dh*/*dg* repeats are plotted separately. Data from two biological replicates of *rct1Δ* mutant cells were analyzed. Error bar indicates standard error from mean (SEM).

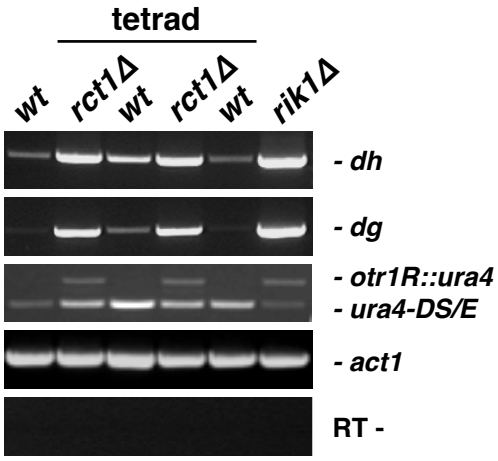

Figure 2.6 Pericentromeric transcript accumulation and impaired transgene silencing in *rct1Δ* mutant cells

Semi-quantitative RT-PCR of *dh*/*dg* and *otr1R*::*ura4* transcript levels in *rct1Δ* mutant cells. Truncated *ura4-DS/E* at endogenous site and *act1* serve as loading controls, RT- omits the reverse transcription step. A full tetrad was analyzed to show the silencing defect phenotype segregates with *rct1Δ* alleles.

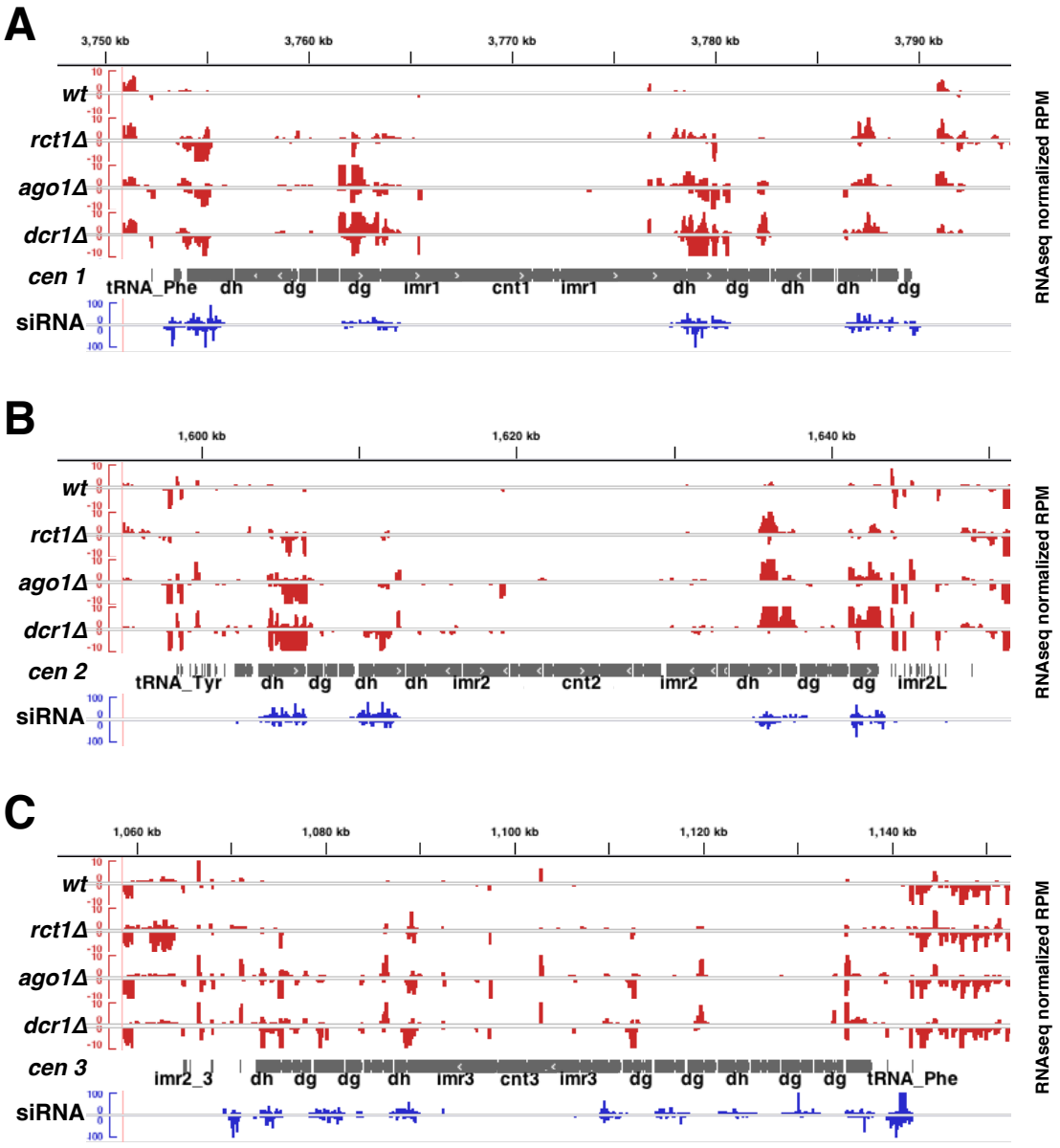

Figure 2.7 Pericentromeric transcript accumulations in RNAi and *rct1Δ* mutant cells

RNAseq reads distribution in indicated strains. RNAseq tracks (red), small RNAseq track (blue), centromeres (grey). Y-axis represents normalized reads in each library (RPM). **(A)** centromere 1 **(B)** centromere 2 **(C)** centromere 3

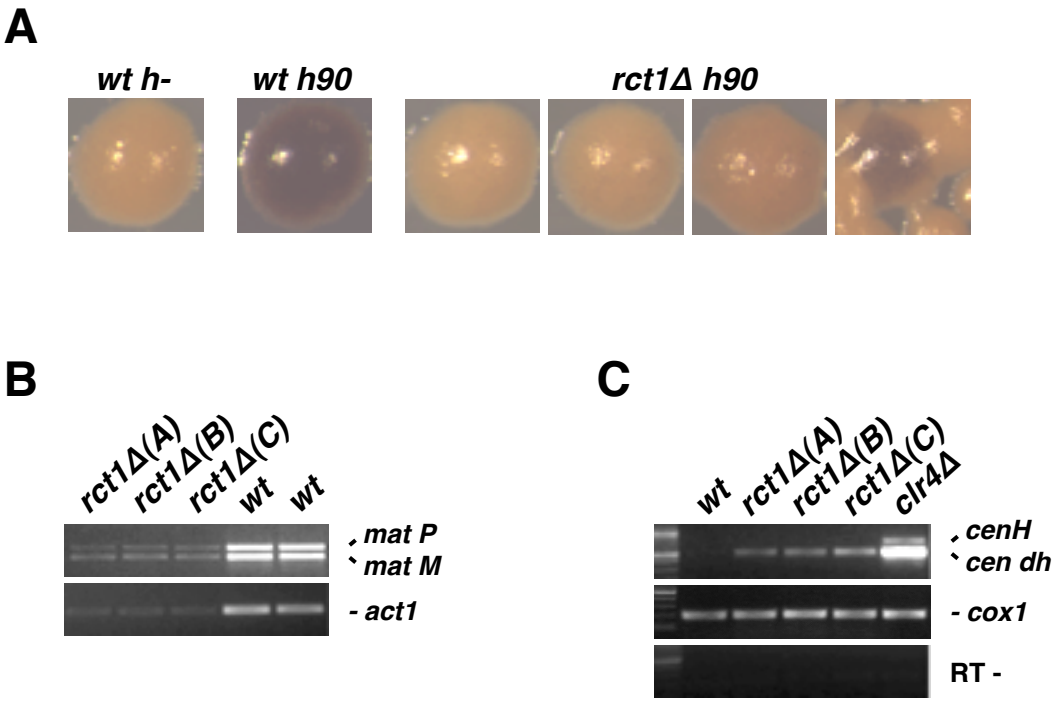

Figure 2.8 Rct1 is not needed for silencing at the mating-type locus

(A) Spore formation in indicated strains detected by iodine staining. Homothallic wild type (*h90*) strain is used as a positive control; heterothallic wild type (*h-*) is used as a negative control.
(B) PCR of genomic DNA to detect plus (*mat P*) and minus (*mat M*) mating type cell ratio in indicated strains. Three individual *rct1Δ* mutant strains in *h90* background were analyzed, labeled as A, B and C. *act1* serves as control.
(C) Semi-quantitative RT-PCR analysis of *cenH* transcripts from mating-type locus. The lower band, *cen dh*, indicates transcripts generated from the pericentromeric *dh* repeats. Three individual *rct1Δ* mutant strains in *h90* background were analyzed, labeled as A, B and C. *cox1* serves as loading control, RT- omits the reverse transcription step.

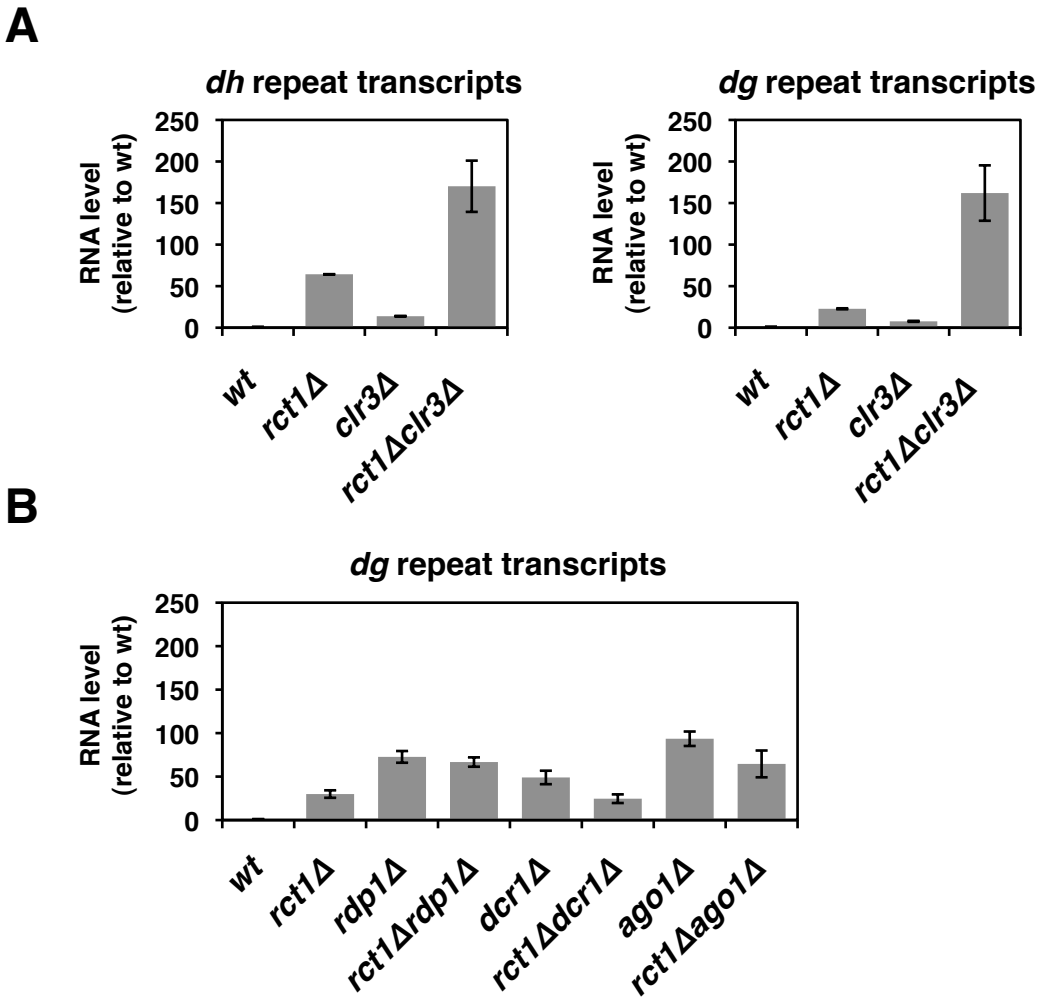

Figure 2.9 Rct1 functions in RNAi machinery and acts in parallel with Clr3 to establish pericentromeric silencing

(A) and **(B)** RT-qPCR analysis of *dh*/*dg* transcript expression levels in mutant strains as indicated. *actin* transcript levels were used for normalization by ΔΔCT method. Y-axis represents RNA expression levels relative to wild type. At least two biological replicates were used for each genotype and qPCR reaction was performed at least twice for each strain. Error bars indicate SEM.

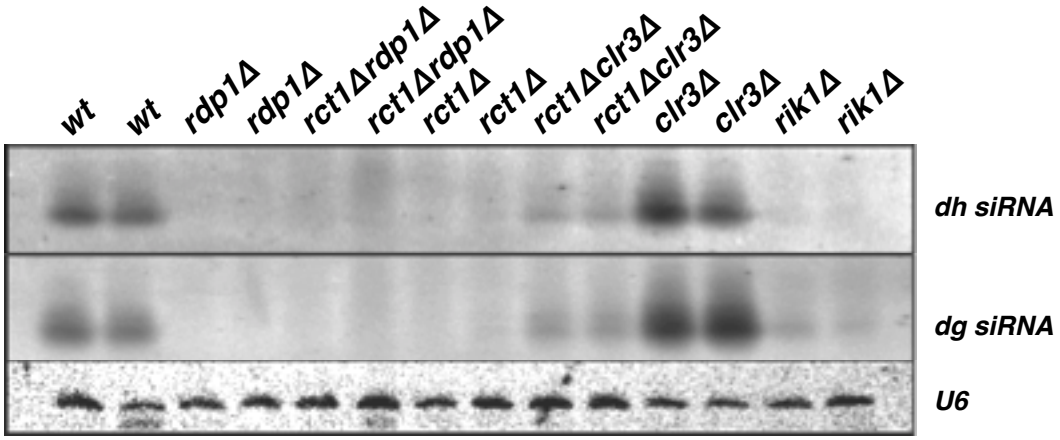

Figure 2.10 Additive effect of Clr3 deletion in pericentromeric siRNA levels in *rct1Δ* mutant cells

Small RNA northern blots of pericentromeric *dh*/*dg* derived siRNAs in indicated strains. Two biological replicates were analyzed for each genotype. *U6* serves as loading control.

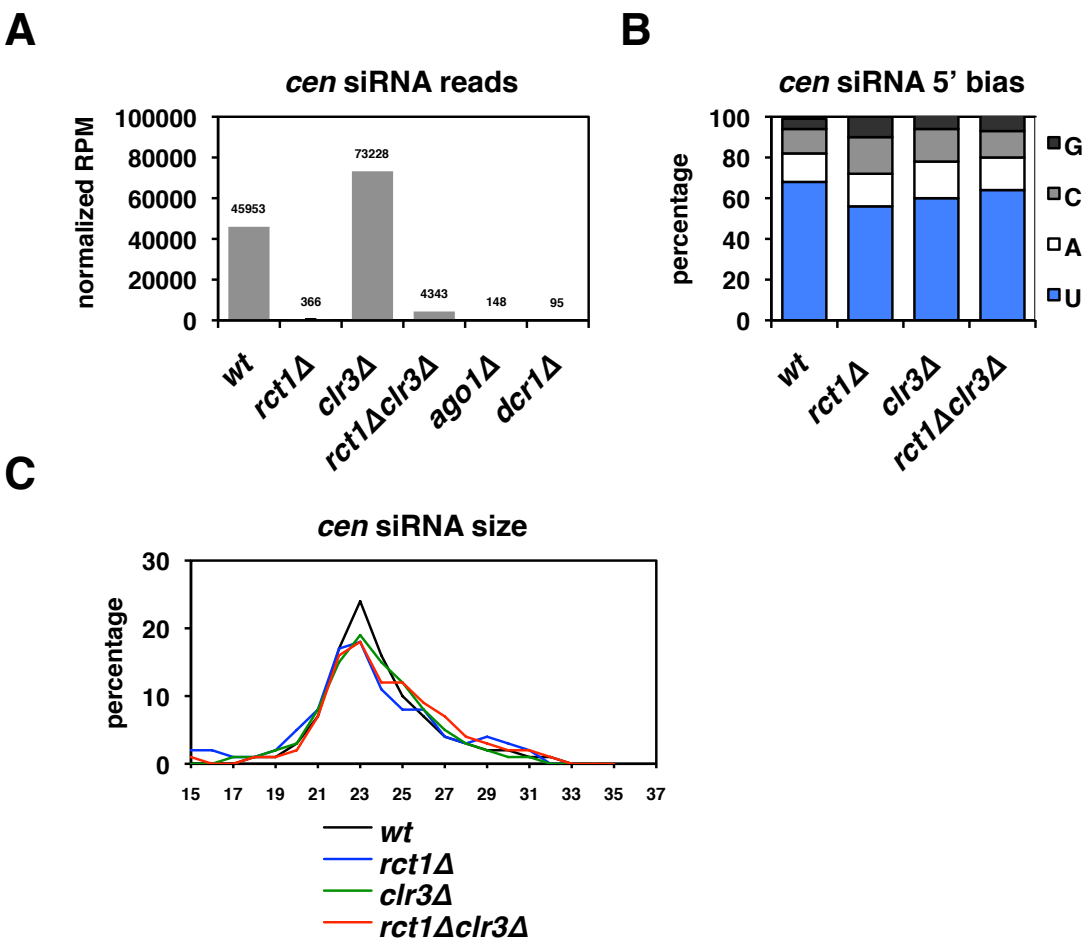

Figure 2.11 Pericentromeric siRNA profiles in *rct1Δclr3Δ* mutant cells

(A) Quantification of *cen* siRNAs in indicated strains. Y-axis represents normalized reads in each library (RPM). Data from two biological replicates of *rct1Δ* mutant cells were analyzed. Error bar indicates SEM.
(B) The frequency of 5' nucleotide occurrence in *cen* siRNA reads in indicated strains. Y-axis represents percentage of each nucleotide.
(C) The size distribution of *cen* siRNA reads in indicated strains. Y-axis represents percentage of each siRNA length between 15 to 35 bp.

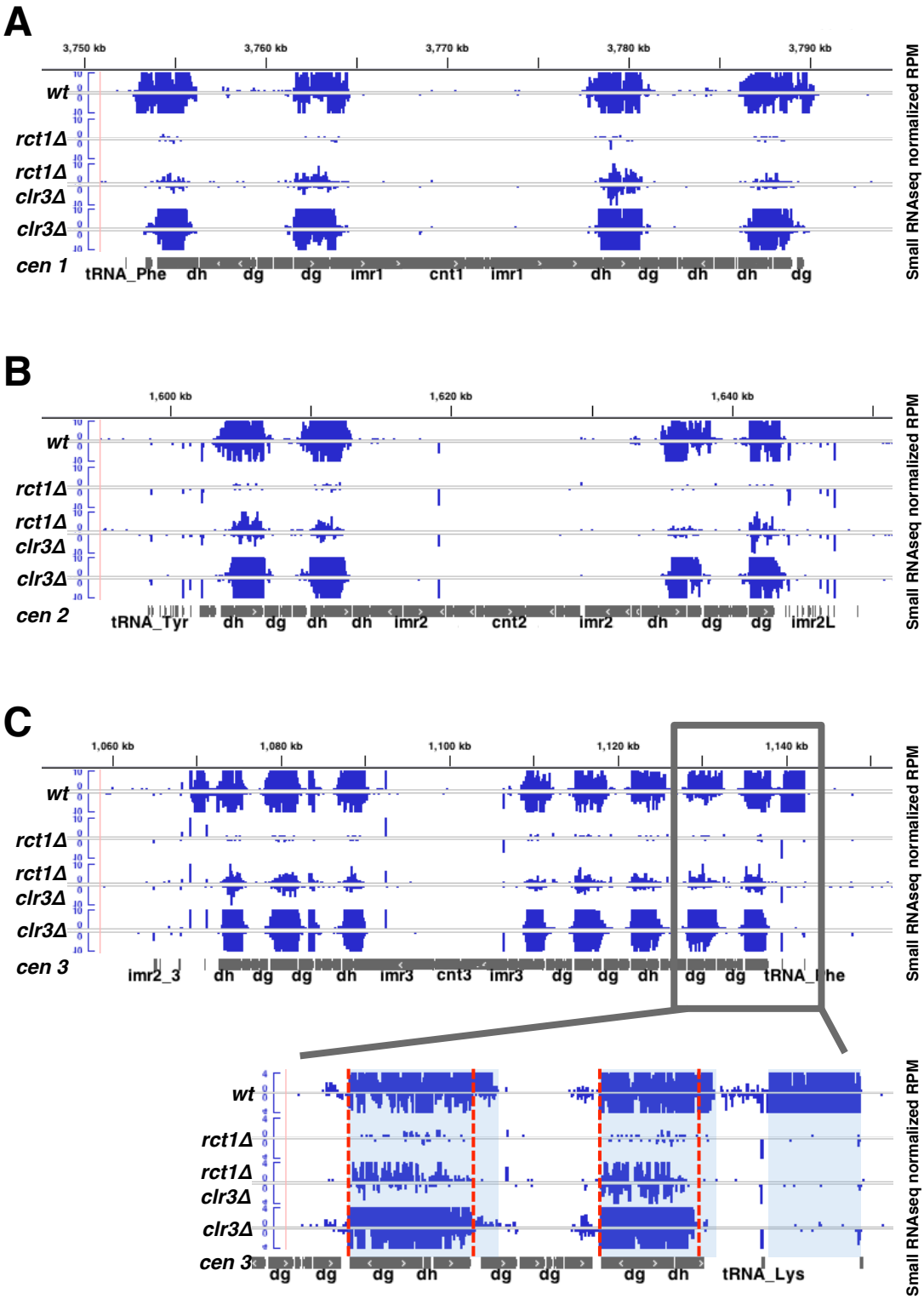

Figure 2.12 Pericentromeric siRNA distribution in *rct1Δclr3Δ* mutant cells

Pericentromeric siRNA levels and distribution in indicated strains. Small RNAseq tracks, (blue), centromeres (grey). Y-axis represents normalized reads in each library (RPM). Lower panel is a blow up view of the pericentromeric boundary located at the right arm of centromere 3, note the difference in scale. Blue shade indicates siRNA distribution from wild type cells, red dashed line marks confined distribution in the mutant cells.

(A) centromere 1 **(B)** centromere 2 **(C)** centromere 3

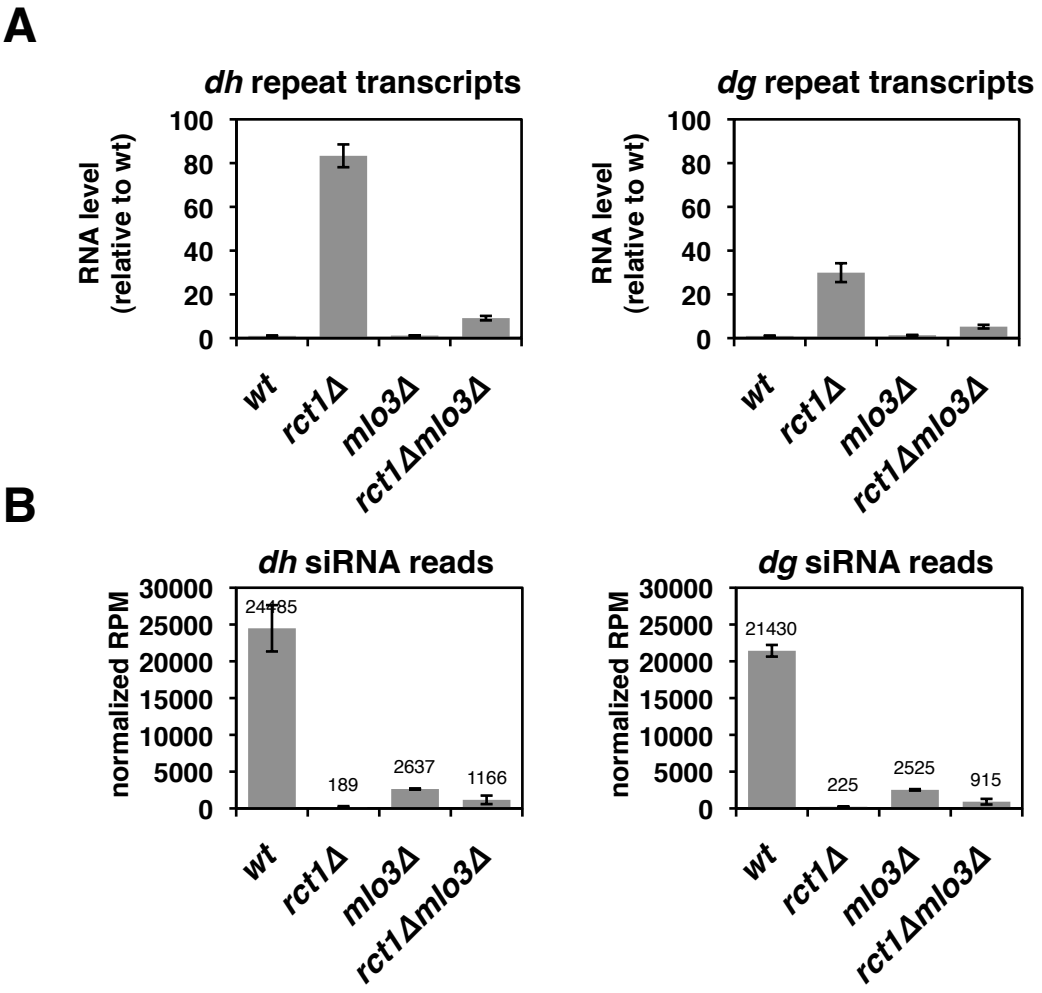

Figure 2.13 *mlo3* suppresses pericentromeric silencing defect in *rct1Δ* mutant cells independent of siRNA biogenesis

(A) RT-qPCR analysis of *dh*/*dg* transcript expression levels in mutant strains as indicated. *actin* transcript levels were used for normalization by ΔΔCT method. Y-axis represents RNA expression levels relative to wild type. Two biological replicates were used for each genotype and qPCR reaction was performed three times for each strain. Error bars indicate SEM.
(B) Quantification of *cen* siRNAs in indicated strains. Y-axis represents normalized reads in each library (RPM). Normalized reads mapped to *dh*/*dg* repeats are plotted separately. Two biological replicates were used for each genotype. Error bar indicates SEM.

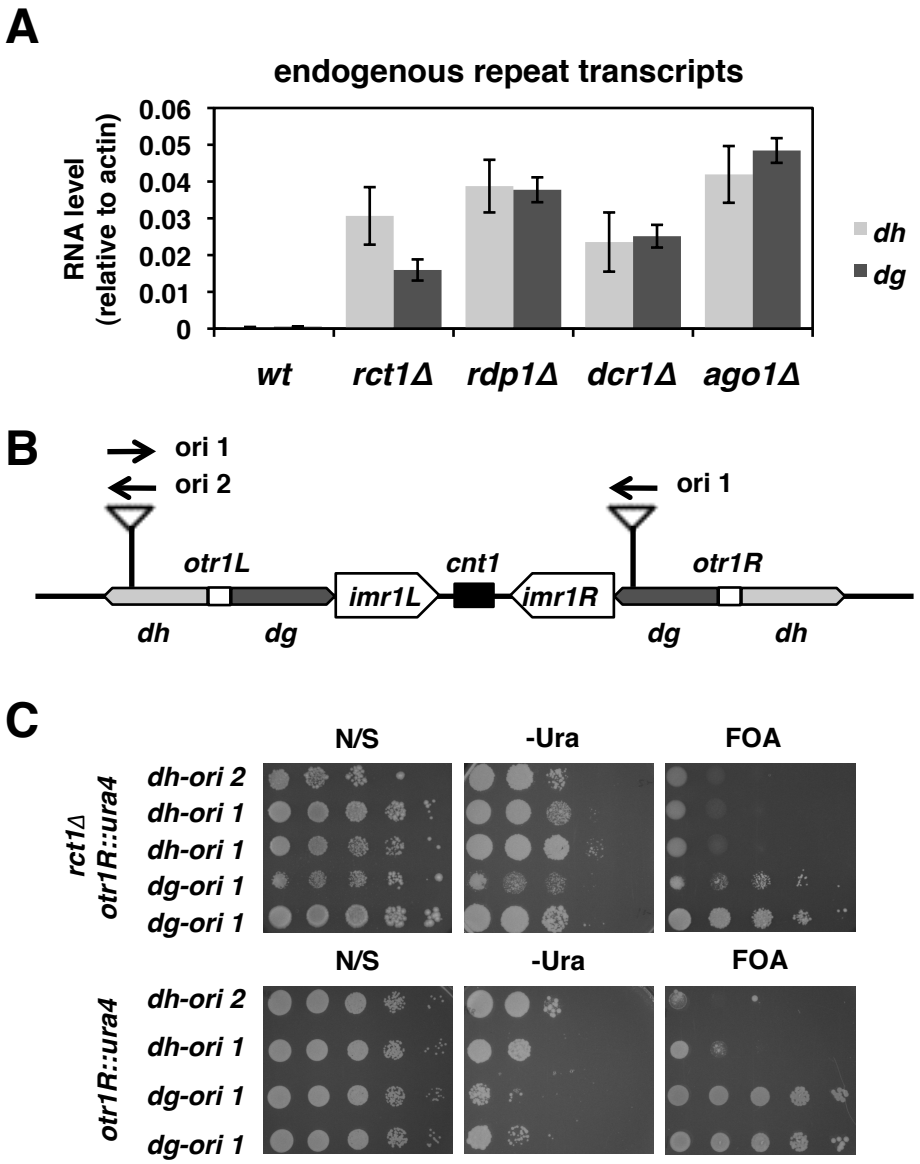

Figure 2.14 *rct1* had no differential effect on transgene silencing when *ura4* is placed in different repeats or orientation

(A) RT-qPCR analysis of *dh*/*dg* transcript expression levels in mutant strains as indicated. Y-axis represents pericentromeric repeat expression levels relative to *actin*. Two biological replicates were used for each genotype and qPCR reaction was performed three times for each strain. Error bars indicate SEM.
(B) Schematic representation of different *otr1::ura4* insertions. Triangle marks *ura4* insertion site and arrows indicate *ura4* insertion orientation (ori).
(C) Spot assay on non-selective (N/S), -Ura and 5-FOA plate to counter select cells expressing Ura4. A ten-fold serial dilution of cells were spotted on the indicated plates, from 10^5 to 10 cells/spot.

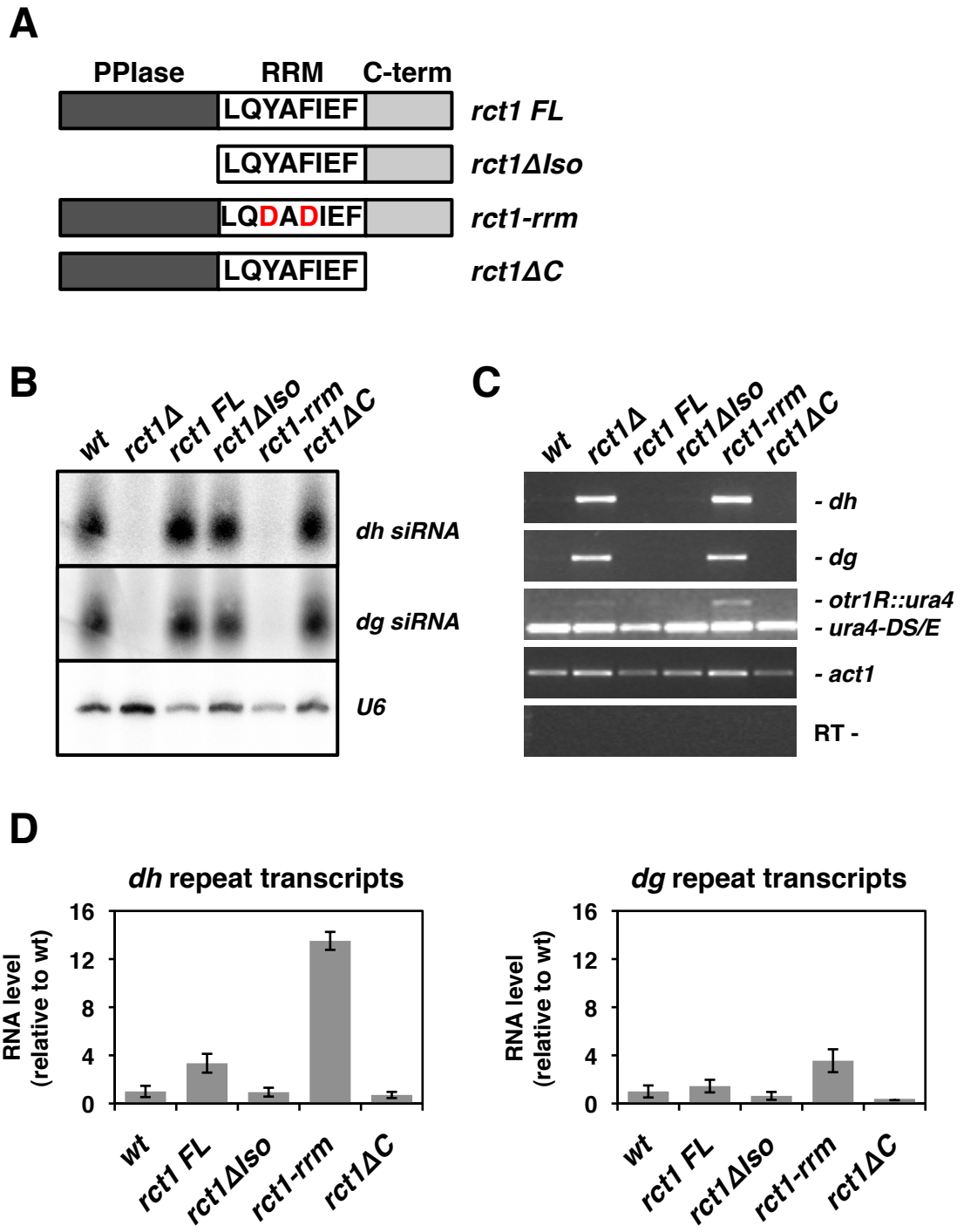

Figure 2.15 The RNA recognition motif of Rct1 is essential for pericentromeric heterochromatin silencing and siRNA biogenesis

(A) Schematic representation of *rct1* alleles. *rct1 FL* contains full-length Rct1 with no mutations. *rct1ΔIso* lacks the first 175 amino acids corresponding to PPIase domain. *rct1-*

rrm includes two amino acid mutations (red) in the RRM, Y287D and F289D, both of which combined were predicted to abolish the RNA-binding ability of Rct1. *rct1ΔC* has amino acids 333-428 removed.
(B) Small RNA northern blots of pericentromeric *dh*/*dg* derived siRNAs in indicated strains. *U6* serves as loading control.
(C) Semi-quantitative RT-PCR showing *dh*/*dg* and *otr1R*::*ura4* transcript levels in *rct1* mutant cells. Truncated *ura4-DS/E* at the endogenous locus and *act1* serve as loading controls, RT- omits the reverse transcription step.
(D) RT-qPCR analysis of *dh*/*dg* transcript expression levels in mutant strains as indicated. *actin* transcript levels were used for normalization by ΔΔCT method. Y-axis represents RNA expression levels relative to wild type. qPCR reaction was performed four times for each strain. Error bars indicate SEM.

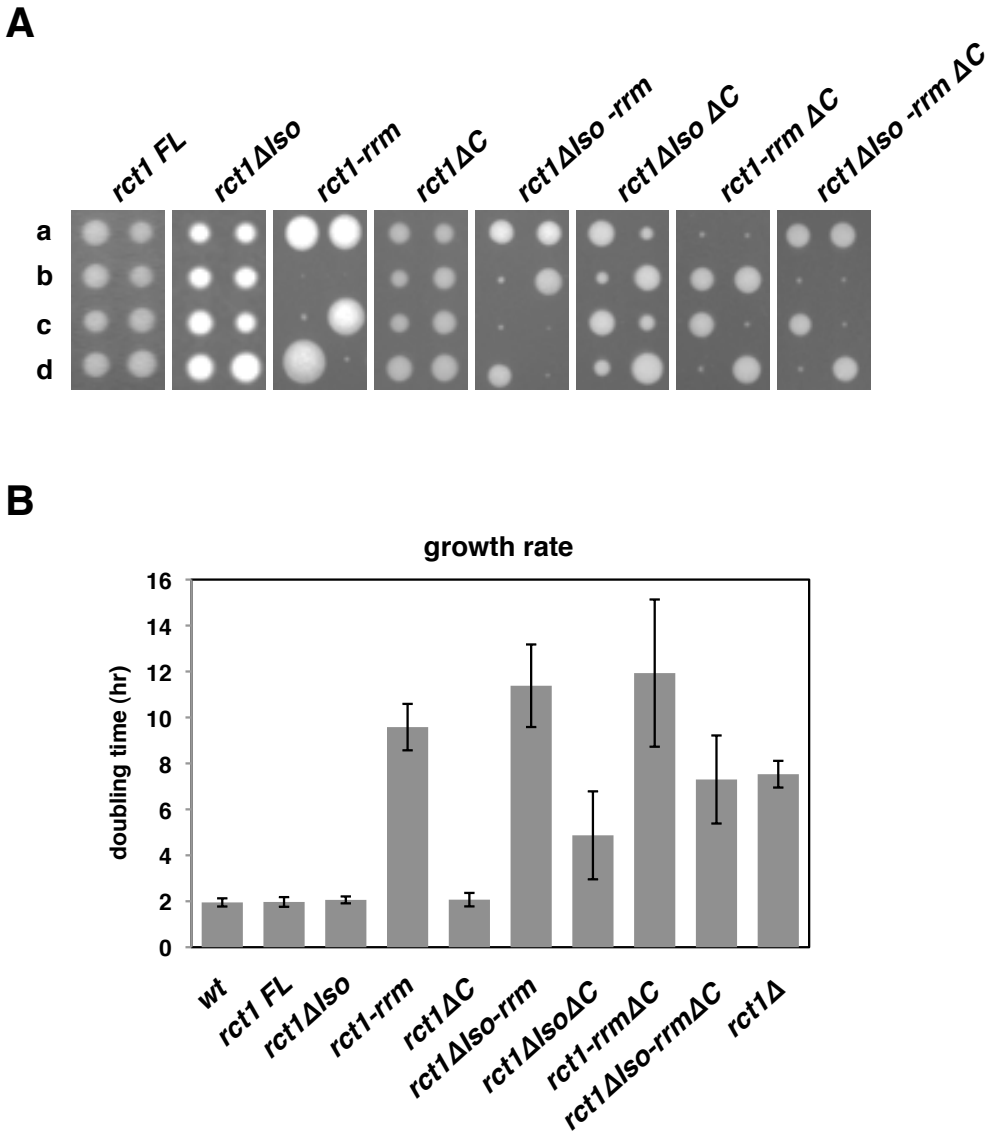

Figure 2.16 The RNA recognition motif of Rct1 is essential for normal cell growth

(A) Heterozygous diploid tetrad dissection plate. a, b, c and d indicates siblings from the same ascus. Haploid cells carry *rct1-rrm* mutant alleles are the small colonies as confirmed by drug resistance and PCR. Two tetrads were shown for each diploid.
(B) Cell growth rate measured by OD_{600} in indicated haploid strains.

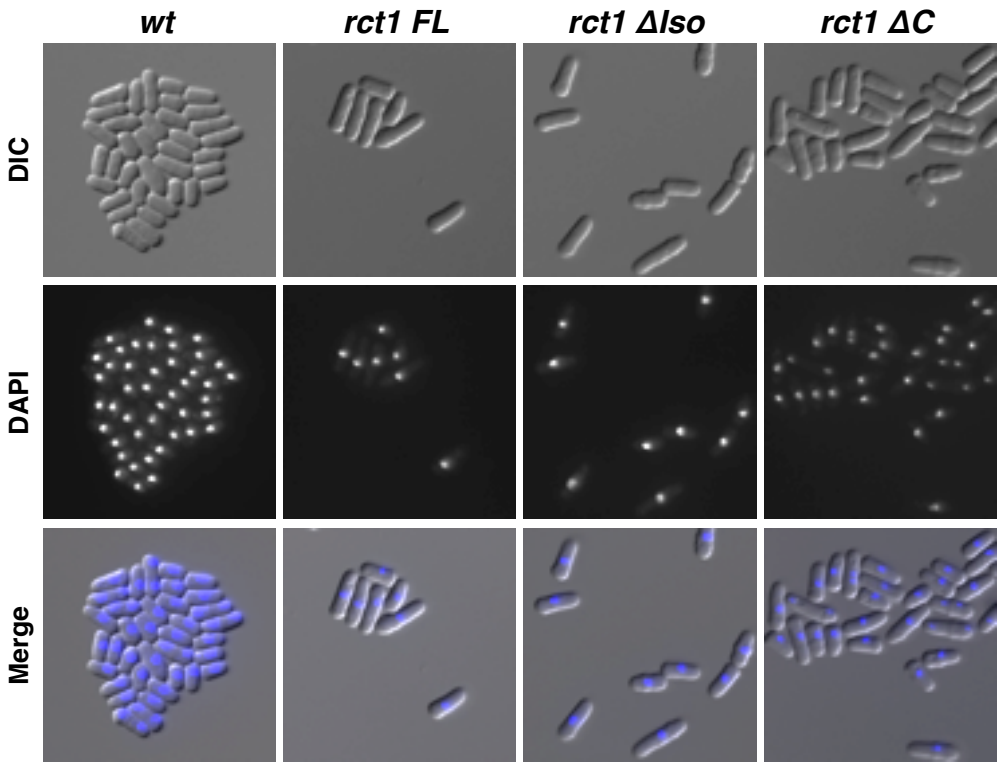

Figure 2.17 The PPIase and C-terminal domains of Rct1 are not required for normal cell morphology

Cell morphology in indicated strains. DIC (differential interference contrast) shows the cell shape, DAPI stains nuclei.

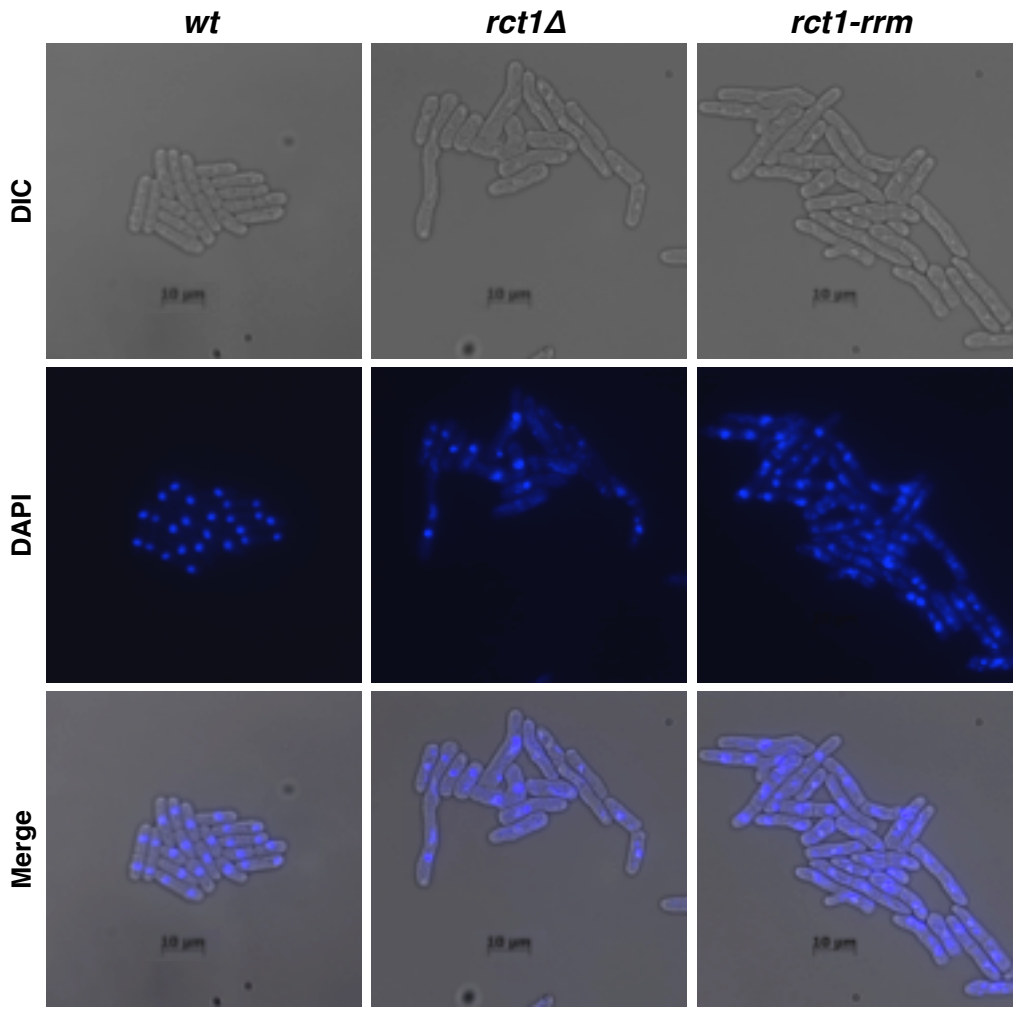

Figure 2.18 The RNA recognition motif of Rct1 is essential for normal cell morphology

Cell morphology in indicated strains. DIC (differential interference contrast) shows the cell shape, DAPI stains nuclei.

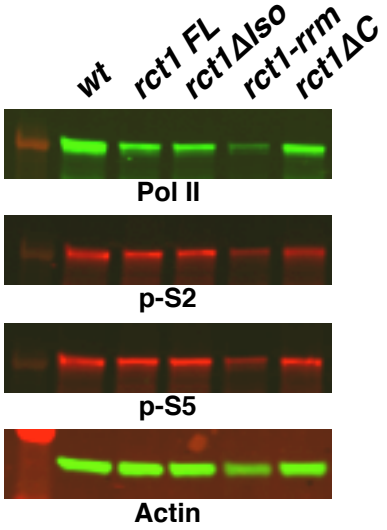

Figure 2.19 Reduced Pol II protein levels in *rct1-rrm* mutant cells

Pol II protein levels were analyzed by western blot in indicated strains. Different phosphorylated forms of Pol II were analyzed. Actin serves as loading control.

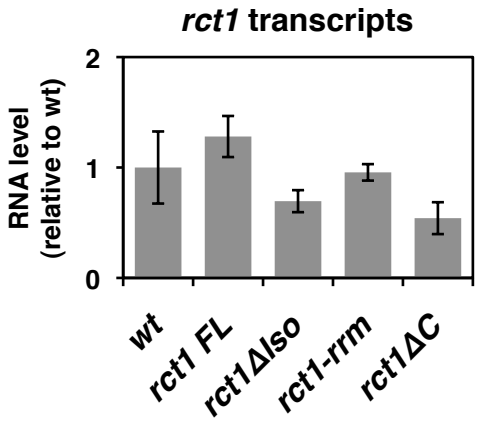

Figure 2.20 *rct1* domain specific mutations had no effect on *rct1* transcript levels

RT-qPCR analysis of *rct1* transcript expression levels in mutant strains as indicated. *actin* transcript levels were used for normalization by ΔΔCT method. Y-axis represents RNA expression levels relative to wild type. qPCR reaction was performed three times for each strain. Error bars indicate SEM.

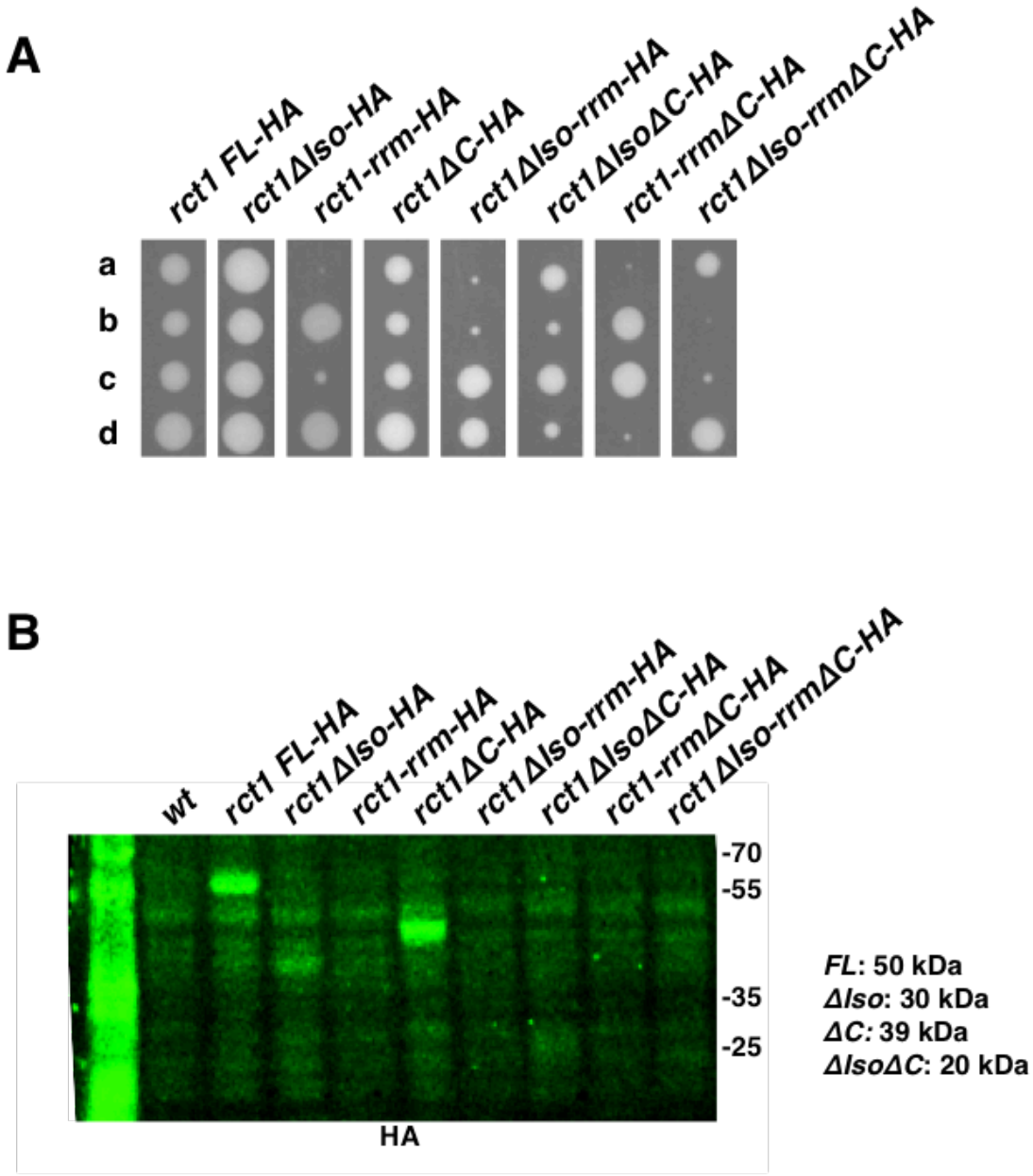

Figure 2.21 Rct1 protein levels are affected in domain specific mutations

(A) Heterozygous diploid tetrad dissection plate. a, b, c and d indicates siblings from the same ascus. Haploid cells carry HA-tagged *rct1-rrm* mutant alleles are the small colonies as confirmed by drug resistance and PCR.
(B) Rct1 protein levels were analyzed by western blot in indicated strains. HA antibody was used to detect C-terminal HA-tagged Rct1.

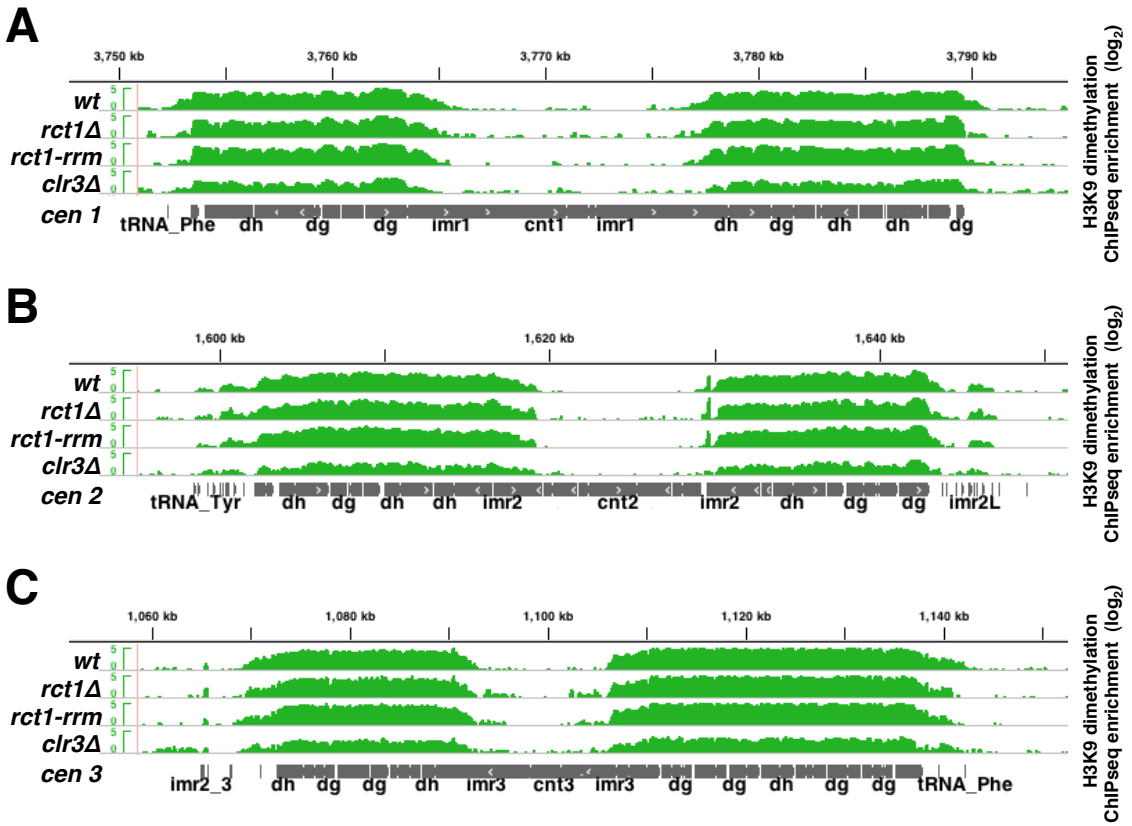

Figure 2.22 The distribution of H3K9 dimethylation at pericentromeric heterochromatin

H3K9me2 enrichment and distribution in indicated strains. ChIPseq tracks (green), centromeres (grey). Y-axis represents the log scale of enrichment. Positive value indicates enrichment after IP as compared to input controls, only positive values were shown.
(A) centromere 1 **(B)** centromere 2 **(C)** centromere 3

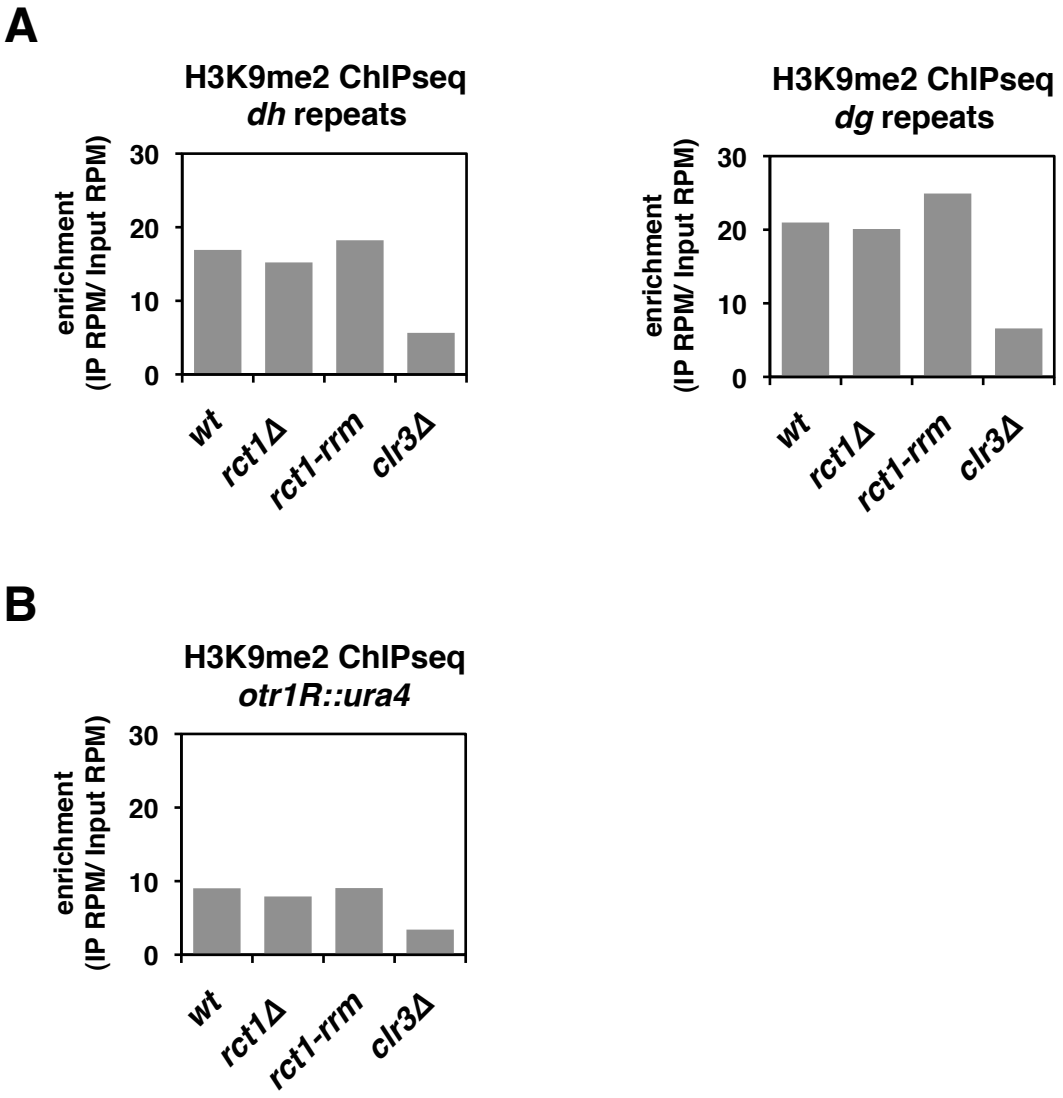

Figure 2.23 Quantification of H3K9 dimethylation levels at pericentromeric heterochromatin

(A) Quantification of H3K9me2 enrichment in indicated strains at endogenous *dh/dg* repeats
(B) Quantification of H3K9me2 enrichment in indicated strains at *otr1R*::*ura4* transgene region

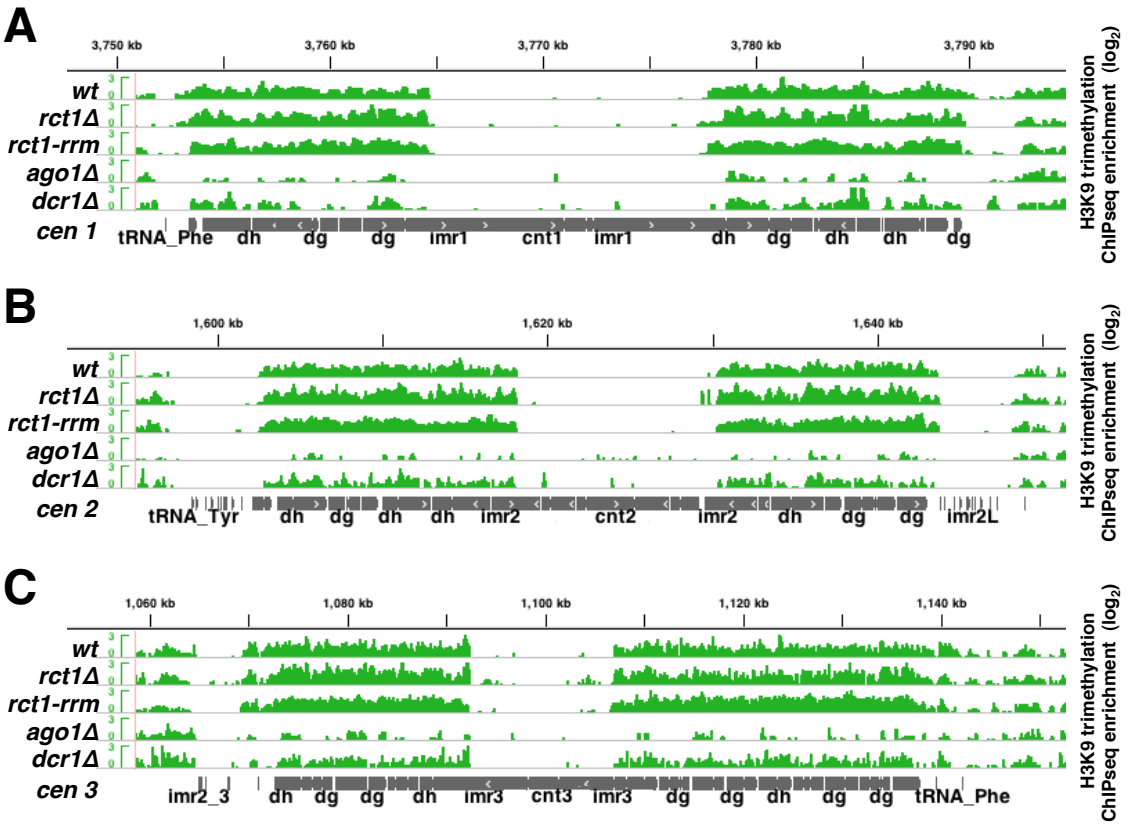

Figure 2.24 The distribution of H3K9 trimethylation at pericentromeric heterochromatin

H3K9me3 enrichment and distribution in indicated strains. ChIPseq tracks (green), centromeres (grey). Y-axis represents the log scale of enrichment. Positive value indicates enrichment after IP as compared to input controls, only positive values were shown.
(A) centromere 1 **(B)** centromere 2 **(C)** centromere 3

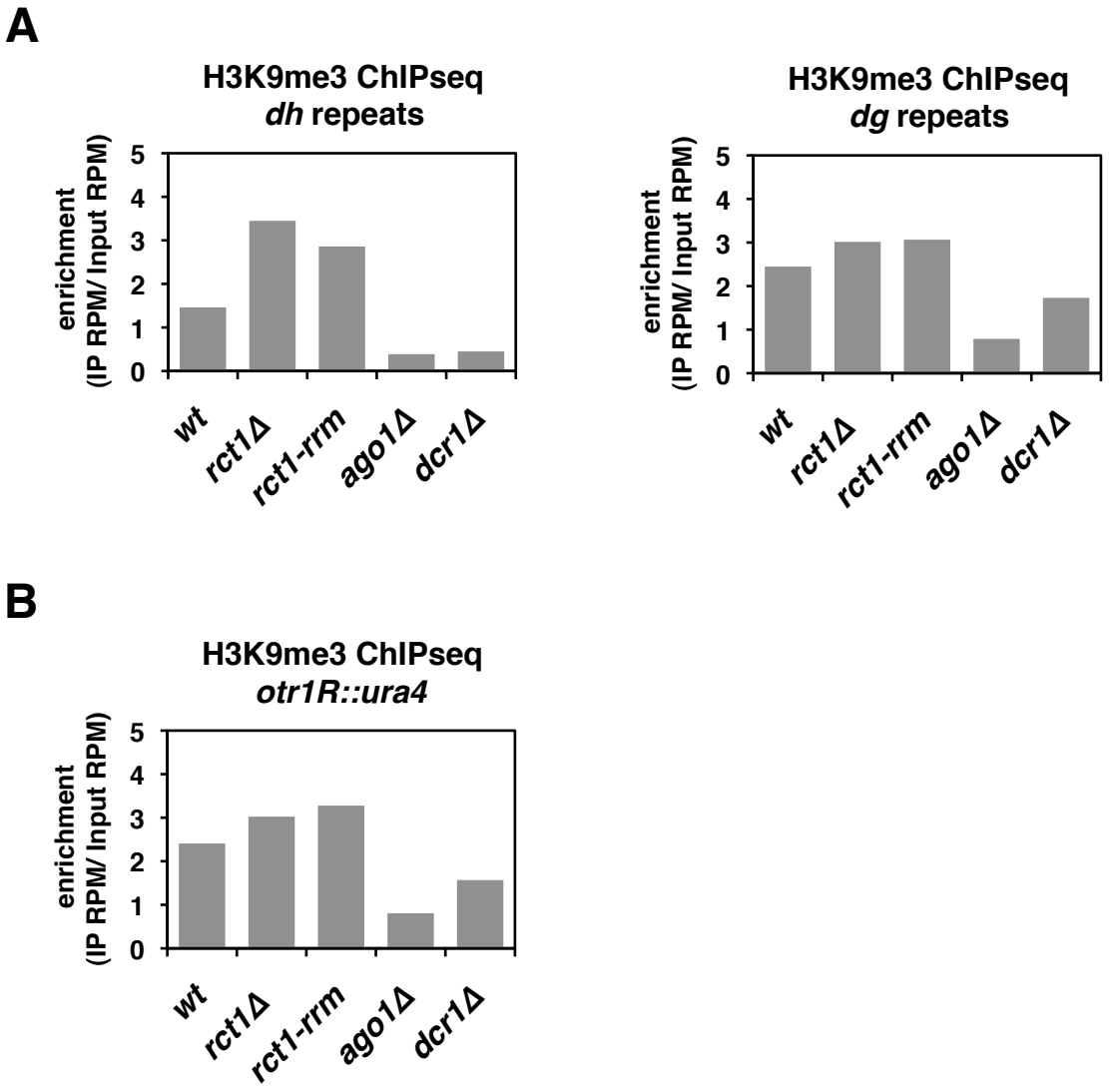

Figure 2.25 Quantification of H3K9 trimethylation levels at pericentromeric heterochromatin

(A) Quantification of H3K9me3 enrichment in indicated strains at endogenous *dh/dg* repeats.
(B) Quantification of H3K9me3 enrichment in indicated strains at *otr1R*::*ura4* transgene region.

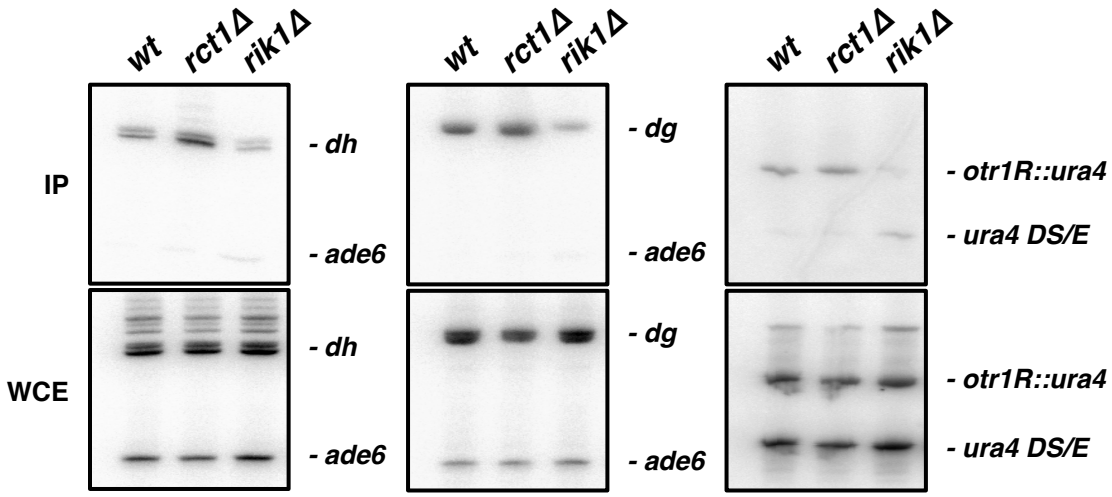

Figure 2.26 Rct1 does not affect Swi6 association at pericentromeric heterochromatin

Chromatin immunoprecipitation with Swi6 antibody in indicated strains. *dh/dg* and *otr1R::ura4* transgene regions were examined. *ade6* and truncated *ura4-DS/E* at the endogenous locus serve as loading controls.

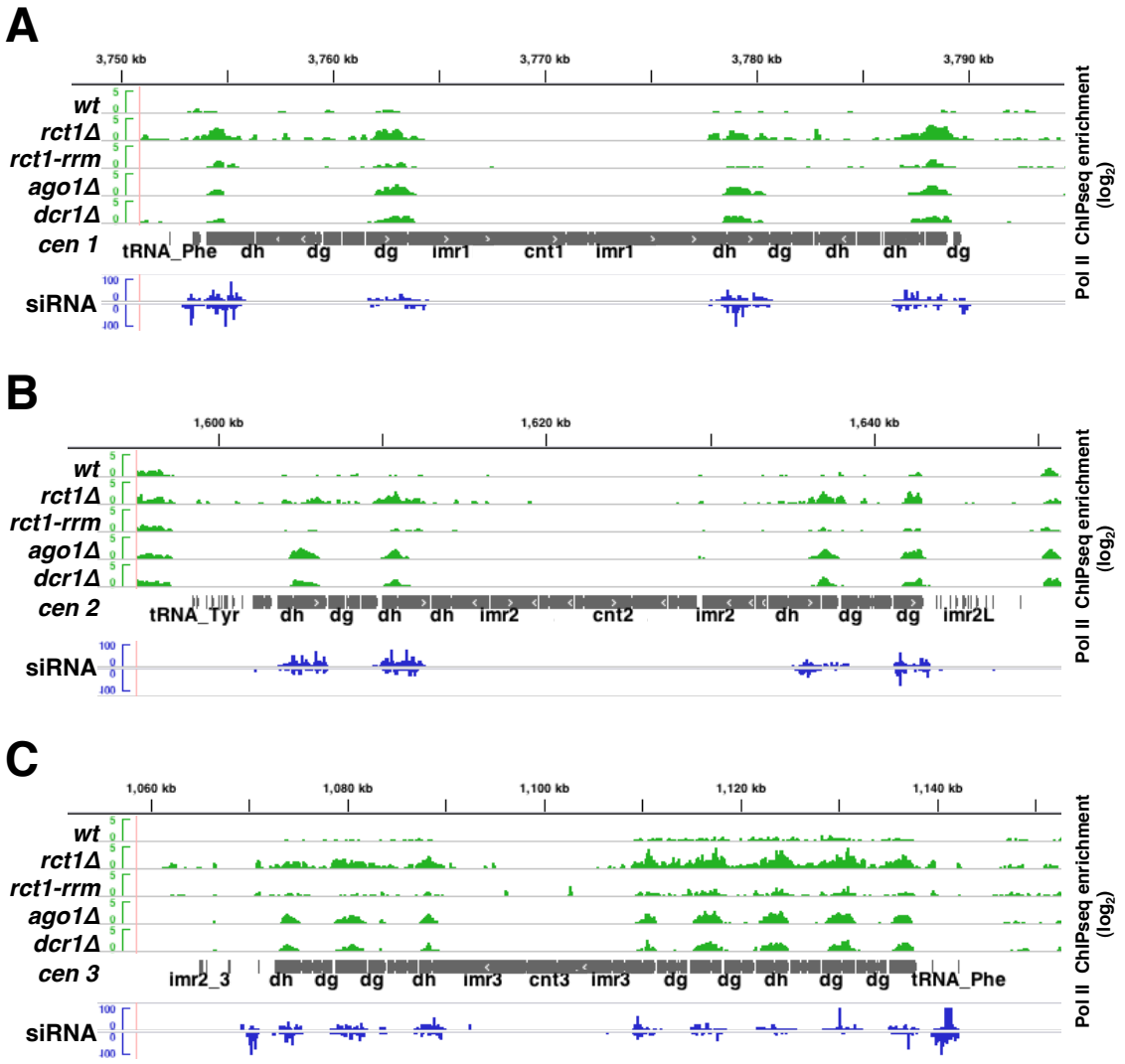

Figure 2.27 The distribution of Pol II at pericentromeric heterochromatin

Total Pol II enrichment and distribution in indicated strains. ChIPseq tracks (green), small RNAseq tracks from wild type (blue), centromeres (grey). Y-axis represents the log scale of enrichment. Positive value indicates enrichment after IP as compared to input controls, only positive values were shown.
(A) centromere 1 **(B)** centromere 2 **(C)** centromere 3

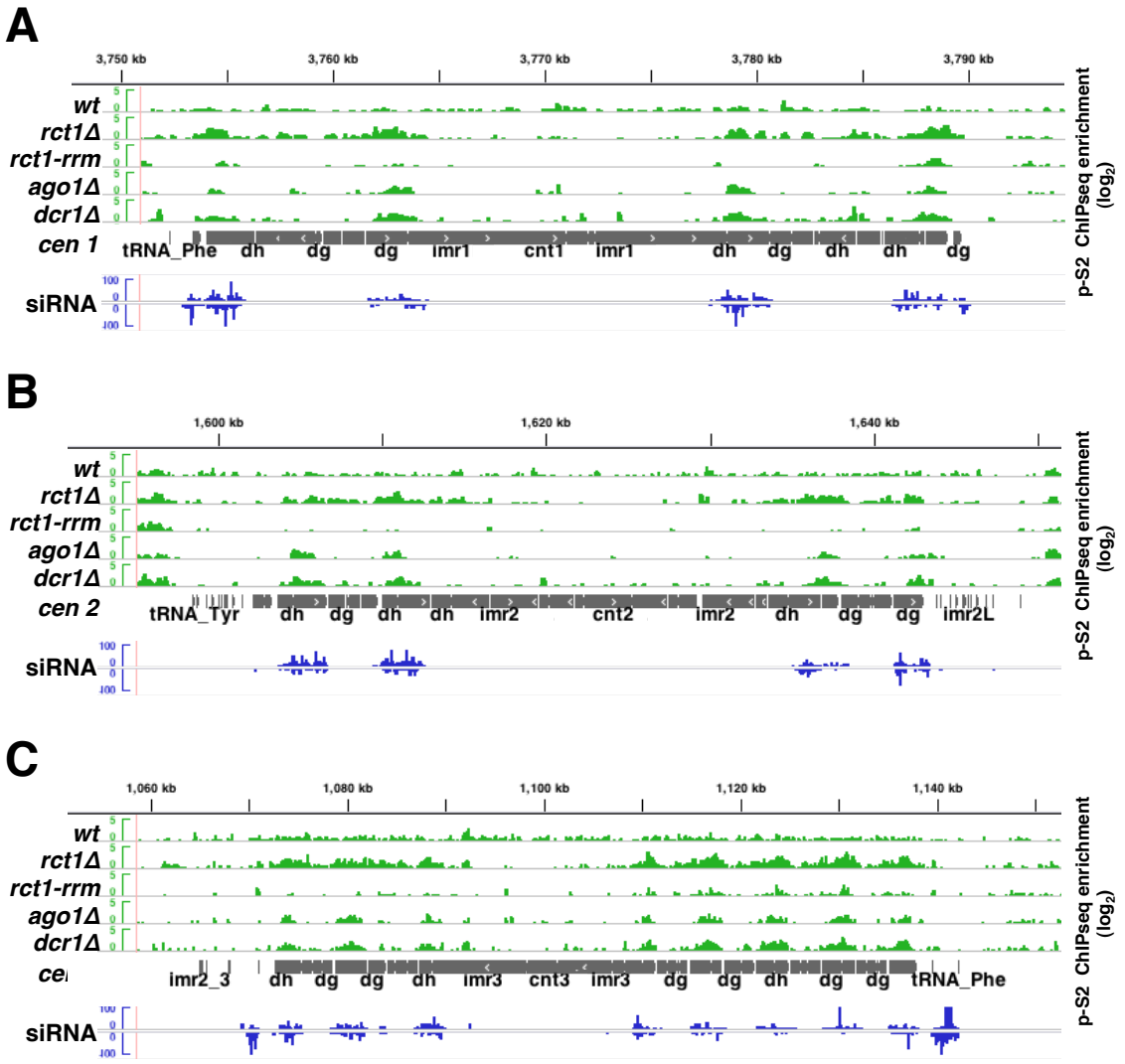

Figure 2.28 The distribution of serine 2 phosphorylated Pol II at pericentromeric heterochromatin

p-S2 Pol II enrichment and distribution in indicated strains. ChIPseq tracks (green), small RNAseq tracks from wild type (blue), centromeres (grey). Y-axis represents the log scale of enrichment. Positive value indicates enrichment after IP as compared to input controls, only positive values were shown.
(A) centromere 1 **(B)** centromere 2 **(C)** centromere 3

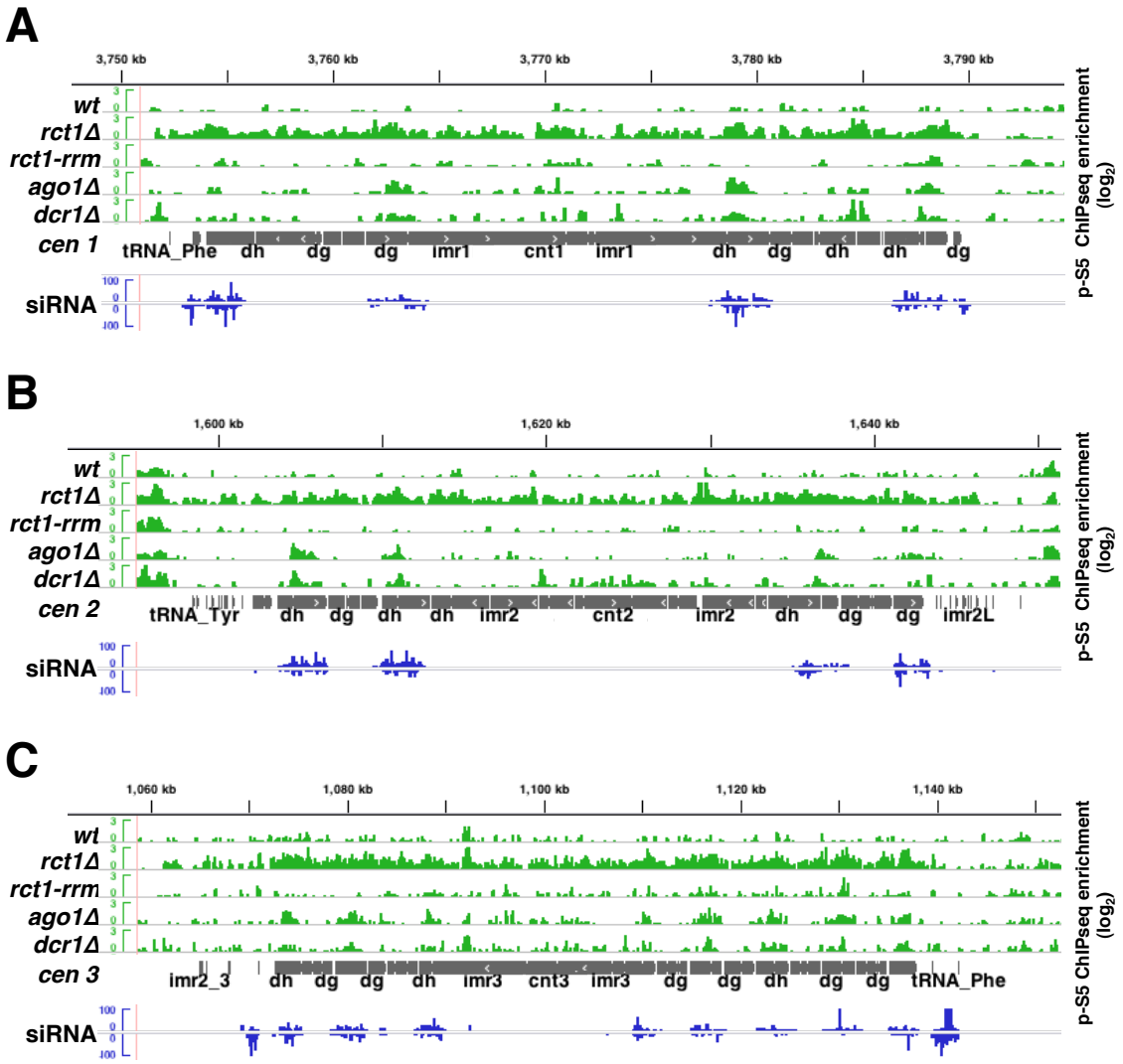

Figure 2.29 The distribution of serine 5 phosphorylated Pol II at pericentromeric heterochromatin

p-S5 Pol II enrichment and distribution in indicated strains. ChIPseq tracks (green), small RNAseq tracks from wild type (blue), centromeres (grey). Y-axis represents the log scale of enrichment. Positive value indicates enrichment after IP as compared to input controls, only positive values were shown.
(A) centromere 1 **(B)** centromere 2 **(C)** centromere 3

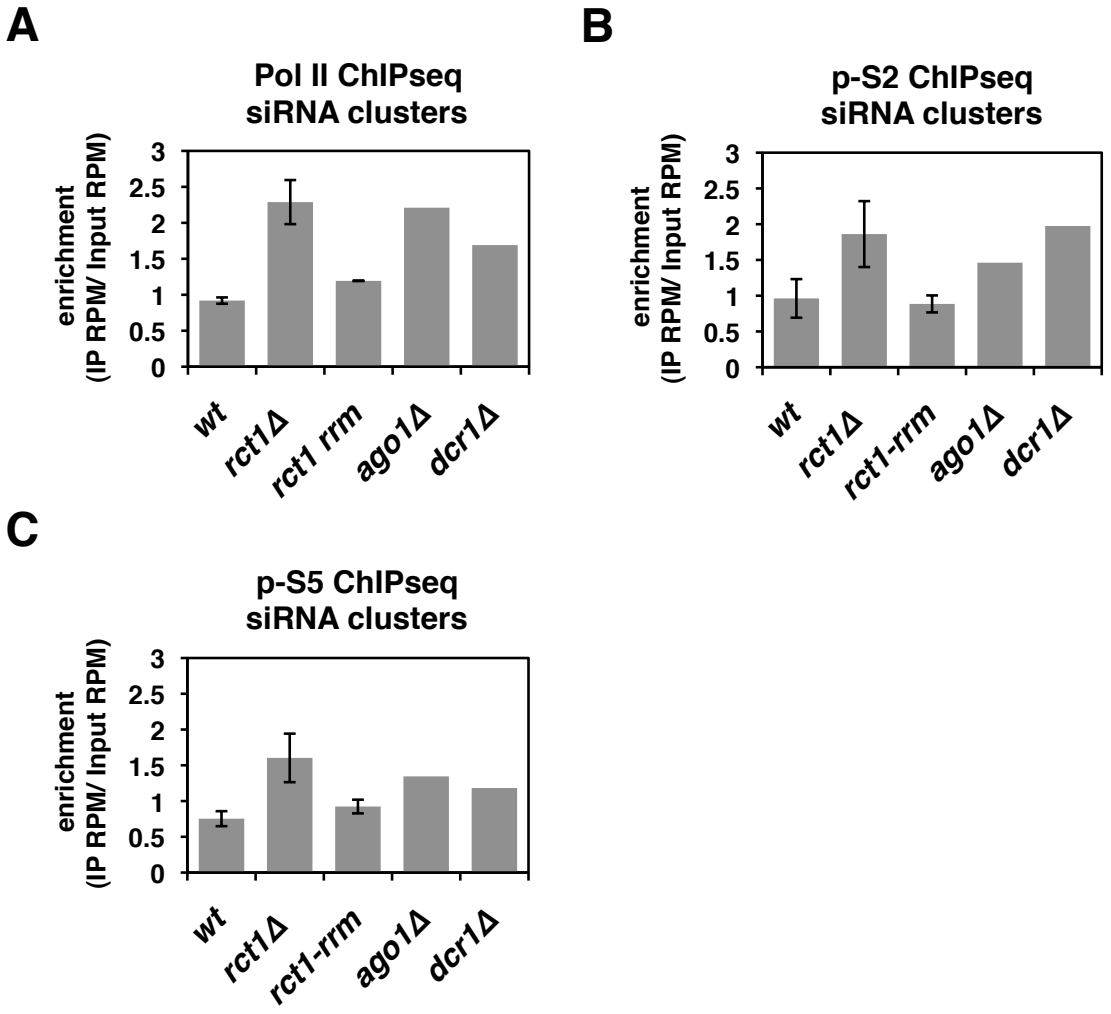

Figure 2.30 Quantification of Pol II accumulation levels at siRNA clusters

Quantification of Pol II enrichment within siRNA clusters in indicated strains. siRNA cluster regions were defined by > 100 siRNA counts on genome browser tracks. Data from two biological replicates of *rct1Δ* mutant cells were analyzed. Two independent ChIP experiments were performed and libraries were constructed independently, with the exception of *ago1Δ* and *dcr1Δ* mutants, where one ChIP experiment was done. Error bar indicates SEM.
(A) Total Pol II
(B) Serine 2 phosphorylated Pol II
(C) Serine 5 phosphorylated Pol II

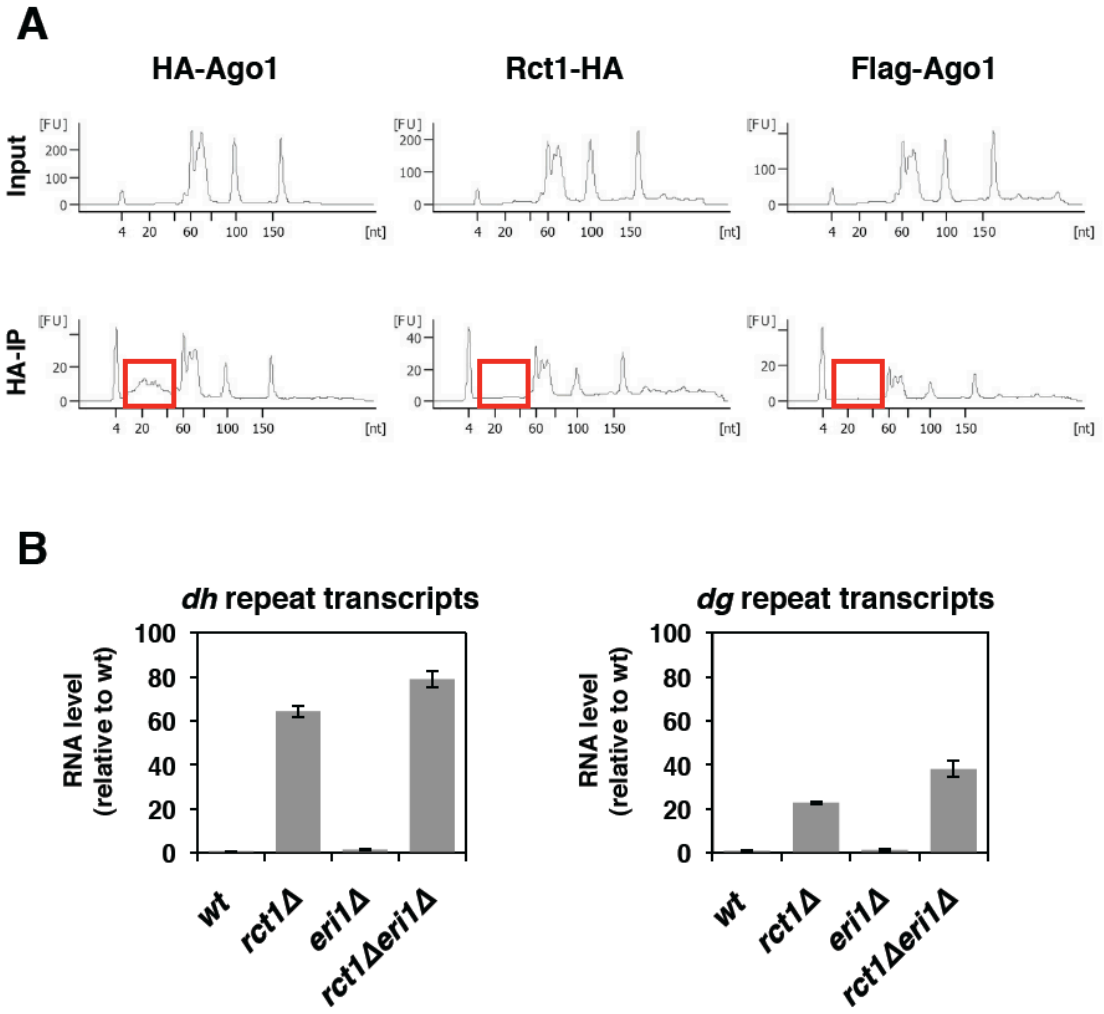

Figure 2.31 Rct1 neither binds to siRNAs nor mediates siRNA stability

(A) RNA-IP was performed in indicated strains by using HA affinity matrix. RNA was purified after IP and ran on a bioanalyzer small RNA chip. HA-Ago1 was used as a positive control, Flag-Ago1 was used as a negative control. Red box marks the region of small RNA enrichment.
(B) RT-qPCR analysis of *dh*/*dg* transcript expression levels in mutant strains as indicated. *actin* transcript levels were used for normalization by ΔΔCT method. Y-axis represents RNA expression levels relative to wild type. At least two biological replicates were used for each genotype and qPCR reaction was performed twice for each strain. Error bars indicate SEM.

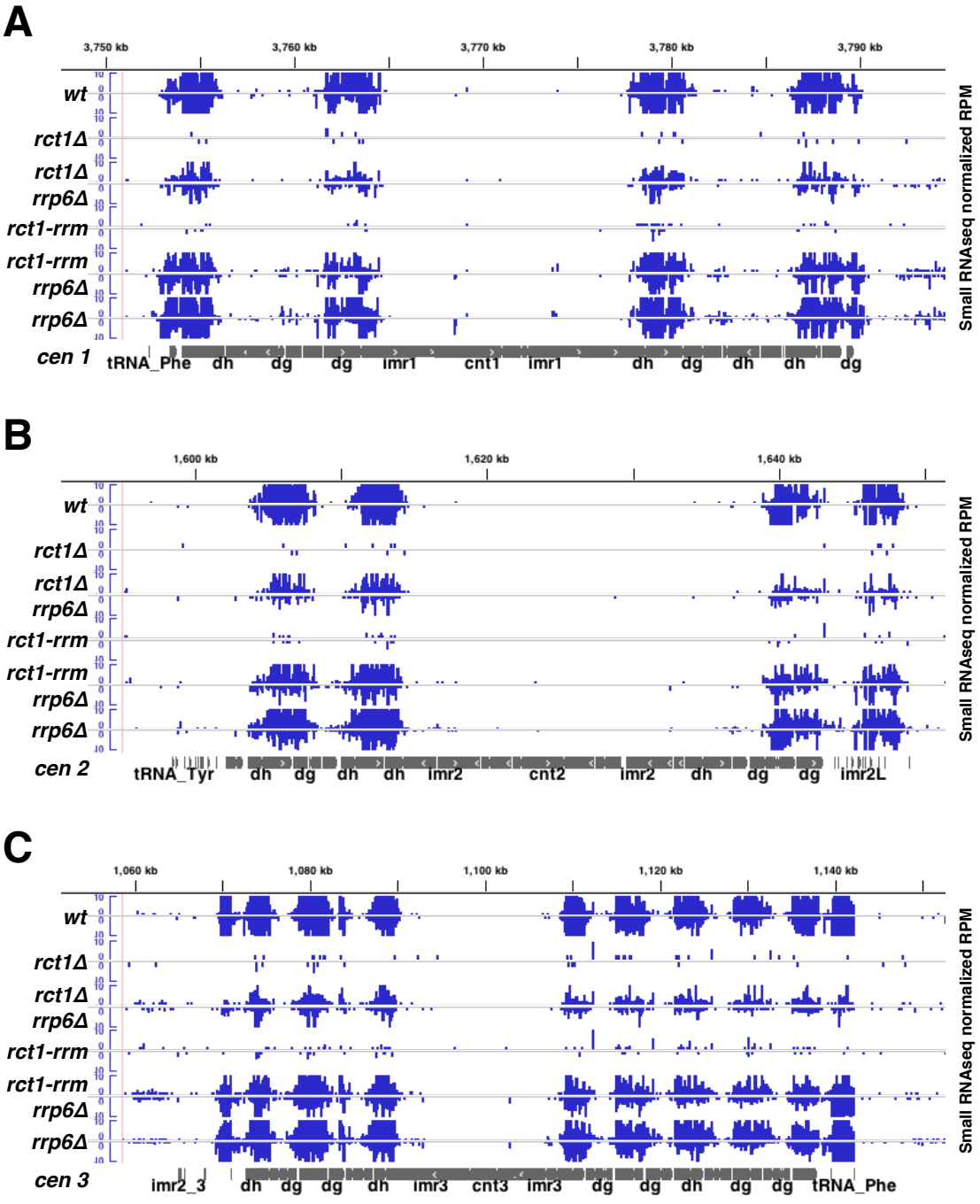

Figure 2.32 siRNA biogenesis triggered by loss of *rrp6* in *rct1* mutant cells

Pericentromeric siRNA levels and distribution in indicated strains. Small RNAseq tracks (blue), centromeres (grey). Y-axis represents normalized reads in each library (RPM). **(A)** centromere 1 **(B)** centromere 2 **(C)** centromere 3

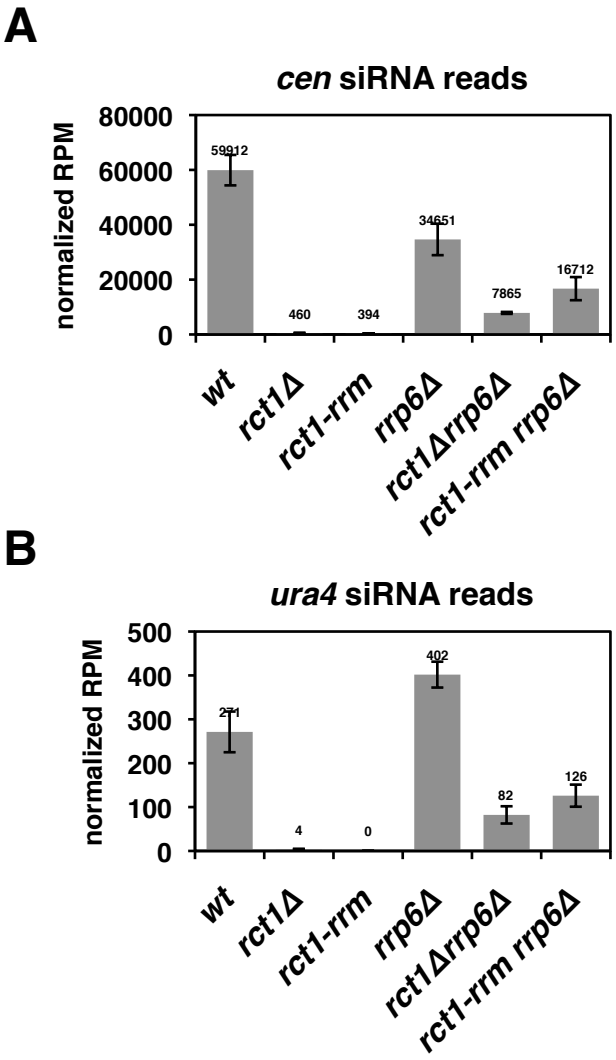

Figure 2.33 Quantification of pericentromeric siRNA biogenesis restored by loss of *rrp6* in *rct1* mutant cells

(A) Quantification of *cen* siRNAs in indicated strains. Y-axis represents normalized reads in each library (RPM). Data from two biological replicates of each strain were analyzed with the exception of *rct1-rrm* mutant cells, where data from one strain was analyzed. Error bars indicate SEM.
(B) Quantitative analysis of *ura4* siRNA levels in indicated strains as described in (A).

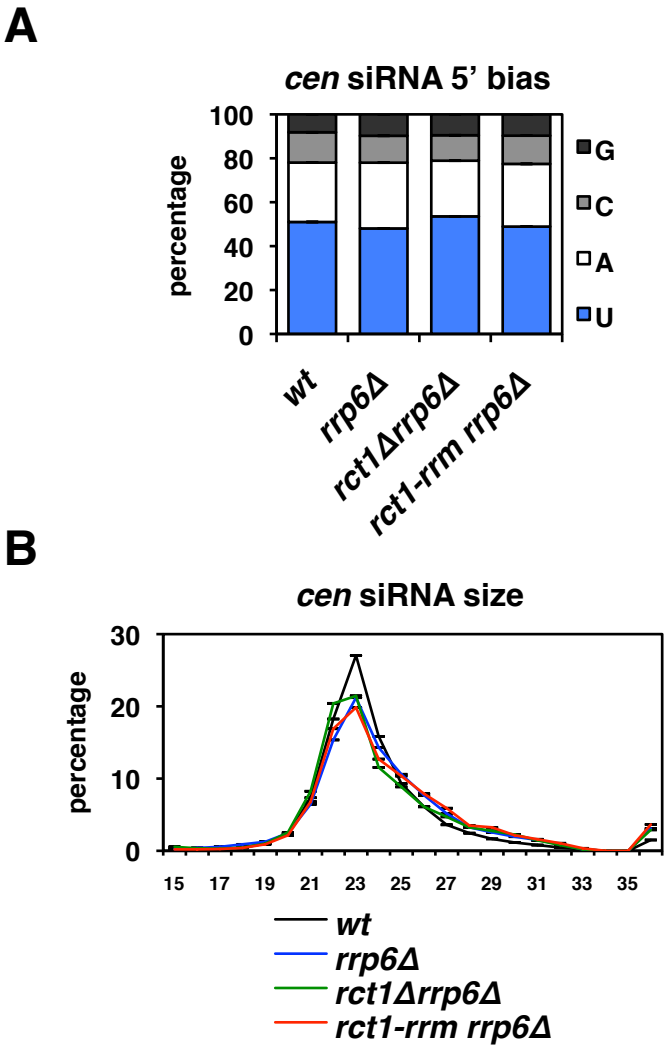

Figure 2.34 Pericentromeric siRNA profiles in *rct1Δrrp6Δ* and *rct1-rrm rrp6Δ* mutant cells

(A) The frequency of 5' nucleotide occurrence in *cen* siRNA reads in indicated strains. Y-axis represents percentage of each nucleotide. Data from two biological replicates were analyzed.
(B) The size distribution of *cen* siRNA reads in indicated strains. Y-axis represents percentage of each siRNA length between 15 to 36 bp. Data from two biological replicates were analyzed.

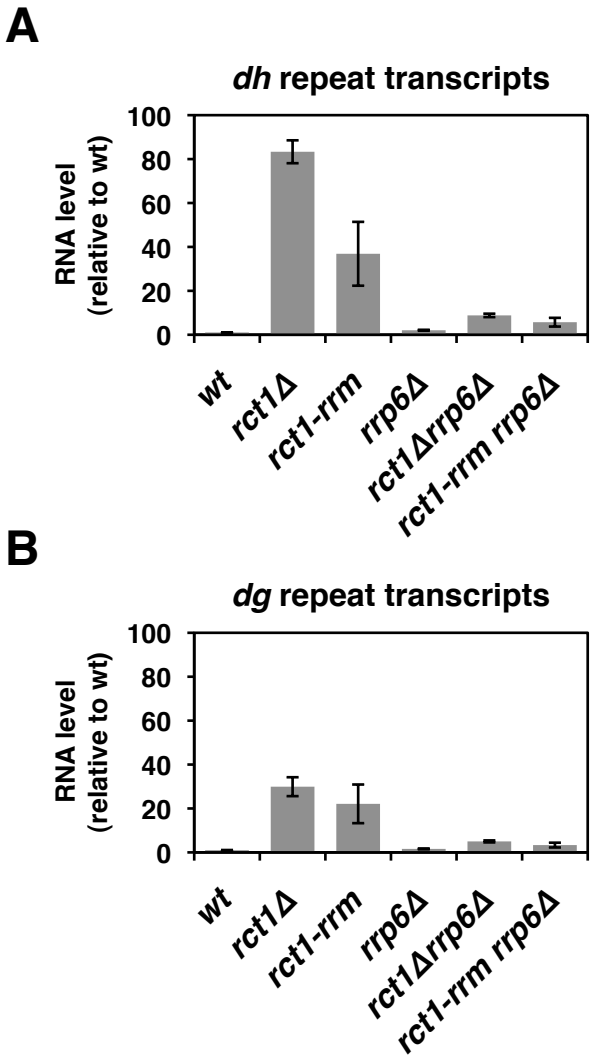

Figure 2.35 Loss of *rrp6* in *rct1* mutant cells induces pericentromeric heterochromatin silencing

RT-qPCR analysis of *dh*/*dg* transcript expression levels in mutant strains as indicated. *actin* transcript levels were used for normalization by ΔΔCT method. Y-axis represents RNA expression levels relative to wild type. Two biological replicates were used for each genotype and qPCR reactions were performed in triplicate for each strain. Error bars indicate SEM.

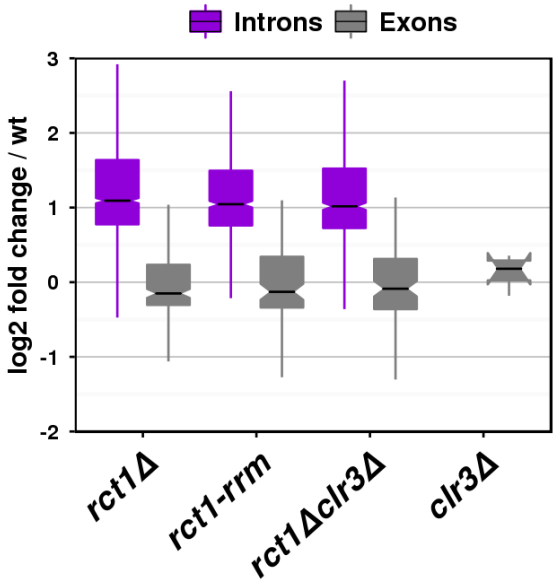

Figure 2.36 Impaired splicing in *rct1* mutant cells

Log_2 fold changes are shown for all differentially expressed introns and exons. RNAseq data were analyzed by DEXSeq with false discovery rate < 0.05. Boxes represent the interquartile range (IQR) bisected by the median. Whiskers extend to the lesser of IQR x 1.5 or the most extreme observation. Introns, purple box; exons, grey box.

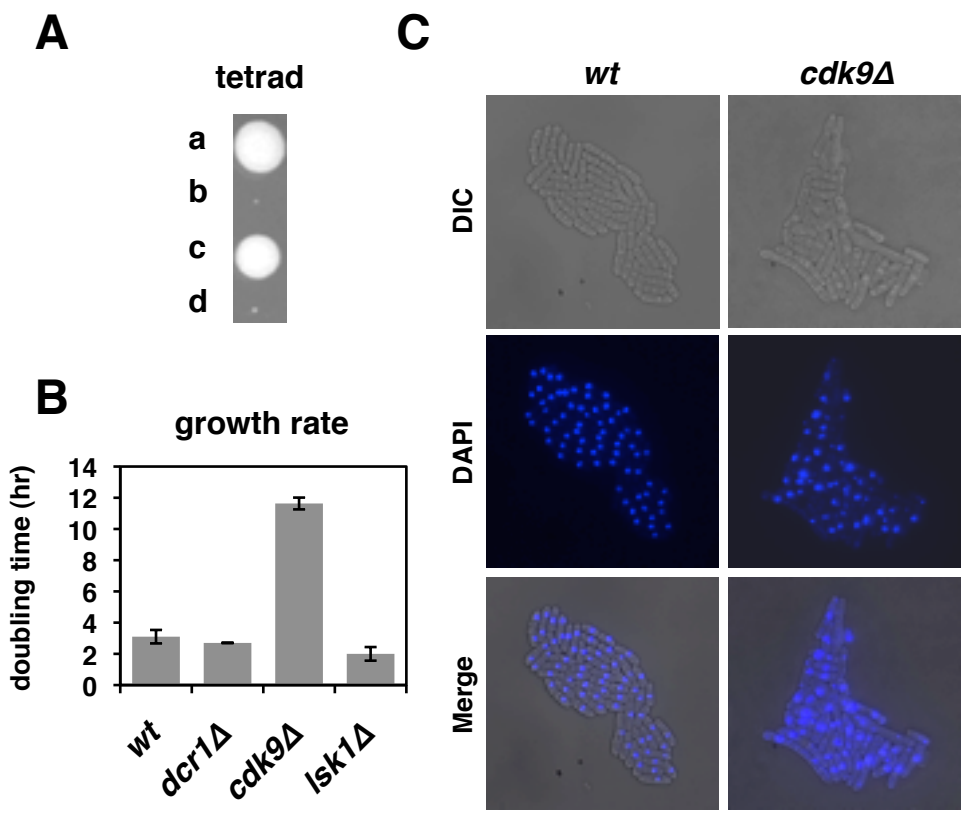

Figure 2.37 *cdk9* is a non-essential gene required for normal cell growth and morphology

(A) A full tetrad. a, b, c and d indicates siblings from the same ascus. Haploid cells carrying *cdk9* null allele are the small colonies as confirmed by drug resistance and PCR.
(B) Cell growth rate measured by OD_{600} in indicated strains.
(C) Cell morphology in indicated strains. DIC (differential interference contrast) shows the cell shape, DAPI stains nuclei.

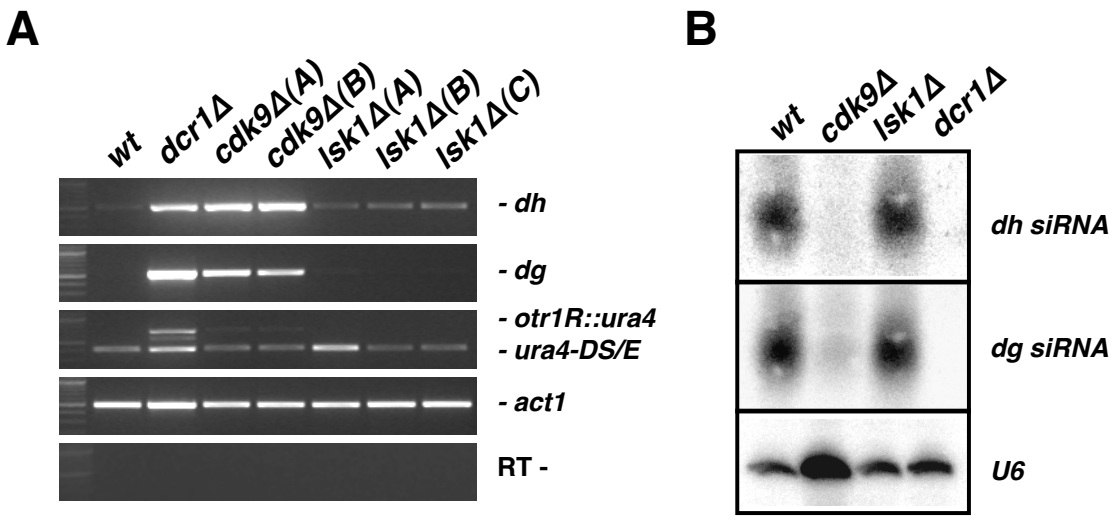

Figure 2.38 Cdk9 is essential for pericentromeric heterochromatin silencing and siRNA biogenesis

(A) Semi-quantitative RT-PCR showing *dh*/*dg* and *otr1R*::*ura4* transcript levels in indicated strains. Biological replicates are labeled as A, B and C. Truncated *ura4-DS/E* at the endogenous locus and *act1* serve as loading controls, RT- omits the reverse transcription step.
(B) Small RNA northern blots of pericentromeric *dh*/*dg* derived siRNAs in indicated strains. *U6* serves as loading control.

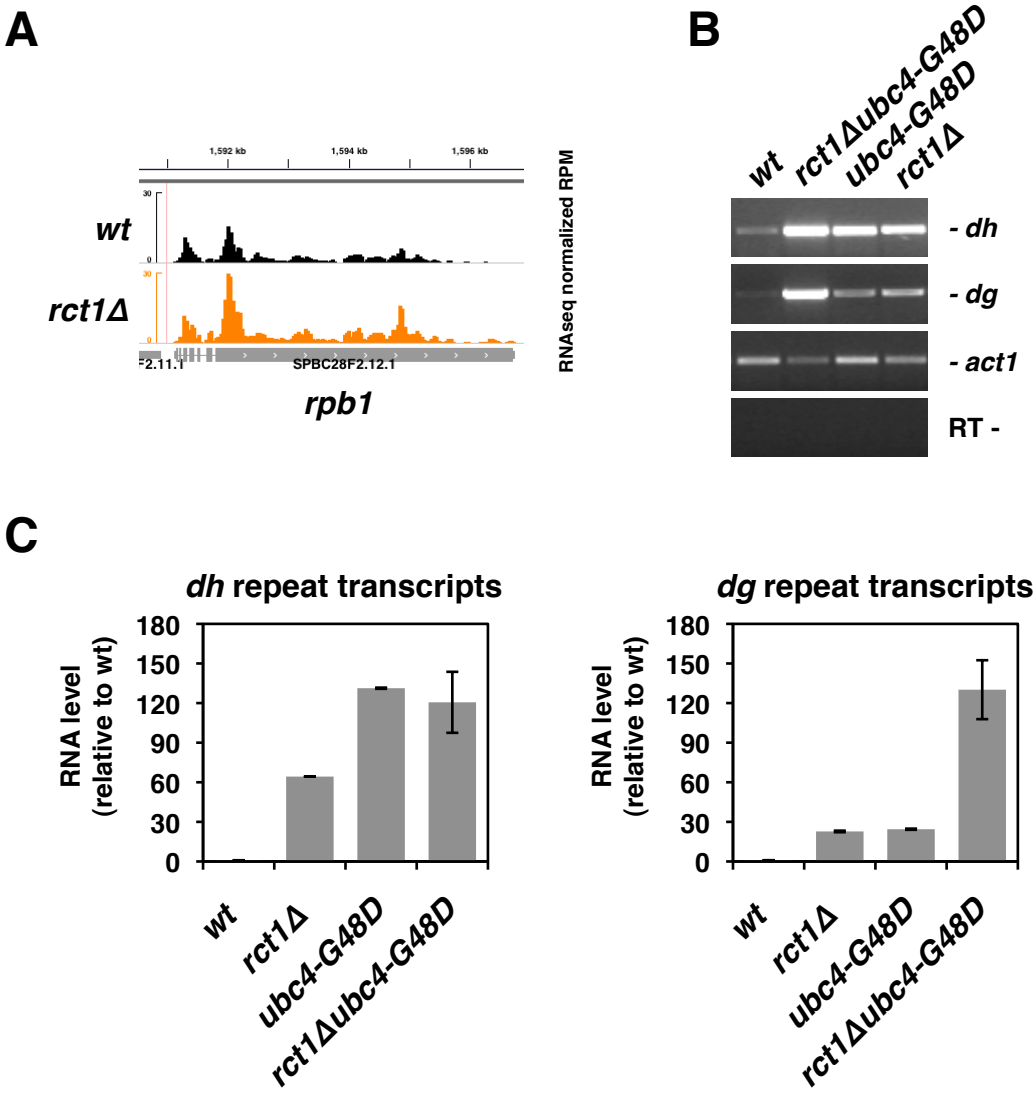

Figure 2.39 Ubc4 is essential for pericentromeric heterochromatin silencing

(A) Pol II large subunit *rpb1* transcript level in indicated strains shown by RNAseq. Y-axis represents normalized reads in each library (RPM).
(B) Semi-quantitative RT-PCR showing *dh*/*dg* and *otr1R*::*ura4* transcript levels in indicated strains. *act1* serve as loading controls, RT- omits the reverse transcription step.
(C) RT-qPCR analysis of *dh*/*dg* transcript expression levels in indicated strains. *actin* transcript levels were used for normalization by ΔΔCT method. Y-axis represents RNA expression levels relative to wild type. Two biological replicates were analyzed for each genotype with the exception of *ubc4-G48D* mutant cells, where data from one strain was analyzed. qPCR reaction was done in duplicates for each strain. Error bars indicate SEM.

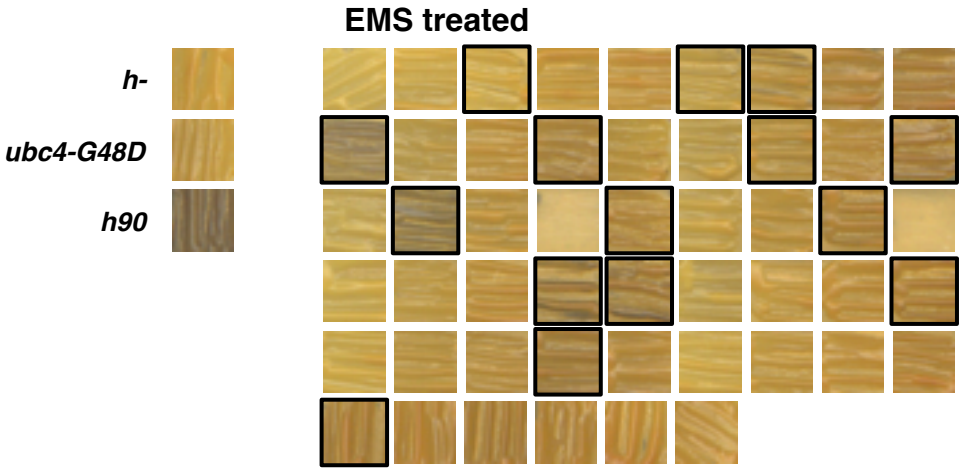

Figure 2.40 *ubc4-G48D* suppressors identified by EMS mutagenesis

Spore formation in indicated strains detected by iodine staining. *h-* is the non-sporulating control; *h90* is the sporulating control. *ubc4-G48D* is the parental strain before EMS mutagenesis. Colonies show increased iodine staining after EMS treatment is marked in black box.

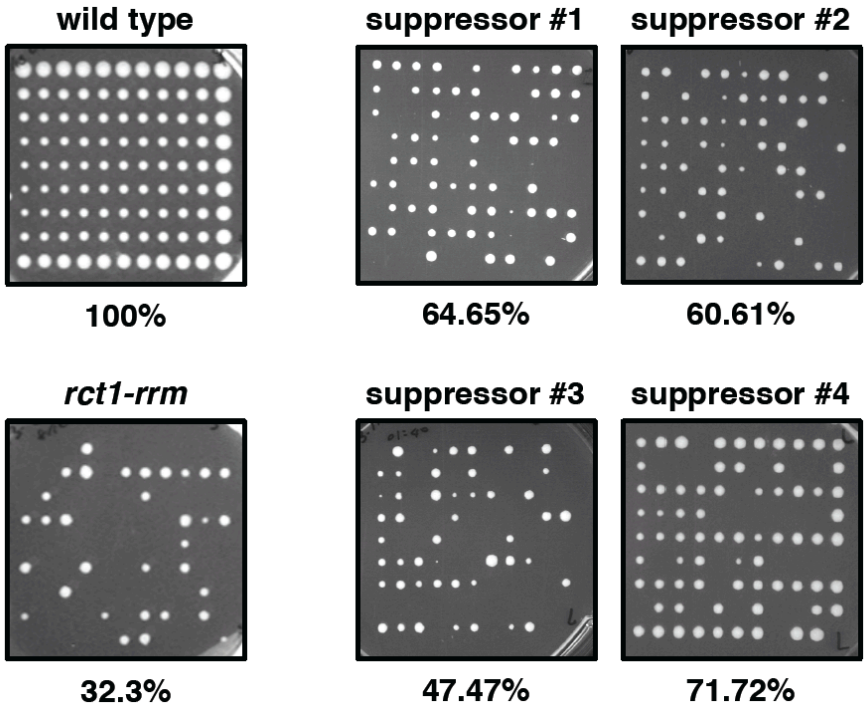

Figure 2.41 Naturally occurred Rct1 suppressors

Four representative strains carrying potential suppressors are shown, percentage indicates survival rate calculated by (visible colony number)/(dissected cell number). Parental *rct1-rrm* mutant cells and wild type cells are included to show the improvement of survival rate.

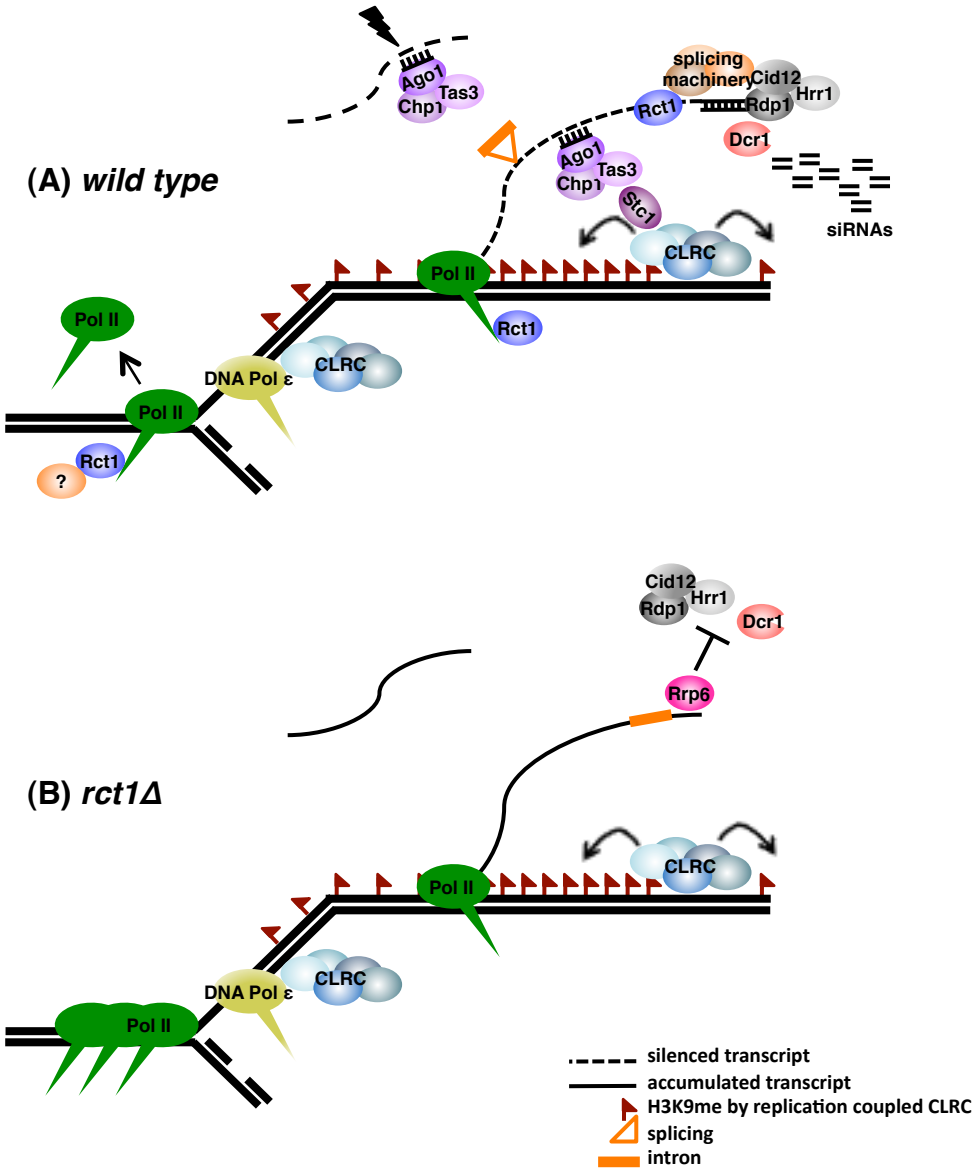

Figure 2.42 Model of Rct1 mediated siRNA biogenesis

This illustration shows a partial replication fork at the pericentromeric repeats.
(A) In wild type cells, Rct1 is engaged with Pol II transcription. Rct1 binds to nascent transcripts via its RRM and recruits the splicing machinery. Weak splice site signals stall splicing and stimulate siRNA production by the RNAi machinery instead. The siRNA-loaded RITS complex recruits the CLRC to deposit H3K9 methylation marks to establish H3K9 methylation. At the transcription and replication collision site, Rct1 mediates Pol II removal to allow replication fork progression and replication coupled H3K9 spreading.
(B) In *rct1Δ* mutant cells, spliceosome fails to assemble at the nascent transcripts. These unspliced transcripts are mis-targeted by Rrp6, preventing RNAi from targeting these transcripts, thereby causing the siRNA biogenesis defect. Full H3K9 methylation is achieved by CLRC recognizing pre-existing H3K9 methylation marks and translocation via slow replication forks.

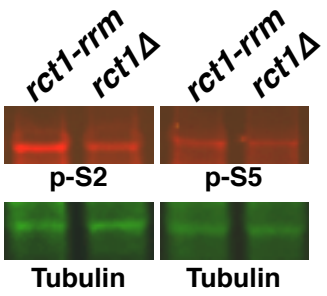

Figure 2.43 Pol II protein levels in *rct1* mutants

Pol II protein levels were analyzed by western blot in indicated strains. Different phosphorylated forms of Pol II were analyzed. Tubulin serves as loading control.

***rct1Δ* RNAseq**

systemic ID	gene	exon number	baseMean	log2FoldChange	pvalue
SPAC13G7.07	arb2	6	238.02	1.44	9.16E-06
SPAC17G8.13c	mst2	3	1459.01	1.31	1.74E-08
SPAC31G5.18c	sde2	1	950.71	1.39	1.19E-16
SPAC3G9.07c	hos2	1	709.93	-1.09	0.000219199
SPBC18E5.03c	sim4	2	735.81	1.05	0.000754247
SPBP8B7.28c	stc1	1	140.34	1.48	0.001095459
SPCC1393.05	ers1	11	359.47	1.52	2.35E-05
SPCC1739.03	hrr1	4	1266.44	1.30	4.54E-06
SPCC188.13c	dcr1	1	1733.90	1.17	2.10E-07
SPCC4G3.18	rix1	1	3020.99	-1.04	0.000229945
SPCC830.03	grc3	2	1339.95	-1.17	2.74E-14
SPCC970.07c	raf2	1	519.24	1.15	8.77E-08

***rct1-rrm* RNAseq**

systemic ID	gene	exon number	baseMean	log2FoldChange	pvalue
SPAC13G7.07	arb2	6	238.02	1.70	1.96E-07
SPAC140.03	arb1	5	1080.58	1.61	6.83E-15
SPBC1105.04c	cbp1	1	1486.37	-1.34	2.17E-05
SPBC16C6.10	chp2	2	497.83	1.66	5.35E-08
SPBC18E5.03c	sim4	2	735.81	1.60	2.75E-07
SPCC1393.05	ers1	11	359.47	1.55	1.79E-05
SPCC1739.03	hrr1	4	1266.44	2.19	1.02E-14
SPCC645.08c	snd1	1	2556.45	-1.38	3.66E-13

Table 2.1 Differentially expressed silencing genes in *rct1* mutants based on a two-fold cut-off

2.4 Materials and Methods

Fission yeast strains and standard manipulation

S. pombe strains and primers used in this study are described in Tables 2.2 and 2.3, respectively. Deletion mutants were generated by standard PCR or plasmid-based methods (Gregan et al., 2006). All yeast strains were cultured in YES (yeast exact with supplements) media at 30 °C.

Western blot

Yeast cells were grown to a concentration of ~1 X 10^7 cells/ml and harvested by centrifugation. Cell pellet was washed in 1XPBS and stored in -80 °C or were lysed immediately. Cells were lysed by either bead-beating or alkaline extraction. Protein samples were quantified with Bradford reagents (Bio-Rad), and equal amounts of protein were loaded. Primary antibodies used were Pol II 8WG16 antibody (Abcam ab817), Pol II pS2 antibody (Abcam 5095), Pol II pS5 antibody (Abcam 5131), high-affinity HA (Roche 11867423001), Tubulin antibody (Sigma T9026) and Actin antibody (Abcam 8224). Secondary antibodies used were goat anti-rabbit IRDye680 (LI-COR 926-32221), anti-mouse IRDye800CW (LI-COR 926-32210) and anti-rat IRDye800CW (LI-COR 926-32219).

Semi-quantitative RT-PCR

DNA-free total RNA was isolated by hot phenol extraction method followed by Turbo DNase (Ambion) treatment. 20 to 30 ng of total RNA were used in one-step RT-PCR reactions (Qiagen) following manufacturer's protocol. Primers used are listed in Table S2. RT- omitted the reverse transcription step and proceeded directly to enzyme mix inactivation at 95 °C.

RT-qPCR

Super Script III First-Strand Synthesis System (Life technologies) was used to reverse transcribe total RNA into cDNA. cDNA was amplified by IQ SYBR Green Super Mix with CFX96 real time PCR detection system (Bio-Rad). Primers used are listed in

Table S2. Expression levels relative to wild type were calculated by $\Delta\Delta C_T$ method using *act1* levels for normalization.

Small RNA northern

Yeast cells were grown to a concentration of ~1 X 10^7 cells/ml. Total RNA was extracted by the hot phenol method (Leed et al., 1991). mirVana miRNA isolation kit (Ambion) was used to enrich the small RNA fraction (<200 bp) from total RNA. 10 to 15 ug of enriched small RNA samples were used for northern blot with RNA chemically cross-linked to membranes (Pall and Hamilton, 2008). Radiolabeled riboprobes were generated by T3/T7 *in vitro* transcription kit (Ambion) using *dh* or *dg* DNA as templates and αP^{32}-UTP for radiolabeling. Riboprobes were further hydrolyzed into desired size before hybridization. *U6* radiolabeled oligoprobe was prepared by P^{32}-ATP end labeling with T4 PNK (Polynucleotide Kinase). Radioactive signals were detected by Fuji phosphoimager.

Small RNA sequencing library construction and data analysis

Small RNA libraries were constructed by NEBNext multiplex Small RNA library prep kit (NEB E7300) following manufacturer's protocol. Libraries were further size selected (125-160 bp) by Blue Pippin machine (Sage Science). Barcoded libraries were pooled and sequenced on Illumina MiSeq platform. Obtained reads were quality filtered using Trimmomatic and aligned to the *S. pombe* genome assembly ASM294v2.21 using Bowtie v2.1.0 and local alignment, with multi-mappers randomly distributed. Only reads between 15 and 36 nucleotides were used for the analysis. Read counts were normalized to reads per million (RPM) using total library size. Reads mapping to the sense strands of tRNA and rRNA were discarded before producing genome browser pileups.

RNA sequencing library construction

ScriptSeq V2 kit (Epicentre) was used to prepare barcoded RNAseq libraries. 50 ng ribosomal RNA (rRNA)-depleted RNA samples were used as starting material following manufacturer's protocol. Ribo-Zero Gold kit (Epicentre) was used to remove

rRNA from total RNA (DNA free) samples. Barcoded libraries were pooled and sequenced on Illumina HiSeq platform.

RNAseq preprocessing, alignment and coverage visualization

Sequencing adapters were trimmed from reads using Trimmomatic 0.30 (Bolger et al., 2014), and surviving read pairs with both mates longer than 25 bp were retained. Reads were then mapped to isolated rDNA annotations with Bowtie 2 2.1.0 with default options (Langmead and Salzberg, 2012). Only read pairs that failed to map concordantly to rDNA were retained. Subsequently, reads were aligned to the Ensembl 21 S. pombe genome release with STAR 2.3.1z (Dobin et al., 2013). Genome index construction was performed with the option --sjdbOverhang 100 and the Ensembl 21 annotations supplied to --sjdbGTFfile. Alignment was performed with the following options: --outFilterMultimapNmax 100 --outFilterMismatchNmax 5. Non-primary and non-concordant alignments were removed with samtools 0.1.19 (Li et al., 2009). One random placement was chosen for multi-mapping reads. Coverage tracks were prepared from STAR alignments with Bedtools 2.19.0-7 and UCSC BigWig utilities (Quinlan and Hall, 2010). BAM alignments were converted to BED format, and the strand of the second read in each aligned pair inverted so base coverage for both mates would be counted on the origin strand. Base coverage was tallied with Bedtools genomecov for each strand and normalized by millions of reads mapped. Figures were produced in IGV (Robinson et al., 2011; Thorvaldsdóttir et al., 2013).

Differential intron and exon usage

Independent pairwise comparisons of *rct1*Δ, *rct1-rrm*, *rct1*Δ-*clr3*Δ and *clr3*Δ with wild type were performed with DEXSeq 1.8.0 (Anders et al., 2012). Two biological replicates were used in all comparisons. A non-overlapping set of exon counting bins in gff format was generated with the dexseq_prepare_annotation.py script. The resulting gff was modified by adding intron counting bins between all exons, which were distinguished by appending an "i" to the preceeding exon ID. dexseq_count.py was run with parameters "-p yes -s yes" to generate raw counts of reads overlapping the bins. DEXSeq routines were called with default arguments to test for differential expression

and estimate $\log_2$ fold changes for the counting bins. Differential exon/intron usage events with a Benjamini-Hochberg adjusted p-value less than 0.05 were considered significant. Boxplots of $\log_2$ fold change estimates for these events were generated with ggplot2 (Wickham, 2009).

Iodine staining

Homothallic strains were streaked on mating/sporulation media (ME + amino acids) and cultured at 25 °C until colonies grew to about 2 mm in size. The agar surface was exposed with Iodine vapor under chemical hood until wild type homothallic yeast colonies turned dark purple.

Genomic DNA extraction

Overnight yeast cultures were harvested by centrifugation. Genomic DNA was extracted by vortexing with phenol:chloroform:isoamyl alcohol (25:24:1) for 5 minute or until 90% of the cells were broken. The aqueous phase was separated by centrifugation and DNA was further precipitated by ethanol precipitation.

ChIP, ChIP sequencing library construction and data analysis

Yeast cells were grown to a concentration of ~1 X 10^7 cells/ml, then fixed in 1% formaldehyde at 25°C for 20 min. Fixation was stopped by adding glysine to a final concentration of 0.125 M, and cells were washed twice in 1XPBS then stored in -80°C until all strains were harvested. Cells were spheroplasted by zymolyase at 37°C and then sonicated using a bioruptor for 8 cycles (30s ON 60s OFF). For each IP, 500-750 ug of chromatin were used with 3 to 5 ul antibody. Antibodies used in ChIP experiments were H3K9 dimethylation antibody (Upstate 07-441), H3K9 trimethylation antibody (Abcam ab8898), Pol II 8WG16 antibody (Abcam ab817), Pol II pS2 antibody (Abcam 5095) and Pol II pS5 antibody (Abcam 5131).

1 ng of DNA purified from ChIP experiments was made into libraries by using NEB enzymes. In brief, DNA was end-repaired by T4 DNA polymerase, Klenow fragment and T4 DNA PNK. “A” bases were added to the 3’ end of end-repaired DNA fragment with Klenow 3’ to 5’ exo minus and dATP. Barcoded Truseq adaptors

(Illumina) were ligated to DNA fragments using quick ligase at 25°C. Five PCR cycles were performed prior to size selection. After size selection, purified DNA was PCR amplified with 6 to 12 cycles (Kapa HiFi HotStart ready mix). Barcoded libraries were pooled and sequenced on Illumina HiSeq platform. Obtained reads were quality filtered using Trimmomatic and aligned to the *S. pombe* genome assembly ASM294v2.21 using Bowtie v2.1.0 and local alignment, with multi-mappers randomly distributed. All read counts were normalized to reads per million (RPM) using total library size. ChIP enrichment was calculated as the $\log_2$ of the ratio of normalized IP reads to normalized input (whole cell extract) reads. Quantification at individual features was performed by intersecting reads with the feature of interest.

RNA immunoprecipitation

RNA-IP was performed as described in (Gilbert and Svejstrup, 2006) with modifications. SUPERase• In™ RNase Inhibitor (Ambion 2696) was added throughout the experiment after cell lysis step. Immunoprecipitation was performed overnight with anti-HA (3F10) high affinity matrices (Roche 11815016001). Immunoprecipitated RNA was subject to bioanalyzer RNA nano (Agilent Technologies RNA 6000 Nano 5067-1511) and small RNA (Agilent Technologies Small RNA 5067-1548) analysis.

EMS mutagenesis

Yeast cells were grown to a concentration of ~1 X 10^7 cells/ml. 1X10^8 cells were transferred to a tube and first washed twice with sterile water, then resuspended in 1.7 ml sodium phosphate buffer (NaH2PO4). Cells were transferred to a glass tube, 50 ul EMS (Sigma) were added to the mutagenesis tube but not the control tube. All tubes were incubated at 30 °C with gentle mixing. At each time point (0, 20, 40, 60, 90 minutes), cells were removed and added to another tube containing 5% sodium thiosulfate buffer to stop EMS mutagenesis. Cells were washed twice with thiosulfate buffer and plated out on YES plates to determine survival rate at each time point. The time point that showed 50% survival rate was used to select for suppressors.

strain name	genotype	source
DG21	*h-, otr1R(SphI)::ura4, ura4-DS/E, ade6-216, his7-366, leu1-32*	lab stock
FY648	*h+, otr1R(SphI)::ura4 (oril), ura4-DS/E, ade6-210, leu1-32*	lab stock
FY939	*h+, tRNAPhe-otr1(dh)BglII::ura4+ (orilI), ura4-DS/E, ade6-M210, leu1-32*	lab stock
FY988	*h+, tRNAPhe-otr1(dh)BglII::ura4+ (oril), ura4-DS/E, ade6-M210, leu1-32*	lab stock
AY1	*h+/h-, delta-rct1::kanMX6/rct1+, otr1R(SphI)::ura4, ura4-DS/E, ade6-210/216, leu1-32*	this study
AY2	*h+/h-, delta-rct1::kanMX6/rct1+, otr1R(SphI)::ura4, ura4-DS/E, ade6-210/216, leu1-32*	this study
DG712	*h+/h-, delta-rik1::kanMX6/rik1+, otr1R(SphI)::ura4, ura4-DS/E, ade6-M210/ade6-M216, leu1-32, his+/his7-366*	lab stock
AY3	*h-, delta-rct1::kanMX6, otr1R(SphI)::ura4, ura4-DS/E, , leu1-32*	this study
AY7	*h+, delta-rct1::hyg, otr1R(SphI)::ura4, ura4-DS/E, ade6-210, leu1-32*	this study
AY997	*h?, rpb1-gfp*	this study
AY1000	*h?, rpb1-gfp, delta-rct1::nat*	this study
AY1040	*h?, rpb1-HA, delta-rct1::nat*	this study
AY1041	*h?, rpb1-HA*	this study
AY1042	*h?, delta-rct1::nat*	this study
AY1043	*h?*	this study
DG763	*h-, delta-rik1::kanMX6, otr1R(SphI)::ura4+, ura4-DS/E, ade6-210, leu1-32, his7-366*	lab stock
DG770	*h+, delta-rik1::kanMX6, otr1R(SphI)::ura4+, ura4-DS/E, ade6-216, leu1-32, his+*	lab stock
ZB20	*h-, delta-ago1::kanMX6, otr1R(SphI)::ura4, ura4-DS/E, ade6-216, leu1-32, his7-366*	lab stock
DG287	*h+, delta-ago1::kanMX6, otr1R(SphI)::ura4, ura4-DS/E, ade6-216, leu1-32, his+*	lab stock
DG690	*h-, delta-dcr1::kanMX6, otr1R(SphI)::ura4+, ura4-DS/E, ade6-210, leu1-32, his7-366*	lab stock
DG691	*h+, delta-dcr1::kanMX6, otr1R(SphI)::ura4, ade6-210, leu1-32*	lab stock
DG692	*h-, delta-dcr1::kanMX6, otr1R(SphI)::ura4, ade6-216, leu1-32, his7-366*	lab stock
DG124	*h-, delta-rdp1::kanMX6, otr1R(SphI)::ura4+, ura4-DS/E, ade6-216, leu1-32, his7-366*	lab stock
TV238	*h+, delta-rdp1::kanMX6, otr1R(SphI)::ura4, ura4-DS/E, ade6-216, leu1-32*	lab stock
SPK679	*h90, delta-clr4::kanMX*	lab stock
AY14	*h90, delta-rct1::hyg, ura4, ade6-210, leu1-32, his2*	this study
AY15	*h90, delta-rct1::hyg, ura4, ade6-210, leu1-32, his2*	this study
AY16	*h90, delta-rct1::hyg, ura4, ade6-210, leu1-32, his2*	this study
DG784	*h-, delta-clr3::kanMX6, otr1R(SphI)::ura4+, ura4-DS/E, ade6-216, leu1-32, his7-366*	lab stock
DG790	*h+, delta-clr3::kanMX6, otr1R(SphI)::ura4, ura4-DS/E, ade6-210, leu1-32, his+*	lab stock
AY714	*h?, delta-rct1::kanMX6, delta-clr3::hyg, otr1R(SphI)::ura4, ura4-DS/E, ade6-210, leu1-32, his+*	this study
AY722	*h-, delta-rct1::kanMX6, delta-clr3::hyg, otr1R(SphI)::ura4, ura4-DS/E, ade6-216, leu1-32, his-*	this study
AY20	*h+, delta-rct1::hyg, delta-clr3::kanMX6, otr1R(SphI)::ura4, ura4-DS/E, leu1-32*	this study
AY22	*h+, delta-rct1::hyg, delta-clr3::kanMX6, otr1R(SphI)::ura4, ura4-DS/E, leu1-32*	this study
AY1269	*h-, delta-rct1::nat, delta-ago1::kanMX6, otr1R(SphI)::ura4, ura4-DS/E, ade6-216, leu1-32, his7-366*	this study
AY1164	*h?, delta-rct1::nat, delta-ago1::kanMX6, otr1R(SphI)::ura4, ura4-DS/E, leu1-32, his7+*	this study
AY1271	*h-, delta-rct1::nat, delta-dcr1::kanMX6, otr1R(SphI)::ura4+, ura4-DS/E, ade6-210, leu1-32, his7-366*	this study
AY1217	*h?, delta-rct1::nat, delta-dcr1::kanMX6, otr1R(SphI)::ura4, leu1-32, his-*	this study
AY25	*h-, delta-rct1::hyg, delta-rdp1::kanMX6, otr1R(SphI)::ura4+, ura4-DS/E, leu1-32*	this study
AY29	*h-, delta-rct1::hyg, delta-rdp1::kanMX6, otr1R(SphI)::ura4+, ura4-DS/E, leu1-32*	this study
BG_3025H	*h+, delta-mlo3::kanMX6, ura4-D18, leu1-32*	lab stock
AY755	*h?, delta-rct1::hyg, delta-mlo3::kanMX6, leu1-32*	this study
AY759	*h?, delta-rct1::hyg, delta-mlo3::kanMX6, leu1-32*	this study
AY8	*h+, delta-rct1::hyg, otr1R(SphI)::ura4 (oril), ura4-DS/E, ade6-210, leu1-32*	this study
AY10	*h+, delta-rct1::hyg, tRNAPhe-otr1(dh)BglII::ura4+ (orilI), ura4-DS/E, ade6-210, leu1-32*	this study
AY11	*h+, delta-rct1::hyg, tRNAPhe-otr1(dh)BglII::ura4+ (oril), ura4-DS/E, ade6-210, leu1-32*	this study
AY12	*h+, delta-rct1::hyg, tRNAPhe-otr1(dh)BglII::ura4+ (oril), ura4-DS/E, ade6-210, leu1-32*	this study
AY403	*h?, delta-rct1::rct1-FL-hyg, otr1R(SphI)::ura4, ura4-DS/E, ade6-216, leu1-32, his+*	this study
AY416	*h?, delta-rct1::rct1ΔIso-hyg, otr1R(SphI)::ura4, ura4-DS/E, ade6-216, leu1-32, his-*	this study
AY420	*h?, delta-rct1::rct1-rrm-hyg, otr1R(SphI)::ura4, ura4-DS/E, ade6-216, leu1-32, his+*	this study
AY455	*h?, delta-rct1::rct1ΔC-hyg, otr1R(SphI)::ura4, ura4-DS/E, ade6-216, leu1-32, his-*	this study
AY435	*h?, delta-rct1::rct1ΔIso-rrm-hyg, otr1R(SphI)::ura4, ura4-DS/E, leu1-32*	this study
AY466	*h?, delta-rct1::rct1ΔIsoΔC-hyg, otr1R(SphI)::ura4, ura4-DS/E, ade6-216, leu1-32, his-*	this study
AY470	*h?, delta-rct1::rct1-rrm-ΔC-hyg, otr1R(SphI)::ura4, ura4-DS/E, ade6-216, leu1-32, his-*	this study
AY486	*h?, delta-rct1::rct1ΔIso-rrm-ΔC-hyg, otr1R(SphI)::ura4, ura4-DS/E, ade6-216, leu1-32, his-*	this study
AY584	*h?, delta-rct1::rct1-FL-HA-hyg, otr1R(SphI)::ura4, ura4-DS/E, ade6-216, leu1-32, his+*	this study
AY603	*h?, delta-rct1::rct1ΔIso-HA-hyg, otr1R(SphI)::ura4, ura4-DS/E, ade6-216, leu1-32, his-*	this study
AY611	*h?, delta-rct1::rct1-rrm-HA-hyg, otr1R(SphI)::ura4, ura4-DS/E, ade6-216, leu1-32, his-*	this study
AY1245	*h?, delta-rct1::rct1-rrm-HA-hyg, otr1R(SphI)::ura4, ura4-DS/E, leu1-32, his-*	this study
AY629	*h?, delta-rct1::rct1ΔC-HA-hyg, otr1R(SphI)::ura4, ura4-DS/E, ade6-216, leu1-32, his-*	this study
AY638	*h?, delta-rct1::rct1ΔIso-rrm-HA-hyg, otr1R(SphI)::ura4, ura4-DS/E,ade6-216, leu1-32, his-*	this study
AY653	*h?, delta-rct1::rct1ΔIsoΔC-HA-hyg, otr1R(SphI)::ura4, ura4-DS/E, ade6-216, leu1-32, his-*	this study
AY671	*h?, delta-rct1::rct1-rrm-ΔC-HA-hyg, otr1R(SphI)::ura4, ura4-DS/E, leu1-32, his-*	this study
AY693	*h?, delta-rct1::rct1ΔIso-rrm-ΔC-HA-hyg, otr1R(SphI)::ura4, ura4-DS/E, ade6-216, leu1-32, his-*	this study
AY1296	*h+, delta-ago1::Nat-3XFLAG-ago1, delta-rct1::rct1-FL-hyg, otr1R(SphI)::ura4 or ade6, ura4-DS/E, ade6-210, leu1-32*	this study
DI47	*h?, delta-ago::KanMX6-HA-ago1, otr1R(SphI)::ura4 (ori I), ura4-DS/E, leu1-32 his3-*	lab stock
BG_3397H	*h+, delta-eri::kanMX6, ura4-D18, leu1-32*	lab stock
AY853	*h+, delta-eri::kanMX6,ade6-216, leu1-32, his+*	this study

Table 2.2 Strain list

strain name	genotype	source
AY847	*h?, delta-rct1::hyg, delta-eri::kanMX6, ade6-210, leu1-32, his-*	this study
AY848	*h?, delta-rct1::hyg, delta-eri::kanMX6, ade6-210, leu1-32, his-*	this study
AY850	*h?, delta-rct1::hyg, delta-eri::kanMX6, ade6-210, leu1-32, his?*	this study
DG859	*h?, delta-rrp6::kanMX6, otr1R(SphI)::ura4, ura4-DS/E, ade6-216, leu1-32, his?*	lab stock
DG860	*h?, delta-rrp6::kanMX6, otr1R(SphI)::ura4, ura4-DS/E, ade6-216, leu1-32, his?*	lab stock
AY1277	*h?, delta-rct1::nat, delta-rrp6::kanMX6, otr1R(SphI)::ura4, ura4-DS/E, ade6-216, leu1-32, his?*	this study
AY1278	*h?, delta-rct1::nat, delta-rrp6::kanMX6, otr1R(SphI)::ura4, ura4-DS/E, ade6-216, leu1-32, his?*	this study
AY1286	*h?, delta-rct1::rct1-rrm-HA-hyg, delta-rrp6::kanMX6, otr1R(SphI)::ura4, ura4-DS/E, ade6-216, leu1-32, his?*	this study
AY1287	*h?, delta-rct1::rct1-rrm-HA-hyg, delta-rrp6::kanMX6, otr1R(SphI)::ura4, ura4-DS/E, ade6-216, leu1-32, his?*	this study
AY337	*h+, delta-cdk9::hyg, otr1R (sph1)::ura4, ura4 DS/E, ade6-216, leu1- 32*	this study
AY342	*h+, delta-cdk9::hyg, otr1R (sph1)::ura4, ura4 DS/E, ade6-216, leu1- 32*	this study
AY452	*h?, lsk1::KanMX6, leu1-32*	this study
AY453	*h?, lsk1::KanMX6, leu1-32*	this study
AY454	*h?, lsk1::KanMX6, leu1-32*	this study
SPG17	*h90, leu1-32, ura4, his2, ade6-216*	lab stock
SPG18	*h90, leu1-32, ura4, his2, ade6-210*	lab stock
DI301	*h-, ubc4-G48D::kanMX6, otr1R(SphI)::ura4+, ura4-DS/E, ade6-216, leu1-32 , his7-366*	lab stock
DI304	*h90, ubc4-G48D::kanMX6, ura4+, ade6+, leu1-32, his2+*	lab stock
AY502	*h?, delta-rct1::hyg, ubc4-G48D::kanMX6, otr1R(SphI)::ura4+, ura4-DS/E, leu1-32*	this study
AY518	*h?, delta-rct1::hyg, ubc4-G48D::kanMX6, otr1R(SphI)::ura4+, ura4-DS/E, leu1-32*	this study

Table 2.2 Strain list (continued)

name	sequence	purpose
124 USF	CGTATTTAACGAATCACTGCAAATG	strain construction
124USR	GGGGATCCGTCGACCTGCAGCGTACTGAATGGTATTCTTGGATGGTATGATG	strain construction
124DSF	GTTTAAACGAGCTCGAATTCATCGATCCTGAACGAAGGTATAGATATGATAGACG	strain construction
124DSR	CCGTGTCCCCGTGTGGTTAT	strain construction
CHK 124F	TTTCCCAAAGCGTGGCTCGT	strain construction
CHK 124R	CGTGGTTTCCATGCCCTTGT	strain construction
rct1-USF XbaI	AAAATCTAGATTGAATCTTTGCATACCGCTTTTT	strain construction
rct1-USR XhoI	AAAACTCGAGCGATTGTATACATGCAAGAAGGC	strain construction
rct1-DSF BglII	AAAAAGATCTTTGATTAAGACTTCAAATGTATGGAA	strain construction
rct1-DSR XbaI	AAAATCTAGACATTTGCTCAGCCTTGGCAT	strain construction
rct1 CHK USF	GGCTGTGCTGCTAACGAAGAAA	strain construction
rct1 CHK DSR	TTGGCAAATCCCGTCTCCTT	strain construction
uni CHK-R	GTCGTTAGAACGCGGCTACA	strain construction
uni CHK-R2	GGCTGGCTTAACTATGCGGC	strain construction
uni CHK-F	TCTGGGCCTCCATGTCGCTGG	strain construction
uni CHK-F2	GCTGCGCACGTCAAGACTGTC	strain construction
rct1-USF NheI	AAAAGCTAGCTTGAATCTTTGCATACCGCTTTTT	strain construction
rct1-DSR NheI	AAAAGCTAGCCATTTGCTCAGCCTTGGCAT	strain construction
rct1 (3'UTR)-R pvuII	GCAGCAGCTGTACGACGATTTTT	strain construction
rct1-F start Xho1	AAAACTCGAGATGTATGTACTAATTGAAACTACAG	strain construction
rct1-F delta-Iso Xho1	AAAACTCGAGATGCCACCCGATCTAGTGGAGCCTTT	strain construction
rct1 BsaB1-R	TTTTGATATCTATCATTGGAGTTGTAATATTGTCTGTAACGAGCC	strain construction
rct1 RRM mut-F	GGCGATAGTCTTCAAGATGCCGATATCGAATTTGATAACAAAG	strain construction
rct1 RRM mut-R	CTTTGTTATCAAATTCGATATCGGCATCTTGAAGACTATCGCC	strain construction
p30F_T7	TAATACGACTCACTATAGGGAGCCTGTTGATTCGGCACCTTTG	small RNA blot
p30R_T3	AATTAACCCTCACTAAAGGGAGATGGAGAACGACTGTGAAGAGACC	small RNA blot
p33F_T7	TAATACGACTCACTATAGGGAGTGCAAGTGGAAAGTGGCTTCA	small RNA blot
p33R_T3	AATTAACCCTCACTAAAGGGAGATCGACCACCCTGACTTGTTCTC	small RNA blot
U6 oligo	ATGTCGCAGTGTCATCCTTG	small RNA blot
p30F	CCTGTTGA TTCGGCACCTTTG	RT-PCR
p30R	TGGAGAACGACTGTGAAGAGACC	RT-PCR
p33F	TGCAAGTGGAAAGTGGCTTCA	RT-PCR
p33R	TCGACCACCCTGACTTGTTCTC	RT-PCR
act 5'	TACCCCATTGAGCACGGTAT	RT-PCR
act 3'	GGAGGAAGA TTGAGCAGCAG	RT-PCR
ura4#1	GAGGGGATGAAAAATCCCAT	RT-PCR
ura4#2	TTCGACAACAGGATTACGACC	RT-PCR
cox1F	TTGCAATCTCAGCACATGGT	RT-PCR
cox1R	CCACCAGGTCCTTCTTCTGT	RT-PCR
GTO223	GAAAACACATCGTTGTCTTCAGAG	RT-PCR
GTO226	TCGTCTTGTAGCTGCATGTGA	RT-PCR
p30_qPCR_F	CCATATCAATTTCCCATGTTCC	qPCR
p30_qPCR_R	CATCAAGCGAGTCGAGATGA	qPCR
p33_qPCR_F	TATCCTGCGTCTCGGTATCC	qPCR
p33_qPCR_R	CTGTTCGTGAATGCTGAGAAAG	qPCR
act1_qPCR_F	TGCACCTGCCTTTTATGTTG	qPCR
act1_qPCR_R	TGGGAACAGTGTGGGTAACA	qPCR

Table 2.3 Primer list

Chapter III: Identification of novel components involved in the RNAi machinery

3.1 Introduction

To identify novel components in the RNAi machinery, we composed a list of potential candidates as previously described in Chapter II. Here, Chapter III includes the screening process of the potential candidates and positive hits identified so far. A putative chromatin remodeler, Ssr4, was identified in my screen, therefore a brief introduction of chromatin remodelers is given as part of this introduction.

The basic unit of chromatin is the nucleosome. Nucleosomes are composed of 146 bp DNA wrapped around an octamer of histone proteins, each of which contains two copies of H2A, H2B, H3 and H4 (Chung et al., 1978; Eickbush and Moudrianakis, 1978). The formation of this higher order chromatin structure assists DNA packaging into the nucleus. However, at the same time, the access to the underlying DNA sequences by various factors is limited by the formation of nucleosomes. In order to allow DNA replication, DNA repair and transcription to occur, interactions between DNA and histones are modulated by a group of proteins call chromatin remodelers. Chromatin remodelers are ATP-dependent multi-protein complexes that mediate nucleosome sliding, removal and structural alterations. Chromatin remodelers are divided into four subfamilies, which are based on unique ATPase-domain sequences and associated subunits: SWI/SNF (Switching defective/ Sucrose Nonfermentable), ISWI (Imitation Switch), CHD (Chromodomain, Helicase, DNA binding) and INO80 (Inositol requiring 80). All four families contain their own unique catalytic ATPase core and diverse noncatalytic subunits that facilitate nucleosome binding, protein-protein interaction and enzymatic activity regulation. Chromatin remodeler complexes regulate all aspects of DNA metabolic processes and perturbations in chromatin remodeling have been linked to

developmental defects, cancer and mental disorders in higher eukaryotes (Euskirchen et al., 2012; Falbo and Shen, 2006).

Originally identified by two independent screens in *S. cerevisiae*, the SWI/SNF chromatin remodeler complex is the first ATP-dependent chromatin remodeler to be described (Hirschhorn et al., 1992; Neigeborn and Carlson, 1984; Peterson and Herskowitz, 1992). Although it is functionally conserved in eukaryotes, the detailed composition of SWI/SNF complex varies in different organisms. In *S. cerevisiae*, the SWI/SNF complex consists of 8 to 12 subunits, none of which is essential for cell viability. Various cellular processes, including transcription, DNA repair and telomeric and rDNA silencing, are regulated by the SWI/SNF complex (Dror and Winston, 2004; Geng and Laurent, 2004; Lans et al., 2012). The ATPase activity of chromatin remodelers is stimulated by substrate binding, including both nucleosomes and naked DNA, and the energy generated by ATP hydrolysis is used to alter DNA-histone interactions (Laurent et al., 1993). In addition to the ATPase-domain, SWI/SNF chromatin remodeling core proteins contain a bromodomain at the C-terminus that binds acetylated lysine residues in the chromatin. Interestingly, some eukaryotes (including yeast and human) contain two types of SWI/SNF complexes, one of which contains multiple subunits with bromodomains and is called the RSC complex (Remodel the Structure of Chromatin). The RSC complex is much more abundant than the SWI/SNF complex in yeast cells, and is required for cell viability (Cairns et al., 1996; Laurent et al., 1992). In *S. cerevisiae*, the RSC complex is composed of 17 subunits, and although it contains a unique ATPase-domain protein, several other subunits are identical or homologous to the SWI/SNF complex (Mohrmann and Verrijzer, 2005). Both the SWI/SNF and RSC complexes are implicated in transcriptional activation and repression; however, they regulate a distinct non-overlapping set of gene targets (Angus-Hill et al., 2001; Holstege et al., 1998; Sudarsanam et al., 2000). Similarly, while both complexes play key roles in repairing DNA double-strand breaks, they are required at a different step of the repair process (Chai et al., 2005). Additionally, the RSC complex regulates the cell cycle progression through the G2/M phase by promoting sister chromatid cohesion and segregation (Cao et al., 1997; Hsu et al., 2003; Huang et al., 2004).

Valuable advances in understanding chromatin remodeling came from studies done in budding yeast *S. cerevisiae*. However, the chromatin structure in budding yeast, in particular at centromeres, is significantly different from other eukaryotes. Characterization of the SWI/SNF and RSC complexes in *S. pombe* revealed a potential role in chromatin remodeling of a protein named Ssr4. Ssr4 belongs to the conserved Ssr protein family (SWI/SNF and RSC complex subunit), the members of which are found in both SWI/SNF and RSC complexes (Monahan et al., 2008). In *S. pombe*, the SWI/SNF complex is consist of 12 subunits, while the RSC complex contains 13 subunits, with 6 subunits shared between these two complexes. Of the 6 shared components, 2 are actin proteins and the remaining are the Ssr family proteins, Ssr1-4 (Monahan et al., 2008). Interestingly, Ssr4, which is the only member of this protein family that has no apparent *S. cerevisiae* ortholog, was identified in my *S. pombe* specific screen as a potential novel RNAi component.

Ssr4 contains no motifs of known function and very little is known about it other than its association with chromatin remodeling complexes. Ssr4 is conserved in the Ascomycota phylum, but seems to be lacking in the Sacchoromycotina subphylum, just like RNAi components. I showed that in cells lacking *ssr4*, pericentromeric silencing is derepressed and siRNA levels are modestly decreased. In addition, *ssr4Δ* mutant cells are sensitive to UV-induced DNA damage, as expected from defects in subunits of chromatin remodeling complexes.

3.2 Results

3.2.1 Knockout strains generation

Budding yeast *S. cerevisiae* has lost all the key RNAi components found in *S. pombe* (Aravind et al., 2000; Nakayashiki et al., 2006), therefore we hypothesized that any gene that is specific to *S. pombe*, with no apparent *S. cerevisiae* homologue and yet is conserved in other eukaryotes, could potentially be involved in the RNAi pathway, or have co-evolved with RNAi machinery to support its function. Based on these criteria, we composed a list that contains 538 genes, including *rdp1, hrr1, cid12*, *dcr1, chp1* and *ago1* (Table 3.1). Among these 538 genes, I exclude the ones that are previously characterized in our lab or are listed as essential according to the *S. pombe* database (http://www.pombase.org/) from my screen. Of the remaining 442 genes of interest, only 279 knockout strains are available from the Bioneer *S. pombe* knockout collection. Therefore, I needed to generate 163 knockout strains for the remaining targets (Figure 3.1 and Table 3.2).

To complete the strain list needed for my screen, I made knockout constructs specific to each gene and transformed them to wild type diploid cells carrying *otr1R::ura4* transgene. Transformants were selected on complete medium with hygromycin. Four diploid colonies from each knockout construct transformation were chosen and the correct integration at both 5' and 3' ends were confirmed by PCR. All diploids that conferred hygromycin resistance had correct integration at both ends, and tetrad dissection was performed to obtain haploid knockout strains. Haploid knockout strains were identified by their hygromycin drug resistance. I identified six genes that were essential for cell viability in *S. pombe*, based on the observation that only wild type cells grew after dissecting 16 tetrads. A summary of the results is listed in Tables 3.2, 3.3 and Figure 3.2.

3.2.2 Known and novel genes that impaired pericentromeric silencing identified in the screen

Since RNAi machinery is required for efficient pericentromeric silencing, I used semi-quantitative RT-PCR to screen for strains in which silencing was impaired. Both *dh* and *dg* repeat transcript levels were analyzed for all strains (Figures 3.3A and B). In addition, *otr1R::ura4* transgene silencing was analyzed in the "home-made" knockout strains (Figure 3.3B). For each set of RNA extraction and RT-PCR, at least one wild type and one *rik1Δ* mutant strain were included as controls (Figure 3.3). I identified 5 novel genes (excluding *rct1*) and 7 known genes that were involved in silencing by my screen. A summary of my results is listed in Table 3.4.

3.2.3 Chromatin remodeler Ssr4 is needed for siRNA biogenesis and heterochromatin silencing

One novel gene which showed the strongest pericentromeric silencing defect was *ssr4*. Ssr4 is the component of both the SWI/SNF and RSC chromatin remodeling complexes (Monahan et al., 2008). To confirm that Ssr4 is needed for pericentromeric silencing, semi-quantitative RT-PCR was performed with four individual *ssr4Δ* mutant strains. My results showed that, in cells lacking Ssr4, *dh* and *dg* repeat transcripts accumulated in the cell, and *otr1R::ura4* transgene is derepressed, although to a lesser extend than *dcr1Δ* mutant cells (Figure 3.4A). To test if siRNA biogenesis was impaired in *ssr4Δ* mutant cells, I performed a small RNA northern blot to detect *dh* and *dg* repeat derived siRNAs. Repeats derived siRNAs were reduced by about a third in *ssr4Δ* mutant cells while siRNAs were barely detectable in RNAi or CLRC mutants (Figure 3.4B). This is consistent with partially derepressed silencing at pericentromeric regions.

3.2.4 Ssr4 is a nuclear protein essential for normal cell growth

RSC chromatin remodelers are often required for normal cell cycle progression (Cao et al., 1997; Hsu et al., 2003; Huang et al., 2004). In agreement with this observation, *ssr4Δ* mutant cells grew two times slower than wild type cells under standard condition (Figure 3.5A) but exhibit normal cell morphology (Figure 3.5B). To

test the cellular localization of Ssr4, I observed the GFP signal of GFP-tagged endogenous Ssr4 under microscope. Consistent with the previous study, Ssr4 is a nuclear protein as expected from the association with SWI/SNF and RSC complexes (Figure 3.6).

3.2.5 Ssr4 is sensitive to UV-induced DNA damage

SWI/SNF and RSC complex components are required for DNA repair pathways (Mandemaker et al., 2014). Therefore, cells lacking these components are highly sensitive to DNA damaging agents, such as UV light. To test if Ssr4 is needed for DNA repair, I challenged *ssr4Δ* mutant cells with UV light to induce DNA damage. My result demonstrated that *ssr4Δ* mutant cells are sensitive to UV-induced DNA damage, suggesting Ssr4 is a bona fide chromatin remodeler (Figure 3.7).

3.3 Discussion

In addition to six genes essential for cell viability, my screen identified five potential novel RNAi components, one of which is Ssr4, a putative chromatin remodeler that is shared between the SWI/SNF and RSC complexes. While the role of chromatin remodelers in transcription regulation and heterochromatin formation is well established (Zhu et al., 2013), no direct link between a chromatin remodeler and the RNAi machinery has ever been suggested.

I demonstrated that Ssr4 is sensitive to UV light, a characteristic of other chromatin remodelers. However, siRNAs derived from pericentromeric repeats are largely retained in cells lacking Ssr4, as a modest 30 to 40 % reduction was consistently detected. This raised the question as to whether Ssr4 is actually involved in the RNAi machinery, or if Ssr4 inhibits heterochromatic transcription by its chromatin remodeling activity. Examination of Ssr4 distribution across eukaryotic genomes revealed that Ssr4 is conserved in many fungal species except *S. cerevisiae*, but is also missing from higher eukaryotes including plants and mammals. Therefore, whether or not Ssr4 is a bona fide RNAi component still remains to be elucidated.

The other 4 potential genes, mug70, sre2, ely5 and SPAC343.17c, only modestly impair pericentromeric silencing. Sre2 is a sterol regulatory element-binding protein (SREBP) that regulates lipid synthesis and homeostasis in the cell (Hughes et al., 2005; Shao and Espenshade, 2012). SREBPs, a family of transmembrane transcription factors, are synthesized as inactive transmembrane precursors, and their activation requires cleavage by RING domain containing E3 ubiquitin ligases (Stewart et al., 2012; 2011). Interestingly, although the SREBP pathway is highly conserved, it is absent from both *S. cerevisiae* and *C. albicans* (Chang et al., 2007; Hughes et al., 2005; Willger et al., 2009). Mug70 was identified in a large-scale screen for meiotically upregulated genes (*mug*) and is associated with Hhp2 that negatively regulates SREBPs in *S. pombe* (Brookheart et al., 2014; Martín-Castellanos et al., 2005). It is not clear how SREBP could be involved in pericentromeric silencing, but *hhp2* shows positive genetic interaction with several RNAi and silencing genes, including *cid12*, *stc1*, *clr4*, *dos1* and *dos2*, indicating *hhp2* is likely to function in the same pathway (Ryan et al., 2012).

Ely5 is part of the nuclear pore complex, and physically interacts with Nup120 (Bilokapic and Schwartz, 2012). Coincidentally, Dcr1-GFP forms a puncture rim-like structure at the inner face of the nuclear membrane, which highly resembles the nuclear pore localization pattern. Additionally, Dcr1 localization is dependent on Nup120, suggesting a direct association between Dcr1 and nuclear pore complexes (Emmerth et al., 2010). Therefore, Ely5 could be involved in RNAi machinery via mediating Dcr1 localization in the cell.

SPAC343.17c has not been characterized, but was co-purified with spliceosome components Prp17 and Prp19. SPAC343.17c belongs to the WD repeat family, and the human homolog WDR70 has been shown to be ubiqutinated in a genome-wide study (Kim et al., 2011). Furthermore, Prp19 in *S. pombe* encodes a ubiquitin protein ligase E4, suggesting a conversed function of SPAC343.17c.

Further experiments are needed to test if these five potential novel RNAi components are indeed involved in the RNAi machinery or they are required for efficient pericentromeric silencing through other pathways.

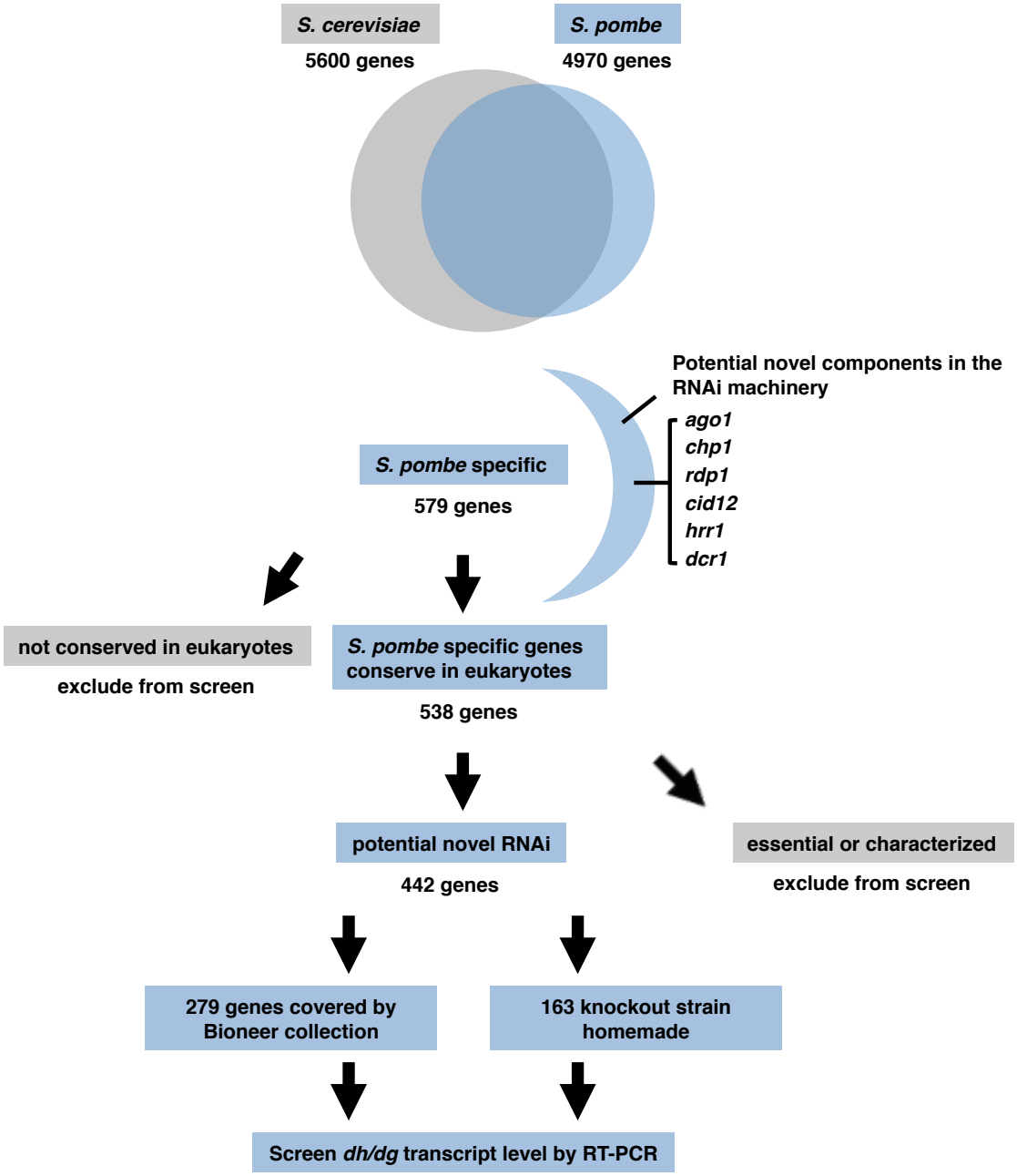

Figure 3.1 The screen set-up

Schematic representation of the screen set-up.

systemic ID	gene	source	phenotype	description
SPCC736.11	ago1	lab stock	loss silencing	argonaute
SPCC663.12	cid12	lab stock	loss silencing	poly(A) polymerase Cid12
SPCC188.13c	dcr1	lab stock	loss silencing	dicer
SPCC613.12c	raf1, clr8, cmc1, dos1	lab stock	loss silencing	CLRC ubiquitin E3 ligase complex specificiy factor Raf1/Dos1
SPCC970.07c	raf2, clr7, cmc2, dos2	lab stock	loss silencing	Rik1-associated factor Raf2
SPBC428.08c	clr4	lab stock	loss silencing	histone H3 lysine methyltransferase Clr4
SPAC17H9.10c	ddb1	lab stock	loss silencing	damaged DNA binding protein Ddb1
SPAC637.07	moe1	lab stock	loss silencing	translation initiation factor eIF3d Moe1
SPAC694.02		lab stock	loss silencing	DEAD/DEAH box helicase
SPCC825.05c		lab stock	loss silencing	splicing coactivator SRRM1 (predicted)
SPCC364.02c	bis1	lab stock	loss silencing	stress response protein Bis1
SPBP35G2.10	mit1	lab stock	loss silencing	SHREC complex subunit Mit1
SPCC645.08c	snd1	lab stock	loss silencing	RNA-binding protein Snd1
SPAC6F12.09	rdp1	lab stock	loss silencing	RNA-directed RNA polymerase Rdp1
SPCC11E10.08	rik1	lab stock	loss silencing	silencing protein Rik1
SPAC664.01c	swi6	lab stock	loss silencing	HP1 family chromodomain protein Swi6
SPAC1071.09c		lab stock	no loss silencing	DNAJ domain protein, DNAJC9 family (predicted)
SPAC12G12.10	wdr21	lab stock	no loss silencing	WD repeat protein, human WDR21 family
SPAC23A1.09		lab stock	no loss silencing	RNA-binding protein (predicted)
SPAC25H1.04	mug105	lab stock	no loss silencing	ubiquitin-fold modifier-specific protease (predicted)
SPAC26F1.02	pnn1	lab stock	no loss silencing	pinin ortholog, involved in splicing Pnn1 (predicted)
SPAC6G10.10c		lab stock	no loss silencing	human hmmtag2 homolog
SPBC21.03c		lab stock	no loss silencing	DUF55 family protein
SPAC27D7.08c		lab stock	no loss silencing	DUF890 family protein, predicted methyltransferase
SPAC30D11.14c		lab stock	no loss silencing	RNA-binding protein (predicted)
SPAC57A7.13		lab stock	no loss silencing	RNA-binding protein, involved in splicing (predicted)
SPAC821.05		lab stock	no loss silencing	translation initiation factor eIF3h (p40)
SPBC18H10.10c	saf4, cwc16, cwf16	lab stock	no loss silencing	splicing associated factor Saf4
SPBC19F8.02		lab stock	no loss silencing	nuclear distribution protein NUDC homolog
SPAC1006.03c	red1, iss3	lab stock	no loss silencing	RNA elimination defective protein Red1
SPAC13G6.10c	asl1	lab stock	no loss silencing	cell wall protein Asl1, predicted O-glucosyl hydrolase
SPAC1565.07c	knd1	lab stock	no loss silencing	Cullin-associated NEDD8-dissociated protein Knd1 (predicted)
SPBC29A10.09c	tri1	lab stock	no phenotype	triman, ribonuclease involved in priRNA formation Tri1
SPCC4B3.12	set9	lab stock	no phenotype	histone lysine methyltransferase Set9
SPCC70.08c		lab stock	no phenotype	methyltransferase (predicted)
SPCC736.09c		lab stock	no phenotype	TRAX, double-strand break repair
SPAC1687.06c	rpl44, rpl28	lab stock	no phenotype	60S ribosomal protein L28/L44 (predicted)
SPAC1F12.06c		lab stock	no phenotype	inosine-containing RNAs endoribonuclease (predicted)
SPAC25H1.02	jmj1	lab stock	no phenotype	histone demethylase Jmj1 (predicted)
SPAC30.03c	mug90, tsn1	lab stock	no phenotype	translin, double-strand break repair
SPBC902.04	rmn1	lab stock	no phenotype	RNA-binding protein
SPBC30B4.08	eri1	lab stock	no phenotype	double-strand siRNA ribonuclease Eri1
SPBC336.05c	hen1	lab stock	no phenotype	small RNA 2'-O-methyltransferase activity (predicted)
SPBC13G1.02	mpg2	lab stock	urgent	mannose-1-phosphate guanyltransferase (predicted)
SPBC146.08c	tif1102	lab stock	urgent	translation initiation factor eIF1A-like (predicted)
SPBC646.09c	int6, yin6	lab stock	urgent	eIF3e subunit Int6
SPAC20G8.08c	fft1	lab stock		SMARCAD1 family ATP-dependent DNA helicase Fft1 (predicted)
SPBP19A11.06	lid2	lab stock	essential, loss silencing	histone demethylase activity (H3-trimethyl-K4 specific)
SPAC1782.03	saf3	lab stock	essential	splicing associated factor Saf3
SPAC22E12.02		lab stock	essential	RNA-binding protein
SPBC4C3.07		lab stock	essential	translation initiation factor eIF3f
SPBC725.08	pir2	lab stock	essential	zf-C2H2 type zinc finger protein, implicated in RNAi (predicted)
SPCC1281.02c		lab stock	essential	chromatin silencing by small RNA, unpublished
SPCP25A2.03		lab stock	essential	THO complex subunit (predicted)
SPAP8A3.06			essential	U2AF small subunit, U2AF-23, mRNA cis splicing, via spliceosome
SPAC1002.10c	sgt1		essential	SGT1 family transcriptional regulator Sgt1
SPAC1751.03			essential	translation initiation factor eIF3m
SPAC2G11.08c	smn1		essential	SMN family protein Smn1, spliceosomal snRNP assembly (unpublished)
SPAC30D11.08c	phf2, saf60, swp2		essential	Lsd1/2 complex PHD finger containing protein Phf2, H3-K9 demethylation
SPAC23E2.02	lsd2, saf140, swm2		essential	histone demethylase SWIRM2, histone H3-K9 demethylation

Table 3.1 Conserved eukaryotic genes present in *S. pombe* with no apparent *S. cerevisiae* ortholog

Genes encoding RNAi components are labeled in blue.

systemic ID	gene	source	phenotype	description
SPAC13G7.10	teb1		essential	Myb family telomere binding protein (predicted)
SPAC1687.04	mcb1		essential	MCM binding protein homolog Mcb1 (predicted)
SPAC1783.03	fta2		essential	Sim4 and Mal2 associated (4 and 2 associated) protein 2
SPAC18B11.11			essential	GTPase activating protein (predicted)
SPAC19G12.07c	rsd1		essential	RNA-binding protein Rsd1 (predicted)
SPAC1F8.07c			essential	pyruvate decarboxylase (predicted)
SPAC222.10c	byr4		essential	two-component GAP Byr4
SPAC23A1.05			essential	serine palmitoyltransferase subunit A (predicted)
SPAC23D3.08	usp108		essential	U1 snRNP-associated protein Usp108
SPAC29A4.06c			essential	splicing protein, human NSRP1 ortholog
SPAC2F3.14c	saf2		essential	splicing associated factor Saf2
SPAC4F10.12	fta1		essential	CENP-L homolog Fta1
SPAC4H3.11c	ppc89		essential	spindle pole body protein Ppc89
SPAC6C3.09			essential	RNase P subunit (predicted)
SPAC9G1.09	sid1		essential	PAK-related GC kinase Sid1
SPAPB1E7.01c			essential	conserved fungal family
SPAPB24D3.06c			essential	DUF1749 family protein
SPBC1677.02	dpm3		essential	dolichol-phosphate mannosyltransferase subunit 3
SPBC16H5.15			essential	conserved fungal protein
SPBC1861.05			essential	pseudouridine-metabolizing bifunctional protein (predicted)
SPBC18E5.03c	sim4		essential	kinetochore protein, CENP-K ortholog, Sim4
SPBC21B10.11	dpm2		essential	dolichol-phosphate mannosyltransferase subunit 2 (predicted)
SPBC24C6.07	cdc14		essential	SIN component Cdc14
SPBC2A9.10	SPBC2A9.10		essential	Bin3 family, 7SK RNA methyltransferase (predicted)
SPBC337.12	red5		essential	human ZC3H3 homolog
SPBC609.01	SPBC609.01		essential	ribonuclease II (RNB) family, involved in mRNA catabolic process (predicted)
SPBC649.05	cut12		essential	spindle pole body protein Cut12
SPBC800.13	cnp20		essential	histone H4 variant, CENP-T ortholog
SPBC8D2.07c	sfc9		essential	transcription factor TFIIIC complex subunit Sfc9 (predicted)
SPBC947.12	kms2		essential	spindle pole body protein Kms2
SPBP8B7.12c	fta3		essential	CENP-H homolog Fta3
SPCC1235.07	fta7		essential	CENP-Q homolog Fta7
SPCC1281.01	ags1		essential	alpha glucan synthase Ags1
SPCC1393.04	fta4		essential	Sim4 and Mal2 associated (4 and 2 associated) protein 4
SPCC1672.10	mis16		essential	kinetochore protein Mis16
SPCC16C4.02c	SPCC16C4.02c		essential	DUF1941 family protein
SPCC4B3.14	cwf20		essential	complexed with Cdc5 protein Cwf20
SPCC4G3.07c	phf1		essential	PHD finger containing protein Phf1
SPCC74.01	sly1		essential	SNARE binding protein Sly1 (predicted)
SPCC777.14	prp4		essential	serine/threonine protein kinase Prp4
SPCC970.12	mis18		essential	kinetochore protein Mis18
SPBC146.09c	lsd1, saf110, swm1		increase silencing, boundary	histone demethylase SWIRM1
SPBC582.04c	dsh1		loss silencing	RNAi protein, Dsh1
SPAC19G12.17	erh1		new gene	enhancer of rudimentary homolog Erh1
SPAC17G8.15	new1		new gene	histone-like transcription factor and archaeal histone family protein
SPBC839.19	new20		new gene	conserved eukaryotic protein
SPAC3H5.13	new4		new gene	conserved eukaryotic protein
SPAC19A8.16	prl65		new gene	conserved fungal protein
SPAC222.17			new gene	conserved fungal protein
SPAC222.18			new gene	Srp1 family splicing factor (predicted)
SPAC227.19c			new gene	conserved protein
SPAC23D3.17			new gene	conserved fungal protein
SPCC417.16			new gene	NADH-ubiquinone reductase complex subunit (predicted)
SPAC9G1.15c	mzt1		new gene, essential	mitotic spindle organizing protein Mzt1
SPAC21E11.04	aca1			L-azetidine-2-carboxylic acid acetyltransferase Aca1
SPAPB24D3.10c	agl1			alpha-glucosidase Agl1
SPBC19G7.08c	art1			arrestin family protein Art1
SPCC962.05	ast1			asteroid homolog, XP-G family protein
SPAC821.04c	cid13			poly(A) polymerase Cid13
SPBC17G9.08c	cnt5			Centaurin Cnt5

Table 3.1 Conserved eukaryotic genes present in *S. pombe* with no apparent *S. cerevisiae* ortholog (continued)

systemic ID	gene	source	phenotype	description
SPAC26A3.10	cnt6			centaurin ADOP ribosylation factor GTPase activating protein family (predicted
SPAPB17E12.04c	csn2			COP9/signalosome complex subunit Csn2
SPAC22A12.03c	csn4			COP9/signalosome complex subunit Csn4
SPCP1E11.07c	cwf18			complexed with Cdc5 protein Cwf18
SPAC30D11.09	cwf19			complexed with Cdc5 protein Cwf19
SPAC21E11.05c	cyp8			cyclophilin family peptidyl-prolyl cis-trans isomerase Cyp8
SPBC106.17c	cys2			homoserine O-acetyltransferase (predicted)
SPBC646.17c	dic1			meiotic dynein intermediate chain Dic1
SPBC3B8.07c	dsd1			dihydroceramide delta-4 desaturase
SPBC1604.01	egt1			Ergothioneine biosynthesis protein Egt1
SPBC146.06c	fan1			Fanconi-associated nuclease Fan1
SPBC336.01	fbh1			DNA helicase I
SPBC646.12c	gap1			GTPase activating protein Gap1
SPBC29A3.17	gef3			RhoGEF Gef3
SPAC1039.11c	gto1			alpha-glucosidase (predicted)
SPAC144.02	iec1			Ino80 complex subunit Iec1
SPCC1259.04	iec3			Ino80 complex subunit Iec3
SPCC306.05c	ins1			INSIG domain protein
SPCC622.19	jmj4			Jmj4 protein (predicted)
SPBC15D4.01c	klp9			kinesin-like protein Klp9
SPAC3A11.05c	kms1			meiotic spindle pole body protein Kms1
SPCC553.07c	kpa1			DinB translesion DNA repair polymerase, pol kappa
SPAC1296.05c	lcp1			cyclin L family cyclin
SPAC27E2.09	mak2			histidine kinase Mak2
SPBC3B9.08c	mnh1			Mago-nashi homolog Mnh1 (predicted)
SPAC3H1.03	mug151			mouse transcriptional regulator, HCNGP-like (predicted)
SPBC17D11.01	nep1			NEDD8 protease Nep1
SPBC646.15c	pex16			Pex16 family peroxisome import protein Pex16 (predicted)
SPBC56F2.01	pof12			F-box protein Pof12
SPAC1093.01	ppr5			mitochondrial PPR repeat protein Ppr5
SPBC1709.12	rid1			GTPase binding protein Rid1 (predicted)
SPAC1D4.09c	rtf2			replication termination factor Rtf2
SPCC297.04c	set7			histone lysine methyltransferase Set7 (predicted)
SPBC1734.05c	spf31			DNAJ protein Spf31 (predicted)
SPBC19F8.01c	spn7			septin Spn7
SPAC19B12.10	sst2			human AMSH/STAMBP protein homolog, ubiquitin specific-protease
SPBC32C12.02	ste11			transcription factor Ste11
SPCC965.05c	thp1			uracil DNA N-glycosylase Thp1
SPAC212.11	tlh1			RecQ type DNA helicase
SPBCPT2R1.08c	tlh2			RecQ type DNA helicase Tlh1
SPBC800.07c	tsf1			mitochondrial translation elongation factor EF-Ts Tsf1
SPAC1002.19	urg1			GTP cyclohydrolase II Urg1 (predicted)
SPBC19C7.09c	uve1			endonuclease Uve1
SPAC1F7.12	yak3			aldose reductase ARK13 family YakC
SPAC1039.07c				aminotransferase class-III, possible transaminase, unknown specificity
SPAC12G12.16c				Fen1 family nuclease, XP-G family (predicted)
SPAC1399.01c				membrane transporter (predicted)
SPAC1565.02c				Rho-type GTPase activating protein (predicted)
SPAC167.05				Usp (universal stress protein) family protein, meiotic chromosome segregation
SPAC1687.19c				queuine tRNA-ribosyltransferase (predicted)
SPAC20H4.06c				RNA-binding protein
SPAC23D3.03c				GTPase activating protein (predicted)
SPAC23H3.04				conserved fungal protein
SPAC25G10.01				RNA-binding protein
SPAC2F3.13c				queuine tRNA-ribosyltransferase (predicted)
SPAC4C5.03				CTNS domain protein (SMART)
SPAC513.06c				dihydrodiol dehydrogenase (predicted)
SPAC56F8.12				conserved fungal protein
SPAC589.05c				conserved eukaryotic protein
SPAC607.02c				conserved fungal protein

Table 3.1 Conserved eukaryotic genes present in *S. pombe* with no apparent *S. cerevisiae* ortholog (continued)

systemic ID	gene	source	phenotype	description
SPAC637.03				conserved fungal protein
SPAC652.01				BC10 family protein
SPAC8E11.05c				conserved fungal protein
SPAC8F11.08c				esterase/lipase (predicted)
SPAC977.08				short chain dehydrogenase (predicted)
SPAPB2B4.07				ubiquitin family protein, human UBTD1 homolog
SPBC1348.09				short chain dehydrogenase (predicted)
SPBC13G1.14c				RNA-binding protein (predicted)
SPBC14F5.10c				ubiquitin-protein ligase E3 (predicted)
SPBC1539.02				eukaryotic nuclear protein implicated in meiotic chromosome segregation
SPBC15D4.13c				human ASCC1 ortholog, implicated in transcriptional regulation (predicted)
SPBC1604.16c				RNA-binding protein, G-patch type (predicted)
SPBC16E9.19				conserved fungal protein
SPBC1703.07				ATP citrate synthase subunit 1 (predicted)
SPBC21C3.12c				DUF953 thioredoxin family protein
SPBC24C6.09c				phosphoketolase family protein (predicted)
SPBC3H7.08c				conserved fungal protein
SPBC428.12c				RNA-binding protein
SPBC530.02				membrane transporter (predicted)
SPBC557.02c				conserved fungal protein
SPBC56F2.05c				transcription factor (predicted)
SPBC800.14c				DUF1772 family protein
SPBC83.10				transthyretin superfamily, human ER membrane protein complex subunit 7 ortl
SPBP4H10.19c				calreticulin/calnexin homolog (predicted)
SPBPB21E7.04c				human COMT ortholog 2
SPBPB2B2.08				conserved fungal protein
SPCC1322.10				cell wall protein Pwp1
SPCC1494.01				iron/ascorbate oxidoreductase family
SPCC162.01c				U4/U6 x U5 tri-snRNP complex subunit (predicted)
SPCC16C4.16c				conserved eukaryotic protein
SPCC191.05c				nucleoside 2-deoxyribosyltransferase (predicted)
SPCC285.05				purine nucleoside transmembrane transporter (predicted)
SPCC320.08				membrane transporter (predicted)
SPCC4G3.12c				ubiquitin-protein ligase E3 (predicted)
SPCC553.10				conserved fungal protein
SPCC553.12c				transmembrane transporter (predicted)
SPCC569.01c				cell surface glycoprotein (predicted), DUF1773 family protein 5
SPCC569.03				cell surface glycoprotein (predicted), DUF1773 family protein 4
SPCC594.01				DUF1769 family protein
SPCC622.11				LMBR1-like membrane protein
SPCC777.12c				thioredoxin family protein
SPCC794.04c				membrane transporter (predicted)
SPCC825.01				ATPase, Arb family ABCF1-like (predicted)
SPCC965.12				dipeptidyl peptidase (predicted)
SPAC922.03				1-aminocyclopropane-1-carboxylate deaminase (predicted)
SPBC4.06				acid phosphatase (predicted)
SPBC31F10.02				acyl-CoA thioesterase (predicted)
SPBC359.06	mug14			adducin
SPBC1289.14				adducin (predicted)
SPAC26A3.02	myh1			adenine DNA glycosylase Myh1
SPAPB24D3.03				agmatinase (predicted)
SPAC11D3.09				agmatinase (predicted)
SPBC8E4.03				agmatinase 2 (predicted)
SPBC1773.06c				alcohol dehydrogenase (predicted)
SPCC550.10	meu8			aldehyde dehydrogenase Meu8 (predicted)
SPBC13G1.04c				alkB homolog/2-OG-Fe(II) oxygenase family (predicted)
SPAC1527.01	mok11			alpha-1,3-glucan synthase Mok11
SPBC32H8.13c	mok12			alpha-1,3-glucan synthase Mok12
SPBC16D10.05	mok13			alpha-1,3-glucan synthase Mok13
SPCC63.04	mok14			alpha-1,4-glucan synthase Mok14

Table 3.1 Conserved eukaryotic genes present in *S. pombe* with no apparent *S. cerevisiae* ortholog (continued)

systemic ID	gene	source	phenotype	description
SPAC15A10.08	ain1			alpha-actinin
SPAC2F3.08	sut1			alpha-glucoside transporter Sut1
SPBC660.12c				aminotransferase (predicted)
SPBC1773.03c				aminotransferase class-III, unknown specificty
SPAC13G7.07	arb2			argonaute binding protein 2
SPBC1709.16c				aromatic ring-opening dioxygenase (predicted)
SPBPB10D8.02c				arylsulfatase (predicted)
SPCC737.09c	hmt1			ATP-binding cassette-type vacuolar membrane transporter Hmt1
SPAC22A12.16				ATP-citrate synthase subunit 2 (predicted)
SPAC20H4.09				ATP-dependent RNA helicase, spliceosomal (predicted)
SPBC15C4.05				ATP-dependent RNA/DNA helicase (predicted)
SPCC1919.11	mug137			BAR adaptor protein
SPBC19C2.10				BAR adaptor protein
SPBC19C7.10	bqt4			bouquet formation protein Bqt4
SPCC330.11	btb1			BTB/POZ domain protein Btb1
SPCC417.12				carboxylesterase-lipase family protein
SPCC736.08	cbf11			CBF1/Su(H)/LAG-1 family transcription factor Cbf11
SPCC1223.13	cbf12			CBF1/Su(H)/LAG-1 family transcription factor Cbf12
SPCC613.11c	meu23			cell surface glycoprotein (predicted), DUF1773 family protein 2
SPAC1B3.17	clr2			chromatin silencing protein Clr2
SPAC18G6.02c	chp1			chromodomain protein Chp1
SPAC3H8.04				chromosome segregation protein (predicted)
SPBC646.02	cwf11			complexed with Cdc5 protein Cwf11
SPAC17H9.06c				conserved eukaryotic protein
SPAC140.04				conserved eukaryotic protein
SPAC11E3.12				conserved eukaryotic protein
SPBC20F10.03				conserved eukaryotic protein
SPCC126.01c				conserved fungal protein
SPAC17A5.05c				conserved fungal protein
SPAC32A11.02c				conserved fungal protein
SPAC11D3.01c				conserved fungal protein
SPAC4D7.11	dsc4			conserved fungal protein
SPAC12G12.07c				conserved fungal protein
SPAC1952.10c				conserved fungal protein
SPAC1F12.04c				conserved fungal protein
SPAC22H10.02				conserved fungal protein
SPAC343.12	rds1			conserved fungal protein
SPBC1E8.03c				conserved fungal protein
SPBC16H5.12c				conserved fungal protein
SPAC19G12.16c	adg2			conserved fungal protein Adg2
SPCC1259.08				conserved fungal protein, DUF2457 family
SPACUNK4.09				conserved protein
SPAC6G9.01c				conserved protein
SPAC11D3.03c				conserved protein
SPAC12B10.16c	mug157			conserved protein Mug157
SPAC24C9.05c	mug70			conserved protein Mug20
SPAC4A8.02c				conserved protein, UPF0047 family
SPAC1952.12c	csn71			COP9/signalosome complex subunit 7a (predicted)
SPBC215.03c	csn1			COP9/signalosome complex subunit Csn1
SPAC222.16c	csn3			COP9/signalosome complex subunit Csn3 (predicted)
SPAC2E1P3.04	cao1			copper amine oxidase Cao1
SPBC1289.16c	cao2			copper amine oxidase-like protein Cao2
SPAC57A10.03	cyp1			cyclophilin family peptidyl-prolyl cis-trans isomerase Cyp1
SPBC1709.04c	cyp3			cyclophilin family peptidyl-prolyl cis-trans isomerase Cyp3
SPCC1450.07c				D-amino acid oxidase (predicted)
SPCC297.05				diacylglycerol binding protein (predicted)
SPAC3A11.10c				dipeptidyl peptidase (predicted)
SPBC19C2.02	pmt1			DNA methyltransferase homolog
SPBC12D12.02c	cdm1			DNA polymerase delta subunit Cdm1
SPCC63.03				DNAJ domain protein, DNAJC11 family

Table 3.1 Conserved eukaryotic genes present in *S. pombe* with no apparent *S. cerevisiae* ortholog (continued)

systemic ID	gene	source	phenotype	description
SPBC543.02c				DNAJ/TPR domain protein DNAJC7 family
SPAC5H10.01				DUF1445 family protein
SPAC1002.18	urg3			DUF1688 family protein
SPAC1952.06c				DUF1716 family protein
SPBC20F10.02c				DUF1741 family protein
SPAC15E1.02c				DUF1761 family protein
SPBC409.17c				DUF1769 family protein
SPAC14C4.01c				DUF1770 family protein
SPAC20G4.03c	hri1			eIF2 alpha kinase Hri1
SPAC222.07c	hri2			eIF2 alpha kinase Hri2
SPCC757.02c				epimarase (predicted)
SPAC1039.03				esterase/lipase (predicted)
SPAC4A8.06c				esterase/lipase (predicted)
SPAC29E6.01	pof11			F-box protein Pof11
SPAC869.04				formamidase-like protein (predicted)
SPAC2E1P3.05c				fungal cellulose binding domain protein
SPCC4G3.19	alp16			gamma tubulin complex subunit Alp16
SPBC211.06	gfh1			gamma tubulin complex subunit Gfh1
SPAC806.08c	mod21			gamma tubulin complex subunit Mod21
SPBC577.03c				GCN5-related N-acetyltransferase (predicted)
SPAC14C4.09	agn1			glucan endo-1,3-alpha-glucosidase Agn1
SPBC646.06c	agn2			glucan endo-1,3-alpha-glucosidase Agn2
SPBC1198.01				glutathione-dependent formaldehyde dehydrogenase (predicted)
SPBC1778.09				GTPase activating protein (predicted)
SPAC1952.17c				GTPase activating protein (predicted)
SPAC1B3.11c	ypt4			GTPase Ypt4
SPBC215.10				haloacid dehalogenase-like hydrolase
SPAC22F3.13	tsc1			hamartin
SPCC1739.03	hrr1			Helicase Required for RNAi-mediated heterochromatin assembly Hrr1
SPCC1020.09	gnr1			heterotrimeric G protein beta subunit Gnr1
SPAC869.06c				HHE domain cation binding protein (predicted)
SPAC1834.08	mak1			histidine kinase Mak1
SPCC74.06	mak3			histidine kinase Mak3
SPCC126.13c				histone deacetylase complex subunit, SAP128 family (predicted)
SPBP8B7.07c	set6			histone lysine methyltransferase Set6 (predicted)
SPBC2F12.12c				human c19orf29 ortholog
SPBC119.03				human COMT homolog 1
SPAC31G5.21				human FAM32A homolog
SPAC29B12.11c				human WW domain binding protein-2 ortholog
SPAC19B12.07c				human ZNF277 ortholog
SPBC30D10.09c				HVA22/TB2/DP1 family protein
SPBC18E5.10				iron sulfur cluster assembly protein (predicted)
SPAC144.14	klp8			kinesin-like protein Klp8
SPAC186.08c				L-lactate dehydrogenase (predicted)
SPBC354.15	fap1			L-pipecolate oxidase
SPAC139.04c	fap2			L-saccharopine oxidase
SPCC126.08c				lectin family glycoprotien receptor (predicted)
SPAC926.06c				leucine-rich repeat protein, unknown
SPBC19C7.01	mni1			Mago Nashi interacting protein (predicted)
SPBC29A10.02	spo5			meiotic RNA-binding protein 1
SPAC25H1.03	mug66			meiotically upregulated gene Mug66
SPAPB1E7.08c				membrane transporter (predicted)
SPCC18.02				membrane transporter (predicted)
SPBC354.05c	sre2			membrane-tethered transcription factor (predicted)
SPAC11D3.05	mfs2			MFS family membrane transporter (predicted)
SPAC806.05				mitochondrial ANC9 family protein
SPBC18H10.11c	ppr2			mitochondrial PPR repeat protein Ppr2
SPCC777.17c				mitochondrial ribosomal protein subunit L9 (predicted)
SPBC18E5.13				mitochondrial translation initiation factor (predicted)
SPCC1183.11				MS ion channel protein 1 (predicted)

Table 3.1 Conserved eukaryotic genes present in *S. pombe* with no apparent *S. cerevisiae* ortholog (continued)

systemic ID	gene	source	phenotype	description
SPAC2C4.17c				MS ion channel protein 2 (predicted)
SPAC15A10.10	mde6			Muskelin homolog (predicted)
SPAC29A4.05	cam2			myosin I light chain Cam2
SPAC1002.07c	ats1			N-acetyltransferase Ats1 (predicted)
SPBC12C2.04				NAD binding dehydrogenase family protein
SPACUNK4.17				NAD binding dehydrogenase family protein
SPAC1071.11				NADH-dependent flavin oxidoreductase (predicted)
SPCC1884.02	nic1			NiCoT heavy metal ion transporter Nic1
SPAC869.02c				nitric oxide dioxygenase (predicted)
SPBC20F10.05	nrl1			NRDE-2 family protein (predicted)
SPAC12G12.12				NST UDP-galactose transporter (predicted)
SPBC29A10.06c	ely5			nuclear pore protein Ely5
SPBC15D4.10c	amo1			nuclear rim protein Amo1
SPBPB2B2.11				nucleotide-sugar 4,6-dehydratase (predicted)
SPAC14C4.10c				Nudix family hydrolase
SPBC1703.11				optic atrophy 3 family protein
SPBC577.14c	spa1			ornithine decarboxylase antizyme
SPAC23G3.03	sib2			ornithine N5 monooxygenase (predicted)
SPBC1711.12				oxidised protein hydrolase (predicted)
SPAC13A11.05				peptidase family M17
SPAC513.02				phosphoglycerate mutase family
SPAC9G1.08c				phospholipase (predicted)
SPAC8E11.04c				phospholipase (predicted)
SPBC106.11c	plg7			phospholipase A2, PAF family homolog
SPAC3H1.10				phytochelatin synthetase
SPAC19D5.03	cid1			poly(A) polymerase Cid1
SPBC1685.06	cid11			poly(A) polymerase Cid11 (predicted)
SPAC17H9.01	cid16			poly(A) polymerase Cid16 (predicted)
SPCC965.06				potassium channel subunit (predicted)
SPBP35G2.02				poteasome interacting protein (predicted)
SPAPYUG7.06	mug67			PPPDE peptidase family (predicted)
SPBC16G5.07c				prohibitin (predicted)
SPAC869.08	pcm2			protein-L-isoaspartate O-methyltransferase Pcm2 (predicted)
SPAC8F11.10c	pvg1			pyruvyltransferase Pvg1
SPAC24H6.09	gef1			RhoGEF Gef1
SPAC31A2.16	gef2			RhoGEF Gef2
SPCC1223.10c	eaf1			RNA polymerase II transcription elongation factor SpEAF
SPBP23A10.14c	ell1			RNA polymerase II transcription elongation factor SpELL
SPAC10F6.06	vip1			RNA-binding protein Vip1
SPAC1B3.10c				SEL1 repeat protein, unknown biological role
SPAC1039.08				serine acetyltransferase (predicted)
SPBC18H10.15	ppk23			serine/threonine protein kinase Ppk23
SPCC162.10	ppk33			serine/threonine protein kinase Ppk33 (predicted)
SPCC162.03				short chain dehydrogenase (predicted)
SPAC3A11.04				siepin homolog
SPAC31G5.18c	sde2			silencing defective protein Sde2
SPBC3B8.08				Sjogren's syndrome/scleroderma autoantigen 1 family (predicted)
SPAC19B12.12c	yip11			SMN family protein Yip11
SPAC11D3.04c				SnoaL
SPBC1289.11	spf38			splicing factor Spf38
SPAC17A5.04c	mde10			spore wall assembly ADAM family peptidase Mde10
SPBC11C11.08	srp1			SR family protein, human SRFS2 ortholog Srp1
SPCC594.04c				steroid oxidoreductase superfamily protein (predicted)
SPAC9.08c				steroid reductase (predicted)
SPBC2G5.06c	hmt2			sulfide-quinone oxidoreductase
SPAC22E12.03c				ThiJ domain protein
SPAC823.09c				threonine aspartase (predicted)
SPBP35G2.11c				transcription related zf-ZZ type zinc finger protein
SPBC887.17				transmembrane transporter (predicted)
SPCC285.04				transthyretin (predicted)

Table 3.1 Conserved eukaryotic genes present in *S. pombe* with no apparent *S. cerevisiae* ortholog (continued)

systemic ID	gene	source	phenotype	description
SPAC22F8.04				triose phosphate transporter (predicted)
SPAP8A3.12c	tpp2			tripeptidyl-peptidase II Tpp2
SPCC1322.03				TRP-like ion channel (predicted)
SPBC725.10				tspO homolog/ peripheral benzodiazepine receptor homolog (predicted)
SPAC630.13c	tsc2			tuberin
SPBC8D2.10c	rmt3			type I ribosomal protein arginine N-methyltransferase Rmt3
SPBC29A3.07c	sab14			U2 snRNP-associated protein SF3B14 ortholog (predicted)
SPBC11C11.01				U2-associated protein (predicted)
SPAC1B3.06c				UbiE family methyltransferase (predicted)
SPBC4.05	mlo2			ubiquitin protein ligase E3 component human N-recognin 7 homolog Mlo2
SPAC6B12.07c				ubiquitin-protein ligase E3 (predicted)
SPAC2F3.16				ubiquitin-protein ligase E3 (predicted)
SPCC1795.03	gms1			UDP-galactose transporter Gms1
SPAC3A12.09c				urease accessory protein UreD (predicted)
SPAC29A4.13				urease accessory protein UreF (predicted)
SPCPB16A4.05c				urease accessory protein UREG (predicted)
SPAC1952.11c	ure2			urease Ure2
SPCC1223.09				uricase (predicted)
SPBC25B2.10				Usp (universal stress protein) family protein
SPAC1834.09	mug51			variant protein kinase 19 family protein
SPCC553.04	cyp9			WD repeat containing cyclophilin family PPIase Cyp9 (predicted)
SPAC17H9.19c	cdt2			WD repeat protein Cdt2
SPBC713.05				WD repeat protein, human MAPK organizer 1 (MORG1) family (predicted)
SPAC12B10.03	bun62			WD repeat protein, human WDR20 family, Bun62
SPBC609.03	iqw1			WD repeat protein, Iqw1
SPAC4F10.18	nup37			WD repeat protein, nucleoporin Nup37 (predicted)
SPBC2A9.03				WD40/YVTN repeat-like
SPBC18H10.07				WW domain-binding protein 4 (predicted)
SPBC18A7.01				X-Pro dipeptidase (predicted)
SPCC1020.12c	xap5			xap-5-like protein
SPBC2A9.07c				zf-PARP type zinc finger protein
SPBC577.04				human THOC5 ortholog (predicted)
SPBC16C6.10	chp2			chromodomain protein 2
SPAC1782.12c				DUF423 protein
SPAC25B8.12c				nucleotide-sugar phosphatase (predicted)
SPAC7D4.03c				conserved fungal family
SPAC890.02c	alp7			centrosomal transforming acidic coiled-coil (TACC) protein ortholog Alp7
SPAPB17E12.02	yip12			SMN family protein Yip12
SPBC106.08c	mug2			cell surface glycoprotein (predicted), DUF1773 family protein 1
SPBC16E9.15				heat shock factor binding protein (predicted)
SPBC1709.03				conserved fungal protein
SPBC32H8.09				WD repeat protein, human WDR8 family
SPBC577.08c	txl1			thioredoxin-like I protein Txl1
SPBP4H10.07				ubiquitin-protein ligase E3 (predicted)
SPCC737.06c				glutamate-cysteine ligase regulatory subunit (predicted)
SPAC343.17c				WD repeat protein, human WDR70 family
SPBP23A10.05	ssr4			SWI/SNF and RSC complex subunit Ssr4
SPAC3A11.08	pcu4			cullin 4
SPAC12B10.08c				mitochondrial tRNA(Ile)-lysidine synthetase family (predicted)
SPAC22G7.11c				conserved fungal protein
SPAC23H4.09	cdb4			curved DNA-binding protein Cdb4, peptidase family
SPAC25B8.13c	isp7			2-OG-Fe(II) oxygenase superfamily protein
SPAC6B12.14c				conserved fungal protein
SPAC6F6.04c				membrane transporter (predicted)
SPAC869.09				conserved fungal protein
SPAC9E9.15				CIA30 protein (predicted)
SPAPB8E5.03	mae1			malic acid transport protein Mae1
SPBC1685.11	rlp1			RecA family ATPase Rlp1
SPBC17A3.05c				DNAJ/DUF1977 DNAJB12 homolog (predicted)
SPBC1E8.05				conserved fungal protein

Table 3.1 Conserved eukaryotic genes present in *S. pombe* with no apparent *S. cerevisiae* ortholog (continued)

systemic ID	gene	source	phenotype	description
SPBC29A10.12				HMG-box variant
SPBP23A10.12	frg1			FRG1 family protein, involved in mRNA processing (predicted)
SPCC1753.05	rsm1			RNA export factor Rsm1
SPCC737.03c	ima1			integral inner nuclear membrane protein Ima1
SPCC794.06				TDT malic acid transporter (predicted)
SPBC17G9.05	rct1			RRM-containing cyclophilin regulating transcription Rct1
SPAC140.03	arb1	Bioneer	loss silencing	argonaute inhibitor protein 1
SPAC10F6.14c		Bioneer		ABC1 kinase family protein (predicted)
SPAC12B10.14c	tea5	Bioneer		pseudokinase Tea5
SPAC13G7.09c		Bioneer		conserved fungal protein
SPAC16A10.07c	taz1, myb, myb1	Bioneer	loss silencing (*mat, telomere*)	human TRF ortholog Taz1
SPAC16E8.12c		Bioneer		ING family homolog Png3 (predicted)
SPAC1783.01		Bioneer		methionine synthase reductase (predicted)
SPAC17C9.05c	pmc3	Bioneer		mediator complex subunit Pmc3/Med27
SPAC17C9.11c		Bioneer		zf-C2H2 type zinc finger protein/UBA domain protein
SPAC186.09		Bioneer		pyruvate decarboxylase (predicted)
SPAC1952.16	rga9	Bioneer		RhoGAP, GTPase activator towards Rho/Rac/Cdc42-like small GTPases (prec
SPAC1D4.01		Bioneer		human C9orf78 ortholog
SPAC22H10.13	zym1	Bioneer		metallothionein Zym1
SPAC24C9.15c	spn5	Bioneer		septin Spn5
SPAC27D7.09c		Bioneer		But2 family protein
SPAC27D7.11c		Bioneer		But2 family protein
SPAC29B12.08	clr5	Bioneer	loss silencing (*mat*)	Clr5 protein
SPAC2C4.07c	dis32	Bioneer		3'-5'-exoribonuclease activity Dis3L2
SPAC30D11.01c	gto2	Bioneer		alpha-glucosidase (predicted)
SPAC343.11c	msc1	Bioneer		multi-copy suppressor of Chk1
SPAC57A7.09		Bioneer		human RNF family homolog
SPAC959.04c	omh6	Bioneer		alpha-1,2-mannosyltransferase Omh6 (predicted)
SPAC959.06c		Bioneer		conserved fungal protein
SPAP11E10.02c	mam3	Bioneer		cell agglutination protein Mam3
SPAP32A8.03c		Bioneer		ubiquitin-protein ligase E3 (predicted)
SPBC106.12c		Bioneer		THO complex subunit (predicted)
SPBC12C2.03c		Bioneer		methionine synthase reductase (predicted)
SPBC1347.03	meu14	Bioneer		sporulation specific PIL domain protein Meu14
SPBC13E7.06	msd1	Bioneer		mitotic-spindle disanchored Msd1
SPBC1604.03c		Bioneer		conserved fungal protein
SPBC16C6.04	dbl6	Bioneer		double strand break localizing protein Dbl6
SPBC16G5.03		Bioneer		ubiquitin-protein ligase E3 (predicted)
SPBC16H5.13		Bioneer		WD repeat protein, human WDR7 ortholog
SPBC1778.05c		Bioneer		human LAMTOR2 ortholog
SPBC1861.02	abp2	Bioneer		ARS binding protein Abp2
SPBC1921.06c	pvg3	Bioneer		galactosylxylosylprotein 3-beta-galactosyltransferase Pvg1
SPBC19C2.09	sre1	Bioneer		sterol regulatory element binding protein, transcription factor Sre1
SPBC21D10.10	bdc1	Bioneer		bromodomain containing protein 1, Bdc1
SPBC26H8.13c		Bioneer		Siva family protein (predicted)
SPBC365.16		Bioneer		conserved protein
SPBC36B7.02		Bioneer		Svf1 family protein Svf2
SPBC3D6.02	but2	Bioneer		But2 family protein But2
SPBC3E7.04c		Bioneer		Ric8 family guanine nucleotide exchange factor synembryn family
SPBC409.06	uch2	Bioneer		ubiquitin C-terminal hydrolase Uch2
SPCC11E10.09c		Bioneer		alpha-amylase homolog (predicted)
SPCC1682.15	mug122	Bioneer		PX/PXA domain protein
SPCC16C4.20c		Bioneer		HMG box protein (predicted)
SPCC18.17c		Bioneer		26S proteasome non-ATPase regulatory subunit (predicted)
SPCC24B10.16c		Bioneer		proteasome assembly chaperone 4 (predicted)
SPCC74.09	mug24	Bioneer		RNA-binding protein, rrm type
SPCC777.06c		Bioneer		hydrolase (predicted)
SPCC895.05	for3	Bioneer		formin For3

Table 3.1 Conserved eukaryotic genes present in *S. pombe* with no apparent *S. cerevisiae* ortholog (continued)

category	total	characterized/ screened	essential	uncharacterized
genes total	538	47	49	442
genes of interest	442	262	6	174
Bioneer collection	279	227	0	52
Homemade strains	163	35	6	122

Table 3.2 Summary of screen progress

systemic ID	gene	description
SPCC4G3.07c	phf1	PHD finger containing protein Phf1
SPBC337.12	red5	human ZC3H3 homolog
SPBC8D2.07c	sfc9	transcription factor TFIIIC complex subunit Sfc9 (predicted)
SPAC19G12.07c	rsd1	RNA-binding protein Rsd1 (predicted)
SPBC16H5.15		conserved fungal protein
SPCC162.01c		U4/U6 x U5 tri-snRNP complex subunit (predicted)

Table 3.3 Essential genes

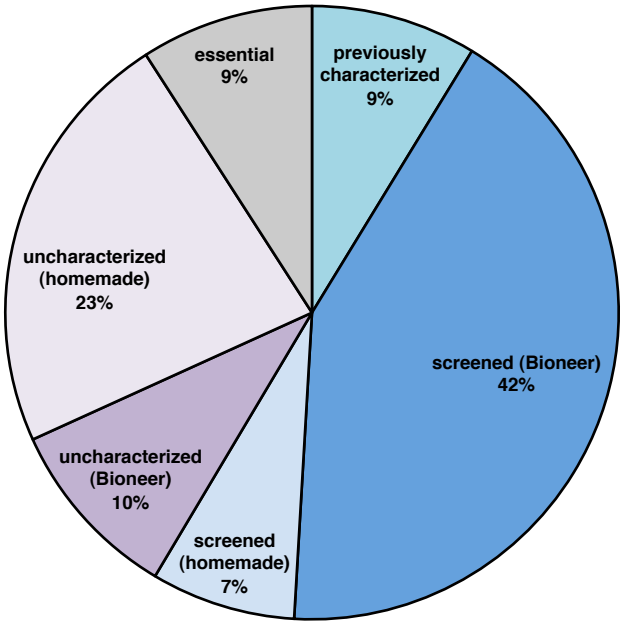

Figure 3.2 The screen progress

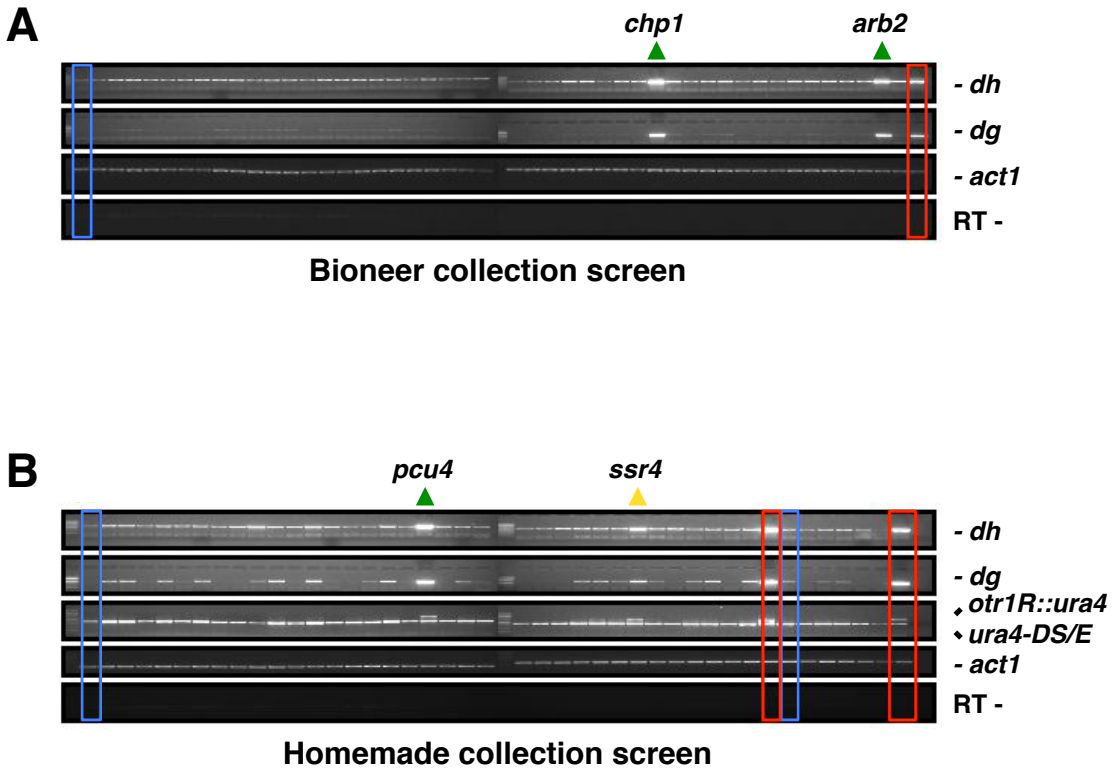

Figure 3.3 Identification of silencing impaired mutants

Representative results of semi-quantitative RT-PCR. Wild type controls are marked by blue boxes; *rik1Δ* mutant controls are marked by red boxes. Previously identified silencing genes are labeled by green triangles; novel gene involved in silencing is labeled by yellow triangle.
(A) Bioneer knockout collection screen
(B) Homemade knockout collection screen

systemic ID	gene	source	*dh*	*dg*	*otr:ura4*	description
SPAC922.03		Bioneer			n.a.	1-aminocyclopropane-1-carboxylate deaminase (predicted)
SPBC4.06		Bioneer	+	+	n.a.	acid phosphatase (predicted)
SPBC31F10.02		Bioneer	+	+	n.a.	acyl-CoA thioesterase (predicted)
SPBC359.06	mug14	Bioneer	+		n.a.	adducin
SPBC1289.14		Bioneer			n.a.	adducin (predicted)
SPAC26A3.02	myh1	Bioneer			n.a.	adenine DNA glycosylase Myh1
SPAPB24D3.03		Bioneer	+	+	n.a.	agmatinase (predicted)
SPAC11D3.09		Bioneer			n.a.	agmatinase (predicted)
SPBC8E4.03		Bioneer	+	+	n.a.	agmatinase 2 (predicted)
SPBC1773.06c		Bioneer		+	n.a.	alcohol dehydrogenase (predicted)
SPCC550.10	meu8	Bioneer	+	+	n.a.	aldehyde dehydrogenase Meu8 (predicted)
SPBC13G1.04c		Bioneer		+	n.a.	alkB homolog/2-OG-Fe(II) oxygenase family (predicted)
SPAC1527.01	mok11	Bioneer		+	n.a.	alpha-1,3-glucan synthase Mok11
SPBC32H8.13c	mok12	Bioneer			n.a.	alpha-1,3-glucan synthase Mok12
SPBC16D10.05	mok13	Bioneer		+	n.a.	alpha-1,3-glucan synthase Mok13
SPCC63.04	mok14	Bioneer		+	n.a.	alpha-1,4-glucan synthase Mok14
SPAC15A10.08	ain1	Bioneer	+	+	n.a.	alpha-actinin
SPAC2F3.08	sut1	Bioneer	+	+	n.a.	alpha-glucoside transporter Sut1
SPBC660.12c		Bioneer			n.a.	aminotransferase (predicted)
SPBC1773.03c		Bioneer			n.a.	aminotransferase class-III, unknown specificty
SPAC13G7.07	arb2	Bioneer	+++	+++	n.a.	argonaute binding protein 2
SPBC1709.16c		Bioneer		+	n.a.	aromatic ring-opening dioxygenase (predicted)
SPBPB10D8.02c		Bioneer	+	+	n.a.	arylsulfatase (predicted)
SPCC737.09c	hmt1	Bioneer		+	n.a.	ATP-binding cassette-type vacuolar membrane transporter Hmt1
SPAC22A12.16		Bioneer		+	n.a.	ATP-citrate synthase subunit 2 (predicted)
SPAC20H4.09		Bioneer		+	n.a.	ATP-dependent RNA helicase, spliceosomal (predicted)
SPBC15C4.05		Bioneer	+	+	n.a.	ATP-dependent RNA/DNA helicase (predicted)
SPCC1919.11	mug137	Bioneer		+	n.a.	BAR adaptor protein
SPBC19C2.10		Bioneer			n.a.	BAR adaptor protein
SPBC19C7.10	bqt4	Bioneer		+	n.a.	bouquet formation protein Bqt4
SPCC330.11	btb1	Bioneer	+	+	n.a.	BTB/POZ domain protein Btb1
SPCC417.12		Bioneer	+	+	n.a.	carboxylesterase-lipase family protein
SPCC736.08	cbf11	Bioneer		+	n.a.	CBF1/Su(H)/LAG-1 family transcription factor Cbf11
SPCC1223.13	cbf12	Bioneer			n.a.	CBF1/Su(H)/LAG-1 family transcription factor Cbf12
SPCC613.11c	meu23	Bioneer	+	+	n.a.	cell surface glycoprotein (predicted), DUF1773 family protein 2
SPAC1B3.17	clr2	Bioneer	++	+	n.a.	chromatin silencing protein Clr2
SPAC18G6.02c	chp1	Bioneer	+++	+++	n.a.	chromodomain protein Chp1
SPAC3H8.04		Bioneer		+	n.a.	chromosome segregation protein (predicted)
SPBC646.02	cwf11	Bioneer			n.a.	complexed with Cdc5 protein Cwf11
SPAC17H9.06c		Bioneer	+	+	n.a.	conserved eukaryotic protein
SPAC140.04		Bioneer	+	+	n.a.	conserved eukaryotic protein
SPAC11E3.12		Bioneer		+	n.a.	conserved eukaryotic protein
SPBC20F10.03		Bioneer			n.a.	conserved eukaryotic protein
SPCC126.01c		Bioneer	+	+	n.a.	conserved fungal protein
SPAC17A5.05c		Bioneer	+	+	n.a.	conserved fungal protein
SPAC32A11.02c		Bioneer	+	+	n.a.	conserved fungal protein
SPAC11D3.01c		Bioneer	+	+	n.a.	conserved fungal protein
SPAC4D7.11	dsc4	Bioneer	+	+	n.a.	conserved fungal protein
SPAC12G12.07c		Bioneer	+		n.a.	conserved fungal protein
SPAC1952.10c		Bioneer	+		n.a.	conserved fungal protein
SPAC1F12.04c		Bioneer		+	n.a.	conserved fungal protein
SPAC22H10.02		Bioneer		+	n.a.	conserved fungal protein
SPAC343.12	rds1	Bioneer		+	n.a.	conserved fungal protein
SPBC1E8.03c		Bioneer			n.a.	conserved fungal protein
SPBC16H5.12c		Bioneer			n.a.	conserved fungal protein
SPAC19G12.16c	adg2	Bioneer			n.a.	conserved fungal protein Adg2
SPCC1259.08		Bioneer	+	+	n.a.	conserved fungal protein, DUF2457 family
SPACUNK4.09		Bioneer	+	+	n.a.	conserved protein
SPAC6G9.01c		Bioneer		+	n.a.	conserved protein
SPAC11D3.03c		Bioneer			n.a.	conserved protein

Table 3.4 Summary of screen result

Genes known to be involved in silencing are labeled in green, novel genes identified in the screen are labeled in yellow. (+) indicates pericentromeric transcript accumulation. (n.a.) indicates analysis not applicable.

systemic ID	gene	source	*dh*	*dg*	*otr:ura4*	description
SPAC12B10.16c	mug157	Bioneer	+		n.a.	conserved protein Mug157
SPAC24C9.05c	mug70	Bioneer	++	+	n.a.	conserved protein Mug20
SPAC4A8.02c		Bioneer			n.a.	conserved protein, UPF0047 family
SPAC1952.12c	csn71	Bioneer			n.a.	COP9/signalosome complex subunit 7a (predicted)
SPBC215.03c	csn1	Bioneer	+		n.a.	COP9/signalosome complex subunit Csn1
SPAC222.16c	csn3	Bioneer			n.a.	COP9/signalosome complex subunit Csn3 (predicted)
SPAC2E1P3.04	cao1	Bioneer			n.a.	copper amine oxidase Cao1
SPBC1289.16c	cao2	Bioneer	+	+	n.a.	copper amine oxidase-like protein Cao2
SPAC57A10.03	cyp1	Bioneer		+	n.a.	cyclophilin family peptidyl-prolyl cis-trans isomerase Cyp1
SPBC1709.04c	cyp3	Bioneer			n.a.	cyclophilin family peptidyl-prolyl cis-trans isomerase Cyp3
SPCC1450.07c		Bioneer		+	n.a.	D-amino acid oxidase (predicted)
SPCC297.05		Bioneer	+		n.a.	diacylglycerol binding protein (predicted)
SPAC3A11.10c		Bioneer	+	+	n.a.	dipeptidyl peptidase (predicted)
SPBC19C2.02	pmt1	Bioneer		+	n.a.	DNA methyltransferase homolog
SPBC12D12.02c	cdm1	Bioneer			n.a.	DNA polymerase delta subunit Cdm1
SPCC63.03		Bioneer		+	n.a.	DNAJ domain protein, DNAJC11 family
SPBC543.02c		Bioneer			n.a.	DNAJ/TPR domain protein DNAJC7 family
SPAC5H10.01		Bioneer			n.a.	DUF1445 family protein
SPAC1002.18	urg3	Bioneer	+	+	n.a.	DUF1688 family protein
SPAC1952.06c		Bioneer	+		n.a.	DUF1716 family protein
SPBC20F10.02c		Bioneer			n.a.	DUF1741 family protein
SPAC15E1.02c		Bioneer	+		n.a.	DUF1761 family protein
SPBC409.17c		Bioneer	+	+	n.a.	DUF1769 family protein
SPAC14C4.01c		Bioneer	+	+	n.a.	DUF1770 family protein
SPAC20G4.03c	hri1	Bioneer	+	+	n.a.	eIF2 alpha kinase Hri1
SPAC222.07c	hri2	Bioneer	+	+	n.a.	eIF2 alpha kinase Hri2
SPCC757.02c		Bioneer	+	+	n.a.	epimarase (predicted)
SPAC1039.03		Bioneer	+	+	n.a.	esterase/lipase (predicted)
SPAC4A8.06c		Bioneer			n.a.	esterase/lipase (predicted)
SPAC29E6.01	pof11	Bioneer			n.a.	F-box protein Pof11
SPAC869.04		Bioneer	+	+	n.a.	formamidase-like protein (predicted)
SPAC2E1P3.05c		Bioneer	+		n.a.	fungal cellulose binding domain protein
SPCC4G3.19	alp16	Bioneer	+	+	n.a.	gamma tubulin complex subunit Alp16
SPBC211.06	gfh1	Bioneer		+	n.a.	gamma tubulin complex subunit Gfh1
SPAC806.08c	mod21	Bioneer			n.a.	gamma tubulin complex subunit Mod21
SPBC577.03c		Bioneer			n.a.	GCN5-related N-acetyltransferase (predicted)
SPAC14C4.09	agn1	Bioneer			n.a.	glucan endo-1,3-alpha-glucosidase Agn1
SPBC646.06c	agn2	Bioneer			n.a.	glucan endo-1,3-alpha-glucosidase Agn2
SPBC1198.01		Bioneer			n.a.	glutathione-dependent formaldehyde dehydrogenase (predicted)
SPBC1778.09		Bioneer	+	+	n.a.	GTPase activating protein (predicted)
SPAC1952.17c		Bioneer			n.a.	GTPase activating protein (predicted)
SPAC1B3.11c	ypt4	Bioneer	+	+	n.a.	GTPase Ypt4
SPBC215.10		Bioneer			n.a.	haloacid dehalogenase-like hydrolase
SPAC22F3.13	tsc1	Bioneer			n.a.	hamartin
SPCC1739.03	hrr1	Bioneer			n.a.	Helicase Required for RNAi-mediated heterochromatin assembly Hrr1
SPCC1020.09	gnr1	Bioneer		+	n.a.	heterotrimeric G protein beta subunit Gnr1
SPAC869.06c		Bioneer	+		n.a.	HHE domain cation binding protein (predicted)
SPAC1834.08	mak1	Bioneer			n.a.	histidine kinase Mak1
SPCC74.06	mak3	Bioneer			n.a.	histidine kinase Mak3
SPCC126.13c		Bioneer	+	+	n.a.	histone deacetylase complex subunit, SAP128 family (predicted)
SPBP8B7.07c	set6	Bioneer		+	n.a.	histone lysine methyltransferase Set6 (predicted)
SPBC2F12.12c		Bioneer			n.a.	human c19orf29 ortholog
SPBC119.03		Bioneer			n.a.	human COMT homolog 1
SPAC31G5.21		Bioneer		+	n.a.	human FAM32A homolog
SPAC29B12.11c		Bioneer			n.a.	human WW domain binding protein-2 ortholog
SPAC19B12.07c		Bioneer		+	n.a.	human ZNF277 ortholog
SPBC30D10.09c		Bioneer	+	+	n.a.	HVA22/TB2/DP1 family protein
SPBC18E5.10		Bioneer		+	n.a.	iron sulfur cluster assembly protein (predicted)
SPAC144.14	klp8	Bioneer	+	+	n.a.	kinesin-like protein Klp8
SPAC186.08c		Bioneer			n.a.	L-lactate dehydrogenase (predicted)

Table 3.4 Summary of screen result (continued)

systemic ID	gene	source	*dh*	*dg*	*otr:ura4*	description
SPBC354.15	fap1	Bioneer			n.a.	L-pipecolate oxidase
SPAC139.04c	fap2	Bioneer		+	n.a.	L-saccharopine oxidase
SPCC126.08c		Bioneer		+	n.a.	lectin family glycoprotien receptor (predicted)
SPAC926.06c		Bioneer		+	n.a.	leucine-rich repeat protein, unknown
SPBC19C7.01	mni1	Bioneer		+	n.a.	Mago Nashi interacting protein (predicted)
SPBC29A10.02	spo5	Bioneer		+	n.a.	meiotic RNA-binding protein 1
SPAC25H1.03	mug66	Bioneer		+	n.a.	meiotically upregulated gene Mug66
SPAPB1E7.08c		Bioneer	+	+	n.a.	membrane transporter (predicted)
SPCC18.02		Bioneer	+	+	n.a.	membrane transporter (predicted)
SPBC354.05c	sre2	Bioneer	+	++	n.a.	membrane-tethered transcription factor (predicted)
SPAC11D3.05	mfs2	Bioneer			n.a.	MFS family membrane transporter (predicted)
SPAC806.05		Bioneer	essential		n.a.	mitochondrial ANC9 family protein
SPBC18H10.11c	ppr2	Bioneer	–	–	n.a.	mitochondrial PPR repeat protein Ppr2
SPCC777.17c		Bioneer			n.a.	mitochondrial ribosomal protein subunit L9 (predicted)
SPBC18E5.13		Bioneer		+	n.a.	mitochondrial translation initiation factor (predicted)
SPCC1183.11		Bioneer	+	+	n.a.	MS ion channel protein 1 (predicted)
SPAC2C4.17c		Bioneer			n.a.	MS ion channel protein 2 (predicted)
SPAC15A10.10	mde6	Bioneer	+	+	n.a.	Muskelin homolog (predicted)
SPAC29A4.05	cam2	Bioneer		+	n.a.	myosin I light chain Cam2
SPAC1002.07c	ats1	Bioneer			n.a.	N-acetyltransferase Ats1 (predicted)
SPBC12C2.04		Bioneer		+	n.a.	NAD binding dehydrogenase family protein
SPACUNK4.17		Bioneer		+	n.a.	NAD binding dehydrogenase family protein
SPAC1071.11		Bioneer			n.a.	NADH-dependent flavin oxidoreductase (predicted)
SPCC1884.02	nic1	Bioneer	+		n.a.	NiCoT heavy metal ion transporter Nic1
SPAC869.02c		Bioneer		+	n.a.	nitric oxide dioxygenase (predicted)
SPBC20F10.05	nrl1	Bioneer		+	n.a.	NRDE-2 family protein (predicted)
SPAC12G12.12		Bioneer		+	n.a.	NST UDP-galactose transporter (predicted)
SPBC29A10.06c	ely5	Bioneer	+	++	n.a.	nuclear pore protein Ely5
SPBC15D4.10c	amo1	Bioneer			n.a.	nuclear rim protein Amo1
SPBPB2B2.11		Bioneer			n.a.	nucleotide-sugar 4,6-dehydratase (predicted)
SPAC14C4.10c		Bioneer	+	+	n.a.	Nudix family hydrolase
SPBC1703.11		Bioneer			n.a.	optic atrophy 3 family protein
SPBC577.14c	spa1	Bioneer	+	+	n.a.	ornithine decarboxylase antizyme
SPAC23G3.03	sib2	Bioneer	+	+	n.a.	ornithine N5 monooxygenase (predicted)
SPBC1711.12		Bioneer	+	+	n.a.	oxidised protein hydrolase (predicted)
SPAC13A11.05		Bioneer		+	n.a.	peptidase family M17
SPAC513.02		Bioneer			n.a.	phosphoglycerate mutase family
SPAC9G1.08c		Bioneer		+	n.a.	phospholipase (predicted)
SPAC8E11.04c		Bioneer			n.a.	phospholipase (predicted)
SPBC106.11c	plg7	Bioneer		+	n.a.	phospholipase A2, PAF family homolog
SPAC3H1.10		Bioneer			n.a.	phytochelatin synthetase
SPAC19D5.03	cid1	Bioneer			n.a.	poly(A) polymerase Cid1
SPBC1685.06	cid11	Bioneer	+	+	n.a.	poly(A) polymerase Cid11 (predicted)
SPAC17H9.01	cid16	Bioneer			n.a.	poly(A) polymerase Cid16 (predicted)
SPCC965.06		Bioneer	+	+	n.a.	potassium channel subunit (predicted)
SPBP35G2.02		Bioneer			n.a.	poteasome interacting protein (predicted)
SPAPYUG7.06	mug67	Bioneer		+	n.a.	PPPDE peptidase family (predicted)
SPBC16G5.07c		Bioneer		+	n.a.	prohibitin (predicted)
SPAC869.08	pcm2	Bioneer	+	+	n.a.	protein-L-isoaspartate O-methyltransferase Pcm2 (predicted)
SPAC8F11.10c	pvg1	Bioneer		+	n.a.	pyruvyltransferase Pvg1
SPAC24H6.09	gef1	Bioneer			n.a.	RhoGEF Gef1
SPAC31A2.16	gef2	Bioneer	+	+	n.a.	RhoGEF Gef2
SPCC1223.10c	eaf1	Bioneer			n.a.	RNA polymerase II transcription elongation factor SpEAF
SPBP23A10.14c	ell1	Bioneer	+	+	n.a.	RNA polymerase II transcription elongation factor SpELL
SPAC10F6.06	vip1	Bioneer			n.a.	RNA-binding protein Vip1
SPAC1B3.10c		Bioneer	+	+	n.a.	SEL1 repeat protein, unknown biological role
SPAC1039.08		Bioneer	+	+	n.a.	serine acetyltransferase (predicted)
SPBC18H10.15	ppk23	Bioneer	+	+	n.a.	serine/threonine protein kinase Ppk23
SPCC162.10	ppk33	Bioneer			n.a.	serine/threonine protein kinase Ppk33 (predicted)
SPCC162.03		Bioneer	+	+	n.a.	short chain dehydrogenase (predicted)

Table 3.4 Summary of screen result (continued)

systemic ID	gene	source	dh	dg	otr:ura4	description
SPAC3A11.04		Bioneer		+	n.a.	siepin homolog
SPAC31G5.18c	sde2	Bioneer	+	++	n.a.	silencing defective protein Sde2
SPBC3B8.08		Bioneer		+	n.a.	Sjogren's syndrome/scleroderma autoantigen 1 family (predicted)
SPAC19B12.12c	yip11	Bioneer			n.a.	SMN family protein Yip11
SPAC11D3.04c		Bioneer			n.a.	SnoaL
SPBC1289.11	spf38	Bioneer			n.a.	splicing factor Spf38
SPAC17A5.04c	mde10	Bioneer		+	n.a.	spore wall assembly ADAM family peptidase Mde10
SPBC11C11.08	srp1	Bioneer			n.a.	SR family protein, human SRFS2 ortholog Srp1
SPCC594.04c		Bioneer			n.a.	steroid oxidoreductase superfamily protein (predicted)
SPAC9.08c		Bioneer		+	n.a.	steroid reductase (predicted)
SPBC2G5.06c	hmt2	Bioneer		+	n.a.	sulfide-quinone oxidoreductase
SPAC22E12.03c		Bioneer			n.a.	ThiJ domain protein
SPAC823.09c		Bioneer	+		n.a.	threonine aspartase (predicted)
SPBP35G2.11c		Bioneer			n.a.	transcription related zf-ZZ type zinc finger protein
SPBC887.17		Bioneer			n.a.	transmembrane transporter (predicted)
SPCC285.04		Bioneer			n.a.	transthyretin (predicted)
SPAC22F8.04		Bioneer	+	+	n.a.	triose phosphate transporter (predicted)
SPAP8A3.12c	tpp2	Bioneer	+	+	n.a.	tripeptidyl-peptidase II Tpp2
SPCC1322.03		Bioneer		+	n.a.	TRP-like ion channel (predicted)
SPBC725.10		Bioneer	+	+	n.a.	tspO homolog/ peripheral benzodiazepine receptor homolog, (predicted)
SPAC630.13c	tsc2	Bioneer	+	+	n.a.	tuberin
SPBC8D2.10c	rmt3	Bioneer		+	n.a.	type I ribosomal protein arginine N-methyltransferase Rmt3
SPBC29A3.07c	sab14	Bioneer		+	n.a.	U2 snRNP-associated protein SF3B14 ortholog (predicted)
SPBC11C11.01		Bioneer		+	n.a.	U2-associated protein (predicted)
SPAC1B3.06c		Bioneer			n.a.	UbiE family methyltransferase (predicted)
SPBC4.05	mlo2	Bioneer	+	+	n.a.	ubiquitin protein ligase E3 component human N-recognin 7 homolog Mlo2
SPAC6B12.07c		Bioneer		+	n.a.	ubiquitin-protein ligase E3 (predicted)
SPAC2F3.16		Bioneer			n.a.	ubiquitin-protein ligase E3 (predicted)
SPCC1795.03	gms1	Bioneer			n.a.	UDP-galactose transporter Gms1
SPAC3A12.09c		Bioneer	+		n.a.	urease accessory protein UreD (predicted)
SPAC29A4.13		Bioneer			n.a.	urease accessory protein UreF (predicted)
SPCPB16A4.05c		Bioneer	+	+	n.a.	urease accessory protein UREG (predicted)
SPAC1952.11c	ure2	Bioneer			n.a.	urease Ure2
SPCC1223.09		Bioneer			n.a.	uricase (predicted)
SPBC25B2.10		Bioneer		+	n.a.	Usp (universal stress protein) family protein
SPAC1834.09	mug51	Bioneer			n.a.	variant protein kinase 19 family protein
SPCC553.04	cyp9	Bioneer			n.a.	WD repeat containing cyclophilin family PPIase Cyp9 (predicted)
SPAC17H9.19c	cdt2	Bioneer	+	+	n.a.	WD repeat protein Cdt2
SPBC713.05		Bioneer	+		n.a.	WD repeat protein, human MAPK organizer 1 (MORG1) family (predicted)
SPAC12B10.03	bun62	Bioneer			n.a.	WD repeat protein, human WDR20 family, Bun62
SPBC609.03	iqw1	Bioneer		+	n.a.	WD repeat protein, Iqw1
SPAC4F10.18	nup37	Bioneer			n.a.	WD repeat protein, nucleoporin Nup37 (predicted)
SPBC2A9.03		Bioneer	+	+	n.a.	WD40/YVTN repeat-like
SPBC18H10.07		Bioneer		+	n.a.	WW domain-binding protein 4 (predicted)
SPBC18A7.01		Bioneer	+	+	n.a.	X-Pro dipeptidase (predicted)
SPCC1020.12c	xap5	Bioneer		+	n.a.	xap-5-like protein
SPBC2A9.07c		Bioneer	+	+	n.a.	zf-PARP type zinc finger protein
SPBC577.04		homemade	+	+	+	human THOC5 ortholog (predicted)
SPBC16C6.10	chp2	homemade	++	+	+	chromodomain protein 2
SPAC1782.12c		homemade		+		DUF423 protein
SPAC25B8.12c		homemade		+		nucleotide-sugar phosphatase (predicted)
SPAC7D4.03c		homemade		+	+	conserved fungal family
SPAC890.02c	alp7	homemade		+		centrosomal transforming acidic coiled-coil (TACC) protein ortholog Alp7
SPAPB17E12.02	yip12	homemade		+	+	SMN family protein Yip12
SPBC106.08c	mug2	homemade		+	+	cell surface glycoprotein (predicted), DUF1773 family protein 1
SPBC16E9.15		homemade		+		heat shock factor binding protein (predicted)
SPBC1709.03		homemade		+		conserved fungal protein
SPBC32H8.09		homemade		+	+	WD repeat protein, human WDR8 family
SPBC577.08c	txl1	homemade		+	+	thioredoxin-like I protein Txl1
SPBP4H10.07		homemade		+	+	ubiquitin-protein ligase E3 (predicted)

Table 3.4 Summary of screen result (continued)

systemic ID	gene	source	dh	dg	otr:ura4	description
SPCC737.06c		homemade		+	+	glutamate-cysteine ligase regulatory subunit (predicted)
SPAC343.17c		homemade	++	++	+	WD repeat protein, human WDR70 family
SPBP23A10.05	ssr4	homemade	+++	++	++	SWI/SNF and RSC complex subunit Ssr4
SPAC3A11.08	pcu4	homemade	+++	+++	++	cullin 4
SPAC22G7.11c		homemade				conserved fungal protein
SPAC23H4.09	cdb4	homemade				curved DNA-binding protein Cdb4, peptidase family
SPAC25B8.13c	isp7	homemade				2-OG-Fe(II) oxygenase superfamily protein
SPAC6B12.14c		homemade				conserved fungal protein
SPAC6F6.04c		homemade				membrane transporter (predicted)
SPAC869.09		homemade				conserved fungal protein
SPAC9E9.15		homemade				CIA30 protein (predicted)
SPAPB8E5.03	mae1	homemade				malic acid transport protein Mae1
SPBC1685.11	rlp1	homemade				RecA family ATPase Rlp1
SPBC17A3.05c		homemade				DNAJ/DUF1977 DNAJB12 homolog (predicted)
SPBC1E8.05		homemade				conserved fungal protein
SPBC29A10.12		homemade				HMG-box variant
SPBP23A10.12	frg1	homemade				FRG1 family protein, involved in mRNA processing (predicted)
SPCC1753.05	rsm1	homemade				RNA export factor Rsm1
SPCC737.03c	ima1	homemade				integral inner nuclear membrane protein Ima1
SPCC794.06		homemade				TDT malic acid transporter (predicted)
SPBC17G9.05		homemade	+++	+++	++	RRM-containing cyclophilin regulating transcription Rct1
SPAC12B10.08c		homemade	essential, comfirmed			mitochondrial tRNA(Ile)-lysidine synthetase family (predicted)
SPCC162.01c		homemade	essential, comfirmed			U4/U6 x U5 tri-snRNP complex subunit (predicted)
SPAC19G12.07c	rsd1	homemade	essential, comfirmed			RNA-binding protein Rsd1 (predicted)
SPBC16H5.15		homemade	essential, comfirmed			conserved fungal protein
SPBC337.12	red5	homemade	essential, comfirmed			human ZC3H3 homolog
SPBC8D2.07c	sfc9	homemade	essential, comfirmed			transcription factor TFIIIC complex subunit Sfc9 (predicted)
SPCC4G3.07c	phf1	homemade	essential. comfirmed			PHD finger containing protein Phf1

Table 3.4 Summary of screen result (continued)

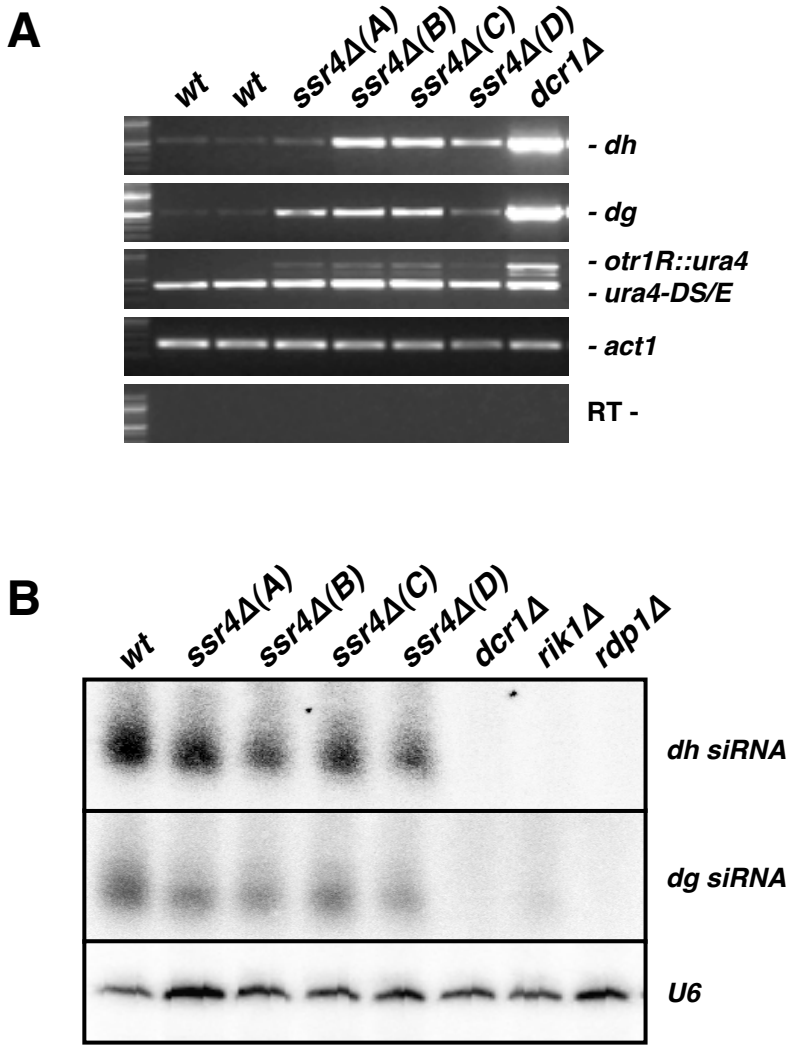

Figure 3.4 Ssr4 is needed for pericentromeric silencing

(A) Semi-quantitative RT-PCR of *dh*/*dg* and *otr1R*::*ura4* transcript levels in *ssr4Δ* mutant cells. Four individual *ssr4Δ* mutant strains were analyzed, labeled as A, B, C and D. Truncated *ura4-DS/E* at endogenous site and *act1* serve as loading controls, RT- omits the reverse transcription step.
(B) Small RNA northern blots of pericentromeric *dh*/*dg* derived siRNAs. *U6* serves as loading control. Four individual *ssr4Δ* mutant strains were analyzed, labeled as A, B, C and D.

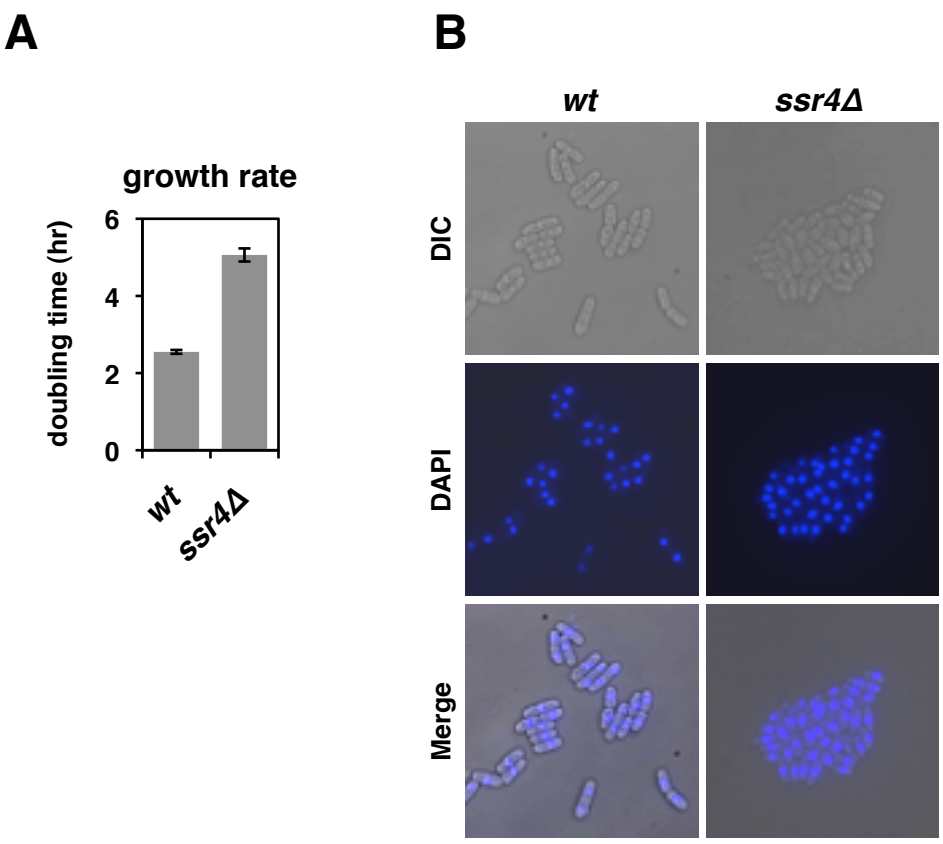

Figure 3.5 Ssr4 is required for normal cell growth and but not morphology

(A) Cell growth rate measured by OD_{600} in indicated strains.
(B) Cell morphology in indicated strains. DIC (differential interference contrast) shows the cell shape, DAPI stains nuclei.

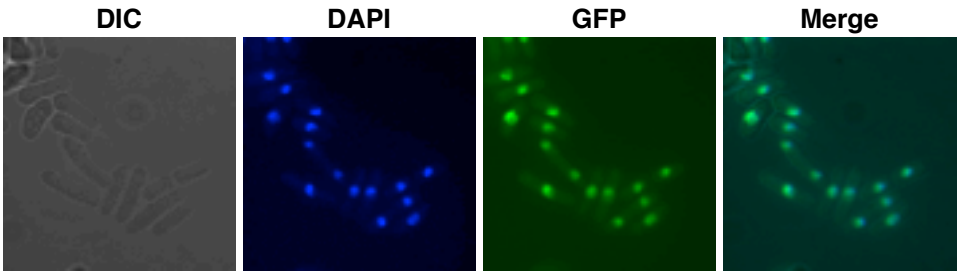

Figure 3.6 Ssr4 is a nuclear protein

GFP-tagged *ssr4* cells observed under microscope. DIC (differential interference contrast) shows the cell shape, DAPI stains nuclei, GFP indicates Ssr4 localization.

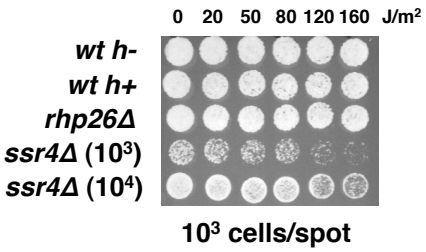

Figure 3.7 Strain lacking *ssr4* is sensitive to UV-induced DNA damage

Indicated strains treated with different dosage of UV light. *ssr4Δ* mutant cells are plated in two concentrations due to the slow growth phenotype.

3.4 Materials and Methods

Deletion construct design and deletion strain generation

Fission yeast deletion plasmid design was based on (Gregan et al., 2006). In brief, each plasmid construct contains an upstream and downstream homology region for each gene of interest, and a hygromycin B selection cassette. Deletion construct plasmids extracted from each *E. coli* strain were linearized by restriction enzymes before transforming into diploid fission yeast. Transformants were selected based on hygromycin B resistance, and correct targeting site was confirmed by PCR. Haploid deletion cells were obtained by tetrad dissection followed by drug resistance test. *S. pombe* strains and primers used in this study are described in Tables 3.5 and 3.6, respectively. Information about deletion mutants obtained from the Bioneer *S. pombe* haploid collection can be found at http://us.bioneer.com/home.aspx.

Semi-quantitative RT-PCR

DNA-free total RNA was isolated by hot phenol extraction method followed by Turbo DNase (Ambion) treatment. 20 to 30 ng of total RNA were used in one-step RT-PCR reactions (Qiagen) following manufacturer's protocol. Primers used are listed in Table 2.3. RT- omitted the reverse transcription step and proceeded directly to enzyme mix inactivation at 95 °C.

Small RNA northern

Yeast cells were grown to a concentration of ~1 X 10^7 cells/ml. Total RNA was extracted by the hot phenol method (Leed et al., 1991). mirVana miRNA isolation kit (Ambion) was used to enrich the small RNA fraction (<200 bp) from total RNA. 10 to 15 ug of enriched small RNA samples were used for northern blot with RNA chemically cross-linked to membranes (Pall and Hamilton, 2008). Radiolabeled riboprobes were generated by T3/T7 *in vitro* transcription kit (Ambion) using *dh* or *dg* DNA as templates and αP^{32}-UTP for radiolabeling. Riboprobes were further hydrolyzed into desired size before hybridization. *U6* radiolabeled oligoprobe was prepared by P^{32}-ATP end labeling

with T4 PNK (Polynucleotide Kinase). Radioactive signals were detected by Fuji phosphoimager.

UV-induced DNA damage

10^3 cells/spot were plated on YES plates unless otherwise noted. UV treatment was performed by the UV crosslinker at 254 nm (Stratalinker 1800). UV dosage used was previously tested to not cause effect on the wild type cells.

strain name	genotype	source
DG21	*h-, otr1R(SphI)::ura4, ura4-DS/E, ade6-216, his7-366, leu1-32*	lab stock
FY648	*h+, otr1R(SphI)::ura4 (oriI), ura4-DS/E, ade6-210, leu1-32*	lab stock
DG763	*h-, delta-rik1::kanMX6, otr1R(SphI)::ura4+, ura4-DS/E, ade6-210, leu1-32, his7-366*	lab stock
DG770	*h+, delta-rik1::kanMX6, otr1R(SphI)::ura4+, ura4-DS/E, ade6-216, leu1-32, his+*	lab stock
AY100	*h?, delta-SPAC25B8.12c-hyg, otr1R(SphI)::ura4, ura4-DS/E, leu1-32*	this study
AY104	*h?, delta-SPCC737.06c-hyg, otr1R(SphI)::ura4, ura4-DS/E, leu1-32*	this study
AY108	*h?, delta-SPAC7D4.03c-hyg, otr1R(SphI)::ura4, ura4-DS/E, leu1-32*	this study
AY115	*h?, delta-SPBC1E8.05c-hyg, otr1R(SphI)::ura4, ura4-DS/E, leu1-32*	this study
AY123	*h?, delta-SPBC17A3.05c-hyg, otr1R(SphI)::ura4, ura4-DS/E, leu1-32*	this study
AY127	*h?, delta-SPAC25B8.13c-hyg, otr1R(SphI)::ura4, ura4-DS/E, leu1-32*	this study
AY131	*h?, delta-SPBP23A10.12-hyg, otr1R(SphI)::ura4, ura4-DS/E, leu1-32*	this study
AY135	*h?, delta-SPBC16C6.10-hyg, otr1R(SphI)::ura4, ura4-DS/E, leu1-32*	this study
AY143	*h?, delta-SPAC343.17c-hyg, otr1R(SphI)::ura4, ura4-DS/E, leu1-32*	this study
AY147	*h?, delta-SPAC6B12.14c-hyg, otr1R(SphI)::ura4, ura4-DS/E, leu1-32*	this study
AY151	*h?, delta-SPAC6F6.04c-hyg, otr1R(SphI)::ura4, ura4-DS/E, leu1-32*	this study
AY155	*h?, delta-SPBC16E9.15-hyg, otr1R(SphI)::ura4, ura4-DS/E, leu1-32*	this study
AY159	*h?, delta-SPCC1753.05-hyg, otr1R(SphI)::ura4, ura4-DS/E, leu1-32*	this study
AY163	*h?, delta-SPBC577.04-hyg, otr1R(SphI)::ura4, ura4-DS/E, leu1-32*	this study
AY167	*h?, delta-SPAC9E9.15-hyg, otr1R(SphI)::ura4, ura4-DS/E, leu1-32*	this study
AY170	*h-, delta-SPAC3A11.08-hyg, otr1R(SphI)::ura4, ura4-DS/E, leu1-32*	this study
AY174	*h?, delta-SPBC29A10.12-hyg, otr1R(SphI)::ura4, ura4-DS/E, leu1-32*	this study
AY178	*h?, delta-SPAC890.02c-hyg, otr1R(SphI)::ura4, ura4-DS/E, leu1-32*	this study
AY182	*h?, delta-SPCC794.06-hyg, otr1R(SphI)::ura4, ura4-DS/E, leu1-32*	this study
AY190	*h?, delta-SPAPB17E12.02-hyg, otr1R(SphI)::ura4, ura4-DS/E, leu1-32*	this study
AY192	*h?, delta-SPAC1782.12c-hyg, otr1R(SphI)::ura4, ura4-DS/E, leu1-32*	this study
AY196	*h?, delta-SPBP23A10.05-hyg, otr1R(SphI)::ura4, ura4-DS/E, leu1-32*	this study
AY197	*h?, delta-SPBP23A10.05-hyg, otr1R(SphI)::ura4, ura4-DS/E, leu1-32*	this study
AY198	*h?, delta-SPBP23A10.05-hyg, otr1R(SphI)::ura4, ura4-DS/E, leu1-32*	this study
AY199	*h?, delta-SPBP23A10.05-hyg, otr1R(SphI)::ura4, ura4-DS/E, leu1-32*	this study
AY200	*h?, delta-SPBC1709.03-hyg, otr1R(SphI)::ura4, ura4-DS/E, leu1-32*	this study
AY204	*h?, delta-SPAC23H4.09-hyg, otr1R(SphI)::ura4, ura4-DS/E, leu1-32*	this study
AY208	*h?, delta-SPAPB8E5.03-hyg, otr1R(SphI)::ura4, ura4-DS/E, leu1-32*	this study
AY216	*h?, delta-SPCC737.03c-hyg, otr1R(SphI)::ura4, ura4-DS/E, leu1-32*	this study
AY221	*h?, delta-SPAC869.09-hyg, otr1R(SphI)::ura4, ura4-DS/E, leu1-32*	this study
AY225	*h?, delta-SPBC1685.11-hyg, otr1R(SphI)::ura4, ura4-DS/E, leu1-32*	this study
AY229	*h?, delta-SPAC22G7.11c-hyg, otr1R(SphI)::ura4, ura4-DS/E, leu1-32*	this study
AY233	*h?, delta-SPBP4H10.07-hyg, otr1R(SphI)::ura4, ura4-DS/E, leu1-32*	this study
AY237	*h?, delta-SPBC577.08c-hyg, otr1R(SphI)::ura4, ura4-DS/E, leu1-32*	this study
AY241	*h?, delta-SPBC32H8.09-hyg, otr1R(SphI)::ura4, ura4-DS/E, leu1-32*	this study
AY245	*h?, delta-SPBC106.08c-hyg, otr1R(SphI)::ura4, ura4-DS/E, leu1-32*	this study
DG494	*h-, delta-dcr1::kanMX6, otr1R(SphI)::ura4, ade6-216, leu1-32*	lab stock
DG124	*h-, delta-rdp1::kanMX6, otr1R(SphI)::ura4+, ura4-DS/E, ade6-216, leu1-32, his7-366*	lab stock
DG763	*h-, delta-rik1::kanMX6, otr1R(SphI)::ura4+, ura4-DS/E, ade6-210, leu1-32, his7-366*	lab stock
BG_5157H	*h+, delta-SPCP25A2.02c::kanMX6, ura4-D18, leu1-32*	lab stock

Table 3.5 Strain list

name	sequence	purpose
p30F	CCTGTTGA TTCGGCACCTTTG	RT-PCR
p30R	TGGAGAACGACTGTGAAGAGACC	RT-PCR
p33F	TGCAAGTGGAAAGTGGCTTCA	RT-PCR
p33R	TCGACCACCCTGACTTGTTCTC	RT-PCR
act 5'	TACCCCATTGAGCACGGTAT	RT-PCR
act 3'	GGAGGAAGA TTGAGCAGCAG	RT-PCR
ura4#1	GAGGGGATGAAAAATCCCAT	RT-PCR
ura4#2	TTCGACAACAGGATTACGACC	RT-PCR
p30F_T7	TAATACGACTCACTATAGGGAGCCTGTTGATTCGGCACCTTTG	small RNA blot
p30R_T3	AATTAACCCTCACTAAAGGGAGATGGAGAACGACTGTGAAGAGACC	small RNA blot
p33F_T7	TAATACGACTCACTATAGGGAGTGCAAGTGGAAAGTGGCTTCA	small RNA blot
p33R_T3	AATTAACCCTCACTAAAGGGAGATCGACCACCCTGACTTGTTCTC	small RNA blot
U6 oligo	ATGTCGCAGTGTCATCCTTG	small RNA blot

Table 3.6 Primer list

Chapter IV- Concluding remarks and future directions

4.1 Summary

During my study, I focused on identifying novel components involved in the RNAi machinery. My main focus was Rct1, a conserved RNA-binding protein that is intimately linked to Pol II transcription. I provide evidence that Rct1 is required for heterochromatin silencing and siRNA biogenesis, but surprisingly dispensable for pericentromeric heterochromatin assembly. In addition, the siRNA biogenesis defect in *rct1* mutant cells can be partially rescued by impairing the RNA surveillance pathway, suggesting Rct1 acts upstream of RNAi and guides Pol II transcripts to their appropriate destinations. Pol II transcripts are inefficiently spliced in cells lacking Rct1, providing a plausible mechanism linking transcript splicing to processing by the RNAi machinery. Furthermore, Cdk9, a central regulator of transcription elongation, is essential for heterochromatin silencing and siRNA biogenesis. Together, my work demonstrates that the RNAi machinery coordinates with Pol II transcription and RNA processing to achieve heterochromatic silencing.

In a related project, I identified several potential candidates whose loss of function impaired heterochromatic silencing, including a putative chromatin remodeler Ssr4. Whether or not these genes are directly involved in RNAi machinery requires further characterization.

My work in genome-wide Pol II accumulation and transcriptome analysis in RNAi mutants contributed partly to the understanding of the role of RNAi machinery outside centromeric heterochromatin.

4.2 Coordinate RNAi targeting by transcript splicing

The ENCODE project revealed an unexpectedly high portion of the human genome is transcribed, but only about 2% contains actual protein-coding potential (Djebali et al., 2012; ENCODE Project Consortium et al., 2012; 2007). The remaining

transcripts are non-coding RNAs (ncRNA) generated from intergenic regions and antisense transcripts. Similar observations have been reported in other eukaryotes, such as mouse, plants and yeasts (Carninci et al., 2005; Chekanova et al., 2007; Marguerat et al., 2012; Nagalakshmi et al., 2008; Willingham and Gingeras, 2006). These ncRNAs are often subjected to rapid degradation by RNA surveillance machinery and were therefore initially thought to be transcriptional noise caused by imperfect transcription (Struhl, 2007). Recent studies have started to shed light on the function of ncRNAs, and although far from complete, the common theme for ncRNA function is as a guide molecule to regulate gene expression (Keller and Bühler, 2013).

A well-studied example is at the pericentromeric region of *S. pombe*, in which the ncRNAs generated from *dh/dg* repeats serve as a platform to guide histone-modifying activities towards heterochromatic regions through RNAi machinery. However, how exactly the RNAi machinery is recruited to pericentromeric ncRNA remains a mystery. One idea is that the suboptimal introns of ncRNAs serve as a platform to assemble the spliceosome along with RNAi factors. Such a complex has been identified in *Cryptococcus neoformans*, termed SCANR (Spliceosome-Coupled And Nuclear RNAi) complex (Dumesic et al., 2013). In *S. pombe*, a subset of splicing factors is required for siRNA biogenesis and pericentromeric silencing, and these splicing factors also interact with the RNAi machinery (Bayne et al., 2008; Chinen et al., 2010). Additionally, splicing factors act at different stages of RNA-directed DNA methylation in plants (Ausin et al., 2012; Dou et al., 2013; Huang et al., 2013; Zhang et al., 2013), suggesting the spliceosome could be used as a conserved apparatus to recruit RNAi components. My work showing Rct1 as a putative splicing factor and a requirement for siRNA biogenesis further strengthens the idea that splicing can regulate Pol II transcript destiny. Interestingly, despite similar gene numbers, the genome of *S. pombe* contains nearly 5000 introns, while *S. cerevisiae* has only about 250 (Kupfer et al., 2004). As expected from a higher number of introns, the splicing machinery in *S. pombe* is more similar to mammals than budding yeast with respect to regulatory factors and 3' splice site sequences (Käufer and Potashkin, 2000; Kuhn and Käufer, 2003). This indicates that the complexity of splicing machinery in *S. cerevisiae* seems to have down-sized along with the loss of the RNAi pathway (Aravind et al., 2000).

A recent study has demonstrated that intron-containing RNAi factors are highly susceptible to perturbations in the splicing machinery when compared to other intron-containing genes. This indicates that splicing factors might only indirectly affect siRNA biogenesis (Kallgren et al., 2014). Although other studies suggested otherwise (Bayne et al., 2008; Chinen et al., 2010), a more careful examination in splicing mutants is needed to fully address the precise role of splicing factors in regulating siRNA biogenesis and heterochromatin silencing.

4.3 Labeling Pol II transcripts for their final destination

A strong argument against the indirect role of splicing factors in siRNA biogenesis is the difference in H3K9 methylation levels between RNAi and splicing mutants. H3K9 methylation is largely retained in splicing mutants and *rct1* mutant cells, but is significantly reduced in RNAi mutants (Bayne et al., 2008; Volpe et al., 2002). This is particularly interesting, as most mutants which lose siRNAs also have reduced pericentromeric H3K9 methylation levels (Alper et al., 2012).

Other than splicing factors and Rct1, Mlo3 and Cid14 are both required only for siRNA biogenesis but not H3K9 methylation (Bühler et al., 2008; Reyes-Turcu et al., 2011; Zhang et al., 2011). Mlo3 and Cid14 physically interact with each other and are thought to be part of the RNA surveillance pathway that channels RNA for degradation. Mlo3 contains an RRM and interacts with pericentromeric transcripts, and it was proposed that the polyadenylation activity of Cid14 marks ncRNAs to be targeted by the exosome or RNAi (Zhang et al., 2011). Strikingly, although Cid14 and Mlo3 are needed for efficient heterochromatic silencing, deleting *mlo3* or *cid14* in RNAi mutant cells rescues the silencing and the H3K9 methylation defect in RNAi mutants, but does not restore siRNAs to wild type levels (Reyes-Turcu et al., 2011). The mechanism of this rescue is currently unknown. However, deleting *rct1* in RNAi mutants does not rescue the silencing defect, and more intriguingly, deleting *mlo3* suppresses the silencing defect observed in *rct1Δ* mutant cells. Similarly, deleting the exosome component *rrp6* restores heterochromatic silencing in *rct1* mutant cells, along with siRNA production.

More and more factors that are involved in RNA metabolic pathways have been discovered to play a role in heterochromatic silencing and siRNA biogenesis, but are not

required for H3K9 methylation. While it is not surprising that these factors can be used to mark Pol II transcripts and channel them into appropriate processing pathways, the complexity of the genetic interactions point to a inter-connected multi-level regulatory mechanism. In addition, similar phenotypes can be caused by completely different reasons, so a direct approach to tackle specific mechanistic questions awaits to be done.

4.4 Small RNAs or RNAi?

Following the discovery that RNAi components are essential for heterochromatin assembly, subsequent studies have shown that their catalytic activity is also required. This seeded the idea that small RNAs are used as a guide molecule to trigger H3K9 methylation (Bühler, 2009).

At the pericentromeric heterochromatin, RNAi factors are needed for both heterochromatin nucleation and maintenance, while in other heterochromatin regions, RNAi factors are only required to rapidly restore heterochromatin when it has been depleted by mutation. My work, along with others, provides evidence that siRNAs are not essential for H3K9 maintenance at the pericentromeric repeats which instead requires an intact RNAi machinery. Consistent with this observation, the H3K9 methylation levels over the embedded transgene reporter are highly dependent on RNAi machinery, while very few siRNAs are detected from the transgene inserted into the pericentromeric repeats (Bühler et al., 2006; Irvine et al., 2006; Volpe et al., 2002). This is likely because the reporter transgene is transcriptionally silenced even in S phase, unlike the centromeric repeats. Instead of siRNA biogenesis, RNAi components could provide a structural base to guide H3K9 methyltransferase activity. Such an idea is supported by a recent study showing that catalytically dead Dcr1 was able to assemble heterochromatin when overexpressed in certain strains (Yu et al., 2014), while siRNA biogenesis depends on Dcr1 catalytic activity (Colmenares et al., 2007).

Furthermore, pericentromeric H3K9 methylation can be partially maintained independent of RNAi components if the Mlo3/TRAMP-mediated RNA surveillance machinery is also compromised. This indicates that an additional pathway can assemble pericentromeric heterochromatin independent of siRNAs and RNAi.

4.5 The role of RNAi-mediated Pol II release

RNAi factors, including Dcr1 and Ago1, are required to release Pol II from pericentromeric repeats during S phase when the replication machinery encounters Pol II. Failure to remove Pol II at pericentromeric repeats in *dcr1Δ* mutant cells interferes with fork progression and results in the loss of H3K9 methylation due to fork restart by homologous recombination (Zaratiegui et al., 2011).

My work on Cdk9, a Pol II CTD kinase, demonstrates that when compromised transcription avoids collision with replication, siRNA biogenesis is impaired along with a loss of pericentromeric silencing. This supports the idea that collision signals Dcr1 recruitment to the conflict site and thereby facilitates Pol II release (Zaratiegui et al., 2011). Additionally, in cells lacking Rct1, H3K9 methylation is retained while Pol II accumulated, suggesting Pol II accumulation can be an active process rather than a passive accumulation due to the loss of H3K9 methylation.

In addition to pericentromeric heterochromatin, several other genomic loci possess a potential conflict between transcription and replication, including rDNA, tDNA and highly transcribed protein-coding genes. We found Dcr1, but not Ago1, is involved in transcription termination of these loci, as Pol II accumulation is only observed in *dcr1Δ* mutant. This is important to maintain genome integrity, and failure to remove Pol II at rDNA results in the reduction of rDNA copy number (Castel et al., submitted).

4.6 Final thoughts

RNAi was originally discovered from its role in post-transcriptional silencing, and studies have now shown that RNAi is involved in a wide variety of cellular processes, including chromatin modification, DNA repair, transcription termination and DNA elimination (Alper et al., 2012; Zaratiegui et al., 2007). However, the requirement for RNAi factors does not necessarily equal the requirement for small RNAs. The detection of small RNAs from a specific locus could simply serve as an RNAi footprint, and careful examination by using catalytic mutants is needed to further dissect the role of RNAi in different cellular processes.

In addition, several Dicers and Argonautes are present in higher eukaryotes, while *S. pombe* contains only one copy of each (Zaratiegui et al., 2007). This diverse pool of

RNAi factors present in higher eukaryotes contributes to the production of different types of small RNAs and regulates their target specificity. *S. pombe* apparently lacks this diversity of small RNA regulation, although the diversity of small RNAs has not yet been extensively explored. However, different small RNA modifications could provide additional small RNA complexity, and carry out specific functions in both *S. pombe* and higher eukaryotes. I look forward to more exciting research in this area.

References

Abraham, J., Nasmyth, K.A., Strathern, J.N., Klar, A.J., and Hicks, J.B. (1984). Regulation of mating-type information in yeast. Negative control requiring sequences both 5“ and 3” to the regulated region. J. Mol. Biol. *176*, 307–331.

Aguilar-Arnal, L., Marsellach, F.-X., and Azorín, F. (2008). The fission yeast homologue of CENP-B, Abp1, regulates directionality of mating-type switching. Embo J. *27*, 1029–1038.

Al-Sady, B., Madhani, H.D., and Narlikar, G.J. (2013). Division of labor between the chromodomains of HP1 and Suv39 methylase enables coordination of heterochromatin spread. Mol. Cell *51*, 80–91.

Allshire, R.C., Nimmo, E.R., Ekwall, K., Javerzat, J.P., and Cranston, G. (1995). Mutations derepressing silent centromeric domains in fission yeast disrupt chromosome segregation. Genes Dev. *9*, 218–233.

Allshire, R.C., and Karpen, G.H. (2008). Epigenetic regulation of centromeric chromatin: old dogs, new tricks? Nat. Rev. Genet. *9*, 923–937.

Alper, B.J., Job, G., Yadav, R.K., Shanker, S., Lowe, B.R., and Partridge, J.F. (2013). Sir2 is required for Clr4 to initiate centromeric heterochromatin assembly in fission yeast. Embo J. *32*, 2321–2335.

Alper, B.J., Lowe, B.R., and Partridge, J.F. (2012). Centromeric heterochromatin assembly in fission yeast--balancing transcription, RNA interference and chromatin modification. Chromosome Res. *20*, 521–534.

Anders, S., Reyes, A., and Huber, W. (2012). Detecting differential usage of exons from RNA-seq data. Genome Res. *22*, 2008–2017.

Angus-Hill, M.L., Schlichter, A., Roberts, D., Erdjument-Bromage, H., Tempst, P., and Cairns, B.R. (2001). A Rsc3/Rsc30 zinc cluster dimer reveals novel roles for the chromatin remodeler RSC in gene expression and cell cycle control. Mol. Cell *7*, 741–751.

Antequera, F., Tamame, M., Villanueva, J.R., and Santos, T. (1984). DNA methylation in the fungi. J. Biol. Chem. *259*, 8033–8036.

Aramayo, R., and Selker, E.U. (2013). Neurospora crassa, a model system for epigenetics research. Cold Spring Harb Perspect Biol *5*, a017921.

Aravind, L., Watanabe, H., Lipman, D.J., and Koonin, E.V. (2000). Lineage-specific loss and divergence of functionally linked genes in eukaryotes. Proc. Natl. Acad. Sci. U.S.a.

97, 11319–11324.

Ausin, I., Greenberg, M.V.C., Li, C.F., and Jacobsen, S.E. (2012). The splicing factor SR45 affects the RNA-directed DNA methylation pathway in Arabidopsis. Epigenetics *7*, 29–33.

Ayoub, N., Goldshmidt, I., Lyakhovetsky, R., and Cohen, A. (2000). A fission yeast repression element cooperates with centromere-like sequences and defines a mat silent domain boundary. Genetics *156*, 983–994.

Baltz, A.G., Munschauer, M., Schwanhäusser, B., Vasile, A., Murakawa, Y., Schueler, M., Youngs, N., Penfold-Brown, D., Drew, K., Milek, M., et al. (2012). The mRNA-bound proteome and its global occupancy profile on protein-coding transcripts. Mol. Cell *46*, 674–690.

Bannikova, O., Zywicki, M., Marquez, Y., Skrahina, T., Kalyna, M., and Barta, A. (2013). Identification of RNA targets for the nuclear multidomain cyclophilin atCyp59 and their effect on PPIase activity. Nucleic Acids Res *41*, 1783–1796.

Bannister, A.J., Zegerman, P., Partridge, J.F., Miska, E.A., Thomas, J.O., Allshire, R.C., and Kouzarides, T. (2001). Selective recognition of methylated lysine 9 on histone H3 by the HP1 chromo domain. Nature *410*, 120–124.

Bayne, E.H., Portoso, M., Kagansky, A., Kos-Braun, I.C., Urano, T., Ekwall, K., Alves, F., Rappsilber, J., and Allshire, R.C. (2008). Splicing factors facilitate RNAi-directed silencing in fission yeast. Science *322*, 602–606.

Bayne, E.H., White, S.A., Kagansky, A., Bijos, D.A., Sanchez-Pulido, L., Hoe, K.-L., Kim, D.-U., Park, H.-O., Ponting, C.P., Rappsilber, J., et al. (2010). Stc1: a critical link between RNAi and chromatin modification required for heterochromatin integrity. Cell *140*, 666–677.

Beach, D.H., and Klar, A.J. (1984). Rearrangements of the transposable mating-type cassettes of fission yeast. Embo J. *3*, 603–610.

Beach, D., Nurse, P., and Egel, R. (1982). Molecular rearrangement of mating-type genes in fission yeast. Nature *296*, 682–683.

Bensasson, D., Zarowiecki, M., Burt, A., and Koufopanou, V. (2008). Rapid evolution of yeast centromeres in the absence of drive. Genetics *178*, 2161–2167.

Bernstein, E., Caudy, A.A., Hammond, S.M., and Hannon, G.J. (2001). Role for a bidentate ribonuclease in the initiation step of RNA interference. Nature *409*, 363–366.

Bilokapic, S., and Schwartz, T.U. (2012). Molecular basis for Nup37 and ELY5/ELYS recruitment to the nuclear pore complex. Proceedings of the National Academy of Sciences *109*, 15241–15246.

Bjerling, P., Silverstein, R.A., Thon, G., Caudy, A., Grewal, S., and Ekwall, K. (2002). Functional divergence between histone deacetylases in fission yeast by distinct cellular localization and in vivo specificity. Molecular and Cellular Biology *22*, 2170–2181.

Blasco, M.A. (2007). The epigenetic regulation of mammalian telomeres. Nat. Rev. Genet. *8*, 299–309.

Bolger, A.M., Lohse, M., and Usadel, B. (2014). Trimmomatic: a flexible trimmer for Illumina sequence data. Bioinformatics.

Bostick, M., Kim, J.K., Estève, P.-O., Clark, A., Pradhan, S., and Jacobsen, S.E. (2007). UHRF1 plays a role in maintaining DNA methylation in mammalian cells. Science *317*, 1760–1764.

Brookheart, R.T., Lee, C.-Y.S., and Espenshade, P.J. (2014). Casein kinase 1 regulates sterol regulatory element-binding protein (SREBP) to control sterol homeostasis. J. Biol. Chem. *289*, 2725–2735.

Brown, S.W. (1966). Heterochromatin. Science *151*, 417–425.

Buker, S.M., Iida, T., Bühler, M., Villén, J., Gygi, S.P., Nakayama, J.-I., and Moazed, D. (2007). Two different Argonaute complexes are required for siRNA generation and heterochromatin assembly in fission yeast. Nat. Struct. Mol. Biol. *14*, 200–207.

Bühler, M., Haas, W., Gygi, S.P., and Moazed, D. (2007). RNAi-dependent and -independent RNA turnover mechanisms contribute to heterochromatic gene silencing. Cell *129*, 707–721.

Bühler, M., Spies, N., Bartel, D.P., and Moazed, D. (2008). TRAMP-mediated RNA surveillance prevents spurious entry of RNAs into the Schizosaccharomyces pombe siRNA pathway. Nat. Struct. Mol. Biol. *15*, 1015–1023.

Bühler, M., Verdel, A., and Moazed, D. (2006). Tethering RITS to a nascent transcript initiates RNAi- and heterochromatin-dependent gene silencing. Cell *125*, 873–886.

Bühler, M. (2009). RNA turnover and chromatin-dependent gene silencing. Chromosoma *118*, 141–151.

Cairns, B.R., Lorch, Y., Li, Y., Zhang, M., Lacomis, L., Erdjument-Bromage, H., Tempst, P., Du, J., Laurent, B., and Kornberg, R.D. (1996). RSC, an essential, abundant chromatin-remodeling complex. Cell *87*, 1249–1260.

Cam, H.P. (2010). Roles of RNAi in chromatin regulation and epigenetic inheritance. Epigenomics *2*, 613–626.

Cam, H.P., Sugiyama, T., Chen, E.S., Chen, X., FitzGerald, P.C., and Grewal, S.I.S. (2005). Comprehensive analysis of heterochromatin- and RNAi-mediated epigenetic control of the fission yeast genome. Nat. Genet. *37*, 809–819.

Cao, Y., Cairns, B.R., Kornberg, R.D., and Laurent, B.C. (1997). Sfh1p, a component of a novel chromatin-remodeling complex, is required for cell cycle progression. Molecular and Cellular Biology *17*, 3323–3334.

Carninci, P., Kasukawa, T., Katayama, S., Gough, J., Frith, M.C., Maeda, N., Oyama, R., Ravasi, T., Lenhard, B., Wells, C., et al. (2005). The transcriptional landscape of the mammalian genome. Science *309*, 1559–1563.

Castel, S.E., and Martienssen, R.A. (2013). RNA interference in the nucleus: roles for small RNAs in transcription, epigenetics and beyond. Nat. Rev. Genet. *14*, 100–112.

Castel, S.E., Ren, J., Bhattacharjee, S., Chang, A-Y., Sánchez, M., Valbuena, A., Antequera, F., and Martienssen, R.A. (2014) Transcriptional termination by Dicer at sites of replication stress maintains genomic stability. (Submitted)

Chai, B., Huang, J., Cairns, B.R., and Laurent, B.C. (2005). Distinct roles for the RSC and Swi/Snf ATP-dependent chromatin remodelers in DNA double-strand break repair. Genes Dev. *19*, 1656–1661.

Chang, Y.C., Bien, C.M., Lee, H., Espenshade, P.J., and Kwon-Chung, K.J. (2007). Sre1p, a regulator of oxygen sensing and sterol homeostasis, is required for virulence in Cryptococcus neoformans. Mol. Microbiol. *64*, 614–629.

Chekanova, J.A., Gregory, B.D., Reverdatto, S.V., Chen, H., Kumar, R., Hooker, T., Yazaki, J., Li, P., Skiba, N., Peng, Q., et al. (2007). Genome-wide high-resolution mapping of exosome substrates reveals hidden features in the Arabidopsis transcriptome. Cell *131*, 1340–1353.

Chen, E.S., Zhang, K., Nicolas, E., Cam, H.P., Zofall, M., and Grewal, S.I.S. (2008). Cell cycle control of centromeric repeat transcription and heterochromatin assembly. Nature *451*, 734–737.

Cheutin, T., Gorski, S.A., May, K.M., Singh, P.B., and Misteli, T. (2004). In vivo dynamics of Swi6 in yeast: evidence for a stochastic model of heterochromatin. Molecular and Cellular Biology *24*, 3157–3167.

Cheutin, T., McNairn, A.J., Jenuwein, T., Gilbert, D.M., Singh, P.B., and Misteli, T. (2003). Maintenance of stable heterochromatin domains by dynamic HP1 binding. Science *299*, 721–725.

Chikashige, Y., Kinoshita, N., Nakaseko, Y., Matsumoto, T., Murakami, S., Niwa, O., and Yanagida, M. (1989). Composite motifs and repeat symmetry in S. pombe centromeres: direct analysis by integration of NotI restriction sites. Cell *57*, 739–751.

Chinen, M., Morita, M., Fukumura, K., and Tani, T. (2010). Involvement of the spliceosomal U4 small nuclear RNA in heterochromatic gene silencing at fission yeast centromeres. J. Biol. Chem. *285*, 5630–5638.

Choi, E.S., Strålfors, A., Castillo, A.G., Durand-Dubief, M., Ekwall, K., and Allshire, R.C. (2011). Identification of noncoding transcripts from within CENP-A chromatin at fission yeast centromeres. J. Biol. Chem. *286*, 23600–23607.

Chung, S.Y., Hill, W.E., and Doty, P. (1978). Characterization of the histone core complex. Proc. Natl. Acad. Sci. U.S.a. *75*, 1680–1684.

Clarke, L. (1990). Centromeres of budding and fission yeasts. Trends Genet. *6*, 150–154.

Clarke, L., and Carbon, J. (1985). The structure and function of yeast centromeres. Annu. Rev. Genet. *19*, 29–55.

Clarke, L., Amstutz, H., Fishel, B., and Carbon, J. (1986). Analysis of centromeric DNA in the fission yeast Schizosaccharomyces pombe. Proc. Natl. Acad. Sci. U.S.a. *83*, 8253–8257.

Cliften, P.F., Fulton, R.S., Wilson, R.K., and Johnston, M. (2006). After the duplication: gene loss and adaptation in Saccharomyces genomes. Genetics *172*, 863–872.

Colmenares, S.U., Buker, S.M., Bühler, M., Dlakić, M., and Moazed, D. (2007). Coupling of double-stranded RNA synthesis and siRNA generation in fission yeast RNAi. Mol. Cell *27*, 449–461.

Cottarel, G., Shero, J.H., Hieter, P., and Hegemann, J.H. (1989). A 125-base-pair CEN6 DNA fragment is sufficient for complete meiotic and mitotic centromere functions in Saccharomyces cerevisiae. Molecular and Cellular Biology *9*, 3342–3349.

de Almeida, S.F., García-Sacristán, A., Custódio, N., and Carmo-Fonseca, M. (2010). A link between nuclear RNA surveillance, the human exosome and RNA polymerase II transcriptional termination. Nucleic Acids Res *38*, 8015–8026.

de Lange, T., Shiue, L., Myers, R.M., Cox, D.R., Naylor, S.L., Killery, A.M., and Varmus, H.E. (1990). Structure and variability of human chromosome ends. Molecular and Cellular Biology *10*, 518–527.

Demerec, M., and Slizynska, H. (1937). Mottled White 258-18 of Drosophila Melanogaster. Genetics *22*, 641–649.

Djebali, S., Davis, C.A., Merkel, A., Dobin, A., Lassmann, T., Mortazavi, A., Tanzer, A., Lagarde, J., Lin, W., Schlesinger, F., et al. (2012). Landscape of transcription in human cells. Nature *489*, 101–108.

Djupedal, I., Kos-Braun, I.C., Mosher, R.A., Söderholm, N., Simmer, F., Hardcastle, T.J., Fender, A., Heidrich, N., Kagansky, A., Bayne, E., et al. (2009). Analysis of small RNA in fission yeast; centromeric siRNAs are potentially generated through a structured RNA. Embo J. *28*, 3832–3844.

Djupedal, I., Portoso, M., Spåhr, H., Bonilla, C., Gustafsson, C.M., Allshire, R.C., and

Ekwall, K. (2005). RNA Pol II subunit Rpb7 promotes centromeric transcription and RNAi-directed chromatin silencing. Genes Dev. *19*, 2301–2306.

Dobin, A., Davis, C.A., Schlesinger, F., Drenkow, J., Zaleski, C., Jha, S., Batut, P., Chaisson, M., and Gingeras, T.R. (2013). STAR: ultrafast universal RNA-seq aligner. Bioinformatics *29*, 15–21.

Doe, C.L., Wang, G., Chow, C., Fricker, M.D., Singh, P.B., and Mellor, E.J. (1998). The fission yeast chromo domain encoding gene chp1(+) is required for chromosome segregation and shows a genetic interaction with alpha-tubulin. Nucleic Acids Res *26*, 4222–4229.

Dou, K., Huang, C.-F., Ma, Z.-Y., Zhang, C.-J., Zhou, J.-X., Huang, H.-W., Cai, T., Tang, K., Zhu, J.-K., and He, X.-J. (2013). The PRP6-like splicing factor STA1 is involved in RNA-directed DNA methylation by facilitating the production of Pol V-dependent scaffold RNAs. Nucleic Acids Res *41*, 8489–8502.

Drinnenberg, I.A., Fink, G.R., and Bartel, D.P. (2011). Compatibility with killer explains the rise of RNAi-deficient fungi. Science *333*, 1592.

Drinnenberg, I.A., Weinberg, D.E., Xie, K.T., Mower, J.P., Wolfe, K.H., Fink, G.R., and Bartel, D.P. (2009). RNAi in budding yeast. Science *326*, 544–550.

Dror, V., and Winston, F. (2004). The Swi/Snf chromatin remodeling complex is required for ribosomal DNA and telomeric silencing in Saccharomyces cerevisiae. Molecular and Cellular Biology *24*, 8227–8235.

Dumesic, P.A., Natarajan, P., Chen, C., Drinnenberg, I.A., Schiller, B.J., Thompson, J., Moresco, J.J., Yates, J.R., Bartel, D.P., and Madhani, H.D. (2013). Stalled spliceosomes are a signal for RNAi-mediated genome defense. Cell *152*, 957–968.

Eberle, A.B., Hessle, V., Helbig, R., Dantoft, W., Gimber, N., and Visa, N. (2010). Splice-site mutations cause Rrp6-mediated nuclear retention of the unspliced RNAs and transcriptional down-regulation of the splicing-defective genes. PLoS ONE *5*, e11540.

Egel, R., Nielsen, O., and Weilguny, D. (1990). Sexual differentiation in fission yeast. Trends Genet. *6*, 369–373.

Eickbush, T.H., and Moudrianakis, E.N. (1978). The histone core complex: an octamer assembled by two sets of protein-protein interactions. Biochemistry *17*, 4955–4964.

Ekwall, K., and Ruusala, T. (1994). Mutations in rik1, clr2, clr3 and clr4 genes asymmetrically derepress the silent mating-type loci in fission yeast. Genetics *136*, 53–64.

Ekwall, K., Olsson, T., Turner, B.M., Cranston, G., and Allshire, R.C. (1997). Transient inhibition of histone deacetylation alters the structural and functional imprint at fission yeast centromeres. Cell *91*, 1021–1032.

Elbashir, S.M., Lendeckel, W., and Tuschl, T. (2001). RNA interference is mediated by 21- and 22-nucleotide RNAs. Genes Dev. *15*, 188–200.

Emmerth, S., Schober, H., Gaidatzis, D., Roloff, T., Jacobeit, K., and Bühler, M. (2010). Nuclear retention of fission yeast dicer is a prerequisite for RNAi-mediated heterochromatin assembly. Dev. Cell *18*, 102–113.

ENCODE Project Consortium, Bernstein, B.E., Birney, E., Dunham, I., Green, E.D., Gunter, C., and Snyder, M. (2012). An integrated encyclopedia of DNA elements in the human genome. Nature *489*, 57–74.

ENCODE Project Consortium, Birney, E., Stamatoyannopoulos, J.A., Dutta, A., Guigó, R., Gingeras, T.R., Margulies, E.H., Weng, Z., Snyder, M., Dermitzakis, E.T., et al. (2007). Identification and analysis of functional elements in 1% of the human genome by the ENCODE pilot project. Nature *447*, 799–816.

Euskirchen, G., Auerbach, R.K., and Snyder, M. (2012). SWI/SNF chromatin-remodeling factors: multiscale analyses and diverse functions. J. Biol. Chem. *287*, 30897–30905.

Falbo, K.B., and Shen, X. (2006). Chromatin remodeling in DNA replication. J. Cell. Biochem. *97*, 684–689.

Festenstein, R., Pagakis, S.N., Hiragami, K., Lyon, D., Verreault, A., Sekkali, B., and Kioussis, D. (2003). Modulation of heterochromatin protein 1 dynamics in primary Mammalian cells. Science *299*, 719–721.

Fire, A., Xu, S., Montgomery, M.K., Kostas, S.A., Driver, S.E., and Mello, C.C. (1998). Potent and specific genetic interference by double-stranded RNA in Caenorhabditis elegans. Nature *391*, 806–811.

Fischer, G., Bang, H., and Mech, C. (1984). [Determination of enzymatic catalysis for the cis-trans-isomerization of peptide binding in proline-containing peptides]. Biomed. Biochim. Acta *43*, 1101–1111.

Fischle, W., Tseng, B.S., Dormann, H.L., Ueberheide, B.M., Garcia, B.A., Shabanowitz, J., Hunt, D.F., Funabiki, H., and Allis, C.D. (2005). Regulation of HP1-chromatin binding by histone H3 methylation and phosphorylation. Nature *438*, 1116–1122.

Fischle, W., Wang, Y., and Allis, C.D. (2003). Binary switches and modification cassettes in histone biology and beyond. Nature *425*, 475–479.

Fishel, B., Amstutz, H., Baum, M., Carbon, J., and Clarke, L. (1988). Structural organization and functional analysis of centromeric DNA in the fission yeast Schizosaccharomyces pombe. Molecular and Cellular Biology *8*, 754–763.

Freeman-Cook, L.L., Gómez, E.B., Spedale, E.J., Marlett, J., Forsburg, S.L., Pillus, L., and Laurenson, P. (2005). Conserved locus-specific silencing functions of Schizosaccharomyces pombe sir2+. Genetics *169*, 1243–1260.

Fujiyama-Nakamura, S., Ito, S., Sawatsubashi, S., Yamauchi, Y., Suzuki, E., Tanabe, M., Kimura, S., Murata, T., Isobe, T., Takeyama, K.-I., et al. (2009). BTB protein, dKLHL18/CG3571, serves as an adaptor subunit for a dCul3 ubiquitin ligase complex. Genes Cells *14*, 965–973.

Garcia, J.F., Dumesic, P.A., Hartley, P.D., El-Samad, H., and Madhani, H.D. (2010). Combinatorial, site-specific requirement for heterochromatic silencing factors in the elimination of nucleosome-free regions. Genes Dev. *24*, 1758–1771.

Geyer, R., Wee, S., Anderson, S., Yates, J., and Wolf, D.A. (2003). BTB/POZ domain proteins are putative substrate adaptors for cullin 3 ubiquitin ligases. Mol. Cell *12*, 783–790.

Gilbert, C., and Svejstrup, J.Q. (2006). RNA immunoprecipitation for determining RNA-protein associations in vivo. Curr Protoc Mol Biol *Chapter 27*, Unit27.4.

Goffeau, A., Barrell, B.G., Bussey, H., Davis, R.W., Dujon, B., Feldmann, H., Galibert, F., Hoheisel, J.D., Jacq, C., Johnston, M., et al. (1996). Life with 6000 genes. Science *274*, 546–563–7.

Gonzalez, M., and Li, F. (2012). DNA replication, RNAi and epigenetic inheritance. Epigenetics *7*, 14–19.

Gregan, J., Rabitsch, P.K., Rumpf, C., Novatchkova, M., Schleiffer, A., and Nasmyth, K. (2006). High-throughput knockout screen in fission yeast. Nat Protoc *1*, 2457–2464.

Grewal, S.I., and Klar, A.J. (1997). A recombinationally repressed region between mat2 and mat3 loci shares homology to centromeric repeats and regulates directionality of mating-type switching in fission yeast. Genetics *146*, 1221–1238.

Grewal, S.I., Bonaduce, M.J., and Klar, A.J. (1998). Histone deacetylase homologs regulate epigenetic inheritance of transcriptional silencing and chromosome segregation in fission yeast. Genetics *150*, 563–576.

Gullerova, M., Barta, A., and Lorkovic, Z.J. (2007). Rct1, a Nuclear RNA Recognition Motif-Containing Cyclophilin, Regulates Phosphorylation of the RNA Polymerase II C-Terminal Domain. Molecular and Cellular Biology *27*, 3601–3611.

Gullerova, M., Barta, A., and Lorkovic, Z.J. (2006). AtCyp59 is a multidomain cyclophilin from Arabidopsis thaliana that interacts with SR proteins and the C-terminal domain of the RNA polymerase II. Rna *12*, 631–643.

Halic, M., and Moazed, D. (2010). Dicer-Independent Primal RNAs Trigger RNAi and Heterochromatin Formation. Cell *140*, 504–516.

Hall, I.M., Noma, K.-I., and Grewal, S.I.S. (2003). RNA interference machinery regulates chromosome dynamics during mitosis and meiosis in fission yeast. Proc. Natl. Acad. Sci. U.S.a. *100*, 193–198.

Hall, I.M., Shankaranarayana, G.D., Noma, K.-I., Ayoub, N., Cohen, A., and Grewal, S.I.S. (2002). Establishment and maintenance of a heterochromatin domain. Science *297*, 2232–2237.

Halverson, D., Gutkin, G., and Clarke, L. (2000). A novel member of the Swi6p family of fission yeast chromo domain-containing proteins associates with the centromere in vivo and affects chromosome segregation. Mol. Gen. Genet. *264*, 492–505.

Hamilton, A.J., and Baulcombe, D.C. (1999). A species of small antisense RNA in posttranscriptional gene silencing in plants. Science *286*, 950–952.

Hansen, K.R., Burns, G., Mata, J., Volpe, T.A., Martienssen, R.A., Bähler, J., and Thon, G. (2005). Global effects on gene expression in fission yeast by silencing and RNA interference machineries. Molecular and Cellular Biology *25*, 590–601.

Hansen, K.R., Ibarra, P.T., and Thon, G. (2006). Evolutionary-conserved telomere-linked helicase genes of fission yeast are repressed by silencing factors, RNAi components and the telomere-binding protein Taz1. Nucleic Acids Res *34*, 78–88.

Heard, E., and Martienssen, R.A. (2014). Transgenerational Epigenetic Inheritance: Myths and Mechanisms. Cell *157*, 95–109.

Heckman, D.S., Geiser, D.M., Eidell, B.R., Stauffer, R.L., Kardos, N.L., and Hedges, S.B. (2001). Molecular evidence for the early colonization of land by fungi and plants. Science *293*, 1129–1133.

Hedges, S.B. (2002). The origin and evolution of model organisms. Nat. Rev. Genet. *3*, 838–849.

Heitz, E. (1928). Das Heterochromatin der Moose.

Hicks, J.B., and Herskowitz, I. (1977). Interconversion of Yeast Mating Types II. Restoration of Mating Ability to Sterile Mutants in Homothallic and Heterothallic Strains. Genetics *85*, 373–393.

Hiraoka, Y., Henderson, E., and Blackburn, E.H. (1998). Not so peculiar: fission yeast telomere repeats. Trends Biochem. Sci. *23*, 126.

Hirota, T., Lipp, J.J., Toh, B.-H., and Peters, J.-M. (2005). Histone H3 serine 10 phosphorylation by Aurora B causes HP1 dissociation from heterochromatin. Nature *438*, 1176–1180.

Hirschhorn, J.N., Brown, S.A., Clark, C.D., and Winston, F. (1992). Evidence that SNF2/SWI2 and SNF5 activate transcription in yeast by altering chromatin structure. Genes Dev. *6*, 2288–2298.

Holstege, F.C., Jennings, E.G., Wyrick, J.J., Lee, T.I., Hengartner, C.J., Green, M.R., Golub, T.R., Lander, E.S., and Young, R.A. (1998). Dissecting the regulatory circuitry of

a eukaryotic genome. Cell *95*, 717–728.

Hong, E.-J.E., Villén, J., Gerace, E.L., Gygi, S.P., and Moazed, D. (2005). A cullin E3 ubiquitin ligase complex associates with Rik1 and the Clr4 histone H3-K9 methyltransferase and is required for RNAi-mediated heterochromatin formation. RNA Biol *2*, 106–111.

Horn, P.J., Bastie, J.-N., and Peterson, C.L. (2005). A Rik1-associated, cullin-dependent E3 ubiquitin ligase is essential for heterochromatin formation. Genes Dev. *19*, 1705–1714.

Houseley, J., LaCava, J., and Tollervey, D. (2006). RNA-quality control by the exosome. Nat. Rev. Mol. Cell Biol. *7*, 529–539.

Hsu, J.-M., Huang, J., Meluh, P.B., and Laurent, B.C. (2003). The yeast RSC chromatin-remodeling complex is required for kinetochore function in chromosome segregation. Molecular and Cellular Biology *23*, 3202–3215.

Huang, C.-F., Miki, D., Tang, K., Zhou, H.-R., Zheng, Z., Chen, W., Ma, Z.-Y., Yang, L., Zhang, H., Liu, R., et al. (2013). A Pre-mRNA-splicing factor is required for RNA-directed DNA methylation in Arabidopsis. PLoS Genet. *9*, e1003779.

Huang, J., Hsu, J.-M., and Laurent, B.C. (2004). The RSC nucleosome-remodeling complex is required for Cohesin's association with chromosome arms. Mol. Cell *13*, 739–750.

Hughes, A.L., Todd, B.L., and Espenshade, P.J. (2005). SREBP pathway responds to sterols and functions as an oxygen sensor in fission yeast. Cell *120*, 831–842.

Iida, T., Kawaguchi, R., and Nakayama, J.-I. (2006). Conserved ribonuclease, Eri1, negatively regulates heterochromatin assembly in fission yeast. Curr. Biol. *16*, 1459–1464.

Iida, T., Nakayama, J.-I., and Moazed, D. (2008). siRNA-mediated heterochromatin establishment requires HP1 and is associated with antisense transcription. Mol. Cell *31*, 178–189.

Irvine, D.V., Goto, D.B., Vaughn, M.W., Nakaseko, Y., McCombie, W.R., Yanagida, M., and Martienssen, R. (2009). Mapping epigenetic mutations in fission yeast using whole-genome next-generation sequencing. Genome Res. *19*, 1077–1083.

Irvine, D.V., Zaratiegui, M., Tolia, N.H., Goto, D.B., Chitwood, D.H., Vaughn, M.W., Joshua-Tor, L., and Martienssen, R.A. (2006). Argonaute slicing is required for heterochromatic silencing and spreading. Science *313*, 1134–1137.

Ivanova, A.V., Bonaduce, M.J., Ivanov, S.V., and Klar, A.J. (1998). The chromo and SET domains of the Clr4 protein are essential for silencing in fission yeast. Nat. Genet. *19*, 192–195.

Jeppesen, P., and Turner, B.M. (1993). The inactive X chromosome in female mammals is distinguished by a lack of histone H4 acetylation, a cytogenetic marker for gene expression. Cell *74*, 281–289.

Jeppesen, P., Mitchell, A., Turner, B., and Perry, P. (1992). Antibodies to defined histone epitopes reveal variations in chromatin conformation and underacetylation of centric heterochromatin in human metaphase chromosomes. Chromosoma *101*, 322–332.

Ji, L., and Chen, X. (2012). Regulation of small RNA stability: methylation and beyond. Cell Res. *22*, 624–636.

Jia, S., Kobayashi, R., and Grewal, S.I.S. (2005). Ubiquitin ligase component Cul4 associates with Clr4 histone methyltransferase to assemble heterochromatin. Nat. Cell Biol. *7*, 1007–1013.

Jia, S., Noma, K.-I., and Grewal, S.I.S. (2004). RNAi-independent heterochromatin nucleation by the stress-activated ATF/CREB family proteins. Science *304*, 1971–1976.

Kagansky, A., Folco, H.D., Almeida, R., Pidoux, A.L., Boukaba, A., Simmer, F., Urano, T., Hamilton, G.L., and Allshire, R.C. (2009). Synthetic heterochromatin bypasses RNAi and centromeric repeats to establish functional centromeres. Science *324*, 1716–1719.

Kallgren, S.P., Andrews, S., Tadeo, X., Hou, H., Moresco, J.J., Tu, P.G., Yates, J.R., Nagy, P.L., and Jia, S. (2014). The Proper Splicing of RNAi Factors Is Critical for Pericentric Heterochromatin Assembly in Fission Yeast. PLoS Genet. *10*, e1004334.

Kato, H., Goto, D.B., Martienssen, R.A., Urano, T., Furukawa, K., and Murakami, Y. (2005). RNA polymerase II is required for RNAi-dependent heterochromatin assembly. Science *309*, 467–469.

Käufer, N.F., and Potashkin, J. (2000). Analysis of the splicing machinery in fission yeast: a comparison with budding yeast and mammals. Nucleic Acids Res *28*, 3003–3010.

Keller, C., and Bühler, M. (2013). Chromatin-associated ncRNA activities. Chromosome Res.

Keller, C., Adaixo, R., Stunnenberg, R., Woolcock, K.J., Hiller, S., and Bühler, M. (2012). HP1(Swi6) mediates the recognition and destruction of heterochromatic RNA transcripts. Mol. Cell *47*, 215–227.

Keller, C., Kulasegaran-Shylini, R., Shimada, Y., Hotz, H.-R., and Bühler, M. (2013). Noncoding RNAs prevent spreading of a repressive histone mark. Nat. Struct. Mol. Biol. *20*, 994–1000.

Keller, C., Woolcock, K., Hess, D., and Bühler, M. (2010). Proteomic and functional analysis of the noncanonical poly(A) polymerase Cid14. Rna *16*, 1124–1129.

Kellum, R., and Alberts, B.M. (1995). Heterochromatin protein 1 is required for correct

chromosome segregation in Drosophila embryos. J. Cell. Sci. *108 (Pt 4)*, 1419–1431.

Kennedy, S., Wang, D., and Ruvkun, G. (2004). A conserved siRNA-degrading RNase negatively regulates RNA interference in C. elegans. Nature *427*, 645–649.

Kim, W., Bennett, E.J., Huttlin, E.L., Guo, A., Li, J., Possemato, A., Sowa, M.E., Rad, R., Rush, J., Comb, M.J., et al. (2011). Systematic and quantitative assessment of the ubiquitin-modified proteome. Mol. Cell *44*, 325–340.

Klar, A.J., Hicks, J.B., and Strathern, J.N. (1982). Directionality of yeast mating-type interconversion. Cell *28*, 551–561.

Kloc, A., Zaratiegui, M., Nora, E., and Martienssen, R. (2008). RNA interference guides histone modification during the S phase of chromosomal replication. Curr. Biol. *18*, 490–495.

Kuhn, A.N., and Käufer, N.F. (2003). Pre-mRNA splicing in Schizosaccharomyces pombe: regulatory role of a kinase conserved from fission yeast to mammals. Curr. Genet. *42*, 241–251.

Kupfer, D.M., Drabenstot, S.D., Buchanan, K.L., Lai, H., Zhu, H., Dyer, D.W., Roe, B.A., and Murphy, J.W. (2004). Introns and splicing elements of five diverse fungi. Eukaryotic Cell *3*, 1088–1100.

LaCava, J., Houseley, J., Saveanu, C., Petfalski, E., Thompson, E., Jacquier, A., and Tollervey, D. (2005). RNA degradation by the exosome is promoted by a nuclear polyadenylation complex. Cell *121*, 713–724.

Lachner, M., O'Carroll, D., Rea, S., Mechtler, K., and Jenuwein, T. (2001). Methylation of histone H3 lysine 9 creates a binding site for HP1 proteins. Nature *410*, 116–120.

Lachner, M., Sengupta, R., Schotta, G., and Jenuwein, T. (2004). Trilogies of histone lysine methylation as epigenetic landmarks of the eukaryotic genome. Cold Spring Harbor Symposia on Quantitative Biology *69*, 209–218.

Langmead, B., and Salzberg, S.L. (2012). Fast gapped-read alignment with Bowtie 2. Nat. Methods *9*, 357–359.

Lans, H., Marteijn, J.A., and Vermeulen, W. (2012). ATP-dependent chromatin remodeling in the DNA-damage response. Epigenetics Chromatin *5*, 4.

Laurent, B.C., Treich, I., and Carlson, M. (1993). The yeast SNF2/SWI2 protein has DNA-stimulated ATPase activity required for transcriptional activation. Genes Dev. *7*, 583–591.

Laurent, B.C., Yang, X., and Carlson, M. (1992). An essential Saccharomyces cerevisiae gene homologous to SNF2 encodes a helicase-related protein in a new family. Molecular and Cellular Biology *12*, 1893–1902.

Lee, Y., Ahn, C., Han, J., Choi, H., Kim, J., Yim, J., Lee, J., Provost, P., Rådmark, O., Kim, S., et al. (2003). The nuclear RNase III Drosha initiates microRNA processing. Nature *425*, 415–419.

Li, F., Goto, D.B., Zaratiegui, M., Tang, X., Martienssen, R., and Cande, W.Z. (2005). Two novel proteins, dos1 and dos2, interact with rik1 to regulate heterochromatic RNA interference and histone modification. Curr. Biol. *15*, 1448–1457.

Li, F., Huarte, M., Zaratiegui, M., Vaughn, M.W., Shi, Y., Martienssen, R., and Cande, W.Z. (2008). Lid2 is required for coordinating H3K4 and H3K9 methylation of heterochromatin and euchromatin. Cell *135*, 272–283.

Li, F., Martienssen, R., and Cande, W.Z. (2011). Coordination of DNA replication and histone modification by the Rik1-Dos2 complex. Nature *475*, 244–248.

Li, H., Handsaker, B., Wysoker, A., Fennell, T., Ruan, J., Homer, N., Marth, G., Abecasis, G., Durbin, R., 1000 Genome Project Data Processing Subgroup (2009). The Sequence Alignment/Map format and SAMtools. Bioinformatics *25*, 2078–2079.

Lippman, Z., and Martienssen, R. (2004). The role of RNA interference in heterochromatic silencing. Nature *431*, 364–370.

Lyon, M.F. (1961). Gene action in the X-chromosome of the mouse (Mus musculus L.). Nature *190*, 372–373.

Ma, J.-B., Ye, K., and Patel, D.J. (2004). Structural basis for overhang-specific small interfering RNA recognition by the PAZ domain. Nature *429*, 318–322.

Mandemaker, I., Vermeulen, W., and Marteijn, J. (2014). Role of chromatin remodeling during the transcriptional restart upon DNA damage. Nucleus *5*.

Marasovic, M., Zocco, M., and Halic, M. (2013). Argonaute and Triman generate dicer-independent priRNAs and mature siRNAs to initiate heterochromatin formation. Mol. Cell *52*, 173–183.

Marguerat, S., Schmidt, A., Codlin, S., Chen, W., Aebersold, R., and Bähler, J. (2012). Quantitative analysis of fission yeast transcriptomes and proteomes in proliferating and quiescent cells. Cell *151*, 671–683.

Martín-Castellanos, C., Blanco, M., Rozalén, A.E., Pérez-Hidalgo, L., García, A.I., Conde, F., Mata, J., Ellermeier, C., Davis, L., San-Segundo, P., et al. (2005). A large-scale screen in S. pombe identifies seven novel genes required for critical meiotic events. Curr. Biol. *15*, 2056–2062.

McClintock, B. (1950). The origin and behavior of mutable loci in maize. Proc. Natl. Acad. Sci. U.S.a. *36*, 344–355.

Merrill, B.M., Stone, K.L., Cobianchi, F., Wilson, S.H., and Williams, K.R. (1988).

Phenylalanines that are conserved among several RNA-binding proteins form part of a nucleic acid-binding pocket in the A1 heterogeneous nuclear ribonucleoprotein. J. Biol. Chem. *263*, 3307–3313.

Mitchell, P., Petfalski, E., Shevchenko, A., Mann, M., and Tollervey, D. (1997). The exosome: a conserved eukaryotic RNA processing complex containing multiple 3“-->5” exoribonucleases. Cell *91*, 457–466.

Mohrmann, L., and Verrijzer, C.P. (2005). Composition and functional specificity of SWI2/SNF2 class chromatin remodeling complexes. Biochim. Biophys. Acta *1681*, 59–73.

Monahan, B.J., Villén, J., Marguerat, S., Bähler, J., Gygi, S.P., and Winston, F. (2008). Fission yeast SWI/SNF and RSC complexes show compositional and functional differences from budding yeast. Nat. Struct. Mol. Biol. *15*, 873–880.

Motamedi, M.R., Hong, E.-J.E., Li, X., Gerber, S., Denison, C., Gygi, S., and Moazed, D. (2008). HP1 proteins form distinct complexes and mediate heterochromatic gene silencing by nonoverlapping mechanisms. Mol. Cell *32*, 778–790.

Motamedi, M.R., Verdel, A., Colmenares, S.U., Gerber, S.A., Gygi, S.P., and Moazed, D. (2004). Two RNAi complexes, RITS and RDRC, physically interact and localize to noncoding centromeric RNAs. Cell *119*, 789–802.

Muller, H.J. (1930). Types of visible variations induced by X-rays inDrosophila. Journ. of Gen. *22*, 299–334–334.

Murakami, H., Goto, D.B., Toda, T., Chen, E.S., Grewal, S.I., Martienssen, R.A., and Yanagida, M. (2007). Ribonuclease activity of Dis3 is required for mitotic progression and provides a possible link between heterochromatin and kinetochore function. PLoS ONE *2*, e317.

Murakami, S., Matsumoto, T., Niwa, O., and Yanagida, M. (1991). Structure of the fission yeast centromere cen3: direct analysis of the reiterated inverted region. Chromosoma *101*, 214–221.

Murnane, J.P., and Sabatier, L. (2004). Chromosome rearrangements resulting from telomere dysfunction and their role in cancer. Bioessays *26*, 1164–1174.

Nagalakshmi, U., Wang, Z., Waern, K., Shou, C., Raha, D., Gerstein, M., and Snyder, M. (2008). The transcriptional landscape of the yeast genome defined by RNA sequencing. Science *320*, 1344–1349.

Nakaseko, Y., Adachi, Y., Funahashi, S., Niwa, O., and Yanagida, M. (1986). Chromosome walking shows a highly homologous repetitive sequence present in all the centromere regions of fission yeast. Embo J. *5*, 1011–1021.

Nakaseko, Y., Kinoshita, N., and Yanagida, M. (1987). A novel sequence common to the

centromere regions of Schizosaccharomyces pombe chromosomes. Nucleic Acids Res *15*, 4705–4715.

Nakayama, J., Klar, A.J., and Grewal, S.I. (2000). A chromodomain protein, Swi6, performs imprinting functions in fission yeast during mitosis and meiosis. Cell *101*, 307–317.

Nakayama, J., Rice, J.C., Strahl, B.D., Allis, C.D., and Grewal, S.I. (2001). Role of histone H3 lysine 9 methylation in epigenetic control of heterochromatin assembly. Science *292*, 110–113.

Nakayashiki, H., Kadotani, N., and Mayama, S. (2006). Evolution and diversification of RNA silencing proteins in fungi. J. Mol. Evol. *63*, 127–135.

Natsume, T., Tsutsui, Y., Sutani, T., Dunleavy, E.M., Pidoux, A.L., Iwasaki, H., Shirahige, K., Allshire, R.C., and Yamao, F. (2008). A DNA polymerase alpha accessory protein, Mcl1, is required for propagation of centromere structures in fission yeast. PLoS ONE *3*, e2221.

Neigeborn, L., and Carlson, M. (1984). Genes affecting the regulation of SUC2 gene expression by glucose repression in Saccharomyces cerevisiae. Genetics *108*, 845–858.

Nicolas, E., Yamada, T., Cam, H.P., FitzGerald, P.C., Kobayashi, R., and Grewal, S.I.S. (2007). Distinct roles of HDAC complexes in promoter silencing, antisense suppression and DNA damage protection. Nat. Struct. Mol. Biol. *14*, 372–380.

Nonaka, N., Kitajima, T., Yokobayashi, S., Xiao, G., Yamamoto, M., Grewal, S.I.S., and Watanabe, Y. (2002). Recruitment of cohesin to heterochromatic regions by Swi6/HP1 in fission yeast. Nat. Cell Biol. *4*, 89–93.

Ohno, S., Kaplan, W.D., and Kinosita, R. (1959). Formation of the sex chromatin by a single X-chromosome in liver cells of Rattus norvegicus. Exp. Cell Res. *18*, 415–418.

Oshima, Y., and Takano, I. (1971). Mating types in Saccharomyces: their convertibility and homothallism. Genetics *67*, 327–335.

Pak, J., and Fire, A. (2007). Distinct populations of primary and secondary effectors during RNAi in C. elegans. Science *315*, 241–244.

Pall, G.S., and Hamilton, A.J. (2008). Improved northern blot method for enhanced detection of small RNA. Nat Protoc *3*, 1077–1084.

Partridge, J.F., Borgstrøm, B., and Allshire, R.C. (2000). Distinct protein interaction domains and protein spreading in a complex centromere. Genes Dev. *14*, 783–791.

Partridge, J.F., Scott, K.S.C., Bannister, A.J., Kouzarides, T., and Allshire, R.C. (2002). cis-acting DNA from fission yeast centromeres mediates histone H3 methylation and recruitment of silencing factors and cohesin to an ectopic site. Curr. Biol. *12*, 1652–1660.

Pemberton, T.J., and Kay, J.E. (2005). The cyclophilin repertoire of the fission yeast Schizosaccharomyces pombe. Yeast *22*, 927–945.

Peterson, C.L., and Herskowitz, I. (1992). Characterization of the yeast SWI1, SWI2, and SWI3 genes, which encode a global activator of transcription. Cell *68*, 573–583.

Petrie, V.J., Wuitschick, J.D., Givens, C.D., Kosinski, A.M., and Partridge, J.F. (2005). RNA interference (RNAi)-dependent and RNAi-independent association of the Chp1 chromodomain protein with distinct heterochromatic loci in fission yeast. Molecular and Cellular Biology *25*, 2331–2346.

Pintard, L., Willems, A., and Peter, M. (2004). Cullin-based ubiquitin ligases: Cul3-BTB complexes join the family. Embo J. *23*, 1681–1687.

Pollex, T., and Heard, E. (2012). Recent advances in X-chromosome inactivation research. Curr Opin Cell Biol *24*, 825–832.

Provost, P., Dishart, D., Doucet, J., Frendewey, D., Samuelsson, B., and Rådmark, O. (2002a). Ribonuclease activity and RNA binding of recombinant human Dicer. Embo J. *21*, 5864–5874.

Provost, P., Silverstein, R.A., Dishart, D., Walfridsson, J., Djupedal, I., Kniola, B., Wright, A., Samuelsson, B., Rådmark, O., and Ekwall, K. (2002b). Dicer is required for chromosome segregation and gene silencing in fission yeast cells. Proc. Natl. Acad. Sci. U.S.a. *99*, 16648–16653.

Quinlan, A.R., and Hall, I.M. (2010). BEDTools: a flexible suite of utilities for comparing genomic features. Bioinformatics *26*, 841–842.

Rea, S., Eisenhaber, F., O'Carroll, D., Strahl, B.D., Sun, Z.W., Schmid, M., Opravil, S., Mechtler, K., Ponting, C.P., Allis, C.D., et al. (2000). Regulation of chromatin structure by site-specific histone H3 methyltransferases. Nature *406*, 593–599.

Reddy, B.D., Wang, Y., Niu, L., Higuchi, E.C., Marguerat, S.B., Bähler, J., Smith, G.R., and Jia, S. (2011). Elimination of a specific histone H3K14 acetyltransferase complex bypasses the RNAi pathway to regulate pericentric heterochromatin functions. Genes Dev. *25*, 214–219.

Reinhart, B.J., and Bartel, D.P. (2002). Small RNAs correspond to centromere heterochromatic repeats. Science *297*, 1831.

Reyes-Turcu, F.E., Zhang, K., Zofall, M., Chen, E., and Grewal, S.I.S. (2011). Defects in RNA quality control factors reveal RNAi-independent nucleation of heterochromatin. Nat. Struct. Mol. Biol. *18*, 1132–1138.

Ribar, B., Prakash, L., and Prakash, S. (2007). ELA1 and CUL3 are required along with ELC1 for RNA polymerase II polyubiquitylation and degradation in DNA-damaged yeast cells. Molecular and Cellular Biology *27*, 3211–3216.

Rice, J.C., and Allis, C.D. (2001). Histone methylation versus histone acetylation: new insights into epigenetic regulation. Curr Opin Cell Biol *13*, 263–273.

Robinson, J.T., Thorvaldsdóttir, H., Winckler, W., Guttman, M., Lander, E.S., Getz, G., and Mesirov, J.P. (2011). Integrative genomics viewer. Nat. Biotechnol. *29*, 24–26.

Roy, B., and Sanyal, K. (2011). Diversity in requirement of genetic and epigenetic factors for centromere function in fungi. Eukaryotic Cell *10*, 1384–1395.

Ryan, C.J., Roguev, A., Patrick, K., Xu, J., Jahari, H., Tong, Z., Beltrao, P., Shales, M., Qu, H., Collins, S.R., et al. (2012). Hierarchical modularity and the evolution of genetic interactomes across species. Mol. Cell *46*, 691–704.

Sadaie, M., Iida, T., Urano, T., and Nakayama, J.-I. (2004). A chromodomain protein, Chp1, is required for the establishment of heterochromatin in fission yeast. Embo J. *23*, 3825–3835.

Saitoh, S., Chabes, A., McDonald, W.H., Thelander, L., Yates, J.R., and Russell, P. (2002). Cid13 is a cytoplasmic poly(A) polymerase that regulates ribonucleotide reductase mRNA. Cell *109*, 563–573.

Sanders, S.L., Portoso, M., Mata, J., Bähler, J., Allshire, R.C., and Kouzarides, T. (2004). Methylation of histone H4 lysine 20 controls recruitment of Crb2 to sites of DNA damage. Cell *119*, 603–614.

Scott, K.C., Merrett, S.L., and Willard, H.F. (2006). A heterochromatin barrier partitions the fission yeast centromere into discrete chromatin domains. Curr. Biol. *16*, 119–129.

Scott, K.C., White, C.V., and Willard, H.F. (2007). An RNA polymerase III-dependent heterochromatin barrier at fission yeast centromere 1. PLoS ONE *2*, e1099.

Shankaranarayana, G.D., Motamedi, M.R., Moazed, D., and Grewal, S.I.S. (2003). Sir2 regulates histone H3 lysine 9 methylation and heterochromatin assembly in fission yeast. Curr. Biol. *13*, 1240–1246.

Shao, W., and Espenshade, P.J. (2012). Expanding roles for SREBP in metabolism. Cell Metab. *16*, 414–419.

Sharif, J., Muto, M., Takebayashi, S.-I., Suetake, I., Iwamatsu, A., Endo, T.A., Shinga, J., Mizutani-Koseki, Y., Toyoda, T., Okamura, K., et al. (2007). The SRA protein Np95 mediates epigenetic inheritance by recruiting Dnmt1 to methylated DNA. Nature *450*, 908–912.

Sijen, T., Steiner, F.A., Thijssen, K.L., and Plasterk, R.H.A. (2007). Secondary siRNAs result from unprimed RNA synthesis and form a distinct class. Science *315*, 244–247.

Sipiczki, M. (2000). Where does fission yeast sit on the tree of life? Genome Biol. *1*, REVIEWS1011.

Somesh, B.P., Reid, J., Liu, W.-F., Søgaard, T.M.M., Erdjument-Bromage, H., Tempst, P., and Svejstrup, J.Q. (2005). Multiple mechanisms confining RNA polymerase II ubiquitylation to polymerases undergoing transcriptional arrest. Cell *121*, 913–923.

Steiner, N.C., and Clarke, L. (1994). A novel epigenetic effect can alter centromere function in fission yeast. Cell *79*, 865–874.

Stewart, E.V., Lloyd, S.J.-A., Burg, J.S., Nwosu, C.C., Lintner, R.E., Daza, R., Russ, C., Ponchner, K., Nusbaum, C., and Espenshade, P.J. (2012). Yeast sterol regulatory element-binding protein (SREBP) cleavage requires Cdc48 and Dsc5, a ubiquitin regulatory X domain-containing subunit of the Golgi Dsc E3 ligase. J. Biol. Chem. *287*, 672–681.

Stewart, E.V., Nwosu, C.C., Tong, Z., Roguev, A., Cummins, T.D., Kim, D.-U., Hayles, J., Park, H.-O., Hoe, K.-L., Powell, D.W., et al. (2011). Yeast SREBP cleavage activation requires the Golgi Dsc E3 ligase complex. Mol. Cell *42*, 160–171.

Strathern, J.N., and Herskowitz, I. (1979). Asymmetry and directionality in production of new cell types during clonal growth: the switching pattern of homothallic yeast. Cell *17*, 371–381.

Struhl, K. (2007). Transcriptional noise and the fidelity of initiation by RNA polymerase II. Nat. Struct. Mol. Biol. *14*, 103–105.

Sudarsanam, P., Iyer, V.R., Brown, P.O., and Winston, F. (2000). Whole-genome expression analysis of snf/swi mutants of Saccharomyces cerevisiae. Proc. Natl. Acad. Sci. U.S.a. *97*, 3364–3369.

Sugiyama, T., Cam, H., Verdel, A., Moazed, D., and Grewal, S.I.S. (2005). From The Cover: RNA-dependent RNA polymerase is an essential component of a self-enforcing loop coupling heterochromatin assembly to siRNA production. Proceedings of the National Academy of Sciences *102*, 152–157.

Sugiyama, T., Cam, H.P., Sugiyama, R., Noma, K.-I., Zofall, M., Kobayashi, R., and Grewal, S.I.S. (2007). SHREC, an effector complex for heterochromatic transcriptional silencing. Cell *128*, 491–504.

Tamura, K., Stecher, G., Peterson, D., Filipski, A., and Kumar, S. (2013). MEGA6: Molecular Evolutionary Genetics Analysis version 6.0. Mol. Biol. Evol. *30*, 2725–2729.

Thon, G., and Klar, A.J. (1993). Directionality of fission yeast mating-type interconversion is controlled by the location of the donor loci. Genetics *134*, 1045–1054.

Thon, G., and Verhein-Hansen, J. (2000). Four chromo-domain proteins of Schizosaccharomyces pombe differentially repress transcription at various chromosomal locations. Genetics *155*, 551–568.

Thon, G., Cohen, A., and Klar, A.J. (1994). Three additional linkage groups that repress

transcription and meiotic recombination in the mating-type region of Schizosaccharomyces pombe. Genetics *138*, 29–38.

Thon, G., Hansen, K.R., Altes, S.P., Sidhu, D., Singh, G., Verhein-Hansen, J., Bonaduce, M.J., and Klar, A.J.S. (2005). The Clr7 and Clr8 directionality factors and the Pcu4 cullin mediate heterochromatin formation in the fission yeast Schizosaccharomyces pombe. Genetics *171*, 1583–1595.

Thorvaldsdóttir, H., Robinson, J.T., and Mesirov, J.P. (2013). Integrative Genomics Viewer (IGV): high-performance genomics data visualization and exploration. Brief. Bioinformatics *14*, 178–192.

Trojer, P., and Reinberg, D. (2007). Facultative heterochromatin: is there a distinctive molecular signature? Mol. Cell *28*, 1–13.

Turner, B.M. (1991). Histone acetylation and control of gene expression. J. Cell. Sci. *99 (Pt 1)*, 13–20.

Tuzon, C.T., Borgstrom, B., Weilguny, D., Egel, R., Cooper, J.P., and Nielsen, O. (2004). The fission yeast heterochromatin protein Rik1 is required for telomere clustering during meiosis. J. Cell Biol. *165*, 759–765.

Vanácová, S., Wolf, J., Martin, G., Blank, D., Dettwiler, S., Friedlein, A., Langen, H., Keith, G., and Keller, W. (2005). A new yeast poly(A) polymerase complex involved in RNA quality control. PLoS Biol. *3*, e189.

Vaucheret, H., Béclin, C., Elmayan, T., Feuerbach, F., Godon, C., Morel, J.B., Mourrain, P., Palauqui, J.C., and Vernhettes, S. (1998). Transgene-induced gene silencing in plants. Plant J. *16*, 651–659.

Verdaasdonk, J.S., and Bloom, K. (2011). Centromeres: unique chromatin structures that drive chromosome segregation. Nat. Rev. Mol. Cell Biol. *12*, 320–332.

Verdel, A., Jia, S., Gerber, S., Sugiyama, T., Gygi, S., Grewal, S.I.S., and Moazed, D. (2004). RNAi-Mediated Targeting of Heterochromatin by the RITS Complex. Science *303*, 672–676.

Viladevall, L., St Amour, C.V., Rosebrock, A., Schneider, S., Zhang, C., Allen, J.J., Shokat, K.M., Schwer, B., Leatherwood, J.K., and Fisher, R.P. (2009). TFIIH and P-TEFb coordinate transcription with capping enzyme recruitment at specific genes in fission yeast. Mol. Cell *33*, 738–751.

Volpe, T.A., Kidner, C., Hall, I.M., Teng, G., Grewal, S.I.S., and Martienssen, R.A. (2002). Regulation of heterochromatic silencing and histone H3 lysine-9 methylation by RNAi. Science *297*, 1833–1837.

Volpe, T., Schramke, V., Hamilton, G.L., White, S.A., Teng, G., Martienssen, R.A., and Allshire, R.C. (2003). RNA interference is required for normal centromere function in

fission yeast. Chromosome Res. *11*, 137–146.

Waddington, C.H. (1942). Canalization of development and the inheritance of acquired characters. Nature.

Wang, S.S., and Zakian, V.A. (1990). Sequencing of Saccharomyces telomeres cloned using T4 DNA polymerase reveals two domains. Molecular and Cellular Biology *10*, 4415–4419.

Wang, S.-W., Stevenson, A.L., Kearsey, S.E., Watt, S., and Bähler, J. (2008). Global role for polyadenylation-assisted nuclear RNA degradation in posttranscriptional gene silencing. Molecular and Cellular Biology *28*, 656–665.

Wickham, H. (2009). ggplot2 (Springer).

Wickner, R.B. (1996). Double-stranded RNA viruses of Saccharomyces cerevisiae. Microbiol. Rev. *60*, 250–265.

Willger, S.D., Grahl, N., and Cramer, R.A. (2009). Aspergillus fumigatus metabolism: clues to mechanisms of in vivo fungal growth and virulence. Med. Mycol. *47 Suppl 1*, S72–S79.

Willingham, A.T., and Gingeras, T.R. (2006). TUF love for "junk" DNA. Cell *125*, 1215–1220.

Win, T.Z., Draper, S., Read, R.L., Pearce, J., Norbury, C.J., and Wang, S.-W. (2006a). Requirement of fission yeast Cid14 in polyadenylation of rRNAs. Molecular and Cellular Biology *26*, 1710–1721.

Win, T.Z., Stevenson, A.L., and Wang, S.-W. (2006b). Fission yeast Cid12 has dual functions in chromosome segregation and checkpoint control. Molecular and Cellular Biology *26*, 4435–4447.

Wolfe, K.H., and Shields, D.C. (1997). Molecular evidence for an ancient duplication of the entire yeast genome. Nature *387*, 708–713.

Wood, V., Gwilliam, R., Rajandream, M.-A., Lyne, M., Lyne, R., Stewart, A., Sgouros, J., Peat, N., Hayles, J., Baker, S., et al. (2002). The genome sequence of Schizosaccharomyces pombe. Nature *415*, 871–880.

Wyers, F., Rougemaille, M., Badis, G., Rousselle, J.-C., Dufour, M.-E., Boulay, J., Régnault, B., Devaux, F., Namane, A., Séraphin, B., et al. (2005). Cryptic pol II transcripts are degraded by a nuclear quality control pathway involving a new poly(A) polymerase. Cell *121*, 725–737.

Yamada, T., Fischle, W., Sugiyama, T., Allis, C.D., and Grewal, S.I.S. (2005). The nucleation and maintenance of heterochromatin by a histone deacetylase in fission yeast. Mol. Cell *20*, 173–185.

Yamanaka, S., Mehta, S., Reyes-Turcu, F.E., Zhuang, F., Fuchs, R.T., Rong, Y., Robb, G.B., and Grewal, S.I.S. (2013). RNAi triggered by specialized machinery silences developmental genes and retrotransposons. Nature *493*, 557–560.

Yamane, K., Mizuguchi, T., Cui, B., Zofall, M., Noma, K.-I., and Grewal, S.I.S. (2011). Asf1/HIRA facilitate global histone deacetylation and associate with HP1 to promote nucleosome occupancy at heterochromatic loci. Mol. Cell *41*, 56–66.

Yang, Z., Ebright, Y.W., Yu, B., and Chen, X. (2006). HEN1 recognizes 21-24 nt small RNA duplexes and deposits a methyl group onto the 2“ OH of the 3” terminal nucleotide. Nucleic Acids Res *34*, 667–675.

Yu, R., Jih, G., Iglesias, N., and Moazed, D. (2014). Determinants of heterochromatic siRNA biogenesis and function. Mol. Cell *53*, 262–276.

Zakian, V.A. (1995). Telomeres: beginning to understand the end. Science *270*, 1601–1607.

Zaratiegui, M., Castel, S.E., Irvine, D.V., Kloc, A., Ren, J., Li, F., de Castro, E., Marín, L., Chang, A.-Y., Goto, D., et al. (2011). RNAi promotes heterochromatic silencing through replication-coupled release of RNA Pol II. Nature *479*, 135–138.

Zaratiegui, M., Irvine, D.V., and Martienssen, R.A. (2007). Noncoding RNAs and gene silencing. Cell *128*, 763–776.

Zhang, C.-J., Zhou, J.-X., Liu, J., Ma, Z.-Y., Zhang, S.-W., Dou, K., Huang, H.-W., Cai, T., Liu, R., Zhu, J.-K., et al. (2013). The splicing machinery promotes RNA-directed DNA methylation and transcriptional silencing in Arabidopsis. Embo J. *32*, 1128–1140.

Zhang, H., Kolb, F.A., Brondani, V., Billy, E., and Filipowicz, W. (2002). Human Dicer preferentially cleaves dsRNAs at their termini without a requirement for ATP. Embo J. *21*, 5875–5885.

Zhang, H., Kolb, F.A., Jaskiewicz, L., Westhof, E., and Filipowicz, W. (2004). Single processing center models for human Dicer and bacterial RNase III. Cell *118*, 57–68.

Zhang, K., Fischer, T., Porter, R.L., Dhakshnamoorthy, J., Zofall, M., Zhou, M., Veenstra, T., and Grewal, S.I.S. (2011). Clr4/Suv39 and RNA Quality Control Factors Cooperate to Trigger RNAi and Suppress Antisense RNA. Science *331*, 1624–1627.

Zhang, K., Mosch, K., Fischle, W., and Grewal, S.I.S. (2008). Roles of the Clr4 methyltransferase complex in nucleation, spreading and maintenance of heterochromatin. Nat. Struct. Mol. Biol. *15*, 381–388.

Zhu, Y., Rowley, M.J., Böhmdorfer, G., and Wierzbicki, A.T. (2013). A SWI/SNF chromatin-remodeling complex acts in noncoding RNA-mediated transcriptional silencing. Mol. Cell *49*, 298–309.